

# Extensions of the Standard Model and their Influence on Single-Top

Erik Lascaris

May 2006

A Master's Thesis in Theoretical High Energy Physics  
under the supervision of  
prof. dr. E.L.M.P. Laenen  
and  
prof. dr. ing. B. van Eijk.



NIKHEF  
Kruislaan 409  
1098 SJ Amsterdam  
The Netherlands



**Universiteit Twente**  
*de ondernemende universiteit*

University of Twente  
Postbus 217  
7500 AE Enschede  
The Netherlands



# Abstract

With particle accelerators like the Tevatron and the LHC we can reach such high energies that it is very likely that we will soon find clear signatures of physics beyond the Standard Model. Some of the most interesting processes to examine are single-top processes; interactions with in the final state only one top quark and some other particle. The top quark has a mass almost 5 orders of magnitude larger than the lightest quarks ( $\sim 175$  GeV), a strange property that some theories explain by predicting interactions with new particles. In this thesis some extensions of the Standard Model are analyzed. With the use of a Monte Carlo these theories have been simulated, resulting in several predictions for experimental results for the single-top process.



# Acknowledgements

Even though this report was written by only one person, it was impossible to create it without the help of many people. I would like to thank my supervisor Eric Laenen for giving answers to the many questions I had, and for giving me the opportunity to do this thesis project in the first place. It has been a very enlightening experience that has introduced me to the world of theoretical physics, provided me with a deeper understanding of the Standard Model, and helped me to get more familiarized with some of the most recent theoretical developments. I believe that this thesis project has provided me a solid foundation for any further studies in high energy physics.

I like to give a special thanks to Patrick Motylinski, who has spent a lot of his time helping me with the Monte Carlo program. He helped me with numerous bug-fixes and helped me to obtain a better insight to the program. Furthermore this man has a gift for making people laugh, which makes working with him a most pleasant experience.

I would like to thank Kristen Sunter for proofreading this thesis, and for helping me with the more linguistic matters.

I must not forget to thank Tim Dijkstra, Hylke Koers, and Gideon Koekoek as well, for all their help when I had problems again with Linux, Gnuplot, LateX, and all kinds of physics-related issues. I have enjoyed the many interesting discussions we had.

Finally I would like to thank the NIKHEF institute for their hospitality and support. The numerous facilities they offered, like free coffee in the morning, an extensive library, 24-hour access, and their computer services, made it a pleasant and productive place to work and made it a lot easier for me to write this thesis.



# Contents

<b>1</b>	<b>Introduction</b>	<b>7</b>
1.1	Conventions . . . . .	8
<b>2</b>	<b>Gauge Theories</b>	<b>10</b>
2.1	Lagrangian mechanics . . . . .	10
2.2	Symmetries . . . . .	12
2.3	Feynman diagrams . . . . .	15
<b>3</b>	<b>The Standard Model</b>	<b>21</b>
3.1	Experimental basis for electroweak theory . . . . .	21
3.2	Building the Lagrangian . . . . .	22
3.3	Spontaneous symmetry breaking . . . . .	25
3.4	Eigenstates of the gauge bosons . . . . .	29
3.5	Fermion masses . . . . .	32
3.6	Quantum chromodynamics . . . . .	34
3.7	Summary . . . . .	35
<b>4</b>	<b>Top physics in the Standard Model</b>	<b>37</b>
4.1	Top quark production via $t\bar{t}$ . . . . .	37
4.2	Single-top production . . . . .	40
4.3	Numerical results for top production . . . . .	44
4.4	Top decay . . . . .	54
<b>5</b>	<b>The Monte Carlo program</b>	<b>57</b>
5.1	Classical numerical integration . . . . .	57
5.2	Monte Carlo techniques . . . . .	60
5.3	The program . . . . .	63
<b>6</b>	<b>Topflavor models</b>	<b>70</b>
6.1	The Topflavor Lagrangian . . . . .	70
6.2	Breaking of $SU(2)_l \times SU(2)_h \rightarrow SU(2)_w$ . . . . .	75
6.3	Electroweak symmetry breaking . . . . .	76
6.4	Fermion - gauge boson couplings . . . . .	79
6.5	Single-top in the Topflavor model . . . . .	81
6.6	Monte Carlo results . . . . .	82
<b>7</b>	<b>Little Higgs models</b>	<b>93</b>
7.1	The hierarchy problem . . . . .	93
7.2	The Littlest Higgs . . . . .	94
7.3	Electroweak symmetry breaking . . . . .	100
7.4	Single-top in the Littlest Higgs model . . . . .	102
7.5	Monte Carlo results . . . . .	103
<b>8</b>	<b>Conclusions</b>	<b>107</b>
<b>A</b>	<b>Differential cross sections</b>	<b>109</b>
<b>B</b>	<b>Special unitary groups</b>	<b>112</b>

# Chapter 1

## Introduction

The Standard Model (SM) has been one of the most successful theories in physics. After its development in the early 70's, it predicted several new particles including the existence of the  $W^\pm, Z$  bosons which were discovered at CERN in 1983. The most recent discovery is the detection of the top quark, done by the CDF and  $D\bar{O}$  experiments at the Tevatron (Fermilab), in 1995. The only particle predicted by the SM that has not been found yet is the Higgs boson. If it truly exists, the LHC will certainly find it.

Now that we have found almost all of the particles predicted by the Standard Model, one could ask 'Is there any physics beyond the Standard Model?'. Most physicists believe that the answer to this is 'yes'. It is highly unlikely that the Standard Model is the ultimate theory of everything because gravity is not included in the model, and it possesses some esthetical problems like, most notably, the hierarchy problem (see Chapter 7).

Because the Standard Model has been so successful, all new fundamental theories should converge to the SM at energies below the electroweak symmetry breaking scale ( $v = 254$  GeV). The obvious way to create such a theory, is by starting with the Standard Model and make some simple extension. In this thesis we describe two of such extensions, the *Topflavor* model and the *Littlest Higgs* model. Both models have been conceived quite recently (1996 and 2002), and are therefore not fully studied yet.

An interesting method for testing these theories can be done with the aid of precise measurements of the cross sections of different kinds of top production. The reason why the top quark can be used as a probe for new interactions, is because it is so heavy. In this thesis we focus on one particular type of top production, namely the *single-top* processes. These are processes in which only one single top quark is created, plus some other particle(s).

Before we analyze extensions of the Standard Model, it is important to have a thorough understanding of the Standard Model itself and the theoretical foundation it is built upon. For this reason we start in Chapter 2 with a brief introduction to gauge theories, symmetries, and quantum field theory, followed by a complete analysis of the Standard Model in Chapter 3. Subsequently we investigate in Chapter 4 what the Standard Model predictions are for single-top production. We expect that the more literate reader will enjoy these first chapters as a good review, while the less experienced reader will appreciate the level of detail with which the Standard Model and single-top are examined.

As part of this thesis project it was necessary to develop a Monte Carlo program for doing single-top simulations. In Chapter 5 we explain the basics of Monte Carlo integration and demonstrate how the Monte Carlo program is implemented. This program has been used to produce almost all of the cross sections and plots presented in this report. Several tests have been done to confirm that the program is working properly.

Finally, in Chapter 6 and 7 we examine the two Standard Model extensions: Topflavor and the Littlest Higgs. Both chapters start with a thorough analysis of the model, followed by the determination of mass eigenstates and the couplings. At the end of each chapter we present the Monte Carlo results, together with a short discussion. In Chapter 8 we give a short summary about what we can conclude from the results found in the previous chapters.



## 1.1 Conventions

For this report we have adopted the following conventions.

### Natural units

In all calculations we will work with units such that

$$\hbar = c = 1. \tag{1.1}$$

In this system length, time, energy and mass have the following units:

$$[\text{length}] = \text{GeV}^{-1}, \tag{1.2a}$$

$$[\text{time}] = \text{GeV}^{-1}, \tag{1.2b}$$

$$[\text{energy}] = \text{GeV}, \tag{1.2c}$$

$$[\text{mass}] = \text{GeV}. \tag{1.2d}$$

### Metric

All calculations are done in Minkowski space. The metric tensor is therefore defined as

$$g_{\mu\nu} = g^{\mu\nu} = \begin{pmatrix} 1 & 0 & 0 & 0 \\ 0 & -1 & 0 & 0 \\ 0 & 0 & -1 & 0 \\ 0 & 0 & 0 & -1 \end{pmatrix}. \tag{1.3}$$

Unless noted otherwise, repeated indices will imply Einstein summation.

### Group generators

For the generators of SU(2), SU(3), and SU(5) we refer to Appendix B. To prevent confusion with  $\sigma$ -fields and cross sections, we write the Pauli matrices as  $\tau^a$  (the  $\tau$ -lepton is rarely encountered).

### Monte Carlo parameters

For all our simulations we have used the RANMAR random generator, the CTEQ5L table for the PDF's, and all scales set to  $\mu_F = \mu_R = m_t$ . For the top mass  $m_t$  we use 175 GeV, the mass of the  $W$  vector boson is set to  $m_W = 80.4$  GeV. The CKM matrix we have used is

$$V = \begin{pmatrix} V_{ud} & V_{us} & V_{ub} \\ V_{cd} & V_{cs} & V_{cb} \\ V_{td} & V_{ts} & V_{tb} \end{pmatrix} = \begin{pmatrix} 0.9751 & 0.2215 & 0.0035 \\ 0.2210 & 0.9743 & 0.0410 \\ 0.0 & 0.0 & 1.0 \end{pmatrix}.$$

The coupling constants are given by

$$\alpha_s = \alpha_s(m_t) \approx 0.114089, \tag{1.4a}$$

$$\alpha_w = g_w^2/4\pi \approx 0.03394, \tag{1.4b}$$

$$g_w^2 = \frac{8}{\sqrt{2}} G_F m_W^2 \approx 0.42651, \tag{1.4c}$$

with Fermi's constant given by

$$G_F = 1.16639 \times 10^{-5} \text{ GeV}^{-2}. \tag{1.5}$$

See Chapter 5 for more information about the Monte Carlo program.

## Cross sections

All cross sections are given in picobarn (pb),

$$1 \text{ pb} = 10^3 \text{ fb} = 10^{-40} \text{ m}^2 = 10^{-36} \text{ cm}^2. \quad (1.6)$$

Given the luminosity  $L$  of an accelerator, one can determine the event rate of a process with

$$\frac{dN}{dt} = \sigma L, \quad (1.7)$$

where  $\sigma$  is the cross section of the process. In Table 1.1 we present the luminosity of the Tevatron (as of May 2006) and LHC, and also indicate the event rate of a process with  $\sigma = 1 \text{ pb}$ . Unfortunately it is impossible to run an accelerator 24 hours a day, 365 days a year. Therefore we have also indicated the integrated luminosity, which should be used for calculating the number of events per year.

	Tevatron	LHC	
	Run II	low- $L$	high- $L$
$\sqrt{s}$ (in TeV)	2	14	14
Luminosity $L$ (in $\text{cm}^{-2}\text{s}^{-1}$ )	$10^{32}$	$10^{33}$	$10^{34}$
Integrated luminosity (in $\text{fb}^{-1}/\text{year}$ )	1.5	10	100
Event rate, for $\sigma = 1 \text{ pb}$ (in events/day)	9	86	864
Events per year, for $\sigma = 1 \text{ pb}$	$1.5 \times 10^3$	$10^4$	$10^5$

Table 1.1: Luminosity for the Tevatron and the LHC. The luminosity of the LHC will be increased by a factor of 10 after several years operating at low-luminosity. For each accelerator the event rate and the number of events per year for a  $\sigma = 1 \text{ pb}$  process is given.

# Chapter 2

## Gauge Theories

In this chapter we introduce the basic principles of gauge theories. It is meant as an easy appetizer for the rest of the thesis and summarizes the knowledge that can be found in many textbooks about particle physics. In the first section we briefly explain the use of Lagrangians and present the expressions for the Lagrangians of scalar bosons, fermions, and vector bosons. The second section the symmetries of Lagrangians are discussed, and we introduce local gauge symmetries. Finally, in the third section we quickly review quantum field theory in order to explain some things about the origin of Feynman diagrams and the Feynman rules.

### 2.1 Lagrangian mechanics

One of the most elegant and far-reaching principles in classical dynamics is Hamilton's principle. It can be stated as follows [1]:

Of all the possible paths  $\mathbf{x}(t)$  along which a dynamical system may move from one point to another within a specified time interval, the actual path followed is that for which the action has a stationary value (a minimum, maximum or saddle point).

The action is defined as the time integral of the difference between the kinetic and the potential energies:

$$S[x] \equiv \int_{t_1}^{t_2} (T - U) dt = \int_{t_1}^{t_2} L dt. \quad (2.1)$$

The functional  $L(\dot{\mathbf{x}}, \mathbf{x}, t)$  is the Lagrangian of the system. In mathematical terms, Hamilton's principle is written as

$$\delta S[x] = \delta \int_{t_1}^{t_2} L dt = 0. \quad (2.2)$$

According to the calculus of variations this integral can only have a stationary value if it satisfies the Euler-Lagrange equations

$$\frac{\partial L}{\partial x_i} - \frac{d}{dt} \frac{\partial L}{\partial \dot{x}_i} = 0, \quad (2.3)$$

where  $\mathbf{x} = (x_1, x_2, x_3)$ .

Given a Lagrangian, we can quickly find the equations of motion. For example, a one-dimensional harmonic oscillator has the Lagrangian

$$L = T - U = \frac{1}{2}m\dot{x}^2 - \frac{1}{2}kx^2, \quad (2.4)$$

and the Euler-Lagrange equations immediately lead to the correct equation of motion:

$$kx + m\ddot{x} = 0. \quad (2.5)$$

Evidently, everything that is to say about a physical system can be derived from the Lagrangian.

## Lagrangians in quantum field theories

In quantum field theory things are a bit different. Particles are described by relativistic fields that allow a particle to choose between several different paths (transitions from one state to another), each path with its own probability.

Because in a relativistic theory space and time should be on equal footing, we rewrite the action as

$$S[\phi] = \int_{t_1}^{t_2} L dt = \int_{t_1}^{t_2} \int_V (\mathcal{L} d\mathbf{x}) dt = \int \mathcal{L} d^4x. \quad (2.6)$$

The function  $\mathcal{L}(\partial_\mu\phi(x), \phi(x), x)$  is called the Lagrangian density, but in particle physics it is often simply referred to as the Lagrangian. For this Lagrangian the Euler-Lagrange equations become

$$\frac{\partial \mathcal{L}}{\partial \phi_i} - \partial_\mu \frac{\partial \mathcal{L}}{\partial (\partial_\mu \phi_i)} = 0. \quad (2.7)$$

As an example, the motion of a spin-0 particle with mass  $m$  is described by the Klein-Gordon equation,

$$(\partial_\mu \partial^\mu + m^2) \phi = 0, \quad (2.8)$$

therefore a valid Lagrangian is

$$\mathcal{L}_{\text{KG}} = \frac{1}{2} (\partial_\mu \phi)^2 - \frac{1}{2} m^2 \phi^2. \quad (2.9)$$

It is easy to see that this Lagrangian indeed leads to the Klein-Gordon equation, by using the Euler-Lagrange equations of (2.7). For complex scalar fields, the conventional Lagrangian is

$$\mathcal{L}_{\text{KG}^*} = (\partial_\mu \phi^*) (\partial_\mu \phi) - m^2 \phi^* \phi, \quad (2.10)$$

where the complex field  $\phi$  can be considered to be the sum of two real scalar fields,

$$\phi = \frac{1}{\sqrt{2}} (\phi_1 + i\phi_2). \quad (2.11)$$

The factors 1/2 are chosen such that the equations of motion become

$$(\partial_\mu \partial^\mu + m^2) \phi = 0, \quad (2.12a)$$

$$(\partial_\mu \partial^\mu + m^2) \phi^* = 0. \quad (2.12b)$$

In a similar way we can find the Lagrangians for a spin- $\frac{1}{2}$  field and spin-1 field. The Dirac Lagrangian

$$\mathcal{L}_{\text{Dirac}} = i\bar{\psi}\gamma^\mu \partial_\mu \psi - m\bar{\psi}\psi, \quad (2.13)$$

leads to the Dirac equation for both the  $\psi$  and  $\bar{\psi}$ :

$$i\gamma^\mu \partial_\mu \psi - m\psi = 0, \quad (2.14a)$$

$$i\partial_\mu \bar{\psi} \gamma^\mu - m\bar{\psi} = 0. \quad (2.14b)$$

The Proca Lagrangian

$$\mathcal{L}_{\text{Proca}} = -\frac{1}{4} F^{\mu\nu} F_{\mu\nu} + \frac{1}{2} m^2 A^\nu A_\nu, \quad (2.15)$$

with

$$F^{\mu\nu} = \partial^\mu A^\nu - \partial^\nu A^\mu, \quad (2.16)$$

leads to the equation of motion for a massive vector field:

$$\partial_\mu F^{\mu\nu} + m^2 A^\nu = 0. \quad (2.17)$$

Note that if we take  $m = 0$  and interpret  $A^\mu = (\phi, \mathbf{A})$  as the electromagnetic four-vector potential, that the equations (2.17) are exactly the Maxwell equations in a vacuum without sources.

## 2.2 Symmetries

Symmetries are in physics a very important tool. An important theorem that deals with symmetries is Noether's theorem, which states that for each global symmetry of the Lagrangian there is a conserved current and a conserved charge involved. An example of such a Noether current is the current of electric charges in Quantum Electrodynamics (QED) which is a direct consequence of a symmetry in the QED Lagrangian,

$$\mathcal{L}_{\text{QED}} = \bar{\psi} (i\gamma^\mu \partial_\mu - m) \psi - \frac{1}{4} F^{\mu\nu} F_{\mu\nu} - q\bar{\psi}\gamma^\mu \psi A_\mu. \quad (2.18)$$

### Local U(1) symmetries: QED

As one can easily see, the Dirac Lagrangian (2.13) is invariant under the global U(1) transformation

$$\psi(x) \rightarrow \psi'(x) = e^{iq\lambda} \psi(x), \quad (2.19)$$

because then  $\bar{\psi} \rightarrow e^{-iq\lambda} \bar{\psi}$  and thus

$$\mathcal{L}_{\text{Dirac}} \rightarrow ie^{-iq\lambda} \bar{\psi} \gamma^\mu \partial_\mu e^{iq\lambda} \psi - me^{-iq\lambda} \bar{\psi} e^{iq\lambda} \psi = i\bar{\psi} \gamma^\mu \partial_\mu \psi - m\bar{\psi} \psi = \mathcal{L}_{\text{Dirac}}. \quad (2.20)$$

An interesting thing happens if we demand that this Lagrangian is not just globally invariant, but also locally invariant to the U(1) transformation:

$$\psi(x) \rightarrow \psi'(x) = e^{iq\lambda(x)} \psi(x). \quad (2.21)$$

In order to do this, we must replace the ordinary derivative  $\partial_\mu$  with the covariant derivative  $D_\mu$ ,

$$D_\mu = \partial_\mu + iqA_\mu, \quad (2.22)$$

where  $A_\mu$  is the gauge field which transforms as

$$A_\mu(x) \rightarrow A_\mu(x) - \partial_\mu \lambda(x). \quad (2.23)$$

A local transformation of the Lagrangian

$$\mathcal{L} = i\bar{\psi} \gamma^\mu D_\mu \psi - m\bar{\psi} \psi = i\bar{\psi} \gamma^\mu \partial_\mu \psi - q\bar{\psi} \gamma^\mu A_\mu \psi - m\bar{\psi} \psi, \quad (2.24)$$

now results in

$$\begin{aligned} \mathcal{L}' &= ie^{-iq\lambda} \bar{\psi} \gamma^\mu \partial_\mu e^{iq\lambda} \psi - qe^{-iq\lambda} \bar{\psi} \gamma^\mu (A_\mu - (\partial_\mu \lambda)) e^{iq\lambda} \psi - me^{-iq\lambda} \bar{\psi} e^{iq\lambda} \psi \\ &= ie^{-iq\lambda} \bar{\psi} \gamma^\mu e^{iq\lambda} (\partial_\mu \psi) + ie^{-iq\lambda} \bar{\psi} \gamma^\mu (\partial_\mu e^{iq\lambda}) \psi \\ &\quad - qe^{-iq\lambda} \bar{\psi} \gamma^\mu e^{iq\lambda} A_\mu \psi + qe^{-iq\lambda} \bar{\psi} \gamma^\mu e^{iq\lambda} (\partial_\mu \lambda) \psi - m\bar{\psi} \psi \\ &= i\bar{\psi} \gamma^\mu (\partial_\mu \psi) - qe^{-iq\lambda} \bar{\psi} \gamma^\mu e^{iq\lambda} (\partial_\mu \lambda) \psi \\ &\quad - q\bar{\psi} \gamma^\mu A_\mu \psi + qe^{-iq\lambda} \bar{\psi} \gamma^\mu e^{iq\lambda} (\partial_\mu \lambda) \psi - m\bar{\psi} \psi \\ &= i\bar{\psi} \gamma^\mu (\partial_\mu \psi) - q\bar{\psi} \gamma^\mu A_\mu \psi - m\bar{\psi} \psi = \mathcal{L}. \end{aligned} \quad (2.25)$$

It is impossible to have a local gauge invariance without adding a gauge field to the Lagrangian. If we add a vector field to the Lagrangian, then we must also add the Proca Lagrangian (2.17) for  $A_\mu$ . The kinetic term,  $-\frac{1}{4} F^{\mu\nu} F_{\mu\nu}$ , is invariant under the local U(1). This is not so strange, because  $iqF_{\mu\nu} = [D_\mu, D_\nu]$ , as one can see with

$$\begin{aligned} [D_\mu, D_\nu] \psi &= [\partial_\mu, \partial_\nu] \psi + iq([\partial_\mu, A_\nu] - [\partial_\nu, A_\mu]) \psi - e^2 [A_\mu, A_\nu] \psi \\ &= (\partial_\mu A_\nu - \partial_\nu A_\mu) \psi \\ &= iqF_{\mu\nu} \psi. \end{aligned} \quad (2.26)$$

The mass term  $\frac{1}{2} m^2 A^\nu A_\nu$  however, is not locally invariant. Therefore the gauge boson must be massless. The total Lagrangian is then

$$\begin{aligned} \mathcal{L} &= \bar{\psi} (i\gamma^\mu D_\mu - m) \psi - \frac{1}{4} F^{\mu\nu} F_{\mu\nu} \\ &= \bar{\psi} (i\gamma^\mu \partial_\mu - m) \psi - \frac{1}{4} F^{\mu\nu} F_{\mu\nu} - q\bar{\psi} \gamma^\mu \psi A_\mu. \end{aligned} \quad (2.27)$$

But this is exactly the Lagrangian of QED! The local gauge invariance dictates that photon must be massless and that the interaction between two electrons and a photon is given by

$$\mathcal{L}_{\text{int}} = -q\bar{\psi}\gamma^\mu\psi A_\mu \equiv j_\mu A^\mu, \quad (2.28)$$

where  $j_\mu \equiv -q\bar{\psi}\gamma^\mu\psi$  is the current density. With the Euler-Lagrange equations we find for the photon field

$$\partial_\mu F^{\mu\nu} = j^\nu, \quad (2.29)$$

which are the Maxwell equations for an electromagnetic field produced by an electric current  $j^\nu$ . From this equation follows that the current must be conserved:

$$\partial_\nu j^\nu = 0. \quad (2.30)$$

All this comes from the Dirac Lagrangian and the demand that we have a local U(1) symmetry!

But why a local symmetry? What does it mean? A global transformation is performing a transformation at all points in space-time at once. A local transformation on the other hand means that you do a different transformation at each point. The most basic local transformation is to execute the transformation only at one point<sup>1</sup>. This cannot be done without consequences: the transformation of the electron field  $\psi$  leads to the change of the photon field  $A_\mu$ . A heuristic point of view is to compare this with a space full of electric charges. Moving them all does not change the fields (if we move along). However, moving only a single charge creates an electromagnetic field.

In any case, it is a remarkable fact that by demanding the symmetry to be local, that the Dirac Lagrangian demands the existence of the photon field with the same interactions as found in nature.

## Local SU(2) symmetries: isospin

The concept of using a gauge symmetry to implement interactions into a theory can be extended to other symmetry groups. However, if we want to keep  $\bar{\psi}\psi$  invariant then the transformation  $\psi \rightarrow U\psi$  must be unitary,

$$\bar{\psi}\psi \rightarrow \bar{\psi}U^\dagger U\psi = \bar{\psi}\psi \quad \Rightarrow \quad U^\dagger = U^{-1}. \quad (2.31)$$

Therefore the gauge groups are almost always SU( $N$ ) or U(1). As a specific example we introduce here isospin theory, which uses SU(2) as the gauge group.

The idea of isospin was first introduced by Heisenberg<sup>2</sup>. He noticed that the neutron is almost identical to the proton, apart from its electric charge. They almost have the same mass and the strong force couples just as strong to the proton as it does for the neutron. It was believed that the strong force is mediated by pions, three light mesons that strongly interact with the proton and the neutron. According to Heisenberg the proton and neutron can be imagined as two different states of the same particle called the nucleon. The pions in this theory are the gauge bosons, similar to the photon in QED.

The nucleon is written as an isospin doublet,

$$\psi = \begin{pmatrix} p \\ n \end{pmatrix}, \quad (2.32)$$

with isospin  $I = \frac{1}{2}$ . The state of the nucleon transforms as

$$\psi \rightarrow \psi' = U \begin{pmatrix} p \\ n \end{pmatrix} \quad (2.33)$$

where  $U$  is a unitary  $2 \times 2$  matrix and therefore a U(2) transformation. This however is a reducible group: it can be reduced to SU(2) $\times$ U(1). To see this more clearly, we write the matrix  $U$  in terms of four real parameters:

$$U = e^{iH}, \quad (2.34)$$

where  $H = H^\dagger$  is an Hermitian  $2 \times 2$  matrix,

$$H = Y \mathbf{1}_{2 \times 2} + I_a \frac{\tau_a}{2}. \quad (2.35)$$

---

<sup>1</sup>Any other local transformation can be considered as the result of performing several different single-point transformations at once, one at each point in space-time.

<sup>2</sup>Even though the idea of a SU(2) isospin was proposed by Heisenberg, the idea of using a *local* SU(2) was invented by Yang and Mills. Perhaps a better name for the theory described here is “Yang-Mills theory with isospin”.

The  $\tau_a$  are the three Pauli matrices, the vector  $I_a = (I_1, I_2, I_3)$  is the isospin vector, and  $Y$  is called the hypercharge because it is very similar to the electric charge of the U(1) group in QED. The U(2) group is clearly reducible: the SU(2) part of the transformation mixes the different isospin states, while the U(1) part only changes the phase of each state but does not mix them.

The proton is the eigenstate with eigenvalue  $I_3 = +\frac{1}{2}$  and the neutron the eigenstate with  $I_3 = -\frac{1}{2}$ . The relation between  $I_a$ ,  $Y$  and the electric charge  $Q$  is given by the Gell-Mann-Nishijima formula:

$$Q = I_3 + \frac{1}{2}Y. \quad (2.36)$$

So, for the nucleon we must have  $Y = 1$ . This formula also holds for other particles, like the pions ( $I = 1$ ):

$$\pi^a = \begin{pmatrix} \pi^+ \\ \pi^0 \\ \pi^- \end{pmatrix}. \quad (2.37)$$

The quantum numbers for the  $\pi^+, \pi^0, \pi^-$  are  $I_3 = 1, 0, -1$  and  $Y = 0$ . The more interesting part of the theory lies in the isospin. Therefore in the rest of the section we ignore the hypercharge and only work with isospin.

The strong force sees no difference between the isospin states, and hence the Lagrangian describing the strong force should be isospin invariant. If we imply the symmetry to be a *local* SU(2) isospin invariance, the Lagrangian becomes

$$\mathcal{L} = \bar{\psi} (i\gamma^\mu D_\mu - m) \psi - \frac{1}{4} F^{\mu\nu} F_{\mu\nu}^a, \quad (2.38)$$

where  $F_{\mu\nu}^a$  can be written as [2]

$$-igF_{\mu\nu}^a \frac{\tau^a}{2} = [D_\mu, D_\nu], \quad (2.39)$$

with the covariant derivative

$$D_\mu = \partial_\mu - igA_\mu^a \frac{\tau^a}{2}. \quad (2.40)$$

Putting (2.39) and (2.40) together we find an explicit expression for  $F_{\mu\nu}^a$ :

$$F_{\mu\nu}^a = \partial_\mu A_\nu^a - \partial_\nu A_\mu^a + g\epsilon^{abc} A_\mu^b A_\nu^c. \quad (2.41)$$

The antisymmetric tensor  $\epsilon^{abc}$  are the structure constants of the SU(2) group.

The expression for  $D_\mu$  is not as arbitrary as it seems. Because the group SU(2) has three generators (meaning that the transformation is parameterized by three real numbers) there are also three real gauge fields, represented by the pions:

$$A_\mu^a = \begin{pmatrix} A_\mu^1 \\ A_\mu^2 \\ A_\mu^3 \end{pmatrix} = \begin{pmatrix} \pi^+ \\ \pi^0 \\ \pi^- \end{pmatrix}. \quad (2.42)$$

Because also the pions carry isospin, the triplet must be able to rotate under SU(2):

$$A_\mu^a \rightarrow U A_\mu^a = e^{iH} A_\mu^a. \quad (2.43)$$

However, in this case  $H$  is a Hermitian  $3 \times 3$  matrix,

$$H = I^a T^a, \quad (2.44)$$

with  $T^a$  the 3-dimensional SU(2) generators. We are searching for a  $D_\mu$  that gives us something similar to (2.28), for example

$$\mathcal{L}_{\text{int}} = j_\mu A^\mu = g\bar{\psi}\gamma^\mu A_\mu^a \psi. \quad (2.45)$$

But we cannot have an interaction term like that, because the vectors are of different sizes and the Lagrangian has to be a singlet under any transformation.

To solve this, we need to write  $A_\mu^a$  in a different representation of SU(2) that has the same dimension as the nucleon doublet. That representation is the adjoint representation:

$$A_\mu \equiv A_\mu^a \frac{\tau^a}{2}. \quad (2.46)$$

One could call  $A_\mu$  a  $2 \times 2$  matrix field, but it is actually just a  $SU(2)$  triplet in the adjoint representation. The  $A_\mu$  we can use in the same way as we did in (2.28), and so we find

$$D_\mu = \partial_\mu - igA_\mu = \partial_\mu - igA_\mu^a \frac{\tau^a}{2}, \quad (2.47)$$

as stated in (2.40). Evidently, we need the generators of the gauge group to couple the gauge field with fermions.

There are several problems with this theory as stated here. The pions are massless, but in reality they have a mass of  $\sim 140$  GeV. Also the pions have the wrong spin. In this theory they are vector bosons, while in reality they are (pseudo)scalar bosons with spin 0. As a fundamental theory this theory failed. Later it became clear that the pions and nucleons were actually composed of quarks, transforming under a color  $SU(3)$ . This is the theory of QCD, where the strong force is mediated by gauge bosons called gluons. Because  $SU(3)$  is parametrized with 8 real values, there are 8 real fields and hence 8 gluons.

Even though the isospin theory never gave a perfect description of the strong force, it is a very useful tool for calculating e.g. the branch ratios of nucleon-pion scattering [3]. Also the idea of using a gauged  $SU(2)$  symmetry became a foundation stone for further theories, in particular electroweak theory.

## 2.3 Feynman diagrams

To actually do calculations with the Lagrangians, we need to find a set of rules to convert the Lagrangian to something useful: the invariant amplitude  $\mathcal{M}$ . With this it is then possible to calculate cross sections and decay widths, things that can actually be measured in an experiment.

In this section we give a short introduction to quantum field theory. A more elaborate description of the theory can be found in several textbooks, e.g. [4] and [5].

### Feynman's extension of Hamilton's principle

By inventing the path integral formalism, Feynman extended Hamilton's principle for quantum mechanics. Because of the particle-wave duality we can no longer talk about a particle that follows a certain path, instead, it is more as if the particle follows all possible path at once. The principle is nicely illustrated by a quote from F.J. Dyson [6]:

Thirty-one years ago, Dick Feynman told me about his 'sum over histories' version of quantum mechanics. 'The electron does anything it likes', he said. 'It goes in any direction at any speed, forward or backwards in time, however it likes, and then you add up the amplitudes and it gives you the wave-function.' I said to him, 'You're crazy'. But he wasn't.

### The generating functional

In quantum mechanics the probability for a particle to go from an initial state  $|\psi_i\rangle$  to a final state  $|\psi_f\rangle$  is given by the absolute square of the amplitude,

$$P_{i \rightarrow f} = |\langle \psi_f, t_f | \psi_i, t_i \rangle|^2 = \left| \langle \psi_f | e^{-iH(t_f - t_i)} | \psi_i \rangle \right|^2. \quad (2.48)$$

where  $H(t)$  is the Hamilton operator<sup>3</sup>. By cutting the time interval  $[t_i, t_f]$  into infinitesimally small intervals, the amplitude turns into a functional integral:

$$\langle \psi_f, t_f | \psi_i, t_i \rangle = \int \mathcal{D}q \frac{\mathcal{D}p}{2\pi} \exp \left( i \int_{t_i}^{t_f} d\tau [p\dot{q} - H(p, q)] \right) = \int \mathcal{D}q \exp \left( i \int_{t_i}^{t_f} d\tau L(q, \dot{q}) \right), \quad (2.49)$$

where  $L(t)$  is the Lagrangian.

---

<sup>3</sup>Note that we are working in the *Heisenberg picture*, the states  $|\psi\rangle$  are time-independent and the operators are time-dependent. The notation  $|\psi, t\rangle$  should be interpreted as "the state  $|\psi\rangle$  as measured by operators at time  $t$ ".



In the same way the expectation value of any operator  $Q(t)$  can also be turned into a path integral. If  $q(t)$  is the eigenvalue given by  $Q(t)|\psi, t'\rangle = q(t)|\psi, t'\rangle$  then

$$\langle \psi_f, t_f | Q(t) | \psi_i, t_i \rangle = \int \mathcal{D}q \, q(t) \exp \left( i \int_{t_i}^{t_f} d\tau L(q, \dot{q}) \right). \quad (2.50)$$

In general, for any product of operators  $Q(t_1)Q(t_2)\cdots Q(t_n)$  we have

$$\langle \psi_f, t_f | \mathcal{T}Q(t_1)Q(t_2)\cdots Q(t_n) | \psi_i, t_i \rangle = \int \mathcal{D}q \, q(t'_n)\cdots q(t'_1) \exp \left( i \int_{t_i}^{t_f} d\tau L(q, \dot{q}) \right), \quad (2.51)$$

where  $\mathcal{T}$  is the time ordering operator, defined as

$$\mathcal{T}Q(t_1)Q(t_2)\cdots Q(t_n) \equiv Q(t'_n)Q(t'_{n-1})\cdots Q(t'_1) \quad (2.52)$$

for  $t'_1 \leq t'_2 \leq \dots \leq t'_n$ . In other words,  $\mathcal{T}$  orders all the operators chronologically.

Sofar we have only considered the Lagrangian in the ground state, the vacuum. But in a real experiment there is more than just the vacuum. At time  $t_i$  particles are created, they have some interactions with each other, and finally at  $t_f$  they are absorbed again by a detector for instance. This situation can be described by adding a source term  $J(t)$  to the Lagrangian,

$$\langle \psi_f, t_f | \psi_i, t_i \rangle^J = \int \mathcal{D}q \exp \left( i \int_{t_i}^{t_f} d\tau [L(q, \dot{q}) + Jq] \right), \quad (2.53)$$

with  $J(t) = 0$  for  $t < t_i$  and  $t > t_f$ . In this way we make sure that before and after the experiment there is nothing but the ground-state  $|0\rangle$ .

The generating functional  $Z[J]$  is defined as the amplitude  $\langle 0_f | 0_i \rangle^J$  of the transition from ground state  $|0_i\rangle$  at time  $-T$  to ground state  $|0_f\rangle$  at  $T$ , in the limit  $T \rightarrow \infty (1 - i\epsilon)$ ,<sup>4</sup>

$$Z[J] \equiv \int \mathcal{D}q \exp \left( i \int d\tau [L(q, \dot{q}) + Jq] \right). \quad (2.54)$$

Note that

$$\begin{aligned} \left. \frac{\delta Z[J]}{\delta J(t)} \right|_{J=0} &= \left. \frac{\delta}{\delta J(t)} \int \mathcal{D}q \exp \left( i \int d\tau [L(q, \dot{q}) + Jq] \right) \right|_{J=0} \\ &= \left. i \int \mathcal{D}q \, q(t) \exp \left( i \int d\tau [L(q, \dot{q}) + Jq] \right) \right|_{J=0} \\ &= i \int \mathcal{D}q \, q(t) \exp \left( i \int d\tau L(q, \dot{q}) \right) \\ &= i \langle 0 | Q(t) | 0 \rangle, \end{aligned} \quad (2.55)$$

and in general

$$\begin{aligned} \left. \frac{\delta^n Z[J]}{\delta J(t_1)\cdots\delta J(t_n)} \right|_{J=0} &= (i)^n \int \mathcal{D}q \, q(t_1)\cdots q(t_n) \exp \left( i \int d\tau L(q, \dot{q}) \right) \\ &= (i)^n \langle 0 | \mathcal{T}Q(t_1)\cdots Q(t_n) | 0 \rangle. \end{aligned} \quad (2.56)$$

This means that with  $Z[J]$  we can find any amplitude for any process described by the  $\mathcal{L}$  at hand.

This also works with quantum fields. For example, the amplitude for the process with one scalar particle in the initial state and one scalar particle in the final state is given by

$$\langle 0 | \phi(y) \phi(x) | 0 \rangle = (-i)^2 \left. \frac{\delta^2 Z[J]}{\delta J(y) \delta J(x)} \right|_{J=0}. \quad (2.57)$$

Here the quantum fields  $\phi$  contain creation and annihilation operators. The creation operator in  $\phi(x)$  creates at  $x$  a particle from the vacuum and the annihilation operator in  $\phi(y)$  destroys that particle at  $y$ , leaving the vacuum behind. Apparently we can use the functional  $Z[J]$  just like a generating function, hence the name.

<sup>4</sup>The small imaginary contribution  $i\epsilon$  (the Wick rotation) is needed to guarantee convergence of the integral.

## Feynman diagrams

In the case of a relativistic scalar field  $\phi$  the generating functional is given by

$$Z[J] \equiv \int \mathcal{D}\phi \exp\left(i \int d^4x [\mathcal{L}(\phi, \partial_\mu \phi) + J\phi]\right). \quad (2.58)$$

The  $n$ -point Green's function is defined by

$$G^{(n)}(x_1, \dots, x_n) \equiv \langle 0 | \mathcal{T} \phi(x_1) \cdots \phi(x_n) | 0 \rangle = (-i)^n \frac{\delta^n Z[J]}{\delta J(x_1) \cdots \delta J(x_n)} \Big|_{J=0}. \quad (2.59)$$

It is also possible to write  $G^{(n)}$  as a diagram:

$$G^{(n)}(x_1, \dots, x_n) = \begin{array}{c} x_1 \\ \circ \\ \diagdown \\ \circ \\ x_2 \\ \diagup \\ \circ \\ x_3 \end{array} \text{---} \text{---} \text{---} \begin{array}{c} \circ \\ x_4 \\ \diagup \\ \circ \\ \diagdown \\ \circ \\ x_n \end{array} . \quad (2.60)$$

This diagram can be regarded as a process where a number particles are created from the vacuum, interact (inside the bubble), and then all are annihilated again. Note that the number of ingoing particles does not have to be equal to the number of outgoing particles.

The simplest example of such a diagram is for the process where one particle is created at  $x_1$  and is then annihilated at  $x_2$ :

$$G^{(2)}(x_1, x_2) = \langle 0 | \phi(x_2) \phi(x_1) | 0 \rangle = \begin{array}{c} \circ \\ x_1 \end{array} \text{---} \text{---} \begin{array}{c} \circ \\ x_2 \end{array} \equiv i\Delta_F(x_2 - x_1). \quad (2.61)$$

The function  $\Delta_F(x)$  is the *propagator* of the field. It is easier to work with the Fourier transform  $\tilde{\Delta}_F(p)$ , than with  $\Delta_F(x)$  itself. The propagator in momentum space is given by

$$i\tilde{\Delta}_F(p) = \begin{array}{c} \circ \\ p \rightarrow \end{array} \text{---} \text{---} \begin{array}{c} \circ \end{array} = \frac{i}{p^2 - m^2 + i\epsilon}. \quad (2.62)$$

For higher values of  $n$  the diagrams become more and more complicated. For example, if there is an interaction term in the Lagrangian like

$$\mathcal{L}_{\text{int}} = -\frac{\lambda}{4!} \phi^4, \quad (2.63)$$

there will be diagrams with points where four lines meet. These points are called *vertices*. For the interaction term of (2.63) we have

$$\begin{array}{c} \diagup \\ \bullet \\ \diagdown \end{array} \text{---} \text{---} \begin{array}{c} \diagdown \\ \bullet \\ \diagup \end{array} = -i\lambda. \quad (2.64)$$

If we had used a different  $\mathcal{L}_{\text{int}}$  as an example, we would have had a different vertex with a different expression.

There are all kinds of diagrams possible. Some diagrams have all lines connected, and some do not. As it happens, the sum of all diagrams can be written as the sum of all connected diagrams times some factor that represents vacuum to vacuum transitions. In most cases this factor disappears during the calculation and is therefore ignored. Also, to calculate the amplitude of a process in which we start with some set of particles and end with some other set, we are not interested in the part of particle creation and annihilation. Therefore the only diagrams that are used, are the diagrams without the legs. These are called *amputated diagrams*. We are now left with diagrams that are made only out of propagators, vertices and external lines. An example of such a Feynman diagram is

$$\begin{array}{c} \diagdown \\ \bullet \\ \diagup \end{array} \text{---} \text{---} \begin{array}{c} \bullet \\ \diagdown \\ \diagup \end{array} \quad (2.65)$$

The *external lines* represent the initial and final particles in the diagram. In the case of real scalar fields all external lines are mathematically expressed in momentum space with

$$\begin{array}{c} \diagdown \\ \bullet \\ \diagup \end{array} \text{---} \text{---} = 1. \quad (2.66)$$

For the fermions however, the particle is not described by a simple scalar, but by a 2-component spinor  $u$  with spin  $s = \pm\frac{1}{2}$ . The expression for the external fermion line with momentum  $p$  and spin  $s$  is therefore

$$\begin{array}{c} \nearrow \\ \leftarrow \\ \leftarrow p \end{array} = u(s, p). \quad (2.67)$$

This represents a fermion going *into* the diagram, an initial fermion. A final state fermion is represented by the adjoint spinor:

$$\begin{array}{c} \nearrow \\ \rightarrow \\ p \rightarrow \end{array} = \bar{u}(s, p). \quad (2.68)$$

For the real scalar boson there is no such difference, because  $\phi^\dagger = \phi$ . Finally, the external lines for the antifermions with spin  $s$  and momentum  $p$  are given by

$$\begin{array}{c} \nearrow \\ \rightarrow \\ \leftarrow p \end{array} = \bar{v}(s, p), \quad (2.69a)$$

$$\begin{array}{c} \nearrow \\ \leftarrow \\ p \rightarrow \end{array} = v(s, p). \quad (2.69b)$$

The  $v$  and  $\bar{v}$  are the same type of spinors as the  $u$  and  $\bar{u}$ ; we use a different notation only to make clear that these are antifermions.

In momentum space the vector bosons are described with the polarization vector  $\epsilon^\mu(\lambda, p)$ . The spin  $\lambda = -1, 0, +1$  is in this context called the helicity. The helicity of a particle is defined as the projection of a spin vector  $\mathbf{s}$  in the direction of its momentum vector,

$$\lambda \equiv \frac{\mathbf{s} \cdot \mathbf{p}}{|\mathbf{s} \cdot \mathbf{p}|}. \quad (2.70)$$

For a vector boson of mass  $M$  and four-momentum  $p = (E, 0, 0, |\mathbf{p}|)$  the polarization vectors become [7]

$$\epsilon^\mu(\pm 1, p) = (0, \mp 1, i, 0) / \sqrt{2}, \quad (2.71a)$$

$$\epsilon^\mu(0, p) = (|\mathbf{p}|, 0, 0, E) / M. \quad (2.71b)$$

These equations are clearly not valid for  $M = 0$ . For massless vector bosons, like e.g. the photon, there is no polarization state with  $\lambda = 0$  and therefore it has only transverse polarization states. The constraint  $m = 0$  means that the photon has one degree of freedom less.

With the allowed values for  $\lambda$  in mind, both massive and massless vector bosons have the same expressions for the external lines:

$$\begin{array}{c} \nearrow \\ \text{~~~~~} \\ \leftarrow p \end{array} = \epsilon_\mu(\lambda, p), \quad (2.72a)$$

$$\begin{array}{c} \nearrow \\ \text{~~~~~} \\ \rightarrow p \end{array} = \epsilon_\mu^*(\lambda, p). \quad (2.72b)$$

These rules to convert Feynman diagrams into mathematical expressions are called Feynman rules. The Feynman rules for the propagators, vertices, and external lines are summarized in Table 2.1. Apart from the rules stated in this section, there are also rules concerning diagrams containing loops. Those rules have been omitted here, because in this thesis all calculations are done at leading order (there are no calculations with loop diagrams).

## The invariant amplitude

To describe all possible scattering processes, we define the  $S$ -matrix. This matrix transforms any initial state  $|\psi_i\rangle$  into a final state  $|\psi_f\rangle$ ,

$$|\psi_f\rangle = S |\psi_i\rangle \quad (2.73)$$

Each element of the  $S$ -matrix can be written as

$$S_{fi} = \delta_{fi} + (2\pi)^4 \delta^4(\sum p_i - \sum p_f) \cdot i\mathcal{M}_{i \rightarrow f} \quad (2.74)$$

where  $\mathcal{M}_{i \rightarrow f}$  is the invariant amplitude for  $|\psi_i\rangle \rightarrow |\psi_f\rangle$ . The Kronecker delta  $\delta_{fi}$  describes the process  $|\psi_f\rangle = |\psi_i\rangle$  when no interactions occur. Evidently, we are more interested in the term with  $\mathcal{M}$ .

By using the Feynman diagrams it is easy to calculate the invariant amplitude. To find  $\mathcal{M}$  we first translate all propagators, vertices, and external points into their mathematical equivalent. Connections in the diagram translate to multiplication in the equation for  $\mathcal{M}$ . For example, a Feynman diagram like



$$(2.75)$$

translates into<sup>5</sup>

$$-i\mathcal{M} = [\bar{v}_{e^+} (-ig_e \gamma^\mu) u_{e^-}] \frac{-ig_{\mu\nu}}{q^2} [\bar{u}_{\mu^-} (-ig_e \gamma^\nu) v_{\mu^+}]. \quad (2.76)$$

In the center-of-mass frame, the differential cross section for the process  $A + B \rightarrow C + D$  is given by

$$\frac{d\sigma}{d\Omega} = \frac{S |\mathcal{M}|^2 |\mathbf{p}_A|}{64\pi^2 s |\mathbf{p}_C|}. \quad (2.77)$$

In this equation  $s$  is the center-of-mass energy  $s = (E_A + E_B)^2$ , the  $d\Omega$  is given by  $d\Omega = \sin\theta d\theta d\phi$ , and  $S$  is a product of statistical factors:  $1/j!$  for each group of  $j$  identical particles in the final state. Coincidentally, none of the processes discussed in this thesis have identical particles in the final state, and therefore we shall simply leave  $S$  out of the equation.

For energies that are high enough we can neglect the masses in  $e^- e^+ \rightarrow \mu^- \mu^+$ . Substituting (2.76) into (2.77) leads in that case to

$$\frac{d\sigma}{d\Omega} = \frac{\alpha^2}{4s} (1 + \cos^2\theta), \quad (2.78)$$

with  $\alpha = g_e^2/4\pi = 1/137$ . In Chapter 4 we shall show in more detail how such a calculation is done.

The invariant amplitude can also be used to calculate the lifetime of a particle. The lifetime  $\tau$  follows from  $\tau = 1/\Gamma$ , where  $\Gamma$  is the decay rate or the *width*. If particle  $A$  decays into two particles  $B$  and  $C$ , the width is

$$\Gamma = \frac{S |\mathbf{p}_C|}{8\pi m_A^2} |\mathcal{M}|^2. \quad (2.79)$$

If the decay products are both massless,  $|\mathbf{p}_B| = |\mathbf{p}_C| = m_A/2$ , and this equation simplifies to

$$\Gamma = \frac{S}{16\pi m_A} |\mathcal{M}|^2. \quad (2.80)$$

---

<sup>5</sup>Most often we write the spinor  $u_A(s_A, p_A)$  simply as  $u_A$ . When there is a summation over the spin, we must remember that  $u_A$  always carries spin  $-1$  or  $+1$ . Of course we do the same thing for  $e^\mu$ .

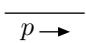
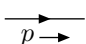

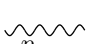
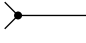
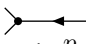
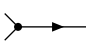
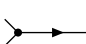

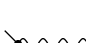
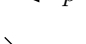

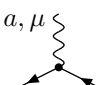
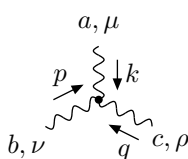
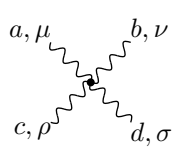
Scalar boson propagator:		$= \frac{i}{p^2 - m^2 + i\epsilon}$
Fermion propagator:		$= \frac{i(\not{p} + m)}{p^2 - m^2 + i\epsilon}$
Vector boson propagator:		$= \frac{-i}{p^2 - m^2 + i\epsilon} \left( g_{\mu\nu} - \frac{p_\mu p_\nu}{p^2 - \xi m^2} (1 - \xi) \right)$
Photon propagator:		$= \frac{-i g_{\mu\nu}}{p^2 + i\epsilon}$
External scalar line:		$= 1$
External fermion line:		$= u^s(p) \quad (\text{initial})$
		$= \bar{u}^s(p) \quad (\text{final})$
External antifermion line:		$= \bar{v}^s(p) \quad (\text{initial})$
		$= v^s(p) \quad (\text{final})$
External photon line:		$= \epsilon_\mu(p) \quad (\text{initial})$
		$= \epsilon_\mu^*(p) \quad (\text{final})$
QED vertex:		$= iQe\gamma^\mu \quad (Q = -1 \text{ for an electron})$
Fermion vertex:		$= ig\gamma^\mu T^a \quad (T^a \text{ is the generator of the group})$
3-boson vertex:		$= gf^{abc} [g^{\mu\nu} (k - p)^\rho + g^{\nu\rho} (p - q)^\mu + g^{\rho\mu} (q - k)^\nu]$
4-boson vertex:		$= -ig^2 [f^{abe} f^{cde} (g^{\mu\rho} g^{\nu\sigma} - g^{\mu\sigma} g^{\nu\rho}) + f^{ace} f^{bde} (g^{\mu\nu} g^{\rho\sigma} - g^{\mu\sigma} g^{\nu\rho}) + f^{ade} f^{bce} (g^{\mu\nu} g^{\rho\sigma} - g^{\mu\rho} g^{\nu\sigma})]$

Table 2.1: The propagators, vertices and external lines in momentum space for any  $SU(N)$  gauge theory. The rules for QED and the photon have been included also. The  $\epsilon$  in the propagators is a small number which can be ignored in most cases. Near the pole of the propagator however, one must replace the  $\epsilon$  by the mass of the particle times its decay width (see e.g. Chapter 6). The gauge  $\xi$  has no influence on calculations [8]. For the gauge  $\xi = 0$  the Goldstone bosons disappear from the theory. Taken from [9].

# Chapter 3

## The Standard Model

The Standard Model of particle physics was developed between 1970 and 1973 and has been one of the most successful theories in physics. Similar to the isospin theory discussed in the previous chapter, the Standard Model is based on the idea of having a Lagrangian that is symmetric under certain local symmetries. These symmetries then determine all of the interactions in the theory.

The model actually consists of two parts, describing two different forces in nature. Quantum chromodynamics (QCD) is the theory that describes the strong nuclear force. Electroweak theory describes the weak interaction unified with the electromagnetic force.

In Section 3.1 we highlight several striking discoveries in high energy experiments that provide for a basis of the electroweak model. After determining which structure the Standard Model should have, we start building the Lagrangian for electroweak theory in Section 3.2. The resulting theory only contains massless particles, and in order to fix this we introduce in Section 3.3 the principle of symmetry breaking. In the sections after that we examine the results of this principle for the gauge bosons (Section 3.4) and for the fermions (Section 3.5). Finally in Section 3.6 we introduce QCD. In Section 3.7 we give a quick summary of the whole Standard Model.

### 3.1 Experimental basis for electroweak theory

The electroweak theory is based mostly on three crucial clues from experiments (the terms left-handed and right-handed will be introduced shortly):

1. Only left-handed fermions feel the (charged-current) weak interaction and those that do, only interact in pairs of two. For leptons these doublets are

$$\begin{pmatrix} \nu_{eL} \\ e_L \end{pmatrix}, \quad \begin{pmatrix} \nu_{\mu L} \\ \mu_L \end{pmatrix}, \quad \begin{pmatrix} \nu_{\tau L} \\ \tau_L \end{pmatrix}, \quad (3.1)$$

and for the quarks

$$\begin{pmatrix} u_L \\ d'_L \end{pmatrix}, \quad \begin{pmatrix} c_L \\ s'_L \end{pmatrix}, \quad \begin{pmatrix} t_L \\ b'_L \end{pmatrix}. \quad (3.2)$$

The quarks  $d'$ ,  $s'$  and  $b'$  are linear combinations of the mass eigenstates  $d$ ,  $s$  and  $b$ :

$$\begin{pmatrix} d' \\ s' \\ b' \end{pmatrix} = \begin{pmatrix} V_{ud} & V_{us} & V_{ub} \\ V_{cd} & V_{cs} & V_{cb} \\ V_{td} & V_{ts} & V_{tb} \end{pmatrix} \begin{pmatrix} d \\ s \\ b \end{pmatrix}. \quad (3.3)$$

This matrix  $V_{qq'}$  is the CKM matrix.

2. All (charged-current) weak interactions are equally strong, the weak force treats e.g. the electron doublet exactly the same as all the other doublets.
3. Neutrinos are massless<sup>1</sup> and therefore travel at the speed of light. This also means that they have a fixed helicity, and hence there are no interaction in the theory that transform a left-handed neutrino into a right-handed one, or vice versa.

---

<sup>1</sup>Recent experiments have indicated that neutrinos actually do carry a tiny mass, but this was unknown during the time that the Standard Model was developed. In this thesis we choose to simply ignore the existence of neutrino mass.

Because the right-handed neutrino does not feel the weak force, is electrically neutral, and has a fixed helicity, it does not interact with anything and is therefore excluded from the model. In other words, we assume that the right-handed neutrino simply does not exist. The consequence is that there are no right-handed doublets in the theory, but only right-handed singlets:

$$(e_R), \quad (\mu_R), \quad (\tau_R). \quad (3.4)$$

Since the right-handed quarks do not feel the weak force either (a  $u_R$ -quark never transforms into a  $d'_R$ -quark), all of them are also singlets:

$$(u_R), \quad (d'_R), \quad (c_R), \quad (s'_R), \quad (t_R), \quad (b'_R). \quad (3.5)$$

Given these experimental observations the task is to construct a Lagrangian that agrees with these experiments. The doublets are very similar to what we had in isospin theory. Therefore we postulate that also the electroweak Lagrangian has an local  $SU(2) \times U(1)$  symmetry.

## 3.2 Building the Lagrangian

Given the symmetry of the theory, we know how to construct the Lagrangian. There must be a kinetic term for the fermions, a covariant derivative and a kinetic term for the gauge bosons.

### Kinetic term of the fermions

To create a Lagrangian that distinguishes between left-handed and right-handed particles, we need to use the helicity projection operators  $P_L = \frac{1}{2}(1 - \gamma_5)$  and  $P_R = \frac{1}{2}(1 + \gamma_5)$ . These operators have several very interesting properties:

$$P_L + P_R = 1, \quad (3.6a)$$

$$P_L P_R = P_R P_L = 0, \quad (3.6b)$$

$$P_L^2 = P_L, \quad P_R^2 = P_R, \quad (3.6c)$$

$$P_L^\dagger = P_L, \quad P_R^\dagger = P_R, \quad (3.6d)$$

$$P_L \gamma^\mu = \gamma^\mu P_R, \quad (3.6e)$$

$$\gamma^\mu P_L = P_R \gamma^\mu. \quad (3.6f)$$

These identities can be easily found using  $(\gamma_5)^2 = 1$ ,  $\gamma_5^\dagger = \gamma_5$ , and  $\gamma_5 \gamma^\mu = -\gamma^\mu \gamma_5$ . The left-handed electron doublet for example, can be written as

$$L_e = \begin{pmatrix} \nu_{eL} \\ e_L \end{pmatrix} = \begin{pmatrix} P_L \nu_e \\ P_L e \end{pmatrix} = P_L \begin{pmatrix} \nu_e \\ e \end{pmatrix}, \quad (3.7)$$

while the right-handed electron singlet is simply

$$R_e = (e_R) = P_R e. \quad (3.8)$$

For the adjoint left-handed spinor we have

$$\bar{\psi}_L \equiv \overline{P_L \psi} = (P_L \psi)^\dagger \gamma^0 = \psi^\dagger P_L^\dagger \gamma^0 = \psi^\dagger P_L \gamma^0 = \psi^\dagger \gamma^0 P_R = \bar{\psi} P_R, \quad (3.9)$$

and similar,

$$\bar{\psi}_R \equiv \overline{P_R \psi} = \bar{\psi} P_L. \quad (3.10)$$

The adjoints of the electron doublet and singlet are then

$$\bar{L}_e = (\bar{\nu}_{eL} \quad \bar{e}_L) = (\bar{\nu}_e \quad \bar{e}) P_R, \quad (3.11a)$$

$$\bar{R}_e = (\bar{e}_R) = \bar{e} P_L. \quad (3.11b)$$

Using the properties of  $P_L$  and  $P_R$ , the mass term of the electron becomes

$$\begin{aligned} -m_e \bar{e} e &= -m_e \bar{e} (P_L + P_R) e \\ &= -m_e \bar{e} (P_L^2 + P_R^2) e \\ &= -m_e (\bar{e} P_L P_L e + \bar{e} P_R P_R e) \\ &= -m_e (\bar{e}_R e_L + \bar{e}_L e_R). \end{aligned} \quad (3.12)$$

This is a problem. The Lagrangian is by definition a scalar quantity, but  $-m_e \bar{e}_R e_L$  and  $-m_e \bar{e}_L e_R$  are clearly not:

$$-m_e \bar{e}_R e_L = -m_e (\bar{e}_R) \begin{pmatrix} 0 \\ e_L \end{pmatrix}, \quad (3.13a)$$

$$-m_e \bar{e}_L e_R = -m_e \begin{pmatrix} 0 & \bar{e}_L \end{pmatrix} (e_R). \quad (3.13b)$$

Adding these two is not even possible because they have different sizes<sup>2</sup>. Conclusively, by dividing a fermion into a left-handed doublet and right-handed singlet, we have excluded any possibility of adding a mass term to the Lagrangian. For now we shall ignore this problem; the solution for giving the fermions a mass is given later in this chapter.

Fortunately, we are allowed to have a kinetic term for the fermions:

$$\begin{aligned} i\bar{e}\gamma^\mu\partial_\mu e &= i\bar{e}\gamma^\mu\partial_\mu (P_L^2 + P_R^2) e \\ &= i\bar{e}(\gamma^\mu\partial_\mu P_L P_L) e + i\bar{e}(\gamma^\mu\partial_\mu P_R P_R) e \\ &= i\bar{e}(P_R\gamma^\mu\partial_\mu P_L) e + i\bar{e}(P_L\gamma^\mu\partial_\mu P_R) e \\ &= i\bar{e}_L\gamma^\mu\partial_\mu e_L + i\bar{e}_R\gamma^\mu\partial_\mu e_R \\ &= i \begin{pmatrix} 0 & \bar{e}_L \end{pmatrix} \gamma^\mu\partial_\mu \begin{pmatrix} 0 \\ e_L \end{pmatrix} + i(\bar{e}_R)\gamma^\mu\partial_\mu (e_R). \end{aligned} \quad (3.14)$$

In this case the doublet is multiplied with its adjoint, resulting in a singlet which can be included to the Lagrangian. Of course, everything said here for the electron is also true for the other leptons and the quarks. The kinetic terms for all fermions are therefore

$$\mathcal{L}_{\text{kF}} = i\bar{L}_\ell\partial\!/\!L_\ell + i\bar{R}_\ell\partial\!/\!R_\ell + i\bar{L}_q\partial\!/\!L_q + i\bar{R}_q\partial\!/\!R_q + i\bar{R}_{q'}\partial\!/\!R_{q'}, \quad (3.15)$$

where summation over  $\ell = e, \mu, \tau$  and  $q = u, c, t$  and  $q' = d', s', c'$  is implied. Using the operators  $P_R$  and  $P_L$  like before, it is easy to shown that this Lagrangian is equal to what we were looking for:

$$\mathcal{L}_{\text{kF}} = i\bar{\nu}_{\ell L}\partial\!/\!\nu_{\ell L} + i\bar{\ell}\partial\!/\!\ell + i\bar{q}\partial\!/\!q + i\bar{q}'\partial\!/\!q'. \quad (3.16)$$

## Symmetries

The Lagrangian is invariant under a global symmetry  $\text{SU}(2)\times\text{U}(1)$ . This was to be expected, because the electroweak theory has the same structure as the isospin theory from Chapter 2. Therefore it should not come as a surprise that the quantum number  $T$  associated with  $\text{SU}(2)_w$  is called *weak-isospin* and that the quantum number  $Y$  of the  $\text{U}(1)_Y$  is called the (weak) *hypercharge*.

The doublets and singlets transform under the  $\text{SU}(2)_w\times\text{U}(1)_Y$  as

$$L(x) \rightarrow L'(x) = \exp\left(ig T^a \frac{\tau^a}{2}\right) \exp(ig'Y) L(x), \quad (3.17a)$$

$$R(x) \rightarrow R'(x) = \exp(ig'Y) R(x). \quad (3.17b)$$

The  $\tau^a$  are the Pauli matrices. Because the right-handed particle  $R$  is a singlet under the  $\text{SU}(2)_w$  it transforms according to the 1-dimensional representation of  $\text{SU}(2)$ , which means that for  $R$  the  $\text{SU}(2)_w$  transformation is the same thing as multiplying with a factor of 1. In other words, right-handed particles do not feel the force of the weak isospin, the weak force. This has already been mentioned in Section 3.1. Consequently, this means that for right-handed particles the weak-isospin is equal to zero.

The adjoints  $\bar{L}$  and  $\bar{R}$  transform as

$$\begin{aligned} \bar{L}'(x) &= [L'(x)]^\dagger \gamma^0 \\ &= L^\dagger(x) \gamma^0 \exp(ig'Y)^\dagger \exp\left(ig T^a \frac{\tau^a}{2}\right)^\dagger \\ &= \bar{L}(x) \exp(-ig'Y) \exp\left(-ig T^a \frac{\tau^a}{2}\right) \end{aligned} \quad (3.18)$$

<sup>2</sup>Actually, this is a different way of saying that a mass term would break the  $\text{SU}(2)$  symmetry of the Lagrangian.



(using the hermiticity of the Pauli matrices,  $\tau_a^\dagger = \tau_a$ ) and

$$\bar{R}(x) \rightarrow \bar{R}'(x) = \exp(-ig'Y) \bar{R}(x). \quad (3.19)$$

With these expressions it is easy to see that the Lagrangian of (3.15) is indeed invariant under  $SU(2)_w \times U(1)_Y$ . Note that if we would have had a mass term, the Lagrangian would not be invariant under the  $SU(2)$ .

### The covariant derivative

We shall now ‘gauge’ the symmetry. If we demand that the Lagrangian stays invariant under the local gauge symmetry  $SU(2)_w \times U(1)_Y$  then we need to replace the  $\partial_\mu$  in (3.15) by<sup>3</sup>

$$D_\mu = \partial_\mu - ig'B_\mu Y - igW_\mu^a \frac{\tau^a}{2}. \quad (3.20)$$

Here the  $B_\mu$  and  $W_\mu^a$  are the gauge bosons of  $U(1)_Y$  and  $SU(2)_w$ . Since  $R$  is a singlet under the  $SU(2)$ , we need to use different expressions for  $D_\mu L$  and  $D_\mu R$ :

$$D_\mu L = \left( \partial_\mu - ig'B_\mu Y - igW_\mu^a \frac{\tau^a}{2} \right) L, \quad (3.21a)$$

$$D_\mu R = (\partial_\mu - ig'B_\mu Y) R. \quad (3.21b)$$

When substituting these into the Lagrangian, we find interaction terms:

$$\begin{aligned} i\bar{L}\gamma^\mu D_\mu L &= i\bar{L}\gamma^\mu \left( \partial_\mu - ig'B_\mu Y - igW_\mu^a \frac{\tau^a}{2} \right) L \\ &= i\bar{L}\gamma^\mu \partial_\mu L + g'B_\mu \bar{L}\gamma^\mu Y L + gW_\mu^a \bar{L}\gamma^\mu \frac{\tau^a}{2} L \\ &= \mathcal{L}_{\text{kin},L} + \mathcal{L}_{\text{int},L}, \end{aligned} \quad (3.22)$$

and

$$\begin{aligned} i\bar{R}\gamma^\mu D_\mu R &= i\bar{R}\gamma^\mu (\partial_\mu - ig'B_\mu Y) R \\ &= i\bar{R}\gamma^\mu \partial_\mu R + g'B_\mu \bar{R}\gamma^\mu Y R \\ &= \mathcal{L}_{\text{kin},R} + \mathcal{L}_{\text{int},R}. \end{aligned} \quad (3.23)$$

In this equations we can see clearly that there is no term for interactions of right-handed particles with the  $W_\mu^a$  bosons.

### Kinetic term of the gauge fields

Now that we have introduced the gauge bosons  $B_\mu$  and  $W_\mu^a$ , we shall add the appropriate kinetic terms. For the  $U(1)$  gauge boson  $B_\mu$  we have to add

$$\mathcal{L} = -\frac{1}{4} B_{\mu\nu} B^{\mu\nu}, \quad (3.24)$$

with  $B_{\mu\nu}$  the field strength given by

$$B_{\mu\nu} = \partial_\mu B_\nu - \partial_\nu B_\mu. \quad (3.25)$$

We can also write this as

$$-ig'B_{\mu\nu} Y = [D_\mu, D_\nu], \quad (3.26)$$

but then we must use  $T = 0$ , i.e.

$$D_\mu = \partial_\mu - ig'B_\mu Y \quad (3.27)$$

---

<sup>3</sup>Often  $D_\mu$  is defined with  $-ig'B_\mu \frac{Y}{2}$  to make it look similar to the  $SU(2)$  term. From a group theory point of view this is an unlogical choice, because  $Y$  is the  $U(1)$  generator and  $\tau^a/2$  is the  $SU(2)$  generator. We shall take here the same approach as Peskin & Schroeder [4] and use  $Y$  instead of  $Y/2$ . This has no influence on the physics, only on the value of  $Y$  assigned to each particle.

because the  $B_\mu$  field carries no weak-isospin. That this is so can be seen from the Lagrangian: there are no interactions between  $B_\mu$  and  $W_\mu^a$ . Of course, this also means that the  $W_\mu^a$  carry no hypercharge. Therefore for the  $W_\mu^a$  field we have

$$D_\mu = \partial_\mu - igW_\mu^a \frac{\tau^a}{2}, \quad (3.28)$$

and we write

$$\mathcal{L} = -\frac{1}{4}W_{\mu\nu}^a W^{a\mu\nu}, \quad (3.29)$$

with the field strength

$$-igW_{\mu\nu}^a \frac{\tau^a}{2} = [D_\mu, D_\nu], \quad (3.30)$$

which can be written as

$$W_{\mu\nu}^a = \partial_\mu W_\nu^a - \partial_\nu W_\mu^a + g\epsilon^{abc}W_\mu^b W_\nu^c. \quad (3.31)$$

## Lagrangian of the massless electroweak theory

We can summarize the total Lagrangian as

$$\mathcal{L} = \mathcal{L}_{\text{kF}} + \mathcal{L}_{\text{kGB}}. \quad (3.32)$$

The  $\mathcal{L}_{\text{kF}}$  are the kinetic terms for the fermions,

$$\begin{aligned} \mathcal{L}_{\text{kF}} &= i\bar{L}_f \gamma^\mu D_\mu L_f + i\bar{R}_f \gamma^\mu D_\mu R_f \\ &= i\bar{L}_f \gamma^\mu \left( \partial_\mu - ig' B_\mu Y - igW_\mu^a \frac{\tau^a}{2} \right) L_f + i\bar{R}_f \gamma^\mu (\partial_\mu - ig' B_\mu Y) R_f, \end{aligned} \quad (3.33)$$

and  $\mathcal{L}_{\text{kGB}}$  the kinetic terms for the gauge bosons,

$$\mathcal{L}_{\text{kGB}} = -\frac{1}{4}(\partial_\mu B_\nu - \partial_\nu B_\mu)^2 - \frac{1}{4}(\partial_\mu W_\nu^a - \partial_\nu W_\mu^a + g\epsilon^{abc}W_\mu^b W_\nu^c)^2. \quad (3.34)$$

Summation over the appropriate flavors  $f = \ell, q, q'$  is implied. The interactions between the gauge bosons and the fermions are inside  $\mathcal{L}_{\text{kF}}$ .

This Lagrangian gives a nice description of electromagnetic and weak interactions with e.g. the  $B_\mu$  field as the photon and the  $W_\mu^a$  as mediators of the weak force. However, there is one big flaw: all particles are massless. The gauge bosons  $W_\mu^a$  cannot be truly massless because otherwise we would have seen them already in experiments. How can we give the bosons and fermions a mass without losing the symmetry  $\text{SU}(2)_w \times \text{U}(1)_Y$  that generated the interaction terms?

## 3.3 Spontaneous symmetry breaking

The reason why all particles are massless is because the symmetry  $\text{SU}(2)_w \times \text{U}(1)_Y$  forbids mass terms, as was shown in (3.13). Therefore the way to solve this is to break the symmetry. But we cannot just leave out the symmetry, because that would ruin our whole theory. We need a more subtle way of symmetry breaking.

There are actually different ways for doing this. We could argue for instance, that the symmetry was never truly exact but just an approximate symmetry. That means that small mass terms in Lagrangian are allowed that do not satisfy the symmetry. This is called *explicit* symmetry breaking.

The Standard Model uses a different way of breaking. By introducing a scalar boson with a specific potential it is possible to induce mass terms for both the gauge bosons and the fermions. This is done in such a way that all interactions still respect the symmetry, although the ground state does not. This mechanism is called *spontaneous* symmetry breaking. How it works is explained in the next few subsections.

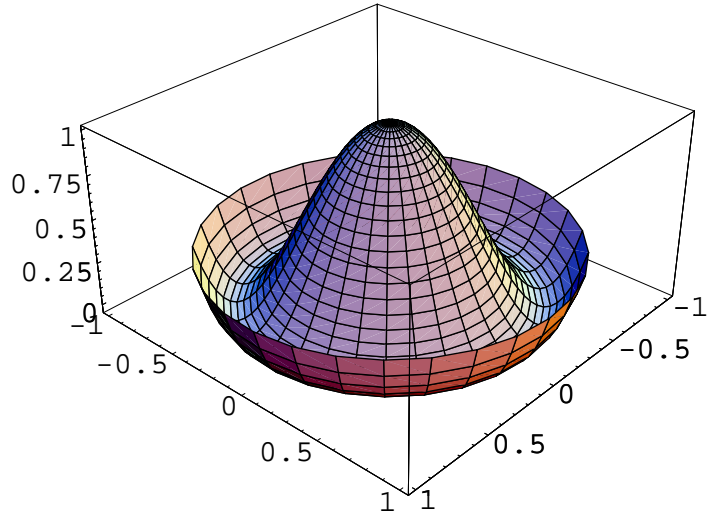


Figure 3.1: Plot of the Higgs potential of Eq. (3.36).

## Goldstone bosons

To obtain a better understanding of the whole principle, we shall first break a global U(1) symmetry. Imagine a complex scalar boson  $\phi$  with the Lagrangian

$$\mathcal{L} = (\partial_\mu \phi^*) (\partial^\mu \phi) - V(\phi), \quad (3.35)$$

where the potential  $V$  is given by

$$V(\phi) = -\mu^2 |\phi|^2 + \lambda |\phi|^4. \quad (3.36)$$

For  $\mu^2 > 0$  and  $\lambda > 0$  the potential will have the shape of a Mexican hat (or the bottom of wine bottle), see Figure 3.1. Note that in this case  $\mu^2$  has the wrong sign to be a scalar mass term. If the system is in its lowest energy state (the vacuum) then  $V$  will be minimal. That minimum occurs at

$$|\phi|^2 = \frac{\mu^2}{2\lambda}. \quad (3.37)$$

In other words, the expectation value for  $\phi$  in the vacuum is  $\langle \phi \rangle = \mu/\sqrt{2\lambda}$ . For obvious reasons  $\langle \phi \rangle$  is called the *vacuum expectation value* (VEV). Note that the vacuum state  $\phi_0$  is degenerate; it can be anything as long as  $|\phi_0| = \langle \phi \rangle$ . For our calculations we shall assume that  $\phi_0$  is real. This assumption is valid, because we can always transform this state with an U(1) transformation to any other possible ground state.

When  $\phi$  is in its ground state, the U(1) symmetry will be broken. This spontaneous breaking of the symmetry is something that also occurs in many other areas of physics. Imagine for example a symmetric chamber filled with water vapor. At high temperatures the vapor will be uniformly distributed throughout the chamber. When the temperature of the chamber is lowered, the vapor will start to condensate. The first tiny drop of water could form anywhere on the walls of the chamber. When this happens, the distribution of the water molecules is no longer uniform. We could say that the symmetry has been broken.

We expand the field  $\phi$  about the ground state:

$$\phi(x) = \phi_0 + \frac{1}{\sqrt{2}} (\phi_1(x) + i\phi_2(x)). \quad (3.38)$$

The Lagrangian becomes

$$\mathcal{L} = (\partial_\mu \phi^*) (\partial^\mu \phi) - V(\phi) = \frac{1}{2} (\partial_\mu \phi_1)^2 + \frac{1}{2} (\partial_\mu \phi_2)^2 - V(\phi), \quad (3.39)$$

with the potential given by

$$V(\phi) = -\frac{\mu^4}{4\lambda} + \mu^2\phi_1^2 + \mu\sqrt{\lambda}\phi_1^3 + \mu\sqrt{\lambda}\phi_1\phi_2^2 + \frac{1}{4}\lambda\phi_1^4 + \frac{1}{2}\lambda\phi_1^2\phi_2^2 + \frac{1}{4}\lambda\phi_2^4. \quad (3.40)$$

Here we have substituted  $\phi_0 = \mu/\sqrt{2\lambda}$ . Apparently, the real  $\phi_1$  field has obtained a mass:

$$\mu^2\phi_1^2 = \frac{1}{2}(2\mu^2)\phi_1^2 = \frac{1}{2}m_1^2\phi_1^2 \quad (3.41)$$

with  $m_1 = \sqrt{2\mu}$ , while the  $\phi_2$  field remains massless.

We have just witnessed an example of Goldstone's theorem: for every spontaneously broken continuous symmetry, the theory must contain a massless particle. These particles are called Goldstone bosons. In this case we have broken a U(1) symmetry, which means that only one of the  $\phi_1$  and  $\phi_2$  fields is allowed to remain massless. If we would have broken SU(2) and had started with a complex doublet like

$$\phi = \begin{pmatrix} \phi_1 + i\phi_2 \\ \phi_3 + i\phi_4 \end{pmatrix}, \quad (3.42)$$

then this would have become a set of three massless Goldstone bosons and one massive particle. Here three fields remain massless because SU(2) consists of three continuous symmetries.

## The Higgs mechanism

When we break a local symmetry, slightly different things happen. As an example we consider again the Lagrangian of (3.35) but replace the ordinary derivatives with the covariant derivative of a local U(1) symmetry:

$$\mathcal{L} = (D_\mu\phi^*)(D^\mu\phi) + \mu^2|\phi|^2 - \lambda|\phi|^4, \quad (3.43)$$

with

$$D_\mu = \partial_\mu - igA_\mu. \quad (3.44)$$

The potential has remained the same and therefore  $\phi$  requires the same VEV  $\langle\phi\rangle$ , we can expand  $\phi(x)$  in the same way as in (3.38)

$$\phi(x) = \phi_0 + \frac{1}{\sqrt{2}}(\phi_1(x) + i\phi_2(x)), \quad (3.45)$$

and the potential becomes again like in (3.40) with  $\phi_2$  massless and  $m_1 = \sqrt{2\mu}$ .

The kinetic term however, has now become

$$\begin{aligned} |D_\mu\phi|^2 &= \frac{1}{2}(\partial_\mu\phi_1)^2 + \frac{1}{2}(\partial_\mu\phi_2)^2 + \sqrt{2}\phi_0g(\partial_\mu\phi_2)A_\mu + \phi_0^2g^2A_\mu A^\mu + g(\partial_\mu\phi_2)A_\mu\phi_1 \\ &\quad + \frac{1}{2}g^2A_\mu A^\mu\phi_1^2 + \sqrt{2}\phi_0g^2A_\mu A^\mu\phi_1 - g(\partial_\mu\phi_1)A^\mu\phi_2 + \frac{1}{2}g^2A_\mu A^\mu\phi_2^2. \end{aligned} \quad (3.46)$$

The terms cubic and quartic in the fields  $A_\mu$ ,  $\phi_1$ , and  $\phi_2$  represent the interactions between these fields. The mass term

$$\phi_0^2g^2A_\mu A^\mu = \frac{\mu^2}{2\lambda}g^2A_\mu A^\mu = \frac{1}{2}m_A^2A_\mu A^\mu \quad (3.47)$$

indicate that the gauge boson has obtained a mass  $m_A = \mu g/\sqrt{\lambda}$ . Evidently, breaking a local gauge symmetry generates a mass term for the gauge boson!

But there is something strange with the Goldstone boson  $\phi_2$ . The term

$$\sqrt{2}\phi_0g(\partial_\mu\phi_2)A_\mu \quad (3.48)$$

would translate into a vertex like [10]:

$$\mu \text{ wavy line } \leftarrow \text{ arrow } \quad \text{with } k \text{ below arrow} = \sqrt{2}\phi_0g(\partial_\mu\phi_2)A_\mu = m_A k^\mu. \quad (3.49)$$

We could interpret this as an indication that  $\phi_2$  has somehow become a part of  $A_\mu$ .

Using the local U(1) transformation,

$$\phi \rightarrow \phi' = \exp(i\alpha(x))\phi, \quad (3.50)$$

we can choose the gauge  $\alpha(x)$  in such a way that  $\phi(x)$  becomes real-valued at every point  $x$ . This means that  $\phi_2 = 0$  in (3.45) and that  $\phi_2$  will vanish from the theory completely. Evidently,  $\phi_2$  can not be an independent physical particle, because the physics is always independent of the choice of gauge.

What has happened? One could say that the Goldstone boson was ‘eaten’ by the gauge boson, thereby giving the gauge boson a mass term. In Section 2.3 we have already seen that a massless vector boson can only have two physical polarization states; the longitudinal state is forbidden. A massive vector boson has an extra degree of freedom: it can have all three polarization states. This extra degree of freedom is provided by the disappearance of the Goldstone boson.

The generation of mass terms for gauge bosons by means of eating Goldstone bosons, is called the Higgs mechanism. It is one of the key principles of electroweak theory and the Standard Model.

## The Higgs in the Standard Model

We shall now use the Higgs mechanism to generate mass terms for the gauge bosons of the electroweak theory. Instead of the local  $U(1)$  we now have  $SU(2)_W \times U(1)_Y$ , which means that we need  $\phi$  to be a complex doublet of scalar fields:

$$\phi = \begin{pmatrix} \phi^+ \\ \phi^0 \end{pmatrix} = \frac{1}{\sqrt{2}} \begin{pmatrix} \phi_1 + i\phi_2 \\ \phi_3 + i\phi_4 \end{pmatrix}. \quad (3.51)$$

In the Standard Model  $\phi$  is called a Higgs doublet. Because  $\phi$  is a doublet under the  $SU(2)$ , its weak-isospin must be equal to  $T = \frac{1}{2}$ . The electric charge of the particles is again given by the Gell-Mann-Nishijima formula,

$$Q = T^3 + Y. \quad (3.52)$$

We choose for the hypercharge  $Y = 1/2$  such that  $\phi^0$  is a neutral particle and  $\phi^+$  is positively charged. The Higgs doublet has the usual Lagrangian

$$\mathcal{L}_H = (D_\mu \phi)^\dagger (D^\mu \phi) - V(\phi^\dagger \phi), \quad (3.53)$$

with the covariant derivative given by

$$\begin{aligned} D_\mu \phi &= \left( \partial_\mu - ig' B_\mu Y - ig W_\mu^a \frac{\tau^a}{2} \right) \phi \\ &= \left( \partial_\mu - \frac{i}{2} g' B_\mu - ig W_\mu^a \frac{\tau^a}{2} \right) \phi. \end{aligned} \quad (3.54)$$

The Higgs potential  $V(\phi^\dagger \phi)$  is equal to

$$V(\phi^\dagger \phi) = -\mu^2 (\phi^\dagger \phi) + \lambda (\phi^\dagger \phi)^2, \quad (3.55)$$

with  $\mu^2 > 0$  and  $\lambda > 0$ . The minimal potential is then

$$\phi^\dagger \phi = \frac{1}{2} (\phi_1^2 + \phi_2^2 + \phi_3^2 + \phi_4^2) = \frac{\mu^2}{2\lambda}. \quad (3.56)$$

A common choice for the ground state is

$$\phi_1 = \phi_2 = \phi_4 = 0, \quad \phi_3^2 = -\frac{\mu^2}{\lambda} \equiv v^2, \quad (3.57)$$

where  $v$  is the vacuum expectation value. With this choice, the field  $\phi(x)$  is neutral which means that also the vacuum is uncharged. The expansion of  $\phi(x)$  about the ground state is then

$$\phi(x) = \langle \phi \rangle + \phi'(x) = \frac{1}{\sqrt{2}} \begin{pmatrix} 0 \\ v + h(x) \end{pmatrix}. \quad (3.58)$$

The neutral scalar field  $h(x)$  is called the Higgs boson. The three Goldstone bosons  $\phi_1$ ,  $\phi_2$ , and  $\phi_4$  will be eaten by the gauge bosons.

The Higgs boson  $h$  will obtain a mass term via the Higgs potential in (3.55). According to Goldstone’s theorem, we must have broken only three out of the four continuous symmetries of

$SU(2)_w \times U(1)_Y$ . Apparently, there is still a symmetry left after the breaking. That symmetry is the  $U(1)_{em}$  of quantum electrodynamics. It is easy to demonstrate that this is the unbroken symmetry.

We have already seen that the VEV leaves the vacuum uncharged,  $q = 0$ . In other words, the charge operator leaves the vacuum invariant:

$$Q \langle \phi \rangle = q \langle \phi \rangle = 0. \quad (3.59)$$

Or in terms of transformations,

$$\langle \phi \rangle \rightarrow \exp(i\alpha(x)Q) \langle \phi \rangle = \left(1 + i\alpha(x)Q - \frac{1}{2}\alpha^2(x)Q^2 + \dots\right) \langle \phi \rangle = \langle \phi \rangle. \quad (3.60)$$

In the next section we shall explore more on the effects of this electroweak symmetry breaking (EWSB).

### 3.4 Eigenstates of the gauge bosons

After determining the VEV acquired by the Higgs doublet, it is time to determine the mass terms of the gauge bosons. To do this, we only need to substitute the VEV into the kinetic part of the Higgs Lagrangian,

$$\mathcal{L}_{\text{KH}} = (D_\mu \phi)^\dagger (D^\mu \phi). \quad (3.61)$$

Inserting the VEV into the potential simply returns the minimum value of the potential, which is just a constant. Adding a constant term to the Lagrangian has no influence on the equations of motion and can therefore be ignored.

By using the explicit form of the Pauli matrices, the covariant derivative can be written as

$$D_\mu = \partial_\mu - \frac{i}{2} \begin{pmatrix} gW_\mu^3 + 2g'B_\mu Y & g(W_\mu^1 - iW_\mu^2) \\ g(W_\mu^1 + iW_\mu^2) & -gW_\mu^3 + 2g'B_\mu Y \end{pmatrix}. \quad (3.62)$$

For  $\phi(x) = \langle \phi \rangle$  we then find

$$D_\mu \phi = \frac{1}{\sqrt{2}} D_\mu \begin{pmatrix} 0 \\ v \end{pmatrix} = \frac{iv}{2\sqrt{2}} \begin{pmatrix} g(W_\mu^1 - iW_\mu^2) \\ -gW_\mu^3 + g'B_\mu \end{pmatrix}, \quad (3.63)$$

and the Hermitian conjugate

$$(D_\mu \phi)^\dagger = \frac{-iv}{2\sqrt{2}} \begin{pmatrix} g(W_\mu^1 + iW_\mu^2) & -gW_\mu^3 + g'B_\mu \end{pmatrix}. \quad (3.64)$$

Hence, the Higgs sector of the Lagrangian becomes

$$\begin{aligned} \mathcal{L}_{\text{H}}(\phi = \langle \phi \rangle) &= (D_\mu \phi)^\dagger (D^\mu \phi) - V \\ &= \frac{1}{2} \frac{v^2 g^2}{4} |W_\mu^1 - iW_\mu^2|^2 + \frac{1}{2} \frac{v^2}{4} (g'B_\mu - gW_\mu^3)^2. \end{aligned} \quad (3.65)$$

The first term is the mass term of a complex (and therefore a charged) vector field:

$$\frac{1}{2} \frac{v^2 g^2}{4} (W_\mu^1 - iW_\mu^2)^* (W^{1\mu} - iW^{2\mu}) = \frac{1}{2} m_W^2 W_\mu^+ W^{-\mu}, \quad (3.66)$$

with mass

$$m_W = vg/2. \quad (3.67)$$

The two mass eigenstates are then

$$W_\mu^\pm = \frac{1}{\sqrt{2}} (W_\mu^1 \mp iW_\mu^2). \quad (3.68)$$

The second term in (3.65) is the mass term of an electrically neutral particle,

$$\frac{1}{2} \frac{v^2}{4} (gW_\mu^3 - g'B_\mu)^2 = \frac{1}{2} m_Z^2 (Z_\mu)^2. \quad (3.69)$$

To find the proper mass eigenstate we write the mass term as

$$\frac{1}{2} \frac{v^2}{4} (g^2 W_\mu^3 W^{3\mu} - 2gg' W_\mu^3 B^\mu + g'^2 B_\mu B^\mu) = \frac{1}{2} \begin{pmatrix} W_\mu^3 & B_\mu \end{pmatrix} \mathbf{M}^2 \begin{pmatrix} W_\mu^3 \\ B_\mu \end{pmatrix}, \quad (3.70)$$

with  $\mathbf{M}^2$  the mass matrix,

$$\mathbf{M}^2 = \frac{v^2}{4} \begin{pmatrix} g^2 & -gg' \\ -gg' & g'^2 \end{pmatrix}. \quad (3.71)$$

The mass eigenstates are then found by diagonalizing this matrix, with the eigenvalues the  $m^2$  of the particles. The normalized eigenstates are found to be:

$$Z_\mu = \frac{gW_\mu^3 - g'B_\mu}{\sqrt{g^2 + g'^2}}, \quad A_\mu = \frac{g'W_\mu^3 + gB_\mu}{\sqrt{g^2 + g'^2}}, \quad (3.72)$$

with the masses given by

$$m_Z = \frac{v}{2} \sqrt{g^2 + g'^2}, \quad m_A = 0. \quad (3.73)$$

These results can also be written in terms of the *weak mixing angle*  $\theta_w$ . Define

$$\cos \theta_w = \frac{g}{\sqrt{g^2 + g'^2}}, \quad \sin \theta_w = \frac{g'}{\sqrt{g^2 + g'^2}}, \quad (3.74)$$

then

$$Z_\mu = \cos \theta_w W_\mu^3 - \sin \theta_w B_\mu, \quad (3.75a)$$

$$A_\mu = \sin \theta_w W_\mu^3 + \cos \theta_w B_\mu. \quad (3.75b)$$

The inverse equations are

$$B_\mu = \cos \theta_w A_\mu - \sin \theta_w Z_\mu, \quad (3.76a)$$

$$W_\mu^3 = \sin \theta_w A_\mu + \cos \theta_w Z_\mu. \quad (3.76b)$$

Using the notation of  $\theta_w$ , we find the important relation

$$\frac{m_W}{m_Z} = \frac{\frac{1}{2}vg}{\frac{1}{2}v\sqrt{g^2 + g'^2}} = \cos \theta_w. \quad (3.77)$$

## The covariant derivative after EWSB

Now that we have found the masses and mass eigenstates of the gauge bosons, we can focus on the remaining  $U(1)_{em}$  symmetry. The best way to do that, is to examine the covariant derivative. When we substitute the eigenstates of  $W_\mu^\pm$ ,  $Z_\mu$ , and  $A_\mu$  into the explicit form of the  $D_\mu$  in (3.62), we find

$$\begin{aligned} D_\mu &= \partial_\mu - \frac{i}{2} \begin{pmatrix} gW_\mu^3 + 2g'B_\mu Y & g(W_\mu^1 - iW_\mu^2) \\ g(W_\mu^1 + iW_\mu^2) & -gW_\mu^3 + 2g'B_\mu Y \end{pmatrix} \\ &= \partial_\mu - \frac{i}{2} \begin{pmatrix} (2Y + 1)g_e A_\mu + \frac{-2Yg'^2 + g^2}{\sqrt{g^2 + g'^2}} Z_\mu & g\sqrt{2}W_\mu^+ \\ g\sqrt{2}W_\mu^- & (2Y - 1)g_e A_\mu + \frac{-2Yg'^2 - g^2}{\sqrt{g^2 + g'^2}} Z_\mu \end{pmatrix}, \end{aligned} \quad (3.78)$$

where we have used

$$\begin{aligned} \pm gW_\mu^3 + 2g'B_\mu Y &= \pm g[\sin \theta_w A_\mu + \cos \theta_w Z_\mu] + 2g'[\cos \theta_w A_\mu - \sin \theta_w Z_\mu] Y \\ &= (2g'Y \cos \theta_w \pm g \sin \theta_w) A_\mu + (-2g'Y \sin \theta_w \pm g \cos \theta_w) Z_\mu \\ &= (2Y \pm 1)g_e A_\mu + \frac{-2Yg'^2 \pm g^2}{\sqrt{g^2 + g'^2}} Z_\mu, \end{aligned} \quad (3.79)$$

and defined

$$g_e \equiv \frac{gg'}{\sqrt{g^2 + g'^2}} = g' \cos \theta_w = g \sin \theta_w. \quad (3.80)$$

Using the operators  $T^\pm$  and  $T^3$  defined by

$$T^\pm = \frac{1}{2}\tau^\pm = \frac{1}{2\sqrt{2}}(\tau^1 \pm i\tau^2), \quad (3.81a)$$

$$T^3 = \frac{1}{2}\tau^3 \quad (3.81b)$$

we can write  $D_\mu$  more elegantly as

$$\begin{aligned} D_\mu &= \partial_\mu - \frac{i}{2}g\sqrt{2}\left(W_\mu^+\sqrt{2}T^+ + W_\mu^-\sqrt{2}T^-\right) - \frac{i}{2}\left[(2Y + 2T^3)g_e A_\mu + \frac{-2Yg'^2 + 2T^3g^2}{\sqrt{g^2 + g'^2}}Z_\mu\right] \\ &= \partial_\mu - ig(W_\mu^+T^+ + W_\mu^-T^-) - ig_e(T^3 + Y)A_\mu - i\frac{(g^2T^3 - g'^2Y)}{\sqrt{g^2 + g'^2}}Z_\mu. \end{aligned} \quad (3.82)$$

If we compare the term with  $A_\mu$  to what we have in QED, we find that

$$Q = T^3 + Y, \quad (3.83)$$

and that  $g_e$  is the QED coupling constant, equal to the (absolute) charge of the electron  $e$ . Note that (3.83) was not put in by hand, but is a direct consequence of the breaking of  $SU(2)_w \times U(1)_Y \rightarrow U(1)_{em}$ .

With (3.83) we can also proof that the definition of the  $W_\mu^\pm$  in (3.68) gives the correct charges. Because the  $W$  particles have no interaction with the  $B_\mu$  field, their hypercharge is zero:  $Y = 0$ . Using the operator  $Q$  on the  $W_\mu^+$  we find

$$Q(W_\mu^+T^+) = (T^3 + Y)(W_\mu^+T^+) = W_\mu^+T^3T^+ = +\frac{1}{2}W_\mu^+T^+, \quad (3.84a)$$

$$Q(W_\mu^-T^-) = (T^3 + Y)(W_\mu^-T^-) = W_\mu^-T^3T^- = -\frac{1}{2}W_\mu^-T^-. \quad (3.84b)$$

Indeed, we see that the charges are correct.

## Interactions between fermions and gauge bosons

Before we can do any calculations with the Standard Model, we need to know the exact form of the interaction terms between the fermions and the gauge bosons. To find these we simply substitute the covariant derivative with  $W_\mu^\pm$ ,  $Z_\mu$ , and  $A_\mu$  into the kinetic Lagrangian of the fermions. For simplicity we shall only consider the charged-current weak interaction of quarks. This is the dominant interaction in single-top processes and actually the only interaction at leading order.

If we ignore the neutral currents the covariant derivative reduces to

$$D_\mu = \partial_\mu - ig(W_\mu^+T^+ + W_\mu^-T^-). \quad (3.85)$$

All right-handed quarks are singlets under the weak  $SU(2)$ , so for them  $T^+ = T^- = 0$ . For the first family of quarks the kinetic Lagrangian (3.33) becomes

$$\begin{aligned} \mathcal{L}_{\text{kF},u} &= i\bar{L}_u\gamma^\mu D_\mu L_u + i\bar{R}_u\gamma^\mu D_\mu R_u + i\bar{R}_d\gamma^\mu D_\mu R_d, \\ &= i\begin{pmatrix} \bar{u}_L & \bar{d}'_L \end{pmatrix} \gamma^\mu \left( \partial_\mu - \frac{ig}{\sqrt{2}} \begin{bmatrix} 0 & W_\mu^+ \\ W_\mu^- & 0 \end{bmatrix} \right) \begin{pmatrix} u_L \\ d'_L \end{pmatrix} + i\bar{u}_R\phi u_R + i\bar{d}'_R\phi d'_R \\ &= i\bar{u}\phi u + i\bar{d}'\phi d' - \frac{ig}{\sqrt{2}}\bar{u}_L\gamma^\mu W_\mu^+ d'_L - \frac{ig}{\sqrt{2}}\bar{d}'_L\gamma^\mu W_\mu^- u_L. \end{aligned} \quad (3.86)$$

In the last step we have used (3.14):

$$i\bar{q}_R\gamma^\mu\partial_\mu q_R + i\bar{q}_L\gamma^\mu\partial_\mu q_L = i\bar{q}\gamma^\mu\partial_\mu q. \quad (3.87)$$

With further use of the operators  $P_L$  and  $P_R$  we see that the interaction terms can be written as

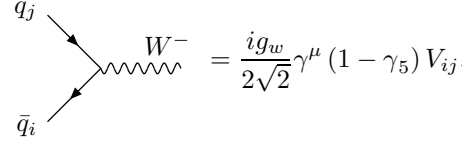
$$\begin{aligned} \mathcal{L}_{\text{int}} &= -\frac{ig}{\sqrt{2}}\bar{u}_L\gamma^\mu W_\mu^+ d'_L = -\frac{ig}{\sqrt{2}}\bar{u}P_R\gamma^\mu P_L d'W_\mu^+ \\ &= -\frac{ig}{\sqrt{2}}\bar{u}\gamma^\mu P_L P_L d'W_\mu^+ = -\frac{ig}{\sqrt{2}}\bar{u}\gamma^\mu P_L d'W_\mu^+ \\ &= -\frac{ig}{2\sqrt{2}}\bar{u}\gamma^\mu (1 - \gamma_5) d'W_\mu^+. \end{aligned} \quad (3.88)$$



The  $d'$ -quark here is not in its mass eigenstate, but is actually a linear combination of quarks as described by the CKM matrix of (3.3):

$$d' = V_{ud}d + V_{us}s + V_{ub}b. \quad (3.89)$$

Apparently, the  $\mathcal{L}_{\text{int}}$  actually consists of three independent interactions. For each of them we can construct the charged-current weak interaction vertex:



$$q_j \begin{array}{c} \nearrow \\ \searrow \end{array} \begin{array}{c} W^- \\ \text{---} \end{array} = \frac{ig_w}{2\sqrt{2}} \gamma^\mu (1 - \gamma_5) V_{ij}. \quad (3.90)$$

This vertex is valid for the quarks  $q_i = u, c, t$  and  $q_j = d, s, b$ .

### 3.5 Fermion masses

The Higgs field can also be used to give the fermions a mass term. This is done by means of a Yukawa interactions between the Higgs doublet, the left-handed doublet and the right-handed singlet:

$$\mathcal{L}_Y = -\lambda \left( \bar{L}\phi R + \bar{R}\phi^\dagger L \right) = -\lambda \bar{L}\phi R + \text{h.c.}, \quad (3.91)$$

where the h.c. stands for Hermitian conjugate. The constant  $\lambda$  is a free parameter of the theory; its value cannot be predicted by the Standard Model itself. Because we need a different constant for each fermion in the model, this means we have to add 9 extra free parameters to the theory.

The generation of the mass is a bit different for the quarks than for leptons. This is because of the fact that there are no right-handed neutrinos in the model.

#### Mass terms for leptons

For the leptons the Yukawa coupling is simply

$$\mathcal{L}_{Y,\ell} = -\lambda_\ell \left( \bar{R}_\ell \phi^\dagger L_\ell + \bar{L}_\ell \phi R_\ell \right), \quad (3.92)$$

with summation over  $\ell = e, \mu, \tau$  implied. Using the expansion of  $\phi$  about its VEV,

$$\phi(x) = \frac{1}{\sqrt{2}} \begin{pmatrix} 0 \\ v + h(x) \end{pmatrix}, \quad (3.93)$$

the Yukawa couplings turns into

$$\begin{aligned} \mathcal{L}_{Y,\ell} &= -\frac{\lambda_\ell}{\sqrt{2}} (\bar{\ell}_R) \begin{pmatrix} 0 & v+h \end{pmatrix} \begin{pmatrix} \nu_{\ell L} \\ \ell_L \end{pmatrix} - \frac{\lambda_\ell}{\sqrt{2}} \begin{pmatrix} \bar{\nu}_{\ell L} & \bar{\ell}_L \end{pmatrix} \begin{pmatrix} 0 \\ v+h \end{pmatrix} (\ell_R) \\ &= -\frac{\lambda_\ell}{\sqrt{2}} \bar{\ell}_R (v+h) \ell_L - \frac{\lambda_\ell}{\sqrt{2}} \bar{\ell}_L (v+h) \ell_R \\ &= -\frac{\lambda_\ell v}{\sqrt{2}} (\bar{\ell}_R \ell_L + \bar{\ell}_L \ell_R) - \frac{\lambda_\ell}{\sqrt{2}} (\bar{\ell}_R \ell_L + \bar{\ell}_L \ell_R) h \\ &= -\frac{\lambda_\ell v}{\sqrt{2}} \bar{\ell}\ell - \frac{\lambda_\ell}{\sqrt{2}} \bar{\ell}\ell h. \end{aligned} \quad (3.94)$$

In the last step we have used (3.12):

$$-m_\ell \bar{\ell}\ell = -m_\ell (\bar{\ell}_R \ell_L + \bar{\ell}_L \ell_R). \quad (3.95)$$

It is clear that the first term in  $\mathcal{L}_{Y,\ell}$  is a lepton mass term with the mass equal to

$$m_\ell = \frac{\lambda_\ell v}{\sqrt{2}}. \quad (3.96)$$

The reason why we can add a fermion mass term in this way, is because the Higgs doublet has exactly the right size to combine the right-handed singlet and the left-handed doublet together in a proper way. Without the Higgs doublet this would have been impossible, as we have seen in (3.13).

The second term in (3.94) is an interaction term with the three-points vertex

$$\begin{array}{c} \ell \\ \swarrow \\ \text{---} \\ \nwarrow \\ \bar{\ell} \end{array} \text{---} h = -i \frac{\lambda_\ell}{\sqrt{2}} = -i m_\ell/v. \quad (3.97)$$

Interestingly enough, the coupling with the Higgs boson is proportional to the mass of the lepton. This is true for all masses in the Standard Model. Evidently, the top quark must have quite a strong coupling to the Higgs, because the top mass is so large. Therefore, by accurately measuring the properties of the top we are able to learn more about the properties of the Higgs boson.

## Mass terms for quarks

In a similar way as with the leptons, we can use Yukawa terms to generate masses for the quarks. However, if we would use the same procedure as for the leptons, only the lower half of each left-handed doublet will acquire a mass. For leptons this is excellent since the neutrinos are considered massless, but for the quarks this would be totally wrong.

The solution is to use not only the regular Higgs doublet with fields  $\phi^0$  and  $\phi^+$ , but also a doublet of its antiparticles,  $\bar{\phi}^0$  and  $\phi^-$ . We can place these fields into a doublet any way we like. However, we don't want to spoil the SU(2) symmetry and therefore we demand that the anti-Higgs doublet transforms in exactly the same way under SU(2) as the original doublet. The correct doublet to use then is

$$\phi^c = -i\tau_2\phi^* = -i \begin{pmatrix} 0 & -i \\ i & 0 \end{pmatrix} \begin{pmatrix} \phi^+ \\ \phi^0 \end{pmatrix}^* = \begin{pmatrix} -\bar{\phi}^0 \\ \phi^- \end{pmatrix}. \quad (3.98)$$

Near the VEV of the  $\phi$  we can expand the doublet  $\phi^c$  as

$$\phi^c(x) = \frac{1}{\sqrt{2}} \begin{pmatrix} v + h(x) \\ 0 \end{pmatrix}. \quad (3.99)$$

The Yukawa terms that we add to the Lagrangian are (taking  $u$  and  $d$  as an example):

$$\mathcal{L}_{Y,u} = -\lambda_d \bar{L}_u \phi R_d - \lambda_u \bar{L}_u \phi^c R_u + \text{h.c.} \quad (3.100)$$

Using the antisymmetric tensor  $\epsilon_{ij} = (-i\tau^2)_{ij}$ , this can also be written quite elegantly as

$$\mathcal{L}_{Y,u} = -\lambda_d \bar{L}_u \phi R_d - \lambda_u \bar{L}_{ua} \epsilon_{ab} \phi_b^\dagger R_u + \text{h.c.} \quad (3.101)$$

Substitution of the expanded  $\phi(x)$  and  $\phi^c(x)$  into these terms leads to

$$\begin{aligned} \mathcal{L}_{Y,u} &= -\lambda_d \left( \bar{L}_u \phi R_d + \bar{R}_u \phi^\dagger L_d \right) - \lambda_u \left( \bar{L}_u \phi^c R_u + \bar{R}_u \phi^{c\dagger} L_u \right) \\ &= -\frac{\lambda_d}{\sqrt{2}} (v+h) \left( \bar{d}'_R d'_L + \bar{d}'_L d'_R \right) - \frac{\lambda_u}{\sqrt{2}} (v+h) (\bar{u}_R u_L + \bar{u}_L u_R) \end{aligned} \quad (3.102)$$

This calculation goes analogously to the one in (3.94). Even though we can write

$$-\frac{\lambda_u}{\sqrt{2}} (v+h) (\bar{u}_R u_L + \bar{u}_L u_R) = -\frac{\lambda_u v}{\sqrt{2}} \bar{u}u - \frac{\lambda_u}{\sqrt{2}} \bar{u}uh, \quad (3.103)$$

we cannot do exactly the same for the  $d'$ , since  $d'$  is not a mass eigenstate. We need again the CKM matrix  $V_{ij}$  of (3.3). Using the notation

$$d'_i = (d'_1, d'_2, d'_3) = (d', s', b'), \quad (3.104a)$$

$$u_i = (u_1, u_2, u_3) = (u, c, t), \quad (3.104b)$$

then the expression of (3.89) becomes

$$d'_i = V_{ij}d_j. \quad (3.105)$$

Therefore

$$\vec{d}'_{iR}d'_{iL} + \vec{d}'_{iL}d'_{iR} = V_{ij}(\vec{d}_{jR}d_{jL} + \vec{d}_{jL}d_{jR}) = V_{ij}\vec{d}_j d_j, \quad (3.106)$$

and so the Yukawa Lagrangian for all quarks is then

$$\mathcal{L}_{Y,q} = -\frac{\lambda_{d_i} v V_{ij}}{\sqrt{2}} \vec{d}_j d_j - \frac{\lambda_{d_i} V_{ij}}{\sqrt{2}} \vec{d}_j d_j h - \frac{\lambda_{u_i} v}{\sqrt{2}} \bar{u}_i u_i - \frac{\lambda_{u_i}}{\sqrt{2}} \bar{u}_i u_i h. \quad (3.107)$$

As expected we find similar expressions as with the leptons.

### 3.6 Quantum chromodynamics

Sofar we have only discussed the electroweak part of the Standard Model. The strong force is only felt by the quarks and is described by quantum chromodynamics (QCD). QCD is a gauge theory with an exact SU(3) color symmetry. Each quark is considered to be a color triplet, for example an up quark is written as

$$u = \begin{pmatrix} u_R \\ u_G \\ u_B \end{pmatrix}. \quad (3.108)$$

These triplets transform under the local SU(3)<sub>c</sub> as

$$u(x) \rightarrow u'(x) = \exp\left(ig_s \alpha^b(x) \frac{\lambda^b}{2}\right) u(x). \quad (3.109)$$

The  $\lambda^b$  with  $b = 1, 2, \dots, 8$  are the eight Gell-Mann matrices and are the generators of SU(3), similar to the Pauli matrices of SU(2).

To extend electroweak theory with QCD, we only need to make some small additions. It already contains the correct kinetic Lagrangian for the quarks,

$$\mathcal{L}_{\text{kF},q} = i\bar{q}\gamma^\mu\partial_\mu q = i\bar{q}_R\gamma^\mu\partial_\mu q_R + i\bar{q}_G\gamma^\mu\partial_\mu q_G + i\bar{q}_B\gamma^\mu\partial_\mu q_B, \quad (3.110)$$

but the covariant derivative needs an extra set of gauge bosons, the gluons:

$$D_\mu = \partial_\mu - ig'B_\mu Y - igW_\mu^a \frac{\tau^a}{2} - ig_s G_\mu^b \frac{\lambda^b}{2}. \quad (3.111)$$

Adding the gauge bosons  $G_\mu^b$  to  $D_\mu$  means that we also must add an kinetic term for them:

$$\mathcal{L}_{\text{kGB},G} = -\frac{1}{4}G^{b\mu\nu}G_{\mu\nu}^b, \quad (3.112)$$

with the field strength similar to (2.41):

$$G_{\mu\nu}^b = \partial_\mu G_\nu^b - \partial_\nu G_\mu^b + g_s f^{bcd} G_\mu^c G_\nu^d. \quad (3.113)$$

The antisymmetric tensor  $f^{bcd}$  are the structure constants of the SU(3) group, which means that

$$\left[\frac{\lambda^b}{2}, \frac{\lambda^c}{2}\right] = if^{bcd}\frac{\lambda^d}{2}. \quad (3.114)$$

Most of them are zero, but using the antisymmetry one can obtain all of them with

$$\begin{aligned} f^{123} &= 1, & f^{458} &= f^{678} = \sqrt{3}/2, \\ f^{147} &= f^{246} = f^{257} = f^{345} = f^{516} = f^{637} = \frac{1}{2}. \end{aligned} \quad (3.115)$$

Note that the electroweak symmetry breaking has no influence on QCD; after the breaking the quarks will obtain a mass, but they remain the same color triplet.

### 3.7 Summary

The complete Lagrangian of the Standard Model can be summarized as

$$\mathcal{L}_{\text{SM}} = \mathcal{L}_{\text{kF}} + \mathcal{L}_{\text{kGB}} + \mathcal{L}_{\text{kH}} + \mathcal{L}_{\text{pH}} + \mathcal{L}_{\text{Y}}. \quad (3.116)$$

Here the kinetic terms of the fermions are

$$\mathcal{L}_{\text{kF}} = i\bar{L}_\ell \not{D} L_\ell + i\bar{R}_\ell \not{D} R_\ell + i\bar{L}_{u^i} \not{D} L_{u^i} + i\bar{R}_{u^i} \not{D} R_{u^i} + i\bar{R}_{d^i} \not{D} R_{d^i}. \quad (3.117)$$

The kinetic terms of the Goldstone bosons are

$$\mathcal{L}_{\text{kGB}} = -\frac{1}{4}B^{\mu\nu}B_{\mu\nu} - \frac{1}{4}W^{a\mu\nu}W_{\mu\nu}^a - \frac{1}{4}G^{b\mu\nu}G_{\mu\nu}^b, \quad (3.118)$$

with the field strengths given by

$$B_{\mu\nu} = \partial_\mu B_\nu - \partial_\nu B_\mu, \quad (3.119a)$$

$$W_{\mu\nu}^a = \partial_\mu W_\nu^a - \partial_\nu W_\mu^a + g\epsilon^{abc}W_\mu^b W_\nu^c, \quad (3.119b)$$

$$G_{\mu\nu}^b = \partial_\mu G_\nu^b - \partial_\nu G_\mu^b + g_s f^{bcd}G_\mu^c G_\nu^d, \quad (3.119c)$$

and  $f^{bcd}$  the structure constants of SU(3). The Higgs sector of the Lagrangian consists of the kinetic term for the Higgs boson

$$\mathcal{L}_{\text{kH}} = (D_\mu \phi)^\dagger (D^\mu \phi), \quad (3.120)$$

and the Higgs potential

$$\mathcal{L}_{\text{pH}} = -V(\phi^\dagger \phi) = \mu^2(\phi^\dagger \phi) - \lambda(\phi^\dagger \phi)^2. \quad (3.121)$$

Finally, the Yukawa terms are given by

$$\mathcal{L}_{\text{Y}} = -\lambda_\ell \bar{L}_\ell \phi R_\ell - \lambda_{d^i} \bar{L}_{u^i} \phi R_{d^i} - \lambda_{u^i} \bar{L}_{u^i} \epsilon_{ab} \phi_b^\dagger R_{u^i} + \text{h.c.} \quad (3.122)$$

In all cases the covariant derivative is given by

$$D_\mu = \partial_\mu - ig' B_\mu Y - ig W_\mu^a \frac{\tau^a}{2} - ig_s G_\mu^b \frac{\lambda^b}{2}, \quad (3.123)$$

and is summation over leptons  $\ell = e, \mu, \tau$  and quarks  $u^i = u, c, t$  and  $d^i = d, s, b$  implied.

Table 3.1 lists the representations and quantum numbers of all the particles in the Standard Model. The value for the weak-isospin  $T$  depends on if the particle belongs to a doublet or triplet. The hypercharge  $Y$  is chosen in such a way that the correct charge  $Q$  is obtained. Table 3.2 gives a summary on how to extract masses and interactions from a Lagrangian.

particle	representations	quantum numbers		
	$\text{SU}(3)_c \times \text{SU}(2)_w \times \text{U}(1)_Y$	$T^3$	$Y$	$Q = T^3 + Y$
$\nu_{eL}, \nu_{\mu L}, \nu_{\tau L}$	$(\mathbf{1}, \mathbf{2})_{-1/2}$	+1/2	-1/2	0
$e_L, \mu_L, \tau_L$	$(\mathbf{1}, \mathbf{2})_{-1/2}$	-1/2	-1/2	-1
$e_R, \mu_R, \tau_R$	$(\mathbf{1}, \mathbf{2})_{-1}$	0	-1	-1
$u_L, c_L, t_L$	$(\mathbf{3}, \mathbf{2})_{+1/6}$	+1/2	+1/6	+2/3
$d_L, s_L, b_L$	$(\mathbf{3}, \mathbf{2})_{+1/6}$	-1/2	+1/6	-1/3
$u_R, c_R, t_R$	$(\mathbf{3}, \mathbf{2})_{+2/3}$	0	+2/3	+2/3
$d_R, s_R, b_R$	$(\mathbf{3}, \mathbf{2})_{-1/3}$	0	-1/3	-1/3
$g$	$(\mathbf{8}, \mathbf{2})_0$	0	0	0
$W^\pm, W^0$	$(\mathbf{1}, \mathbf{3})_0$	$\pm 1, 0$	0	$\pm 1, 0$
$B^0$	$(\mathbf{1}, \mathbf{1})_0$	0	0	0
$\phi^+, \phi^0$	$(\mathbf{1}, \mathbf{2})_{+1/2}$	+1/2, -1/2	+1/2	+1, 0

Table 3.1: List of all particles in the Standard Model, how they transform under the groups  $\text{SU}(3)_c \times \text{SU}(2)_w \times \text{U}(1)_Y$ , and their quantum numbers.

Kinetic terms	Substitute $D_\mu = \partial_\mu$ into the appropriate Lagrangian: $\mathcal{L}_{\text{kF}}$ , $\mathcal{L}_{\text{kGB}}$ , or $\mathcal{L}_{\text{kH}}$ .
Mass terms	Fermion mass: substitute $\phi = \langle \phi \rangle$ into $\mathcal{L}_Y$ . Gauge boson mass: substitute $\phi = \langle \phi \rangle$ into $\mathcal{L}_{\text{kH}}$ . Higgs mass: substitute VEV of $\phi$ into $\mathcal{L}_{\text{pH}}$ .
Interactions	Fermions-gauge bosons: expand $D_\mu$ in $\mathcal{L}_{\text{kF}}$ . Fermions-Higgs: substitute $\phi(x) = \langle \phi \rangle + \phi'(x)$ into $\mathcal{L}_Y$ . Gauge bosons-Higgs: expand $D_\mu$ in $\mathcal{L}_{\text{kH}}$ .
Self-interactions	There are no fermion self-interactions. Gauge boson self-interactions: expand $D_\mu$ in $\mathcal{L}_{\text{kF}}$ . Higgs self-interactions: substitute $\phi(x) = \langle \phi \rangle + \phi'(x)$ into $\mathcal{L}_{\text{pH}}$ .

Table 3.2: The procedures to find a specific term in the Lagrangian.

# Chapter 4

## Top physics in the Standard Model

Top physics is an excellent probe for new physics. The top has a mass almost 5 orders of magnitude larger than the lightest quark ( $\sim 175$  GeV). Because of its large mass the top is expected to have a strong coupling to Higgs bosons. Furthermore, the top can also be used to find new heavy particles of beyond the Standard Model. When such a heavy particle decays, it is very likely that it will decay into a top quark, causing the cross section of top production to rise. Besides its heavy mass, the top also has several other interesting properties. The lifetime of the top is about  $10^{-25}$  seconds, which is about 20 times faster than the time scale for strong interactions. Therefore the top decays into a  $b$ -quark and a  $W^+$  before it can hadronize. This feature gives physicists a unique opportunity to learn more about unbound quarks.

Before we look at the predictions made by new theoretical models, we should first review the ins and outs of top production in the Standard Model. Basically there are two distinct ways called *single-top* production, and  $t\bar{t}$  (pronounced as *t-t-bar*). With single-top processes it is possible to directly measure the value of the CKM element  $V_{tb}$ . If that value deviates a lot from unity then that is a sign that there could be a fourth generation of quarks. Even though single-top production is the main subject of this thesis,  $t\bar{t}$  has been included here in order to provide a more complete picture of top physics. Also, the  $t\bar{t}$  processes are expected to be the main source of background signals for the single-top processes.

This chapter starts with an analysis of  $t\bar{t}$  in Section 4.1, followed by the analysis of the single-top process in Section 4.2. In Section 4.3 we present the numerical evaluations of the cross sections calculated in the first two sections. Section 4.4 deals with the decay of the top. Finally, in Section 4.5 we share some thoughts about what influences we can expect from a theory that extends the Standard Model.

### 4.1 Top quark production via $t\bar{t}$

The top quark was first discovered in 1995 by the CDF and DØ experiments at the Tevatron (Fermilab). The process with which this was done, was  $p + \bar{p} \rightarrow t + \bar{t}$ , i.e. a proton-antiproton collision producing a  $t\bar{t}$  pair.

At leading order  $t\bar{t}$  production there are two dominant subprocesses. These are called quark annihilation ( $q\bar{q} \rightarrow g \rightarrow t\bar{t}$ ) and gluon-gluon fusion ( $gg \rightarrow g, t \rightarrow t\bar{t}$ ). For the first subprocess we have only one Feynman diagram and for the latter there are three (see Figure 4.1).

#### Quark-antiquark annihilation

The invariant amplitude for the Feynman diagram of Figure 4.1a is given by

$$\begin{aligned} -i\mathcal{M} &= \left[ \bar{v}_{\bar{q}}(ig_s\gamma^\mu(\lambda^a)_{ij})u_q \right] \left[ \frac{-ig_{\mu\nu}}{k^2} \right] \left[ \bar{u}_t(ig_s\gamma^\nu(\lambda^a)_{kl})v_{\bar{t}} \right] \\ &= -i\frac{-g_s^2}{k^2}(\lambda^a)_{ij}(\lambda^a)_{kl}[\bar{v}_{\bar{q}}\gamma^\mu u_q][\bar{u}_t\gamma_\nu v_{\bar{t}}]. \end{aligned} \tag{4.1}$$

with  $k = p_q + p_{\bar{q}}$  and  $\lambda^a$  the eight Gell-Mann matrices (see Appendix B). The index  $a = 1, \dots, 8$  corresponds to the type of gluon and the indices  $i, j, k, l = 1, 2, 3$  are the colors of the quarks. Just

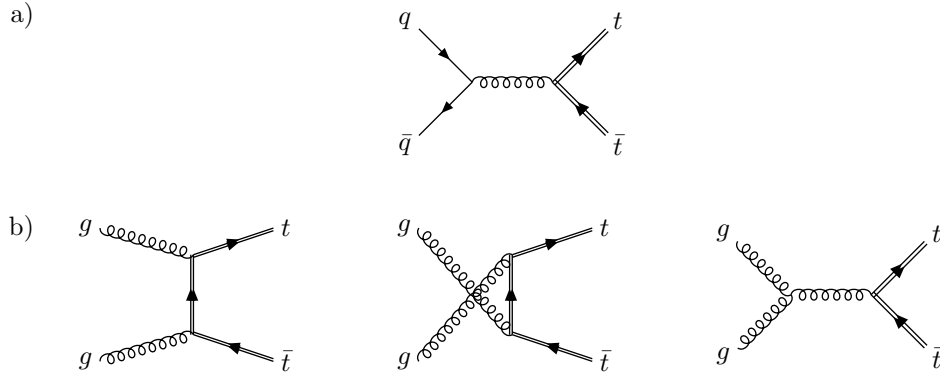


Figure 4.1: The production of  $t\bar{t}$  via quark-annihilation (a) and gluon-gluon fusion (b).

as we always do with spin, we shall sum over final colors and average over initial colors. Note that because the Gell-Mann matrices are Hermitian,

$$(\lambda^a)_{ij}^* = (\lambda^a)_{ij}^{\dagger T} = (\lambda^a)_{ij}^T = (\lambda^a)_{ji}. \quad (4.2)$$

Because there are three colors, averaging over the initial colors leads to a factor of  $1/3 \times 1/3 = 1/9$ :

$$\begin{aligned} |\overline{\mathcal{M}}|^2 &= \frac{1}{4} \sum_{\text{all spin}} \frac{1}{9} \sum_{\text{all color}} \frac{g_s^4}{k^4} (\lambda^a)_{ij} (\lambda^a)_{kl} (\lambda^b)_{ij}^* (\lambda^b)_{kl}^* \\ &\quad \times [\bar{v}_{\bar{q}} \gamma^\mu u_q] [\bar{u}_t \gamma_\mu v_{\bar{t}}] [\bar{v}_{\bar{q}} \gamma^\nu u_q]^* [\bar{u}_t \gamma_\nu v_{\bar{t}}]^* \\ &= \frac{g_s^4}{36k^4} \sum_{\text{all color}} (\lambda^a)_{ij} (\lambda^a)_{kl} (\lambda^b)_{ji} (\lambda^b)_{lk} \sum_{\text{all spin}} [\bar{v}_{\bar{q}} \gamma^\mu u_q] [\bar{u}_t \gamma_\mu v_{\bar{t}}] [\bar{u}_q \gamma^\nu v_{\bar{q}}] [\bar{v}_{\bar{t}} \gamma_\nu u_t] \\ &= \frac{g_s^4}{36k^4} \text{Tr}(\lambda^a \lambda^b) \text{Tr}(\lambda^a \lambda^b) \sum_{\text{all spin}} [\bar{v}_{\bar{q}} \gamma^\mu u_q] [\bar{u}_q \gamma^\nu v_{\bar{q}}] [\bar{u}_t \gamma_\mu v_{\bar{t}}] [\bar{v}_{\bar{t}} \gamma_\nu u_t]. \end{aligned} \quad (4.3)$$

Here we have used

$$[\bar{v}_{\bar{q}} \gamma^\nu u_q]^* = [v_{\bar{q}}^\dagger \gamma^0 \gamma^\nu u_q]^\dagger = u_q^\dagger \gamma^{\nu\dagger} \gamma^0 v_{\bar{q}} = u_q^\dagger \gamma^0 \gamma^\nu v_{\bar{q}} = \bar{u}_q \gamma^\nu v_{\bar{q}}, \quad (4.4)$$

and

$$[\bar{u}_t \gamma_\nu v_{\bar{t}}]^* = \bar{v}_{\bar{t}} \gamma_\nu u_t. \quad (4.5)$$

The Gell-Mann matrices are normalized according to

$$\text{Tr}(\lambda^a \lambda^b) = 2\delta^{ab}, \quad (4.6)$$

and so the product of the traces turns into

$$\text{Tr}(\lambda^a \lambda^b) \text{Tr}(\lambda^a \lambda^b) = 4. \quad (4.7)$$

Using the completeness relations, we find

$$\begin{aligned} \sum_{\text{spin } \bar{q}, q} [\bar{v}_{\bar{q}} \gamma^\mu u_q] [\bar{u}_q \gamma^\nu v_{\bar{q}}] &= \sum_{\text{spin } \bar{q}, q} (\bar{v}_{\bar{q}})_\alpha (\gamma^\mu)_{\alpha\beta} (u_q)_\beta (\bar{u}_q)_\gamma (\gamma^\nu)_{\gamma\delta} (v_{\bar{q}})_\delta \\ &= \left[ \sum_{\text{spin } \bar{q}} (v_{\bar{q}})_\delta (\bar{v}_{\bar{q}})_\alpha \right] (\gamma^\mu)_{\alpha\beta} \left[ \sum_{\text{spin } q} (u_q)_\beta (\bar{u}_q)_\gamma \right] (\gamma^\nu)_{\gamma\delta} \\ &= \text{Tr} \left[ (\not{p}_{\bar{q}} - m_q) \gamma^\mu (\not{p}_q + m_q) \gamma^\nu \right] \\ &= \text{Tr} \left[ \not{p}_{\bar{q}} \gamma^\mu \not{p}_q \gamma^\nu \right]. \end{aligned} \quad (4.8)$$

and

$$\sum_{\text{spin } \bar{t}, t} [\bar{v}_{\bar{t}} \gamma_{\mu} u_t] [\bar{u}_t \gamma_{\nu} v_{\bar{t}}] = \text{Tr} \left[ \left( \not{p}_{\bar{t}} - m_t \right) \gamma_{\mu} \left( \not{p}_t + m_t \right) \gamma_{\nu} \right]. \quad (4.9)$$

Evaluating  $|\overline{\mathcal{M}}|^2$  using the program FORM [11], we quickly find

$$|\overline{\mathcal{M}}|^2 = \frac{4g_s^4}{9\hat{s}^2} (\hat{u}_1^2 + \hat{t}_1^2 + 2m_t^2\hat{s}) = \frac{4}{9} \frac{16\pi^2\alpha_s^2}{\hat{s}^2} (\hat{u}_1^2 + \hat{t}_1^2 + 2m_t^2\hat{s}), \quad (4.10)$$

and thus the cross section becomes (see Appendix A)

$$\frac{d^2\hat{\sigma}}{d\hat{t}_1 d\hat{u}_1} (q\bar{q} \rightarrow t\bar{t}) = \frac{1}{16\pi\hat{s}^2} |\overline{\mathcal{M}}|^2 = \frac{4\pi\alpha_s^2}{9\hat{s}^4} (\hat{u}_1^2 + \hat{t}_1^2 + 2m_t^2\hat{s}). \quad (4.11)$$

The Mandelstam variables used here are defined by

$$\hat{s} = k^2 = (p_q + p_{\bar{q}})^2 = 2p_q p_{\bar{q}}, \quad (4.12a)$$

$$\hat{t}_1 = (p_q - p_t)^2 - m_t^2 = -2p_q p_t, \quad (4.12b)$$

$$\hat{u}_1 = (p_q - p_{\bar{t}})^2 - m_t^2 = -2p_q p_{\bar{t}}. \quad (4.12c)$$

The value of  $\alpha_s$  depends heavily on the energy scale of the process. It is conventional to use the  $\alpha_s$  at the mass scale of the top quark  $m_t$ , so here one should read  $\alpha_s = \alpha_s(m_t^2)$ .

## Gluon-gluon fusion

Calculating the cross section for the gluon-gluon fusion subprocess is much more difficult. As one can see in Figure 4.1b there are three diagrams involved. One of the diagrams contains a triple-gluon vertex which makes calculations even harder. Because the actual calculation is tedious and not so enlightening, we present here only the result [12],

$$\begin{aligned} \frac{d^2\hat{\sigma}}{d\hat{t}_1 d\hat{u}_1} (gg \rightarrow t\bar{t}) &= \frac{\pi\alpha_s^2}{8\hat{s}^2} \left[ \frac{6\hat{t}_1\hat{u}_1}{\hat{s}^2} - \frac{m_t^2(\hat{s} - 4m_t^2)}{3\hat{t}_1\hat{u}_1} \right. \\ &+ \frac{4}{3} \frac{\hat{t}_1\hat{u}_1 - 2m_t^2(\hat{t}_1 + 2m_t^2)}{\hat{t}_1^2} - \frac{4}{3} \frac{\hat{t}_1\hat{u}_1 - 2m_t^2(\hat{u}_1 + 2m_t^2)}{\hat{u}_1^2} \\ &\left. + 3 \frac{\hat{t}_1\hat{u}_1 + m_t^2(\hat{u}_1 - \hat{t}_1)}{\hat{s}\hat{t}_1} + 3 \frac{\hat{t}_1\hat{u}_1 + m_t^2(\hat{t}_1 - \hat{u}_1)}{\hat{s}\hat{u}_1} \right]. \quad (4.13) \end{aligned}$$

## The parton model and $pp, p\bar{p} \rightarrow t\bar{t}$ cross sections

Because of hadronization it is impossible to do experiments with free quarks. Therefore protons are collided with (anti)protons, in an attempt to make one of the partons in the first hadron hit a parton of the second hadron. To do calculations for hadron collisions, we need to know which fraction  $x$  of the proton's momentum is given to the parton. We also need to know the probability that we can hit a certain parton in the proton. However, the probability to find a specific parton depends heavily on the momentum of that parton.

The protons collide with a large momentum,  $P$ . If the momentum is large enough, we can neglect both the mass of the parton and that of the proton,  $|\mathbf{P}| \gg m, M$ . We are then allowed to write the parton momentum  $p$  as

$$p = xP, \quad (4.14)$$

where  $x$  is the momentum fraction, a number between 0 and 1 [13].

The probability to find parton  $i$  with a momentum  $x_i P$  inside the proton is given by the parton distribution function  $f(x_i, \mu)$ , PDF for short. The PDF is a function of the momentum fraction  $x_i$  and the scale  $\mu$ . To be precise,  $f(x_i) dx_i$  represents the number of partons of type  $i$  that have a momentum fraction between  $x_i$  and  $x_i + dx_i$ . The scale  $\mu$  specifies which renormalization scale is used. When the PDF is used to make QCD predictions for a certain process,  $\mu$  should be approximately of the same size as the momenta that is involved in the process. Since all of the top production processes involve momenta in the order of the mass of the top quark, we shall take  $\mu = m_t$ . A plot of  $f(x_i, \mu = m_t)$  is shown in Figure 4.2.



The total differential cross section for  $pp \rightarrow t\bar{t}$  can be found by summing over the different partons for both the cross sections for  $q\bar{q} \rightarrow t\bar{t}$  and  $gg \rightarrow t\bar{t}$ ,

$$\begin{aligned} \frac{d^2 \hat{\sigma}}{d\hat{t}_1 d\hat{u}_1}(pp \rightarrow t\bar{t}) &= \sum_{q,\bar{q}} \int \hat{\sigma}(q\bar{q} \rightarrow t\bar{t}) f(x_q) f(x_{\bar{q}}) dx_q dx_{\bar{q}} \\ &+ \sum_{g_1, g_2} \int \hat{\sigma}(gg \rightarrow t\bar{t}) f(x_{g_1}) f(x_{g_2}) dx_{g_1} dx_{g_2}. \end{aligned} \quad (4.15)$$

To find the total differential cross section for  $p\bar{p} \rightarrow t\bar{t}$ , we need to use the pDF for antiprotons. There is no need for a separate function however; the only difference between the proton and antiproton is that the  $u$ - and  $d$ -quarks are  $\bar{u}$  and  $\bar{d}$  in the antiproton. Hence, we can use the same  $f(x_i)$  but with the interchanges  $u \leftrightarrow \bar{u}$  and  $d \leftrightarrow \bar{d}$ .

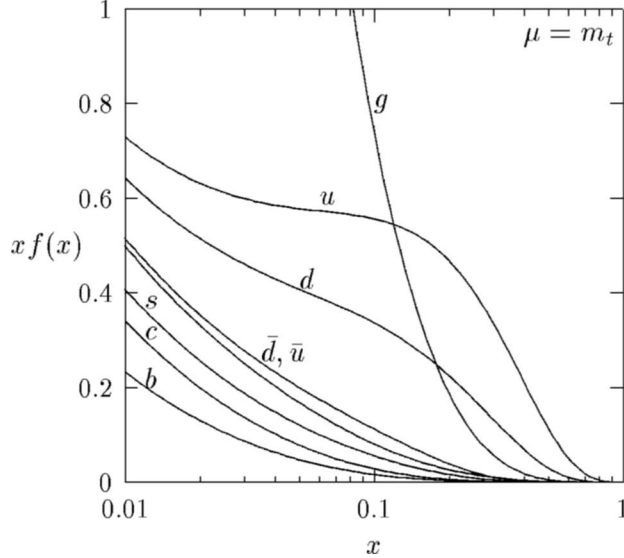


Figure 4.2: Parton distribution functions at the scale  $\mu = m_t$ , relevant for top quark production (taken from [14]).

## 4.2 Single-top production

There are a number of different ways to produce a single top quark. At tree-level there exist three subprocesses. These processes are the  $s$ -channel process,

$$q + \bar{q}' \rightarrow W^+ \rightarrow t + \bar{b}, \quad (4.16)$$

the  $t$ -channel process,

$$q + b \rightarrow W^+ \rightarrow q' + t, \quad (4.17)$$

and the  $Wt$ -associated process,

$$g + b \rightarrow t \rightarrow t + W^-. \quad (4.18)$$

The accents on the  $q'$  and  $\bar{q}'$  are there to indicate that those quarks have a different flavor than the  $q$ . The diagrams for each process are shown in Figures 4.3, 4.4, and 4.5.

### The $s$ -channel single-top

As a particular example of an  $s$ -channel single-top process we calculate here solely the amplitude for  $u + \bar{d} \rightarrow W^+ \rightarrow t + \bar{b}$ . For any other  $s$ -channel single-top process one can simply replace the  $\bar{d}$ -quark by an  $\bar{s}$ - or  $\bar{b}$ -quark, and the  $u$ -quark can be replaced by a  $c$ -quark. The presence of the top quark in the proton is small enough to be neglected. Changing the quark flavors has no effect on the invariant amplitude (4.27), with the exception that the  $V_{ud}$  must also be replaced by the appropriate element of the CKM matrix. The Feynman diagram for the  $s$ -channel process is shown in Figure 4.3.

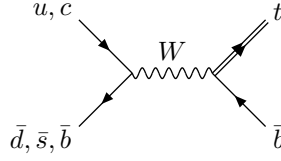


Figure 4.3: The Feynman diagram of the single-top  $s$ -channel subprocess.

Using the Feynman rules of Table 2.1 we translate this diagram into

$$-i\mathcal{M} = \left[ \bar{v}_{\bar{d}} \frac{ig_w}{2\sqrt{2}} \gamma^\mu (1 - \gamma_5) V_{ud} u_u \right] \left[ \frac{-ig_{\mu\nu}}{k^2 - m_W^2} \right] \left[ \bar{u}_t \frac{ig_w}{2\sqrt{2}} \gamma^\nu (1 - \gamma_5) V_{tb} v_{\bar{b}} \right], \quad (4.19)$$

with  $k = p_u + p_{\bar{d}}$  the momentum of the  $W$ . The matrix element squared becomes (averaging over initial spins and summing over final spins):

$$\begin{aligned} \overline{|\mathcal{M}|^2} &= \frac{1}{4} \sum_{\text{all spin}} \frac{g_w^4 |V_{ud}|^2 |V_{tb}|^2}{64} \left| \left[ \bar{v}_{\bar{d}} \gamma^\mu (1 - \gamma_5) u_u \right] \left[ \frac{g_{\mu\nu}}{k^2 - m_W^2} \right] \left[ \bar{u}_t \gamma^\nu (1 - \gamma_5) v_{\bar{b}} \right] \right|^2 \\ &\equiv \frac{1}{256} g_w^4 |V_{ud}|^2 |V_{tb}|^2 X^{\mu\kappa} Y_{\mu\kappa\nu\lambda} Z^{\nu\lambda}. \end{aligned} \quad (4.20)$$

Writing the amplitude in this way will prove to be very useful later on when we examine the Topflavor and the Littlest Higgs model. Here we have defined the tensors  $X^{\mu\kappa}$ ,  $Y_{\mu\kappa\nu\lambda}$  and  $Z^{\nu\lambda}$  as

$$X^{\mu\kappa} = \sum_{\text{spin } u, \bar{d}} \left[ \bar{v}_{\bar{d}} \gamma^\mu (1 - \gamma_5) u_u \right] \left[ \bar{v}_{\bar{d}} \gamma^\kappa (1 - \gamma_5) u_u \right]^*, \quad (4.21a)$$

$$Y_{\mu\kappa\nu\lambda} = \left[ \frac{g_{\mu\nu}}{k^2 - m_W^2} \right] \left[ \frac{g_{\kappa\lambda}}{k^2 - m_W^2} \right]^*, \quad (4.21b)$$

$$Z^{\nu\lambda} = \sum_{\text{spin } t, \bar{b}} \left[ \bar{u}_t \gamma^\nu (1 - \gamma_5) v_{\bar{b}} \right] \left[ \bar{u}_t \gamma^\lambda (1 - \gamma_5) v_{\bar{b}} \right]^*. \quad (4.21c)$$

First we calculate the tensor  $X^{\mu\kappa}$ . Because  $\bar{v}_{\bar{d}} \gamma^\alpha (1 - \gamma_5) u_u$  is a complex  $1 \times 1$  matrix it is the same as its Hermitian conjugate:

$$\begin{aligned} \left[ \bar{v}_{\bar{d}} \gamma^\kappa (1 - \gamma_5) u_u \right]^* &= \left[ v_{\bar{d}} \gamma^0 \gamma^\kappa (1 - \gamma_5) u_u \right]^\dagger = u_u^\dagger (1 - \gamma_5) \gamma^{\kappa\dagger} \gamma^0 v_{\bar{d}} \\ &= u_u^\dagger (1 - \gamma_5) \gamma^0 \gamma^\kappa v_{\bar{d}} = u_u^\dagger \gamma^0 (1 + \gamma_5) \gamma^\kappa v_{\bar{d}} \\ &= \bar{u}_u (1 + \gamma_5) \gamma^\kappa v_{\bar{d}} = \bar{u}_u \gamma^\kappa (1 - \gamma_5) v_{\bar{d}}. \end{aligned} \quad (4.22)$$

Then, using the completeness relations,

$$\begin{aligned} X^{\mu\kappa} &= \sum_{\text{spin } u, \bar{d}} \left[ \bar{v}_{\bar{d}} \gamma^\mu (1 - \gamma_5) u_u \right] \left[ \bar{u}_u \gamma^\kappa (1 - \gamma_5) v_{\bar{d}} \right]^* \\ &= \sum_{\text{spin } u, \bar{d}} (\bar{v}_{\bar{d}})_\alpha (\gamma^\mu (1 - \gamma_5))_{\alpha\beta} (u_u)_\beta (\bar{u}_u)_\gamma (\gamma^\kappa (1 - \gamma_5))_{\gamma\delta} (v_{\bar{d}})_\delta \\ &= \sum_{\text{spin } \bar{d}} (v_{\bar{d}})_\delta (\bar{v}_{\bar{d}})_\alpha (\gamma^\mu (1 - \gamma_5))_{\alpha\beta} \sum_{\text{spin } u} (u_u)_\beta (\bar{u}_u)_\gamma (\gamma^\kappa (1 - \gamma_5))_{\gamma\delta} \\ &= (\not{p}_{\bar{d}} - m_{\bar{d}})_{\delta\alpha} (\gamma^\mu (1 - \gamma_5))_{\alpha\beta} (\not{p}_u + m_u)_{\beta\gamma} (\gamma^\kappa (1 - \gamma_5))_{\gamma\delta} \\ &= \text{Tr} \left[ (\not{p}_{\bar{d}} - m_{\bar{d}}) \gamma^\mu (1 - \gamma_5) (\not{p}_u + m_u) \gamma^\kappa (1 - \gamma_5) \right]. \end{aligned} \quad (4.23)$$

The third tensor  $Z^{\nu\lambda}$  is very similar to  $X^{\mu\kappa}$ , so we can immediately write that down:

$$\begin{aligned} Z^{\nu\lambda} &= \sum_{\text{spin } t, \bar{b}} \left[ \bar{u}_t \gamma^\nu (1 - \gamma_5) v_{\bar{b}} \right] \left[ \bar{u}_t \gamma^\lambda (1 - \gamma_5) v_{\bar{b}} \right]^* \\ &= \text{Tr} \left[ (\not{p}_t + m_t) \gamma^\nu (1 - \gamma_5) (\not{p}_{\bar{b}} - m_{\bar{b}}) \gamma^\lambda (1 - \gamma_5) \right]. \end{aligned} \quad (4.24)$$

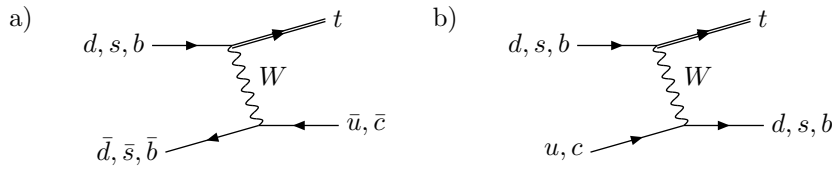


Figure 4.4: The two Feynman diagrams of the single-top  $t$ -channel subprocess.

The final thing we have to do is calculate the tensor  $Y_{\mu\kappa\nu\lambda}$ ,

$$Y_{\mu\kappa\nu\lambda} = \frac{g_{\mu\nu}g_{\kappa\lambda}}{(k^2 - m_W^2)^2}. \quad (4.25)$$

This expression has to be multiplied with  $X^{\mu\kappa}Z^{\nu\lambda}$ . Setting  $m_u = m_{\bar{d}} = m_{\bar{b}} = 0$  and using FORM to calculate the traces, we find a most elegant result:

$$X^{\mu\kappa}Y_{\mu\kappa\nu\lambda}Z^{\nu\lambda} = \frac{64(\hat{u} - m_t^2)\hat{u}}{(\hat{s} - m_W^2)^2}. \quad (4.26)$$

The  $\overline{|\mathcal{M}|^2}$  is then

$$\overline{|\mathcal{M}|^2} = \frac{1}{4}g_w^4 |V_{ud}|^2 |V_{tb}|^2 \frac{(\hat{u} - m_t^2)\hat{u}}{(\hat{s} - m_W^2)^2}, \quad (4.27)$$

with  $\hat{s} = k^2 = (p_u + p_{\bar{d}})^2$  and  $\hat{u} = (p_{\bar{d}} - p_t)^2$ .

The total cross section for the process  $pp \rightarrow t\bar{b}$  via the  $s$ -channel subprocess is

$$\sum_{\text{all partons}} \overline{|\mathcal{M}|^2} = \frac{1}{4}g_w^4 |V_{tb}|^2 \left[ F_{u/s} \frac{(\hat{u} - m_t^2)\hat{u}}{(\hat{s} - m_W^2)^2} + F_{t/s} \frac{(\hat{t} - m_t^2)\hat{t}}{(\hat{s} - m_W^2)^2} \right], \quad (4.28)$$

where  $F_{u/s}$  and  $F_{t/s}$  are flux factors given by

$$F_{u/s} = u_1\bar{d}_2 |V_{ud}|^2 + u_1\bar{s}_2 |V_{us}|^2 + u_1\bar{b}_2 |V_{ub}|^2 + c_1\bar{d}_2 |V_{cd}|^2 + c_1\bar{s}_2 |V_{cs}|^2 + c_1\bar{b}_2 |V_{cb}|^2. \quad (4.29a)$$

$$F_{t/s} = u_2\bar{d}_1 |V_{ud}|^2 + u_2\bar{s}_1 |V_{us}|^2 + u_2\bar{b}_1 |V_{ub}|^2 + c_2\bar{d}_1 |V_{cd}|^2 + c_2\bar{s}_1 |V_{cs}|^2 + c_2\bar{b}_1 |V_{cb}|^2. \quad (4.29b)$$

Here we have used the notation  $q_j$  for the parton distribution function of parton  $q$  in proton  $j$ .

## The $t$ -channel single-top

Let us now examine a close cousin of the  $s$ -channel. The Feynman diagrams for the  $t$ -channel process are shown in Figure 4.4. It is clear that both processes are almost the same: Interchanging  $p_u$  and  $-p_{\bar{b}}$  in the  $s$ -channel process  $u + \bar{d} \rightarrow t + \bar{b}$  gives you the  $t$ -channel process  $b + \bar{d} \rightarrow t + \bar{u}$ , which is exactly the same as interchanging  $\hat{s} \leftrightarrow \hat{t}$ . This means that we can find the amplitude simply by crossing the results of  $u + \bar{d} \rightarrow t + \bar{b}$ :

$$\overline{|\mathcal{M}|^2} = \frac{1}{4}g_w^4 |V_{ud}|^2 |V_{tb}|^2 \frac{(\hat{s} - m_t^2)\hat{s}}{(\hat{t} - m_W^2)^2}. \quad (4.30)$$

Subsequently, by using the interchange  $\hat{s} \leftrightarrow \hat{u}$  we find the amplitude for the second diagram:

$$\overline{|\mathcal{M}|^2} = \frac{1}{4}g_w^4 |V_{ud}|^2 |V_{tb}|^2 \frac{(\hat{u} - m_t^2)\hat{u}}{(\hat{t} - m_W^2)^2}. \quad (4.31)$$

The total cross section for the  $t$ -channel subprocess is then

$$\sum_{\text{all partons}} \overline{|\mathcal{M}|^2} = \frac{1}{4}g_w^4 \left[ F_{s/t} \frac{(\hat{s} - m_t^2)\hat{s}}{(\hat{t} - m_W^2)^2} + F_{u/t} \frac{(\hat{u} - m_t^2)\hat{u}}{(\hat{t} - m_W^2)^2} + F_{s/u} \frac{(\hat{s} - m_t^2)\hat{s}}{(\hat{u} - m_W^2)^2} + F_{t/u} \frac{(\hat{t} - m_t^2)\hat{t}}{(\hat{u} - m_W^2)^2} \right], \quad (4.32)$$

where  $F_{u/s}$  and  $F_{t/s}$  are flux factors given by

$$\begin{aligned}
F_{s/t} &= \bar{d}_1 |V_{td}|^2 \left[ \bar{u}_2 \left( |V_{ud}|^2 + |V_{us}|^2 + |V_{ub}|^2 \right) + \bar{c}_2 \left( |V_{cd}|^2 + |V_{cs}|^2 + |V_{cb}|^2 \right) \right] \\
&+ \bar{s}_1 |V_{ts}|^2 \left[ \bar{u}_2 \left( |V_{ud}|^2 + |V_{us}|^2 + |V_{ub}|^2 \right) + \bar{c}_2 \left( |V_{cd}|^2 + |V_{cs}|^2 + |V_{cb}|^2 \right) \right] \\
&+ \bar{b}_1 |V_{tb}|^2 \left[ \bar{u}_2 \left( |V_{ud}|^2 + |V_{us}|^2 + |V_{ub}|^2 \right) + \bar{c}_2 \left( |V_{cd}|^2 + |V_{cs}|^2 + |V_{cb}|^2 \right) \right]
\end{aligned} \quad (4.33)$$

and

$$\begin{aligned}
F_{u/t} &= \bar{d}_1 |V_{td}|^2 \left[ d_2 \left( |V_{ud}|^2 + |V_{cd}|^2 \right) + s_2 \left( |V_{us}|^2 + |V_{cs}|^2 \right) + b_2 \left( |V_{ub}|^2 + |V_{cb}|^2 \right) \right] \\
&+ \bar{s}_1 |V_{ts}|^2 \left[ d_2 \left( |V_{ud}|^2 + |V_{cd}|^2 \right) + s_2 \left( |V_{us}|^2 + |V_{cs}|^2 \right) + b_2 \left( |V_{ub}|^2 + |V_{cb}|^2 \right) \right] \\
&+ \bar{b}_1 |V_{tb}|^2 \left[ d_2 \left( |V_{ud}|^2 + |V_{cd}|^2 \right) + s_2 \left( |V_{us}|^2 + |V_{cs}|^2 \right) + b_2 \left( |V_{ub}|^2 + |V_{cb}|^2 \right) \right],
\end{aligned} \quad (4.34)$$

and similar for  $F_{t/u}$  and  $F_{s/u}$ .

If we define

$$\hat{t}_1 \equiv \hat{t} - m_t^2 = (p_{\bar{u}} - p_{\bar{d}})^2 - m_t^2, \quad (4.35a)$$

$$\hat{u}_1 \equiv \hat{u} = (p_{\bar{u}} - p_{\bar{d}})^2, \quad (4.35b)$$

such that  $\hat{s} + \hat{t}_1 + \hat{u}_1 = 0$ , then the differential cross section for the first diagram becomes

$$\frac{d^2 \hat{\sigma}}{d\hat{s} d\hat{u}_1} = \frac{1}{64\pi} g_w^4 |V_{ud}|^2 |V_{tb}|^2 \frac{(\hat{s} - m_t^2) \hat{s}}{(\hat{t}_1 + m_t^2 - m_W^2)^2} \delta(\hat{s} + \hat{t}_1 + \hat{u}_1). \quad (4.36)$$

We rather have  $d\hat{t}_1$  in the denominator than  $d\hat{s}$ . Writing  $\hat{s}$  as  $\hat{s} = -\hat{t}_1 - \hat{u}_1$ , then

$$d\hat{s} d\hat{u}_1 = \left( \frac{\partial \hat{s}}{\partial \hat{t}_1} d\hat{t}_1 + \frac{\partial \hat{s}}{\partial \hat{u}_1} d\hat{u}_1 \right) d\hat{u}_1 = -d\hat{t}_1 d\hat{u}_1 - (d\hat{u}_1)^2 = -d\hat{t}_1 d\hat{u}_1. \quad (4.37)$$

Therefore,

$$\frac{d^2 \sigma}{dt_1 du_1} = -\frac{1}{64\pi} g_w^4 |V_{ud}|^2 |V_{tb}|^2 \frac{s(s - m_t^2)}{(t_1 + m_t^2 - m_W^2)^2} \delta(s + t_1 + u_1), \quad (4.38)$$

with  $s = (p_{\bar{d}} + p_b)^2$ ,  $t_1 = (p_{\bar{u}} - p_{\bar{d}})^2 - m_t^2$  and  $u_1 = (p_b - p_{\bar{u}})^2$ .

The invariant amplitudes for both the  $s$ -channel and the  $t$ -channel have been compared to those in the article [15] and were found to be equal (see Tables 4.3 and 4.4).

## $Wt$ -associated production

The Feynman diagrams for  $Wt$ -associated production are shown in Figure 4.5. As one can see, this subprocess is a mixture of strong interactions and weak interactions. At the Tevatron this process can be ignored, but at the LHC the  $Wt$ -associated process will be responsible for 25% of all the single-top events [16].

In this thesis project we have chosen to put our emphasis on single-top processes that only involve weak interactions. Therefore we present here only the Feynman diagrams, we will not perform any calculations for this process.

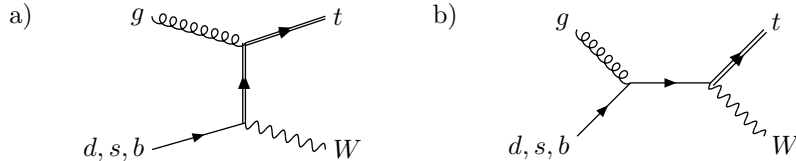


Figure 4.5: The two Feynman diagrams of the single-top  $Wt$ -associated subprocess.

### 4.3 Numerical results for top production

In order to verify a theoretical model we need to be able to turn our calculation into predictions that can be checked in an experiment. In this section we introduce some important variables often used in experiments, followed by the predictions that the Standard Model makes for  $t\bar{t}$  and single-top production.

#### Rapidity, pseudorapidity, and transverse momentum

The most important observable of a process is the cross section, which tells you how often an event of that process may occur. Even if it is not possible to measure the cross section directly, one can often still measure a branching ratio, the ratio between two cross sections.

But in a typical accelerator experiment we can do more than just count the number of events we are interested in. By combining different types of detectors, it is possible to identify the particle, measure its energy  $E$ , and determine its momentum:

$$p = (E, \mathbf{p}) = (E, p_x, p_y, p_z) = (E, |\mathbf{p}| \sin \theta \cos \phi, |\mathbf{p}| \sin \theta \sin \phi, |\mathbf{p}| \cos \theta).$$

The  $z$ -axis is chosen to point along the proton beam<sup>1</sup>, so  $\theta$  is the angle between the beam and the particle. The initial momentum of the protons (and of course the partons) is unknown. Therefore we cannot use conservation of momentum in this way. However, we do can use conservation of the *transverse momentum*,

$$p_T \equiv |\mathbf{p}| \sin \theta = \sqrt{p_x^2 + p_y^2},$$

because  $p_T = 0$  before the collisions and should therefore also be zero after the collisions.

Because the whole system is symmetric under  $\phi$ , the angle does not give us any information about the process. The angle  $\theta$  on the other hand does, and is therefore a very useful quantity to measure. However, instead of working with  $\theta$  particle physicists prefer to use the *pseudorapidity*,

$$\eta = -\ln \left( \tan \left( \frac{1}{2} \theta \right) \right).$$

The reason for this is that it is approximately equal to the *rapidity* of the particle,

$$y = \frac{1}{2} \ln \left( \frac{E + p_z}{E - p_z} \right).$$

The rapidity can be regarded as the relativistic analog of velocity. In special relativity one does not add the velocity of two particles, but adds their rapidities:  $y_{1+2} = y_1 + y_2$ .

For massless particles the rapidity is equal to the pseudorapidity and for massive particles  $\eta > y$ . In single-top processes we have only two particles in the final state: the top quark and a much lighter  $b$ -quark (or  $W$  boson for the  $Wt$  associated process), which means that  $\theta_b = \theta_t + 180^\circ$  and hence  $\eta_b = \eta_t$ . Compared to the large top mass, we can ignore the mass of the  $b$ -quark, so  $y_b \approx \eta_b$ .

#### Results for $t\bar{t}$

Using the Monte Carlo program described in Chapter 5, we find similar results as stated in several articles. Not only is this an good verification of the amplitudes, it is also an excellent test for the Monte Carlo program itself. The cross sections for  $p\bar{p} \rightarrow q\bar{q}, gg \rightarrow t\bar{t}$  and  $pp \rightarrow q\bar{q}, gg \rightarrow t\bar{t}$  are shown in Table 4.1. The results are in rather good agreement with the cross sections of Table 4.2 which is taken from [17].

In the tables it is clear to see that at the Tevatron the  $q\bar{q} \rightarrow t\bar{t}$  subprocess is much more dominant than the  $gg \rightarrow t\bar{t}$  process. The reason for this becomes clear from Figure 4.2. Between  $x = 0.2$  and  $x = 1$  the valance quarks  $u$  and  $d$  carry most of the momentum of the proton. Because the Tevatron is a  $p\bar{p}$ -collider, this means that the biggest source for  $t\bar{t}$  comes from  $u\bar{u}$  and  $d\bar{d}$ , i.e. the  $q\bar{q}$ -channel. The LHC is a proton-proton collider and has therefore much less  $q\bar{q}$  combinations available. Hence, the gluon-fusion process is more dominant at the LHC.

---

<sup>1</sup>In the case of proton-proton collisions the exact direction of the  $z$ -axis is not important. I.e. all LHC plots should show a clear symmetry.

In Figures 4.6-4.11 the transverse momentum, pseudorapidity, and the rapidity of the top quark for both the Tevatron and the LHC are displayed. The transverse momenta all have a very typical shape. The  $p_T$  with the highest occurrence lies around 75 GeV, but one can see that it shifts slightly to the right at higher CM-energies.

The pseudorapidity and rapidity plots all show a clear symmetry around  $\eta = y = 0$ . This is easy to understand for the Tevatron, because the whole process is symmetric ( $p\bar{p} \rightarrow t\bar{t}$ ). However, this is somewhat strange for the LHC, because there we have two protons in the initial state. For the gluon-fusion subprocess this does not make a difference, because there are just as many gluons in a proton as in an antiproton. However, for quark-antiquark annihilation we need an antiquark which can only be a sea quark in this case. If it this is a  $u$ -antiquark or a  $d$ -antiquark, it can annihilate with one of the valence quarks of the other proton, otherwise it will annihilate with one of the sea quarks. In any case, the quark-antiquark annihilation does not see a difference between one proton and the other.

One interesting feature about the pseudorapidity at the LHC, is that it has a small dip near  $\eta = 0$ . This means that the top quark tends to propagate more in the same direction as the initial hadrons. If we compare the rapidity plots of the LHC with the Tevatron, then we see that this effect is absent. Evidently, the origin of this effect is due to the highly relativistic momentum of the top quark (rapidity is invariant under Lorentz boosts, but pseudorapidity is not).

In general we can conclude that the shape of the plots for the Tevatron do not change much if we use a higher CM-energy. The area under the graphs increases slightly, but because the that area must be equal to the cross section, that only tells you that the cross section goes up. The area under a graph can be used as a simple check to tell if the plot can be trusted or not.

	$\sigma_{\text{LO}}(q\bar{q} \rightarrow t\bar{t})$ (pb)	$\sigma_{\text{LO}}(gg \rightarrow t\bar{t})$ (pb)	$\sigma_{\text{LO}}$ (pb)
Tevatron ( $\sqrt{s} = 1.8$ TeV, $p\bar{p}$ )	4.45 (96%)	0.20 (4%)	4.65 (100%)
Tevatron ( $\sqrt{s} = 2.0$ TeV, $p\bar{p}$ )	5.87 (94%)	0.38 (6%)	6.25 (100%)
LHC ( $\sqrt{s} = 14$ TeV, $pp$ )	73.1 (14%)	467 (86%)	540 (100%)

Table 4.1: Cross sections for  $t\bar{t}$  at leading-order in QCD. Behind each value are given in parentheses the percentage of the total cross section. For the Monte Carlo simulation the PDF table CTEQ5L was used, with all scales set to  $\mu = m_t = 175$  GeV.

	$\sigma_{\text{NLO}}$ (pb)	$q\bar{q} \rightarrow t\bar{t}$	$gg \rightarrow t\bar{t}$
Tevatron ( $\sqrt{s} = 1.8$ TeV, $p\bar{p}$ )	$4.87 \pm 10\%$	90%	10%
Tevatron ( $\sqrt{s} = 2.0$ TeV, $p\bar{p}$ )	$6.70 \pm 10\%$	85%	15%
LHC ( $\sqrt{s} = 14$ TeV, $pp$ )	$803 \pm 15\%$	10%	90%

Table 4.2: Cross sections for  $t\bar{t}$  at next-to-leading-order in QCD. Also shown is the percentage of the total cross section from the quark-antiquark-annihilation and gluon-fusion subprocesses [18].

Figure 4.6: Transverse momentum for  $p\bar{p} \rightarrow t\bar{t}$  at the Tevatron for  $\sqrt{s} = 1.8$  TeV, 1.96 TeV and 2.0 TeV.

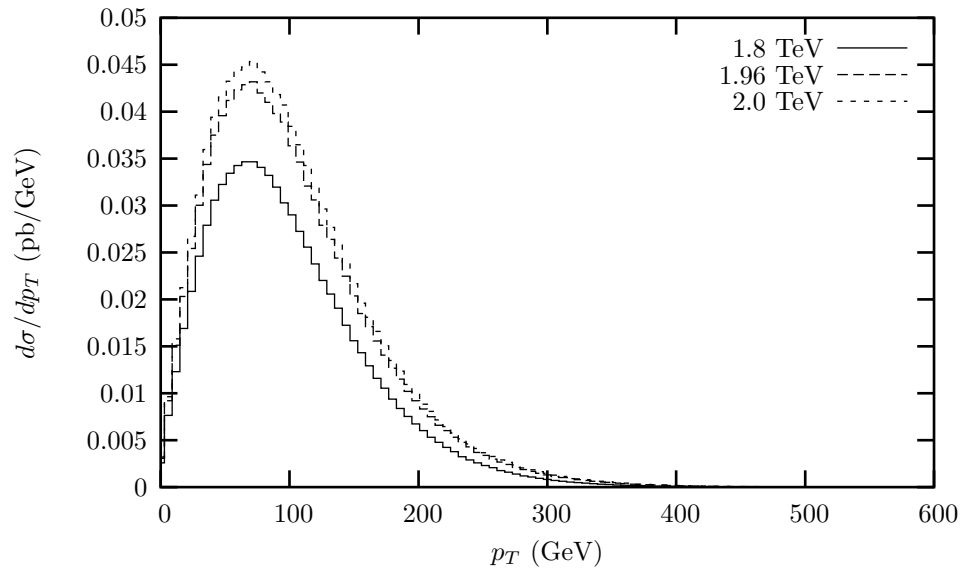


Figure 4.7: Transverse momentum for  $pp \rightarrow t\bar{t}$  at the LHC for  $\sqrt{s} = 14$  TeV.

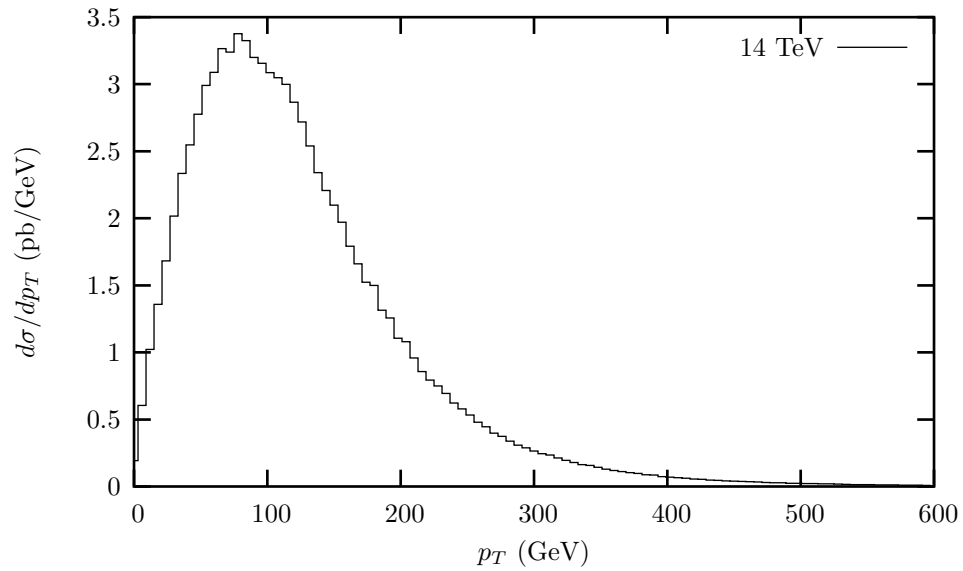


Figure 4.8: Pseudorapidity for  $p\bar{p} \rightarrow t\bar{t}$  at the Tevatron for  $\sqrt{s} = 1.8$  TeV, 1.96 TeV and 2.0 TeV.

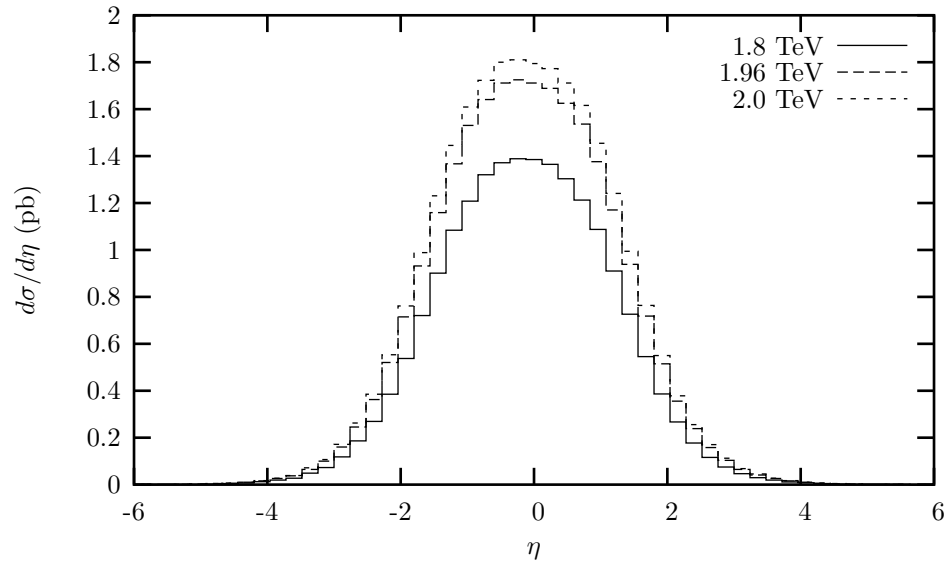


Figure 4.9: Pseudorapidity momentum for  $pp \rightarrow t\bar{t}$  at the LHC for  $\sqrt{s} = 14$  TeV.

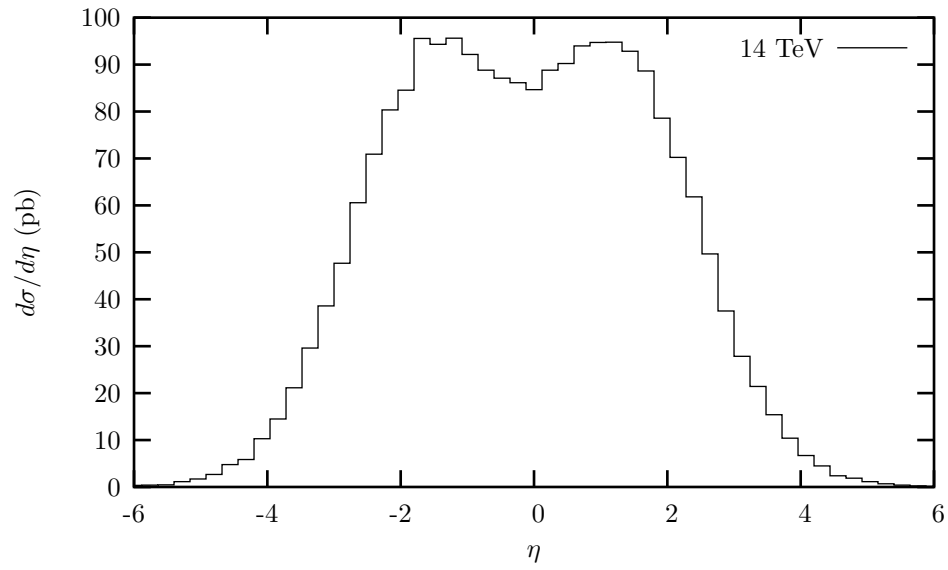




Figure 4.10: Rapidity for  $p\bar{p} \rightarrow t\bar{t}$  at the Tevatron for  $\sqrt{s} = 1.8$  TeV, 1.96 TeV and 2.0 TeV.

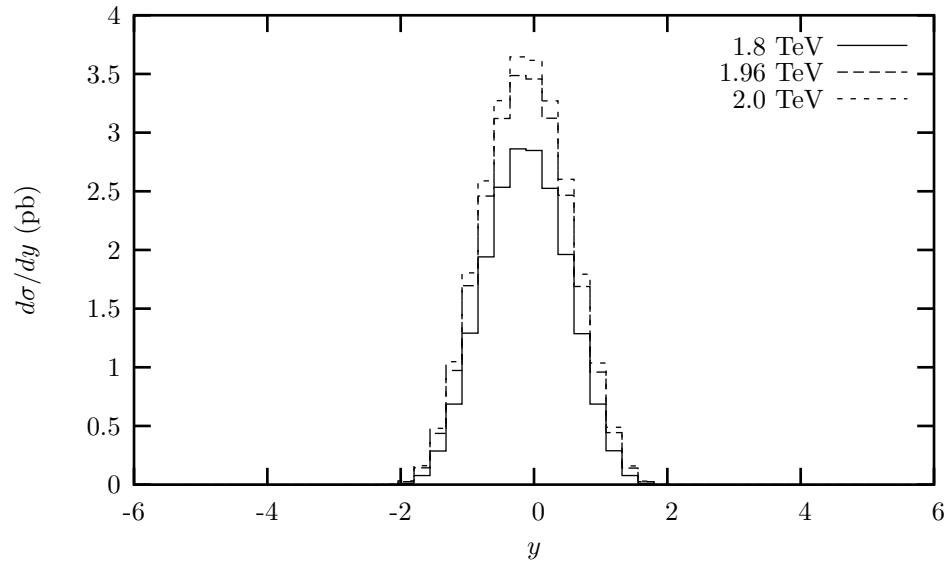
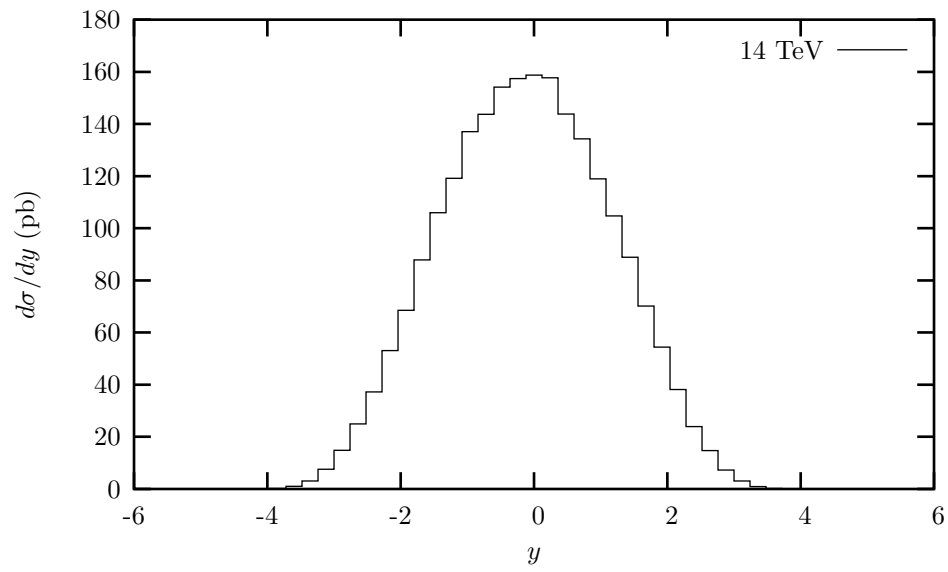


Figure 4.11: Rapidity momentum for  $pp \rightarrow t\bar{t}$  at the LHC for  $\sqrt{s} = 14$  TeV.



## Results for single-top

The results for the single-top simulations are stated in Table 4.3. As a comparison we have added here Table 4.4 that displays the cross sections according to [15]. Our values are a bit higher than those in the article. This could be because of the use of different parameters, e.g. different CKM values, different  $W$  mass, etc.

A noticeable thing is that the cross sections for single-top are all a lot smaller than for  $t\bar{t}$ . This is because  $t\bar{t}$  is a strong process which has an amplitude of  $\propto \alpha_s^2$ , while the  $s$ -channel and  $t$ -channel are weak processes with an amplitude of  $\propto \alpha_w^2 = g_w^4 / (4\pi)^2 \ll \alpha_s^2$ .

$\sqrt{s}$	$\sigma_{\text{LO}}$ (pb)	
	$s$ -channel	$t$ -channel
Tevatron ( $\sqrt{s} = 1.8$ TeV), $p\bar{p} \rightarrow tX$	0.261 $\pm 0.001$	0.654 $\pm 0.001$
Tevatron ( $\sqrt{s} = 1.96$ TeV), $p\bar{p} \rightarrow tX$	0.306 $\pm 0.001$	0.890 $\pm 0.001$
Tevatron ( $\sqrt{s} = 2$ TeV), $p\bar{p} \rightarrow tX$	0.317 $\pm 0.001$	0.956 $\pm 0.001$
LHC ( $\sqrt{s} = 14$ TeV), $pp \rightarrow tX$	4.57 $\pm 0.01$	146.4 $\pm 0.4$
LHC ( $\sqrt{s} = 14$ TeV), $pp \rightarrow \bar{t}X$	2.77 $\pm 0.01$	84.5 $\pm 0.2$

Table 4.3: Leading-order cross sections for single-top production. For the evaluation the CTEQ5L table was used, all scales were set at  $\mu = m_t$ , and we have used 5 iterations with 1,000,000 events per iteration.

Process	$\sqrt{s}$	$\sigma_{\text{LO}}$ (pb)	$\sigma_{\text{NLO}}$ (pb)
$s$ -channel	Tevatron ( $\sqrt{s} = 1.8$ TeV), $p\bar{p} \rightarrow tX$	0.259	0.380 $\pm 0.002$
	Tevatron ( $\sqrt{s} = 1.96$ TeV), $p\bar{p} \rightarrow tX$	0.304	0.447 $\pm 0.002$
	Tevatron ( $\sqrt{s} = 2$ TeV), $p\bar{p} \rightarrow tX$	0.315	0.463 $\pm 0.002$
	LHC ( $\sqrt{s} = 14$ TeV), $pp \rightarrow tX$	4.53	6.55 $\pm 0.03$
	LHC ( $\sqrt{s} = 14$ TeV), $pp \rightarrow \bar{t}X$	2.74	4.07 $\pm 0.02$
$t$ -channel	Tevatron ( $\sqrt{s} = 1.8$ TeV), $p\bar{p} \rightarrow tX$	0.648	0.702 $\pm 0.003$
	Tevatron ( $\sqrt{s} = 1.96$ TeV), $p\bar{p} \rightarrow tX$	0.883	0.959 $\pm 0.002$
	Tevatron ( $\sqrt{s} = 2$ TeV), $p\bar{p} \rightarrow tX$	0.948	1.029 $\pm 0.004$
	LHC ( $\sqrt{s} = 14$ TeV), $pp \rightarrow tX$	144.8	152.6 $\pm 0.6$
	LHC ( $\sqrt{s} = 14$ TeV), $pp \rightarrow \bar{t}X$	83.4	90.0 $\pm 0.5$

Table 4.4: LO and NLO cross sections for single-top production at the Tevatron and LHC for  $m_t = 175$  GeV. Cross sections are evaluated with CTEQ5L and CTEQ5M1 PDFs, and all scales set to  $m_t$ . Errors include only Monte Carlo statistics [15].

In Figures 4.12-4.17 we present the results for the  $p_T$ , and the (pseudo)rapidity for the  $s$ -channel and  $t$ -channel processes, as produced by our Monte Carlo program. Note that in some graphs the differential cross section has been scaled to produce a more meaningful plot. One can see that for low  $p_T$  at the Tevatron the subprocess is very likely to be a  $t$ -channel process, while for  $p_T > 150$  GeV it is more likely that the quark was produced via the  $s$ -channel. However, the cross section is very low for  $p_T > 150$  GeV and therefore we may conclude that at the Tevatron the  $t$ -channel will always be more dominant. We can make the same conclusion for the LHC; there the lines cross at an even higher energy (not shown in the plots).

Why the  $t$ -channel is more dominant than the  $s$ -channel is because of kinetic reasons. As can be seen in the Feynman diagrams in Figures 4.3 and 4.4, the  $s$ -channel process is a back-to-back process, while the  $t$ -channel is more like a scattering process and therefore kinematically favored. Putting it differently, in the  $s$ -channel the  $W$  boson needs to have enough energy to be able to decay into a top and a bottom quark. For the  $t$ -channel the  $W$  boson is allowed to be less energetic.

The (pseudo)rapidity of the top quark shows again a clear symmetry around  $\eta = y = 0$ . Just as with  $t\bar{t}$  production, the single-top processes do not see the difference between one proton and the other, which results therefore in symmetric (pseudo)rapidity plots. However, in contrast to  $t\bar{t}$  there is a clear asymmetry in the Tevatron plots. The asymmetry is most clearly visible in the pseudorapidity plot: the top quark seems to prefer a positive value for  $\eta$ , which means that the top will more likely have its momentum in the same direction as the proton. The top antiquark shows exactly the same asymmetry, but with its maximum at negative values for  $\eta$ . We can explain this by looking at the quark content of the proton and antiproton. If we look at the  $s$ -channel Feynman diagram in Figure 4.3, we see that the most dominant  $s$ -channel process is  $u + \bar{d} \rightarrow t + \bar{b}$  because in the hadrons the  $u$  and  $\bar{d}$  are the most available. There are valence  $u$ -quarks in the proton and valence  $\bar{d}$ -quarks in the antiproton, so some asymmetry was to be expected. Because the  $s$ -channel is a back-to-back process, this asymmetry is not that large.

Why the asymmetry in the  $t$ -channel pseudorapidity is so large at the Tevatron, can be explained with the Feynman diagrams in Figure 4.4. From Figure 4.4a it is clear that we can expect that the top favors the same direction as the proton, because the proton contains a lot of  $d$ -quarks while the antiproton contains the same amount of  $\bar{d}$ -quarks. However, the diagram in 4.4b has the opposite effect. There are approximately twice as many  $u$ -quarks in a proton as there are  $d$ -quarks. For the antiproton the amounts are about the same (they are sea-quarks). Apparently, in this case the top quark is more likely to move in the same direction as the antiproton. The most dominant process however, is the one in Figure 4.4a with  $d + \bar{d} \rightarrow t + \bar{u}$ , because that is the only  $t$ -channel process that does not need sea-quarks. We conclude that for the  $t$ -channel the top momentum is more likely to be in the same direction as the proton (and the momentum of the top antiquark in the same direction as the antiproton of course).

Figure 4.12: Transverse momentum for the single-top process  $p\bar{p} \rightarrow tX$  at the Tevatron ( $\sqrt{s} = 2$  TeV).

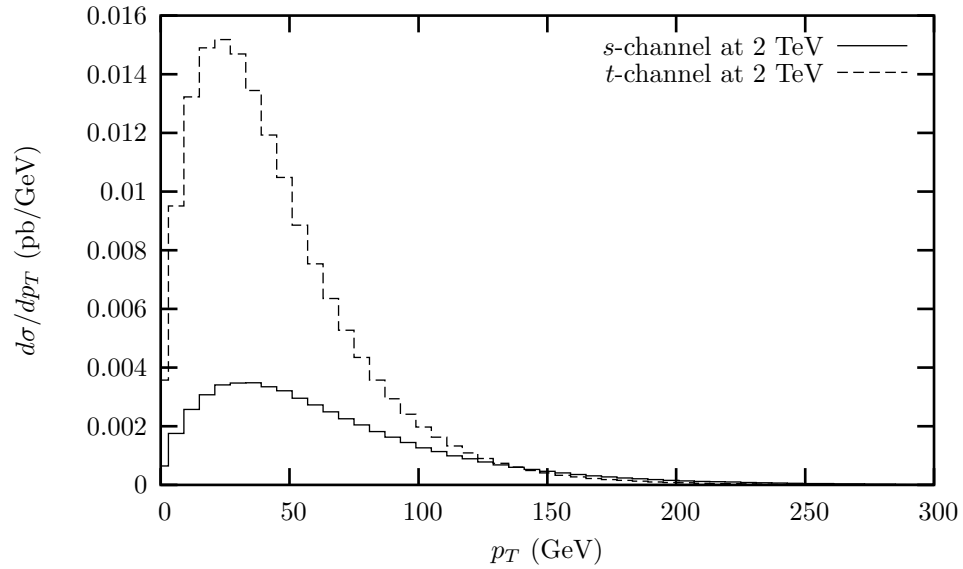


Figure 4.13: Transverse momentum for the single-top processes  $pp \rightarrow tX$  and  $pp \rightarrow \bar{t}X$  at the LHC ( $\sqrt{s} = 14$  TeV). Note that the cross sections for the  $s$ -channels are multiplied with a factor of 10.

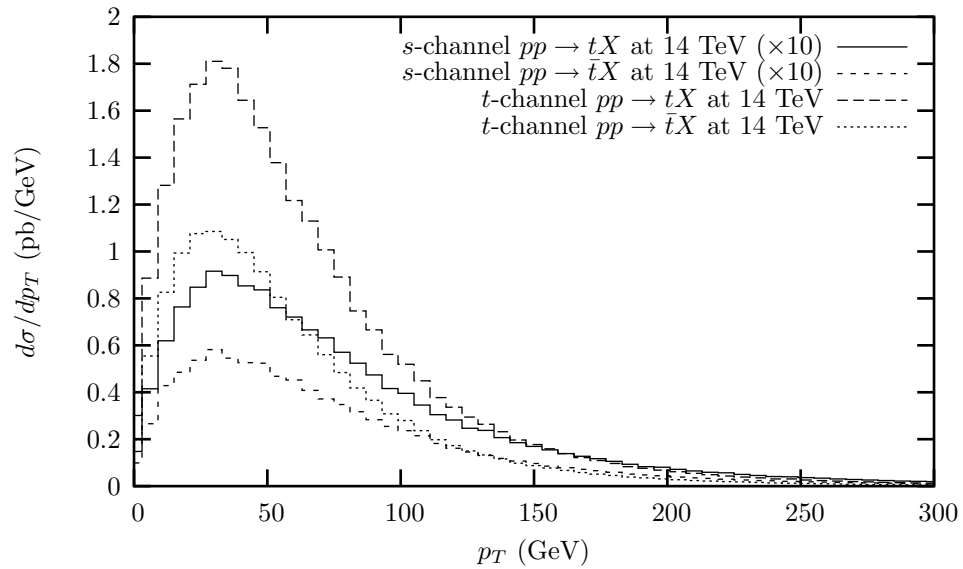


Figure 4.14: Pseudorapidity for the  $s$ -channel single-top process at the Tevatron ( $\sqrt{s} = 2$  TeV) and LHC ( $\sqrt{s} = 14$  TeV). Note that the cross section for the Tevatron is multiplied with a factor of 10.

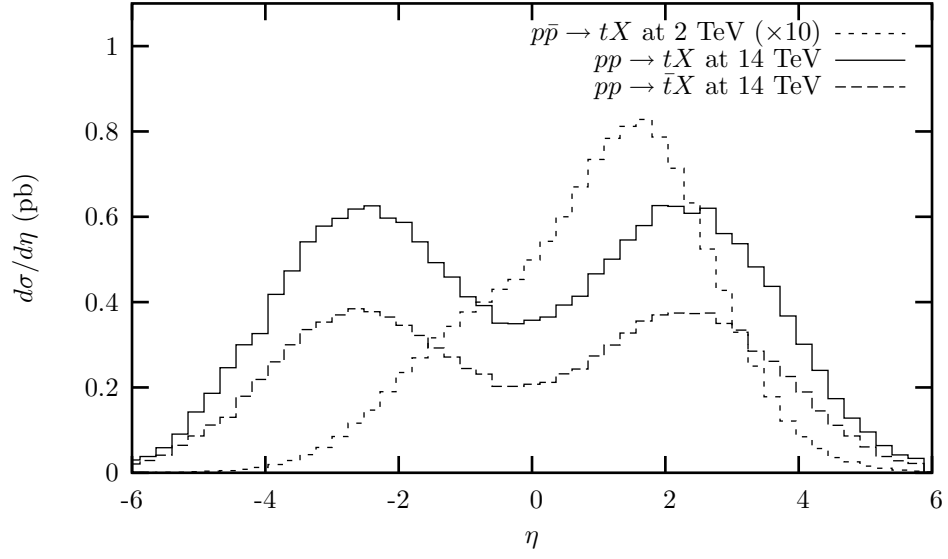


Figure 4.15: Pseudorapidity for the  $t$ -channel single-top process at the Tevatron ( $\sqrt{s} = 2$  TeV) and LHC ( $\sqrt{s} = 14$  TeV). Note that the cross section for the Tevatron is multiplied with a factor of 100.

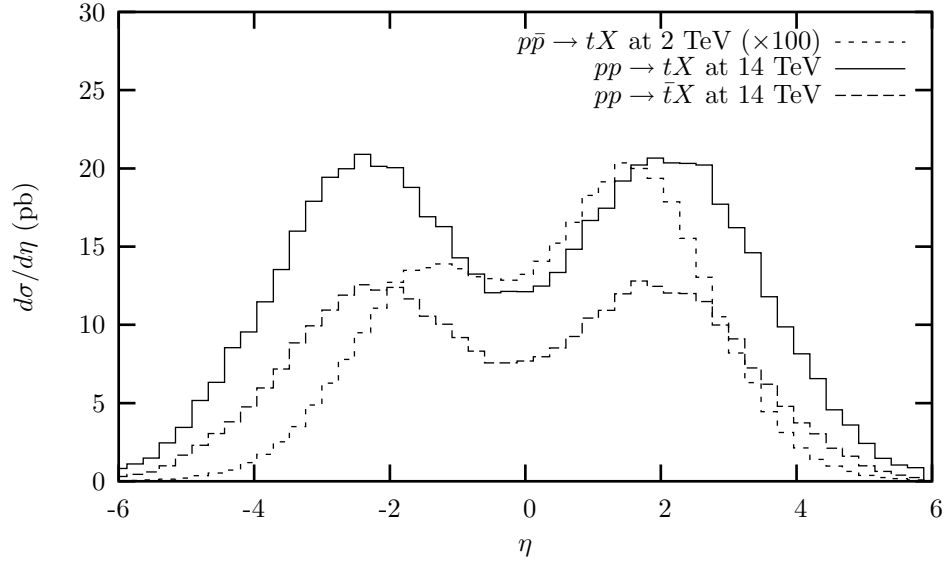


Figure 4.16: Rapidity for the  $s$ -channel single-top process at the Tevatron ( $\sqrt{s} = 2$  TeV) and LHC ( $\sqrt{s} = 14$  TeV). Note that the cross section for the Tevatron is multiplied with a factor of 10.

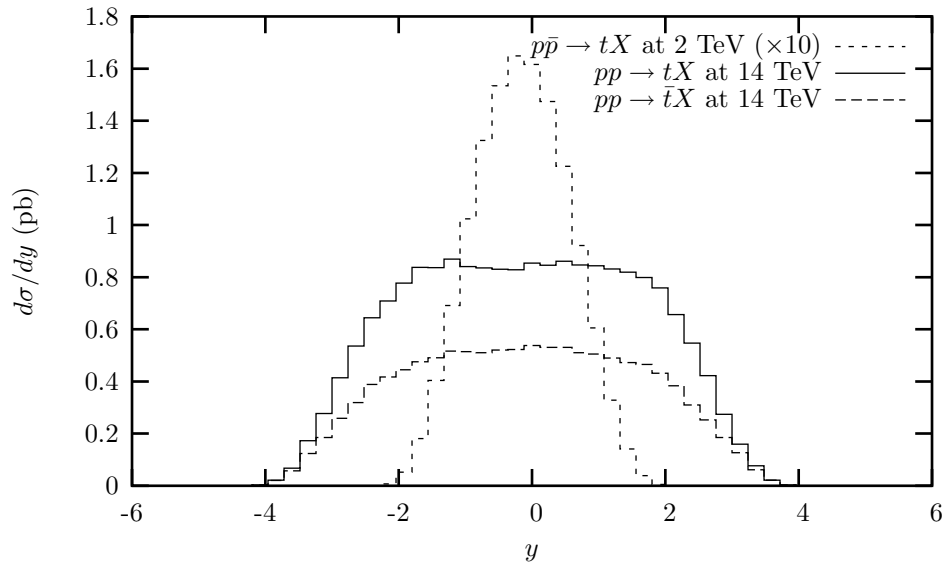
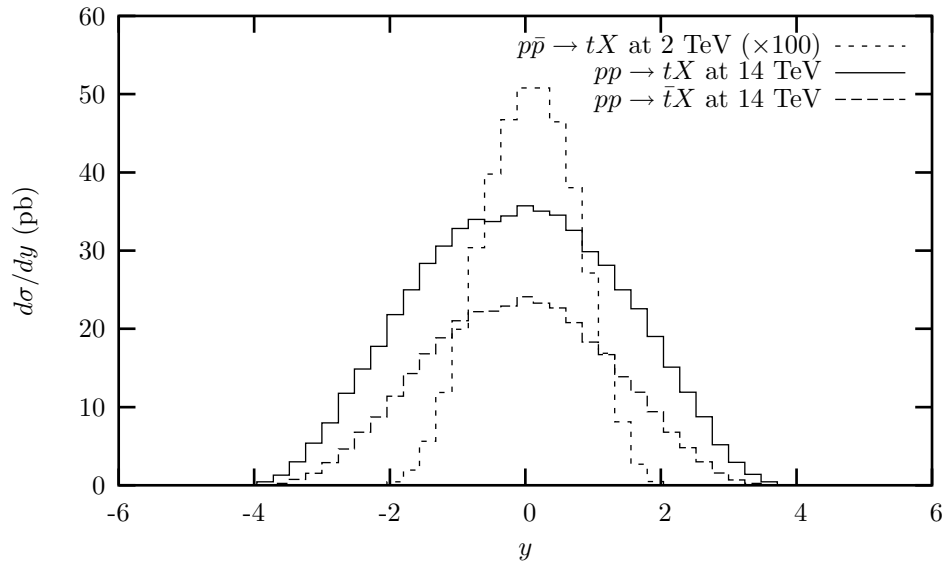


Figure 4.17: Rapidity for the  $s$ -channel single-top process at the Tevatron ( $\sqrt{s} = 2$  TeV) and LHC ( $\sqrt{s} = 14$  TeV). Note that the cross section for the Tevatron is multiplied with a factor of 100.



## 4.4 Top decay

The top quark is really a unique quark. Because of its large mass it has an extremely short lifetime ( $\sim 10^{-25}$  seconds). This lifetime is so short that the top decays before it can hadronize. The top quark is the only known quark that has this property. In general, quarks live long enough to form a bound state with quarks and antiquarks spontaneously that are created from the vacuum. For example, when a  $b$ -quark is created it almost immediately forms a  $B$  meson by hadronizing with an  $\bar{u}$ - or  $\bar{d}$ -quark. After some time the  $B$  meson decays resulting in a jet of hadrons. As it happens, the  $B$  meson has a relative long lifetime and can travel a measurable distance before decaying. By measuring this distance one can determine if a jet originated from a  $b$ -quark. This method is called *b-tagging*.

According to the Standard Model, the dominant top decay mode is  $t \rightarrow W^+b$ . The partial width into the final state  $W^+q$  is proportion to  $|V_{tq}|^2$ . Measurements by CDF Collaboration indicate that [17]

$$\frac{BR(t \rightarrow Wb)}{BR(t \rightarrow Wq)} = \frac{|V_{tb}|^2}{|V_{td}|^2 + |V_{ts}|^2 + |V_{tb}|^2} = 0.94^{+0.31}_{-0.24}. \quad (4.39)$$

This implies that  $|V_{tb}| \gg |V_{td}|, |V_{ts}|$  but does not tell us the absolute magnitude of  $V_{tb}$ .

The  $W$  boson can decay in two different ways. There is leptonic decay,

$$W \rightarrow \ell + \nu_\ell, \quad (4.40)$$

with  $\ell = e, \mu, \tau$ , and there is jet decay

$$W \rightarrow q + \bar{q}' \rightarrow 2 \text{ jets}, \quad (4.41)$$

where  $(q, \bar{q}') = (u, \bar{d}), (c, \bar{s})$ . Other jet decays like  $W \rightarrow q + \bar{b}$  are CKM suppressed. Because the quarks carry color, we find that the decay ratio is approximately

$$\frac{\Gamma(W \rightarrow \ell + \nu_\ell)}{\Gamma(W \rightarrow q + \bar{q}')} = \frac{3}{2 \times 3} = \frac{1}{2}. \quad (4.42)$$

This branching ratio agrees with the data in the Particle Physics Booklet [19]. The  $b$ -quark always decays into a jet. And because the top decays dominantly into a  $b$ -quark and a  $W$ , we see that the top quark only has two decay channels depending on how the  $W$  decays. There is a leptonic decay of the top,

$$t \rightarrow W + b \rightarrow \ell + \nu_\ell + \text{jet}, \quad (4.43)$$

and there is the 3-jets decay of the top

$$t \rightarrow W + b \rightarrow \bar{q} + q' + b \rightarrow 3 \text{ jets}. \quad (4.44)$$

Using  $b$ -tagging it should be easy to detect a top via the leptonic decay. Unfortunately there are several other processes that have the same signature. For this thesis project we have not done any research about background signals of single-top, for more information we refer the interested reader to the literature.

### Decay channels of $t\bar{t}$

There are three different decay channels for the  $t\bar{t}$  process. Dileptonic decay,

$$t + \bar{t} \rightarrow W^+ + b + W^- + \bar{b} \rightarrow \bar{\ell} + \nu_\ell + b + \ell + \bar{\nu}_\ell + \bar{b} \rightarrow \bar{\ell} + \nu_\ell + \ell + \bar{\nu}_\ell + 2 \text{ jets}, \quad (4.45)$$

semileptonic decay,

$$t + \bar{t} \rightarrow W^+ + b + W^- + \bar{b} \rightarrow \bar{\ell} + \nu_\ell + b + q + \bar{q} + \bar{b} \rightarrow \bar{\ell} + \nu_\ell + 4 \text{ jets} \quad (4.46a)$$

$$\rightarrow q + \bar{q} + b + \ell + \bar{\nu}_\ell + \bar{b} \rightarrow \ell + \bar{\nu}_\ell + 4 \text{ jets}, \quad (4.46b)$$

and all-jets decay,

$$t + \bar{t} \rightarrow W^+ + b + W^- + \bar{b} \rightarrow q + \bar{q} + b + q + \bar{q} + \bar{b} \rightarrow 6 \text{ jets}. \quad (4.47)$$

The branching ratios are (ignoring all CKM suppressed decays):

$$\text{dileptonic} : \text{semileptonic} : \text{all-jets} = 1 : 4 : 4. \quad (4.48)$$

## Decay channels of single-top

The decay channels are different for each subprocess. For the  $s$ -channel we have

$$t + \bar{b} \rightarrow W^+ + b + \bar{b} \rightarrow \bar{\ell} + \nu_\ell + b + \bar{b} \rightarrow \bar{\ell} + \nu_\ell + 2 \text{ jets} \quad (4.49a)$$

$$\rightarrow q + \bar{q} + b + \bar{b} \rightarrow 4 \text{ jets}. \quad (4.49b)$$

The  $t$ -channel has exactly the same signature, with the difference that it has only one  $b$ -jet in the final state:

$$t + q \rightarrow W^+ + b + q \rightarrow \bar{\ell} + \nu_\ell + b + q \rightarrow \bar{\ell} + \nu_\ell + 2 \text{ jets} \quad (4.50a)$$

$$\rightarrow q + \bar{q} + b + q \rightarrow 4 \text{ jets}. \quad (4.50b)$$

This difference might be detected with the aid of  $b$ -tagging. Finally, the  $Wt$ -associated single-top production has the decay channels

$$t + W^- \rightarrow W^+ + b + W^- \rightarrow q + \bar{q} + b + q + \bar{q} \rightarrow 5 \text{ jets} \quad (4.51a)$$

$$\rightarrow \bar{\ell} + \nu_\ell + b + q + \bar{q} \rightarrow \bar{\ell} + \nu_\ell + 3 \text{ jets} \quad (4.51b)$$

$$\rightarrow \bar{\ell} + \nu_\ell + b + \ell + \bar{\nu}_\ell \rightarrow \bar{\ell} + \nu_\ell + \ell + \bar{\nu}_\ell + 1 \text{ jet}. \quad (4.51c)$$

## Top decay width

As an exercise we demonstrate in this subsection how one can calculate the lifetime  $\tau = 1/\Gamma$  of the top quark. To find the decay width  $\Gamma$  of the top quark, we first draw the Feynman diagram:



$$(4.52)$$

The invariant amplitude is given by

$$-i\mathcal{M} = \varepsilon_\mu^* \bar{u}_b \left[ \frac{-ig_w}{2\sqrt{2}} \gamma^\mu (1 - \gamma_5) \right] u_t. \quad (4.53)$$

We need to sum over both spin states of the  $b$ , all three helicity states of the  $W$ , and take the average of both spin states of  $t$ . The invariant amplitude squared is then

$$\begin{aligned} \overline{|\mathcal{M}|^2} &= \frac{1}{2} \sum_{\text{all spin}} \sum_{\text{all helicity}} \mathcal{M} \mathcal{M}^* \\ &= \frac{g_w^2}{16} \sum_{\text{all helicity}} \varepsilon_\mu \varepsilon_\nu^* \sum_{\text{all spin}} [\bar{u}_b \gamma^\mu (1 - \gamma_5) u_t] [\bar{u}_b \gamma^\nu (1 - \gamma_5) u_t]^*. \end{aligned} \quad (4.54)$$

With the use of the completeness relations

$$\sum_{\text{helicity}} \varepsilon_\mu \varepsilon_\nu^* = -g_{\mu\nu} + \frac{p_W^\nu p_W^\mu}{m_W^2}, \quad (4.55a)$$

$$\sum_{\text{spin}} u \bar{u} = \not{p} + m, \quad (4.55b)$$

we can write

$$\begin{aligned} \sum_{\text{all spin}} [\bar{u}_b \gamma^\mu (1 - \gamma_5) u_t] [\bar{u}_b \gamma^\nu (1 - \gamma_5) u_t]^* \\ = \sum_{\text{all spin}} [\bar{u}_b (\gamma^\mu - \gamma^\mu \gamma_5) u_t] [\bar{u}_t (\gamma^\nu - \gamma^\nu \gamma_5) u_b] \end{aligned}$$



$$\begin{aligned}
&= \sum_{\text{all spin}} (\bar{u}_b)_\alpha (\gamma^\mu - \gamma^\mu \gamma_5)_{\alpha\beta} (u_t)_\beta (\bar{u}_t)_\gamma (\gamma^\nu - \gamma^\nu \gamma_5)_{\gamma\delta} (u_b)_\delta \\
&= \sum_{\text{spin } b} (u_b)_\delta (\bar{u}_b)_\alpha (\gamma^\mu - \gamma^\mu \gamma_5)_{\alpha\beta} \sum_{\text{spin } t} (u_t)_\beta (\bar{u}_t)_\gamma (\gamma^\nu - \gamma^\nu \gamma_5)_{\gamma\delta} \\
&= (\not{p} + m_b)_{\delta\alpha} (\gamma^\mu - \gamma^\mu \gamma_5)_{\alpha\beta} (\not{p}_t + m_t)_{\beta\gamma} (\gamma^\nu - \gamma^\nu \gamma_5)_{\gamma\delta} \\
&= \text{Tr} \left[ (\not{p} + m_b) \gamma^\mu (1 - \gamma_5) (\not{p}_t + m_t) \gamma^\nu (1 - \gamma_5) \right], \tag{4.56}
\end{aligned}$$

and

$$\begin{aligned}
|\overline{\mathcal{M}}|^2 &= \frac{g_w^2}{16} \left( -g_{\mu\nu} + \frac{p_{W\nu} p_{W\mu}}{m_W^2} \right) \\
&\quad \times \text{Tr} \left[ (\not{p} + m_b) \gamma^\mu (1 - \gamma_5) (\not{p}_t + m_t) \gamma^\nu (1 - \gamma_5) \right]. \tag{4.57}
\end{aligned}$$

This equation can be easily simplified with FORM, resulting in

$$\begin{aligned}
|\overline{\mathcal{M}}|^2 &= \frac{g_w^2}{16} \left[ \frac{4}{m_W^2} (m_t^2 - m_b^2)^2 + 4(m_t^2 + m_b^2) - 8m_W^2 \right] \\
&\approx \frac{g_w^2}{4} \left[ \frac{m_t^4}{m_W^2} + m_t^2 - 2m_W^2 \right]. \tag{4.58}
\end{aligned}$$

In the last step we have neglected the mass of the  $b$ -quark. To find the decay width using (2.79),

$$\Gamma = \frac{|\mathbf{p}_b|}{8\pi m_t^2} |\overline{\mathcal{M}}|^2 = \frac{g_w^2}{32\pi m_t^2} |\mathbf{p}_b| \left[ \frac{m_t^4}{m_W^2} + m_t^2 - 2m_W^2 \right], \tag{4.59}$$

we first need to determine the momentum  $\mathbf{p}_b$ .

In the rest frame of the top quark, the four-momenta of the particle are given by

$$p_t^\mu = (m_t, 0, 0, 0), \tag{4.60a}$$

$$p_b^\mu = (E_b, 0, 0, |\mathbf{p}_b|) = \left( E_b, 0, 0, \sqrt{E_b^2 - m_b^2} \right), \tag{4.60b}$$

$$p_W^\mu = (E_b, 0, 0, -|\mathbf{p}_b|) = \left( E_b, 0, 0, -\sqrt{E_b^2 - m_b^2} \right). \tag{4.60c}$$

Momentum conservation tells us that  $p_t^\mu = p_b^\mu + p_W^\mu$ , and therefore

$$m_t = E_b + E_W, \tag{4.61a}$$

$$E_b^2 - m_b^2 = E_W^2 - m_W^2. \tag{4.61b}$$

Solving this set of equations results in

$$E_b = \frac{m_t^2 + m_b^2 - m_W^2}{2m_t} \approx \frac{m_t^2 - m_W^2}{2m_t} = |\mathbf{p}_b|. \tag{4.62}$$

Substituting the values  $m_W \simeq 80$  GeV,  $m_t \simeq 175$  GeV and  $g_w^2 \simeq 0.43$ , we finally find

$$\begin{aligned}
\Gamma &= \frac{g_w^2}{32\pi m_t^2} |\mathbf{p}_b| \left[ \frac{m_t^4}{m_W^2} + m_t^2 - 2m_W^2 \right] \\
&= \frac{g_w^2}{32\pi m_t^2} \left[ \frac{m_t^2 - m_W^2}{2m_t} \right] \left[ \frac{m_t^4}{m_W^2} + m_t^2 - 2m_W^2 \right] \\
&\approx \frac{g_w^2}{64\pi} \frac{m_t^3}{m_W^2} = 1.79 \text{ GeV}. \tag{4.63}
\end{aligned}$$

The lifetime of the top must then be

$$\tau = \frac{1}{\Gamma} = 0.56 \text{ GeV}^{-1} = 4 \times 10^{-25} \text{ sec}. \tag{4.64}$$

which agrees with the  $10^{-25}$  seconds as stated earlier in this chapter.

## Chapter 5

# The Monte Carlo program

In the previous chapter we have shown how to calculate the invariant amplitude for a process, and we have shown several plots of the (pseudo)rapidity and transverse momentum of the top. In this chapter we explain more about the step between the amplitude and the plots: the Monte Carlo.

If the differential cross section is known, we need to calculate an integral of the form

$$\sigma(pp \rightarrow tX) = \sum_{q,q'} \int \frac{\partial^2 \hat{\sigma}(qq' \rightarrow tX)}{\partial \hat{t}_1 \partial \hat{u}_1} \delta(\hat{s} + \hat{t}_1 + \hat{u}_1) f(x_q) f(x_{q'}) d\hat{t}_1 d\hat{u}_1 dx_q dx_{q'}. \quad (5.1)$$

If there are more than two particles in the final state, we are not able to explicitly determine the differential cross section. In that case we first have to calculate

$$\frac{d\hat{\sigma}}{d\hat{t}_1 d\hat{u}_1} = \overline{|\mathcal{M}|^2} dQ, \quad (5.2)$$

where  $dQ$  is the Lorentz invariant phase space.

In any case, we need to numerically evaluate a multi-dimensional integral. There are several ways to do this, but the Monte Carlo technique as described in this chapter is considered to be the most efficient for high dimensions. Why this is so, is explained in Section 5.1. How the Monte Carlo technique exactly works, is shown in the Section 5.2, including some extensions of the basic idea. In Section 5.3 we talk about the structure of the Monte Carlo program which was used to obtain most of the cross sections and plots in this thesis. In that section we also show some simple ways of testing of the Monte Carlo and state their results.

The first two sections of this chapter are largely based on an excellent introduction to this technique: *Introduction to Monte Carlo methods*, by Stefan Weinzierl [20].

### 5.1 Classical numerical integration

Algorithms for numerical integration have been around for centuries. The classical approach for evaluating 1-dimensional integrals is always the same. Given the integral

$$\int_{x_0}^{x_n} dx f(x), \quad (5.3)$$

first divide the interval  $[x_0, x_n]$  into  $n$  sub-intervals, and evaluate  $f$  for  $n + 1$  points  $x_0, x_1, \dots, x_n$ . Then estimate the area under the curve between each two points  $x_j$  and  $x_{j+1}$ , and sum over all areas. This gives you an estimate of the value of the integral.

Basically there are two ways of doing this: with or without a uniform grid of points. The *Newton-Cotes formulas* work with a uniform grid where each grid point  $x_j$  is given by  $x_j = x_0 + j\Delta x$ , with  $\Delta x = (x_n - x_0)/n$ . The *Gaussian quadrature rules* on the other hand, use orthogonal polynomials to determine the optimal set for  $x_j$ . These are often more efficient than the Newton-Cotes formulas, but are much harder to implement.

## Newton-Cotes formulas

The easiest way to evaluate an integral numerically, is by using the trapezoidal rule

$$\int_{x_0}^{x_0+\Delta x} dx f(x) = \frac{\Delta x}{2} [f(x_0) + f(x_0 + \Delta x)] - \frac{1}{12} (\Delta x)^3 f''(\xi_0), \quad (5.4)$$

where  $x_0 \leq \xi_0 \leq x_0 + \Delta x$ . The area of the function  $f(x)$  between the points  $x_0$  and  $x_0 + \Delta x$  is estimated by the first term, while the second term tells you the size of the error in that estimation. Dividing the integral into  $n$  sub-intervals and summing over the area of each sub-interval, we find

$$\begin{aligned} \int_{x_0}^{x_n} dx f(x) &= \sum_{j=0}^{n-1} \left[ \frac{(x_n - x_0)}{2n} [f(x_j) + f(x_j + \Delta x)] - \frac{1}{12} \frac{(x_n - x_0)^3}{n^3} f''(\xi_j) \right] \\ &= \frac{x_n - x_0}{n} \sum_{j=0}^n w_j f(x_j) - \frac{1}{12} \frac{(x_n - x_0)^3}{n^2} \tilde{f}'', \end{aligned} \quad (5.5)$$

with weights  $w_0 = w_n = 1/2$ , and  $w_j = 1$  for  $1 \leq j \leq n - 1$ . The term

$$\tilde{f}'' = \frac{1}{n} \sum_{j=0}^{n-1} f''(\xi_j) \quad (5.6)$$

can be considered as the average error. Since the exact values of  $\xi_j$  are unknown, we cannot calculate this term and we estimate the value of the integral with

$$\int_{x_0}^{x_n} dx f(x) = \frac{(x_n - x_0)}{n} \sum_{j=0}^n w_j f(x_j), \quad (5.7)$$

while the error is of order  $\mathcal{O}(1/n^2)$ . To do this integration, we need  $n + 1$  evaluations of  $f(x)$ . The number of function-evaluations is important, because this is usually the most time-consuming.

An big improvement to the trapezoidal rule is the so-called Simpson's rule. It uses the evaluation of  $f(x)$  at three points:

$$\int_{x_0-\Delta x}^{x_0+\Delta x} dx f(x) = \frac{\Delta x}{3} [f(x_0 - \Delta x) + 4f(x_0) + f(x_0 + \Delta x)] - \frac{1}{90} (\Delta x)^5 f^{(4)}(\xi_0), \quad (5.8)$$

with  $x_0 - \Delta x \leq \xi_0 \leq x_0 + \Delta x$ . The total integral then becomes

$$\int_{x_0}^{x_n} dx f(x) = \frac{x_n - x_0}{n} \sum_{j=0}^n w_j f(x_j) - \frac{1}{180} \frac{(x_n - x_0)^5}{n^4} \tilde{f}^{(4)}, \quad (5.9)$$

with  $w_0 = w_n = 1/3$ , and  $w_j = 4/3$  for even  $j$ , and  $w_j = 2/3$  if  $j$  is odd. We see that Simpson's rule leads to numerical integration with an error of order  $\mathcal{O}(1/n^4)$ .

Simpson's rule can be improved even further. Boole's rule uses the evaluation of  $f(x)$  at five points,

$$\begin{aligned} \int_{x_0-2\Delta x}^{x_0+2\Delta x} dx f(x) &= \frac{2\Delta x}{45} [7f(x_0 - 2\Delta x) + 32f(x_0 - \Delta x) + 12f(x_0) \\ &\quad + 32f(x_0 + \Delta x) + 7f(x_0 + 2\Delta x)] - \frac{8(\Delta x)^7}{945} f^{(6)}(\xi_0), \end{aligned} \quad (5.10)$$

which leads to an error of order  $\mathcal{O}(1/n^6)$ .

The trapezoidal rule, Simpson's rule, and Boole's rule are all examples of the more general class of Newton-Cotes formulas. If you start with a rule that uses  $2k - 1$  evaluations of  $f(x)$ , one ends up with a numerical integration of order  $\mathcal{O}(1/n^{2k})$ . However, these formulas have two mayor problems. If the function is not smooth, the values for the derivatives  $f^{(2k)}(x)$  can become quite large, causing a large error term. Secondly, when  $k$  becomes large some of the coefficients in the Newton-Cotes formulas become large and of mixed sign. It is well known that when you add or subtract small numbers from big numbers, the result will be substantially large numerical errors. Therefore the trapezoidal rule and Simpson's rule are most often used instead of the rules of higher order.

## Gaussian quadrature rules

The Gaussian quadrature rules are a generalization of the Newton-Cotes formulas. Instead of using a uniform grid of points, we now choose the points in such a way to get the best estimation for the integral. But how do we determine the optimal grid? And how do we find the proper weight for each point?

The trick with Gaussian quadrature rules is that we approximate  $f(x)$  with a polynomial. We can do this only for the interval  $x \in [-1, 1]$ , because for  $|x| \geq 1$  the values of the polynomials tend to become very large. We can extend our interval to  $[0, \infty]$  or  $[-\infty, \infty]$  by using a weight function  $W(x)$ . The integral we wish to evaluate is then

$$I = \int_a^b dx W(x) f(x). \quad (5.11)$$

The weight function makes sure that the integral nicely converges on the given interval. More explicitly,  $W(x)$  is defined such that  $W(x) \geq 0$  for all  $x \in [a, b]$ ,  $\int_a^b dx W(x) > 0$  and  $\int_a^b dx x^n W(x) < \infty$  for all  $n = 0, 1, 2, \dots$

Given the integral of (5.11) the Fundamental Theorem of Gaussian Quadrature [21] states that the optimal choice for a grid of  $n$  points is given by the  $x_j$  for which

$$P_n(x_j) = 0, \quad (5.12)$$

where  $P_n$  is the  $n$ -th orthogonal polynomial with respect to the weight function  $W$ :

$$\int_a^b dx W(x) P_k(x) P_m(x) = \delta_{km}. \quad (5.13)$$

The roots  $x_j$  of the orthogonal polynomials associated with the  $W$  on the interval are real and distinct and are located in the interior of the interval  $[a, b]$ . For example, if  $n = 4$  and  $W(x) = \exp(-x^2)$  for the interval  $(-\infty, \infty)$ ,

$$I = \int_{-\infty}^{\infty} dx \exp(-x^2) f(x), \quad (5.14)$$

then the grid points  $x_j$  are given by the roots of the 4-th Hermite polynomial

$$H_4(x) = 16x^4 - 48x^2 + 12, \quad (5.15)$$

which are

$$x_j = \pm \frac{1}{2} \sqrt{6 \pm 2\sqrt{6}}. \quad (5.16)$$

To find a polynomial that closely approximates the function  $f(x)$ , we use Lagrange interpolation through the  $n$  points  $f(x_j)$ :

$$\phi_n(x) = \sum_{j=1}^n \frac{\pi_n(x)}{(x - x_j) \pi_n'(x_j)} f(x_j), \quad (5.17)$$

where

$$\pi_n(x) = (x - x_0)(x - x_1) \cdots (x - x_n). \quad (5.18)$$

The integral (5.11) is then

$$\int_a^b \phi_n(x) W(x) dx = \int_a^b \sum_{j=1}^n \frac{\pi_n(x)}{(x - x_j) \pi_n'(x_j)} f(x_j) W(x) dx + E_n = \sum_{j=1}^n w_j f(x_j) + E_n \quad (5.19)$$

where  $E_n$  is the error

$$E_n = \frac{f^{(2n)}(\xi)}{(2n)!} \int_a^b dx W(x) [\pi(x)]^2, \quad (5.20)$$

and where  $w_j$  are weight factors given by

$$w_j = \int_a^b \frac{\pi_n(x) W(x)}{(x - x_j) \pi_n'(x_j)} dx. \quad (5.21)$$

This integral is independent of the function  $f(x)$ . In Gaussian quadrature rules the weights are all positive and therefore we do not have here the same problems as with the Newton-Cotes formulas.

## Multi-dimensional integration

It is not hard to extend the Newton-Cotes formulas to multi-dimensional integrals. For example, an integral over the  $d$ -dimensional hypercube  $[0, 1]^d$  can be evaluated with the trapezoidal rule as

$$\int d^d x f(x_1, \dots, x_d) = \frac{1}{n^d} \sum_{j_1=0}^n \cdots \sum_{j_d=0}^n w_{j_1} \cdots w_{j_d} f\left(\frac{j_1}{n}, \dots, \frac{j_d}{n}\right) + \mathcal{O}\left(\frac{1}{n^2}\right). \quad (5.22)$$

For this calculation we need to evaluate the function  $N = (n + 1)^d \approx n^d$  times. For high dimensions this number will get really big which means that the algorithm will be really slow. The error is still of order  $\mathcal{O}(1/n^2)$ , but in terms of the total number of function evaluations  $N$  it is  $\mathcal{O}(1/N^{2/d})$ .

Using Simpson's rule instead of the trapezoidal rule improves the situation a bit, but not by much. The error is of order  $\mathcal{O}(1/n^4) = \mathcal{O}(1/N^{4/d})$ . The real solution to this problem is to use Monte Carlo integration. In the next section we will show that for a Monte Carlo the error goes like  $\mathcal{O}(1/\sqrt{N})$ . In other words, we can halve the error if we take four times as many sample points. This technique is not so fast, but at least it is independent of the dimension. It will therefore be a better option than Simpson's rule when  $d > 8$ .

## 5.2 Monte Carlo techniques

In a way, Monte Carlo integration can be seen as an extension to the classical numerical integration methods. The Gaussian quadrature rules are more efficient than the Newton-Cotes formulas, because a more efficient grid is used, meaning that we need less function evaluations to get to the same accuracy. With Monte Carlo we get a much better efficiency by not using grid points at all. Instead we choose our points randomly in the integration space. That this actually works might seem to be a miracle at first, but will soon be made clear.

There are many advantages in using a Monte Carlo. The implementation is relatively simple, it can easily handle complicated integration boundaries, and as said before, the efficiency is independent of the dimension of the integral. However, the basic Monte Carlo method is far from perfect: it converges quite slowly with a rate of  $\mathcal{O}(1/\sqrt{N})$  to the correct value. There are several techniques to improve this, and these will be discussed in this section after we explain the basic principle of the Monte Carlo method.

### Basic principle

Evaluating an integral is equivalent to calculating the mean value of a function within a certain interval  $[a, b]$ . Therefore we can also estimate the value of an integral by taking a large number of samples from  $[a, b]$  and then determine the average. This is the principle behind Monte Carlo integration.

If  $\mathbf{x}_j = (u_1, \dots, u_d)$  is a random sample from the hypercube  $[0, 1]^d$  then the average value of  $N$  samples is

$$\mu = \frac{1}{N} \sum_{n=1}^N f(\mathbf{x}_n). \quad (5.23)$$

Given the integral

$$I = \int d\mathbf{x} f(\mathbf{x}) = \int d^d u f(u_1, \dots, u_d), \quad (5.24)$$

then according to the law of large numbers our estimate  $\mu$  converges to the true value of the integral,

$$\lim_{N \rightarrow \infty} \frac{1}{N} \sum_{n=1}^N f(\mathbf{x}_n) = I. \quad (5.25)$$

Hence,  $I$  is the mean value of our distribution, with  $\mu$  its estimate. Choosing a finite  $N$  causes an error, which can be estimated by using the variance. It can be shown that if  $f$  is square integrable<sup>1</sup>,

$$\mu^2 = \int d\mathbf{x}_1 \cdots \int d\mathbf{x}_N \left( \frac{1}{N} \sum_{n=1}^N f(\mathbf{x}_n) - I \right)^2 = \frac{\sigma^2(f)}{N}, \quad (5.26)$$

---

<sup>1</sup>If  $f$  is not square integrable the estimate  $E$  will still converge to the value  $I$ , but the error estimate will not be reliable anymore.

where  $\sigma^2(f)$  is the variance of the function  $f(\mathbf{x})$ ,

$$\sigma^2(f) = \int d\mathbf{x} (f(\mathbf{x}) - I)^2. \quad (5.27)$$

From Equation (5.26) we see the statistical error  $E$  of the estimate  $\mu$  is on average  $\sigma(f)/\sqrt{N}$ , i.e. of order  $\mathcal{O}(1/\sqrt{N})$ . Note also that there is no reference to the dimension  $d$  in the error.

That the error is independent of the dimension can also be seen with the following. According to the center limit theorem the probability that the error lies between  $I \pm a\sigma(f)/\sqrt{N}$  is given by

$$\lim_{N \rightarrow \infty} P \left( -a \frac{\sigma(f)}{\sqrt{N}} \leq \frac{1}{N} \sum_{n=1}^N f(\mathbf{x}_n) - I \leq a \frac{\sigma(f)}{\sqrt{N}} \right) = \frac{1}{\sqrt{2\pi}} \int_{-a}^a dt \exp\left(-\frac{t^2}{2}\right). \quad (5.28)$$

Because the integral  $I$  is unknown, we cannot use (5.27) to calculate  $\sigma(f)/\sqrt{N}$ . Instead we must estimate the variance with

$$S^2 = \frac{1}{N} \sum_{n=1}^N (f(\mathbf{x}_n) - \mu)^2 \approx \int dx (f(\mathbf{x}) - I)^2 = \mu^2. \quad (5.29)$$

Using (5.23) this can also be written as

$$S^2 = \frac{1}{N} \sum_{n=1}^N \left( [f(\mathbf{x}_n)]^2 - 2\mu f(\mathbf{x}_n) + \mu^2 \right) = \frac{1}{N} \sum_{n=1}^N [f(\mathbf{x}_n)]^2 - \mu^2. \quad (5.30)$$

## Improvements

Improving the rate of the convergence can be done by lowering the variance in Equation (5.26). This can be done in a number of different ways. In a technique known as *stratified sampling* one divides the full integration space in several subspaces. For example, if we divide the hypercube  $[0, 1]^d$  in two equally large parts  $a$  and  $b$ , the total statistical error becomes

$$\mu = \frac{1}{2} \sqrt{\frac{\sigma_a^2(f)}{N_a} + \frac{\sigma_b^2(f)}{N_b}}, \quad (5.31)$$

where  $\sigma_j^2(f)$  is the variance of  $f(\mathbf{x})$  in the subspace  $j$ , and  $N_j$  is the number of samples drawn from subspace  $j$ . Clearly, if  $\sigma_a^2(f) \gg \sigma_b^2(f)$  it would be wise to take  $N_a \gg N_b$ , because that would lower the total variance. In general, by choosing the correct subspaces one can lower the statistical error significantly. The best results are obtained when  $N_j$  is chosen proportional to  $\sigma_j^2(f)$ .

*Importance sampling* is a different technique which uses random numbers drawn from a pre-defined probability distribution  $P(\mathbf{x})$ . The probability density function for this distribution is then

$$p(\mathbf{x}) = \frac{dP(\mathbf{x})}{d\mathbf{x}} = \frac{\partial^d P(u_1, \dots, u_d)}{\partial u_1 \cdots \partial u_d}, \quad (5.32)$$

with  $p(\mathbf{x}) \geq 0$  and

$$\int d\mathbf{x} p(\mathbf{x}) = 1. \quad (5.33)$$

With the help of this function we can write our integral  $I$  as

$$I = \int d\mathbf{x} f(\mathbf{x}) = \int \frac{f(\mathbf{x})}{p(\mathbf{x})} p(\mathbf{x}) d\mathbf{x} = \int \frac{f(\mathbf{x})}{p(\mathbf{x})} dP(\mathbf{x}). \quad (5.34)$$

Our estimate of  $I$  is then

$$\mu = \frac{1}{N} \sum_{n=1}^N \frac{f(\mathbf{x}_n)}{p(\mathbf{x}_n)}, \quad (5.35)$$

and for the (estimated) variance we have

$$S^2 = \frac{1}{N} \sum_{n=1}^N \left( \frac{f(\mathbf{x}_n)}{p(\mathbf{x}_n)} \right)^2 - \mu^2. \quad (5.36)$$

From this it is clear that if we choose a  $p(\mathbf{x})$  with a similar shape as  $|f(\mathbf{x})|$ , that the variance can become very small. The perfect choice is

$$p(\mathbf{x}) = \frac{f(\mathbf{x})}{\int f(\mathbf{x}) d\mathbf{x}} = \frac{f(\mathbf{x})}{I}, \quad (5.37)$$

for which the error goes to zero for large  $N$ . However, because the integral  $I$  is unknown it is impossible to calculate  $p(\mathbf{x})$  in this way.

We have to be careful with importance sampling techniques: if somewhere  $p(\mathbf{x})$  approaches zero, the variance  $S^2$  might become intolerably large.

## The adaptive VEGAS-algorithm

Stratified sampling and importance sampling can only be used efficiently if one has knowledge about the integral prior to the integration. Unfortunately this information is often not available. The solution to this is to use an adaptive algorithm. Starting from some default setting, the algorithm does a quick numerical integration and uses that result to learn more about the integral itself. With that knowledge the algorithm does another integration, just as quickly, but more efficient. This is then done again and again. After each step, the integration becomes more and more efficient.

An example of such an algorithm is the VEGAS algorithm [22]. It is based upon both importance sampling and stratified sampling. It starts by dividing the integration space in a rectangular grid of subspaces<sup>2</sup>. Using the results of the integration of each subspace the grid is adjusted accordingly, in a similar manner as was done with the stratified sampling technique.

To become even more efficient, the VEGAS algorithm tries to approximate (5.37) with a step function

$$p(\mathbf{x}) = w_j(\mathbf{x}) \approx \frac{|f(\mathbf{x})|}{\int |f(\mathbf{x})| d\mathbf{x}}, \quad (5.38)$$

i.e. by giving each subspace  $j$  a value  $w_j$ . In two dimensions  $p$  would look like a 2-dimensional histogram with  $m^2$  bins, where  $m$  is the number of subspaces per dimension. For  $d$  dimensions that would mean that we need to store  $m^d$  bins in our computer memory, a number that grows exponentially with  $d$ . To prevent that, we assume that  $p(\mathbf{x})$  can be factorized:

$$p(u_1, \dots, u_d) = p_1(u_1) \cdot p_2(u_2) \cdot \dots \cdot p_d(u_d). \quad (5.39)$$

Storing this in our memory would only acquire  $m \times d$  bins. The probability density function  $p$  should approximate  $f$ , so (5.39) is only effective when also  $f$  is approximately factorizable. In other words, using  $p$  only increases the efficiency of the Monte Carlo substantially when the peaks of  $f$  are well-localized.

Each iteration  $i$  results in an estimate for  $I$ ,

$$I \approx \mu_i = \frac{1}{N_i} \sum_{n=1}^{N_i} \frac{f(\mathbf{x}_n)}{p(\mathbf{x}_n)}, \quad (5.40)$$

and an estimate for the statistic error  $E$ ,

$$E^2 \approx S_i^2 = \frac{1}{N_i} \sum_{n=1}^{N_i} \left( \frac{f(\mathbf{x}_n)}{p(\mathbf{x}_n)} \right)^2 - \mu_i^2. \quad (5.41)$$

The results of  $r$  iterations can be combined into one cumulative estimate of  $I$ , weighted by the number of function evaluations  $N_i$  and their variances  $S_i$ :

$$\mu = \left( \sum_{i=1}^r \frac{N_i}{S_i^2} \right)^{-1} \left( \sum_{i=1}^r \frac{N_i E_i}{S_i^2} \right). \quad (5.42)$$

With the VEGAS algorithm it also possible to calculate a  $\chi^2$  per degree of freedom:

$$\chi^2/\text{dof} = \frac{1}{r-1} \sum_{i=1}^r \frac{(\mu_i - \mu)^2}{S_i^2}. \quad (5.43)$$

The value of this should be close to one, and can be used to check if the error estimates  $S_j$  are reliable.

---

<sup>2</sup>Note that in this case we do not choose samples that are points on the grid (as with the classical integration methods). In Monte Carlo's the grid is only there to divide the total integration space in the smaller subspaces.

## 5.3 The program

There are many excellent Monte Carlo programs available for calculating cross sections for many different processes known in high energy physics. For pedagogical reasons however, we have create our own Monte Carlo. In this section we discuss the structure of the final program, in order to give the reader a nice example of the implementation of a Monte Carlo which uses the VEGAS algorithm. An example of the generated output in the terminal is seen in Figure 5.2. The classes and their relations are summarized in the diagram of Figure 5.1.

```

-----
Version:                April 19th, 2006
Random number generator: RANMAR
PDF tabel:              CTEQ5L
Mass of top quark:     m[t] = 175 GeV
Scales:                 mu[R] = mu[F] = 175 GeV
Number of dimensions:   4
Number of iterations:   5
Number of events/iter:  200000
Accelerator/energy:     LHC (pp at 14 TeV)
Process:                Standard Model s-channel single-top
                       (anti-top in final state)

Cross sections in pb.
-----
iteration 1:  2.85539 +/- 0.12043   Total:  2.85539 +/- 0.12043
iteration 2:  2.78367 +/- 0.0183155 Total:  2.78529 +/- 0.0181073
iteration 3:  2.7687 +/- 0.0121595   Total:  2.77386 +/- 0.0100946
iteration 4:  2.77193 +/- 0.0114858   Total:  2.77302 +/- 0.00758238
iteration 5:  2.77369 +/- 0.0119767   Total:  2.77321 +/- 0.00640644

-----
Result = 2.77321 +/- 0.00640644, Chi2 = 0.943374
-----
Area of pT histogram:      2.78784 pb
Area of rapidity histogram: 2.79068 pb
Area of pseudorapidity histogram: 2.7778 pb
-----
Finished! Simulation took 23 seconds (0.383333 minutes)

```

Figure 5.1: Output of the Monte Carlo program for the Standard Model single-top  $s$ -channel process at the LHC, with  $\bar{t}$  in the final state.

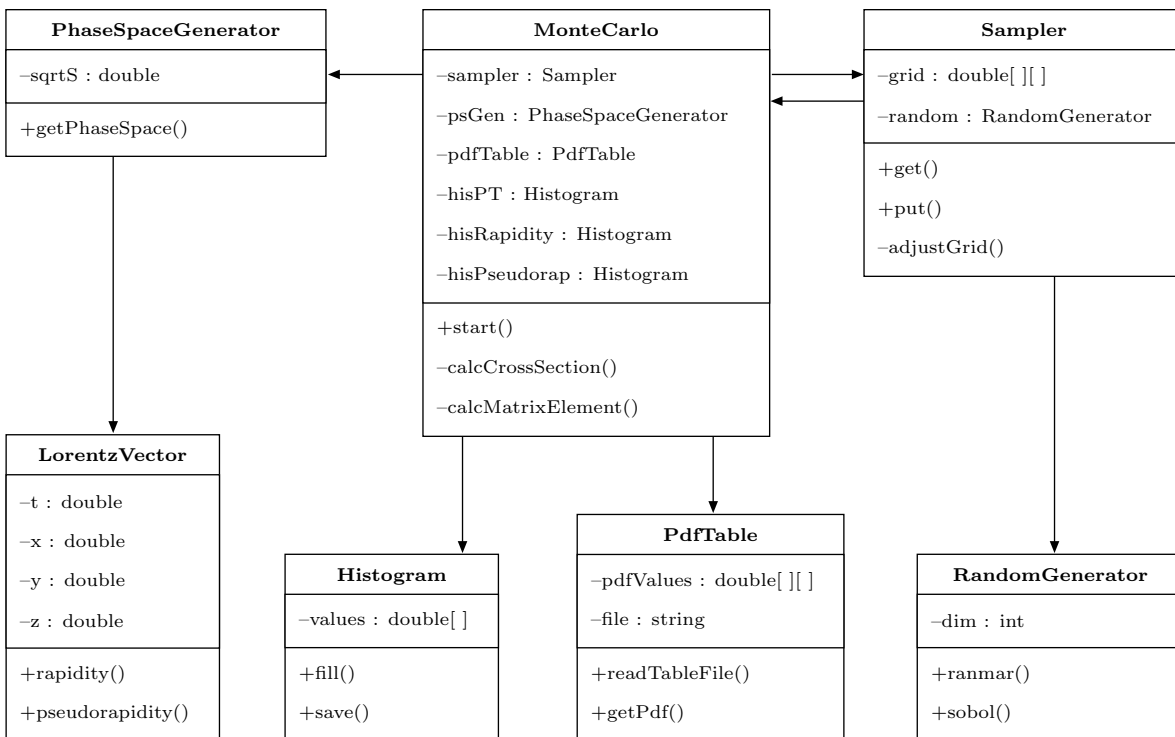


Figure 5.2: Class diagram of the Monte Carlo program. Only the most relevant functions and their relations are shown here.



## The MonteCarlo class

The central nervous system of the program is the `MonteCarlo` class. It contains all the simulation settings including the number of iterations, the number of events (samples) in each iteration, which type of random generator is used, the hadronic center-of-mass energy  $\sqrt{s}$ , and the process that is to be analyzed. The class contains several public functions to make it possible to change these settings.

The main task of this class is quite simple. When the function `start()` is called, the program starts to run a simulation using the given settings. After initializing all the needed objects and printing the settings to the terminal, the program enters a simple loop:

```
while (sampler.get(r, wgt)) {
    dsig = calcDiffCrossSection(r, wgt);
    sampler.put(r, wgt, dsig);
}
```

These lines form the core of the program. In the first line we ask the `sampler` for an event, using the function `get(double r[], double& wgt)`. This function fills the array `r` with random values and assigns to `wgt` the weight of this sample. This weight is proportional to the size of the subspace and is there to correct for the fact that more samples will be drawn from the larger subspaces. The `Sampler` class keeps track of the number of iterations done and makes sure that `get()` will return `false` if it has reached the maximal number of iterations, as specified by the Monte Carlo settings.

In the second line the cross section is calculated for the given event. Finally in the third line the sample `r`, the weight `wgt` and evaluated value `dsig` are given back to the `Sampler`. These values will be used by the `Sampler` to estimate the best adjustment to be made to the grid when the iteration is finished. How this is done exactly is explained in the next section.

## Calculating the cross section

In `calcDiffCrossSection()` the first step in calculating the cross section is to obtain the momentum fractions  $x_1$  and  $x_2$  of the initial two partons. These are two variables over which we need to integrate and therefore we obtain these values by `x1 = r[0]` and `x2 = r[1]`, where `r` is our array with random values.

In order to create a top quark, the initial partons should have an energy large enough to produce the top mass,

$$x_1 x_2 s > m_t^2. \quad (5.44)$$

If this inequality is satisfied, the next step is calculating the phase space. This is done with the function `getPhaseSpace()` of the `PhaseSpaceGenerator` class which calculates the momenta of the initial and final particles, and returns the phase space  $dQ$ . More about this in the section about the `PhaseSpaceGenerator`.

Knowing the momenta of all the particles, we are now able to calculate the total invariant amplitude for this event. This is done by the function `calcMatrixElement()` which uses the PDF values of the `PdfTable` class. For example, we saw in Chapter 4 that the  $|\overline{\mathcal{M}}|^2$  for the  $t\bar{t}$  process via quark-antiquark annihilation was given by

$$|\overline{\mathcal{M}}|^2 = \frac{4}{9} \frac{16\pi^2 \alpha_s^2}{\hat{s}^2} (\hat{u}_1^2 + \hat{t}_1^2 + 2m_t^2 \hat{s}). \quad (5.45)$$

The invariant amplitude summed over all available quarks and anti-quarks is then

$$\sum_{q,\bar{q}} |\overline{\mathcal{M}}|^2 = |\overline{\mathcal{M}}|^2 \Phi_{q\bar{q}}, \quad (5.46)$$

where the  $q\bar{q}$ -flux  $\Phi_{q\bar{q}}$  is given by

$$\begin{aligned} \Phi_{q\bar{q}} = & f_1(x_u) f_2(x_{\bar{u}}) + f_1(x_{\bar{u}}) f_2(x_u) + f_1(x_d) f_2(x_{\bar{d}}) + f_1(x_{\bar{d}}) f_2(x_d) \\ & + f_1(x_c) f_2(x_{\bar{c}}) + f_1(x_{\bar{c}}) f_2(x_c) + f_1(x_s) f_2(x_{\bar{s}}) + f_1(x_{\bar{s}}) f_2(x_s) \\ & + f_1(x_b) f_2(x_{\bar{b}}) + f_1(x_{\bar{b}}) f_2(x_b). \end{aligned} \quad (5.47)$$

Here  $f_i(x_p)$  is the parton distribution function of parton  $p$  for proton  $i$ . After the amplitude and the phase space are determined, the cross section for this particular event is then calculated by

$$d\sigma = \left( |\overline{\mathcal{M}}|^2 \Phi_{q\bar{q}} \right) dQ. \quad (5.48)$$

Also the (pseudo)rapidity and the transverse momentum of the top quark are calculated. These are then added to their corresponding histogram together with a weight factor  $w$  to indicate how much the value should contribute to the histogram. For example, for the histogram of  $d\sigma/dp_T$  we add  $w \times p_T$  instead of  $p_T$ . The weight factor is equal to  $d\sigma$  multiplied by the `wgt` from the event. In this way  $d\sigma/dp_T$  will be proportionally low when  $d\sigma$  is low, and because of the `wgt` we may be sure that the size of the subspace has no influence the histogram<sup>3</sup>.

## The Sampler class

The VEGAS algorithm is hidden inside the `Sampler` class. The `Sampler` fabricates event samples  $\mathbf{x}_j$  for the `MonteCarlo` and receives in return the function evaluations  $f(\mathbf{x}_j)$ . These evaluations are stored in histograms, one for each dimension. After an iteration is finished, these histograms are used to adjust the grid such that the subspace is small for the places where the slope of  $f$  is large.

There are three important functions in this class: `get()` returns a sample  $\mathbf{x}_j$ , `put()` stores the given  $f(\mathbf{x}_j)$  into the histograms and the private function `adjustGrid()` changes the grid after each iteration. When `get(double r[], double& wgt)` is called, the `RandomGenerator` class is used to obtain a pseudorandom number for each dimension. Each random number is then split into two smaller numbers, an integer and a double. The integer is used to randomly pick a subspace, and after that the double is used to randomly pick a position  $x$  within that subspace. This is done for each dimension and the vector of  $x$ -values is then returned as the array `r`. The weight `wgt` is determined by

$$w_j = \frac{1}{N_{\text{ev}} N_{\text{it}}} \frac{1}{V_j}, \quad (5.49)$$

where  $V_j$  is the volume of the subspace, and  $N_{\text{ev}}, N_{\text{it}}$  are the total number of events and iterations.

The function `put(r, wgt, dsig)` is not much more complicated. The goal is to approximate the optimal probability density function  $p$  in (5.38) for which

$$p(u_1, \dots, u_d) = p_1(u_1) \cdot p_2(u_2) \cdot \dots \cdot p_d(u_d), \quad (5.50)$$

where the  $p_i(u_i)$  are treated as histograms. Given a  $f(\mathbf{x}_j) = f(u_{j1}, u_{j2}, \dots, u_{jd})$ , this value is then added to the corresponding bins of each histogram.

The most complicated part of the `Sampler` is in the `adjustGrid()` function. We shall not examine the exact implementation of the function in much detail, because that is beyond the scope of this thesis. We can however show the algorithm in action by evaluating for example the integral

$$\int f(x, y) \, dx \, dy = \int_0^1 \exp\left(-10\left(x - \frac{1}{2}\right)^2 - 10\left(y - \frac{1}{2}\right)^2\right) \, dx \, dy. \quad (5.51)$$

This is also a perfect way for testing the `Sampler`. Notice that the function  $f(x, y)$  can be factorized, we therefore expect a maximal adjustment of the grid.

Each dimension is divided into 50 subspaces. Since  $f(x, y)$  is a function of two dimensions, we have here a 2-dimensional plane divided into  $50 \times 50$  small squares. The program always starts with a uniform grid. After the first iteration the grid points are distributed as can be seen in the left plot of Figure 5.4. After five iterations the grid becomes more and more dense near the center. This can be seen in the right plot of Figure 5.4.

After five iterations, the grid look like Figure 5.4b. It hardly changes anymore after an iteration and one can see clearly that the subspaces are more dense at the places where the integrand  $f(x, y)$  is behaving more wildly: the slope of the function is larger near the origin. The `Sampler` finds the correct value of 0.298. This simple test has convinced us that `Sampler` is doing its work properly.

## The RandomGenerator class

Creating random numbers is not as simple as one might expect. This is because the efficiency and accuracy of the Monte Carlo are directly related to the efficiency and accuracy of the random number generator. We highlight here three points of criteria that indicate how well the generator behaves.

---

<sup>3</sup>Even though the exact size of the subspaces should have no influence, don't forget that deviding the integration space in different subspaces does provoke that most samples are drawn from the largest subspace. Where the integrand behaves more 'wildly', we need a bigger to obtain a better accuracy.

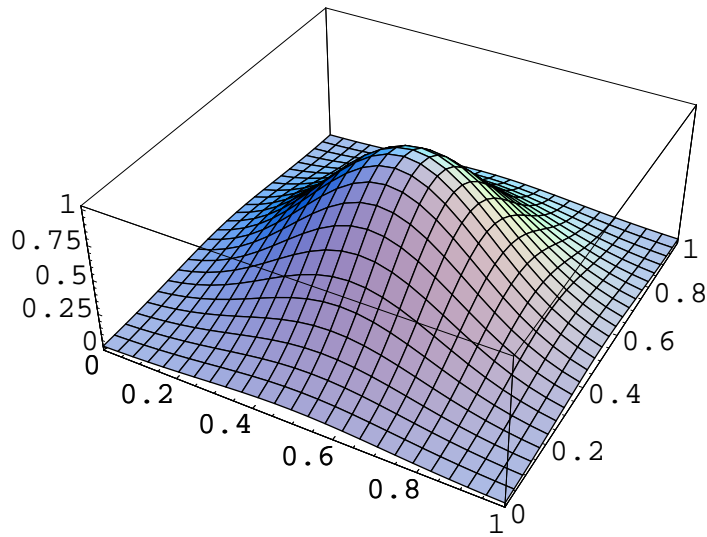


Figure 5.3: Plot of the integrand of Equation (5.51).

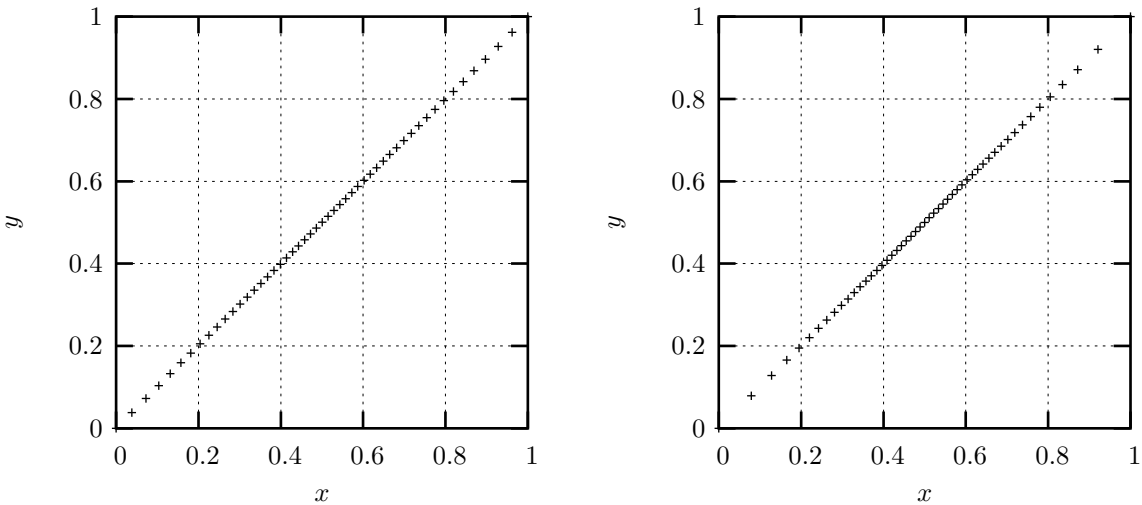


Figure 5.4: The distribution of grid points for (5.51) after the first iteration (left plot) and after 5 iterations (right plot).

First of all, the distribution. To prevent parts of the integration space to be biased, the generated numbers need to have a very uniform distribution. This is not an easy task, since a computer is a deterministic machine and hence can never produce truly random numbers. We need an algorithm that produces numbers that look random (pseudo-random numbers) or numbers that are not random at all, but do have a very uniform distribution (quasi-random numbers).

In many random generators the next random number is determined by using the previous number. Unfortunately, these have the nasty feature of repeating itself after a while. For the Monte Carlo this means that increasing the number of events per iteration no longer increases the accuracy of the calculation. A good random generator should therefore have a very long period.

Finally, the algorithm for generating the random numbers must be very efficient. This is because for  $N_{it}$  iterations,  $N_{ev}$  events per iteration, and an integral of  $d$  dimensions, we need to run the algorithm  $N_{it} \times N_{ev} \times d$  times. The speed of the random generator can therefore have a large impact on the overall speed of the Monte Carlo program.

The `RandomGenerator` class has two algorithms build in. The `ranmar()` function produces pseudo-random numbers by using the RANMAR algorithm, and `sobol()` uses Sobol sequences to return a quasi-random number.

## RANMAR

An easy way to produce random numbers is the multiplicative linear congruential generator:

$$s_i = (as_{i-1} + c) \bmod m. \quad (5.52)$$

The numbers generated are integers between 0 and  $m$ . The integers  $a$  and  $c$  are two predefined constants. If these are chosen wisely, one can get the maximal period of  $m$ . For example, the set with  $a = 69069$ ,  $c = 0$  and  $m = 2^{32}$  has the maximal period.

An improvement of this algorithm is the Lagged Fibonacci generator:

$$s_i = (s_{i-p} + s_{i-q}) \bmod m. \quad (5.53)$$

RANMAR [23] is an extension of this generator. It uses

$$s_i = (s_{i-97} + s_{i-33}) \bmod 2^{24}, \quad (5.54)$$

combined with a simple sequence

$$t_i = \begin{cases} t_{i-1} - 7654321 & \text{if } t_{i-1} - 7654321 \geq 0, \\ t_{i-1} - 7654321 + 2^{24} - 3 & \text{otherwise.} \end{cases} \quad (5.55)$$

The number produced by the algorithm is then

$$s_i = (r_i - t_i) \bmod 2^{24}. \quad (5.56)$$

Dividing the integer  $s_i$  by  $2^{24}$  results in a random number between 0 and 1.

## Sobol sequences

The Sobol generator produces quasi-random numbers that have a very uniform distribution. Instead of arithmetic operations, it uses only bitwise exclusive-OR operations. This makes the algorithm run quite fast on a computer, but unfortunately it also makes the implementation rather complicated. Therefore we shall not go into details here and refer the interested reader to the article of I.M. Sobol, [24].

## Testing

Testing the generator can be easily done by looking at its distribution (this is called the *frequency test*). For both generators we have produced 100,000 random numbers and placed them into a histogram. The result were two histograms with in each bin approximately the same number of values. Our conclusion is that both generators passed the frequency test.

In all simulations done for this thesis, the RANMAR algorithm was used. The main reason for this is that the RANMAR algorithm is better understood and works just as good for our purposes.

## The PhaseSpaceGenerator class

The `PhaseSpaceGenerator` class has two important tasks: determining the momenta of all the initial and final particles, and calculating the phase space factor  $dQ$ . Both are done by the same function, `getPhaseSpace()`. In this thesis project we have worked solely with processes where there are only two particles in the final state. The `PhaseSpaceGenerator` class can also be used to calculate the more general process  $A + B \rightarrow C + D + X$ , but in this section we only discuss the most simple case where there is no  $X$ .

In the lab frame, the hadrons are assumed to collide with equal, but opposite, momenta. In this frame the momenta of the (massless) partons are

$$\begin{aligned} p_A &= (E_A, \mathbf{p}_A) = x_A \cdot \left( \frac{1}{2}\sqrt{s}, 0, 0, \frac{1}{2}\sqrt{s} \right), \\ p_B &= (E_B, \mathbf{p}_B) = x_B \cdot \left( \frac{1}{2}\sqrt{s}, 0, 0, -\frac{1}{2}\sqrt{s} \right). \end{aligned} \quad (5.57)$$

The momentum fractions are determined with the random numbers according to  $\mathbf{x}_A = \mathbf{r}[0]$  and  $\mathbf{x}_B = \mathbf{r}[1]$ . As usual,  $\sqrt{s}$  is the center-of-mass energy of the hadrons.

We need to do the calculations in the center-of-mass (CM) frame of the partons. The boost we need to transform to that frame is

$$\beta_z = \frac{E_A - E_B}{E_A + E_B} = \frac{x_A - x_B}{x_A + x_B}, \quad (5.58)$$

and the rapidity is then

$$y = \frac{1}{2} \ln \left( \frac{1 + \beta_z}{1 - \beta_z} \right) \quad (5.59)$$

Using the rapidity makes it is easier to boost from one frame to another. The parton momenta in the CM frame of the partons is

$$\begin{aligned} \hat{p}_A &= (\cosh(y) E_A - \sinh(y) p_{Az}, 0, 0, -\sinh(y) E_A + \cosh(y) p_{Az}) \\ &= \left( \frac{1}{2} \sqrt{\hat{s}}, 0, 0, \frac{1}{2} \sqrt{\hat{s}} \right) \end{aligned} \quad (5.60)$$

$$\begin{aligned} \hat{p}_B &= (\cosh(y) E_B - \sinh(y) p_{Bz}, 0, 0, -\sinh(y) E_B + \cosh(y) p_{Bz}) \\ &= \left( \frac{1}{2} \sqrt{\hat{s}}, 0, 0, -\frac{1}{2} \sqrt{\hat{s}} \right) \end{aligned} \quad (5.61)$$

$$= \left( \frac{1}{2} \sqrt{\hat{s}}, 0, 0, -\frac{1}{2} \sqrt{\hat{s}} \right) \quad (5.62)$$

where  $\sqrt{\hat{s}}$  is the CM-energy of the partons,

$$\sqrt{\hat{s}} = \sqrt{x_0 x_1} \sqrt{s}. \quad (5.63)$$

The next step is to determine in which direction  $d\Omega$  the particles  $C$  and  $D$  will go. This cannot be calculated, we need to use the random numbers  $\mathbf{r}[2]$  and  $\mathbf{r}[3]$  for that. The angle  $\phi$  should be somewhere between 0 and  $2\pi$ , so

$$\phi = 2\pi r_2, \quad (5.64)$$

because for the random numbers  $r_i \in [0, 1]$ . The angle  $\theta \in [0, \pi]$  is determined with

$$\cos \theta = 1 - 2r_3. \quad (5.65)$$

The reason why we are not using  $\theta = \pi r_3$  is because

$$d\Omega = \sin \theta d\theta d\phi = -d(\cos \theta) d\phi, \quad (5.66)$$

and therefore the distribution of  $\theta$  must be uniform in  $\cos \theta$ .

We have now reached the point that we can almost calculate the phase space [25],

$$dQ = \frac{1}{64\pi^2 \hat{s}} \frac{|\hat{\mathbf{p}}_C|}{|\hat{\mathbf{p}}_A|} d\Omega = \frac{|\hat{\mathbf{p}}_C|}{32\pi^2 \hat{s} \sqrt{\hat{s}}} d\Omega. \quad (5.67)$$

To find an expression for the momenta of the final particles, we note that  $|\hat{\mathbf{p}}_C| = |\hat{\mathbf{p}}_D|$  and

$$\hat{E}_C + \hat{E}_D = \sqrt{m_C^2 + |\hat{\mathbf{p}}_C|^2} + \sqrt{m_D^2 + |\hat{\mathbf{p}}_C|^2} = \sqrt{\hat{s}}. \quad (5.68)$$

Solving this equation for  $|\hat{\mathbf{p}}_C|$ , we find that

$$|\hat{\mathbf{p}}_C| = \frac{1}{2\sqrt{\hat{s}}} \sqrt{\hat{s}^2 + m_C^4 + m_D^4 - 2\hat{s}m_C^2 - 2\hat{s}m_D^2 - 2m_C^2 m_D^2}. \quad (5.69)$$

The phase space weight  $w_{\text{ps}}$  that is returned by the function `getPhaseSpace()` is

$$w_{\text{ps}} = c_u \frac{|\hat{\mathbf{p}}_C|}{32\pi^2 \hat{s} \sqrt{\hat{s}}} 4\pi = \frac{|\hat{\mathbf{p}}_C|}{8\pi \hat{s} \sqrt{\hat{s}}}. \quad (5.70)$$

Instead of  $d\Omega$  we use  $4\pi$ , because summing over all weight factors  $w_{\text{ps}}$ , the  $d\Omega$  will give a contribution of exactly

$$\int d\Omega = 4\pi. \quad (5.71)$$

The constant  $c_u$  is there to give the cross section the correct units.

In the CM frame of the partons, the momenta of particles  $C$  and  $D$  are

$$\begin{aligned}\hat{p}_C &= (|\hat{\mathbf{p}}_C|, 0, 0, |\hat{\mathbf{p}}_C|) \\ \hat{p}_D &= (|\hat{\mathbf{p}}_C|, 0, 0, -|\hat{\mathbf{p}}_C|)\end{aligned}\quad (5.72)$$

Before these momenta are returned by the function, we first have to boost them back to the original CM frame of the hadrons:

$$\begin{aligned}p_C &= (\cosh(-y)\hat{E}_C - \sinh(-y)\hat{p}_{Cz}, 0, 0, -\sinh(-y)\hat{E}_C + \cosh(-y)\hat{p}_{Cz}), \\ p_D &= (\cosh(-y)\hat{E}_D - \sinh(-y)\hat{p}_{Dz}, 0, 0, -\sinh(-y)\hat{E}_D + \cosh(-y)\hat{p}_{Dz}).\end{aligned}\quad (5.73)$$

Here we have used the rapidity  $y$  of Equation (5.59).

## The PdfTable class

The PdfTable class provides the parton distribution function (PDF) that is used by the MonteCarlo class to calculate the total invariant amplitude. This class basically contains only two functions: readTableFile(string file) for reading the CTEQ files, and the function getPdf(double x, double mu) which returns an array with the PDF value for each parton. The argument  $x$  is the momentum fraction and  $\mu$  is the renormalization scale, usually set to  $m_t = 175$  GeV. Because the table only contains a limited amount of data points, getPdf() is essentially an interpolation algorithm that evaluates the correct PDF values.

To check if the class is working properly, we have tried to reproduce the graphs in Figure 4.2. The result is shown in Figure 5.5. Comparing both figures one sees an excellent agreement. We conclude that the PdfTable class is working as expected.

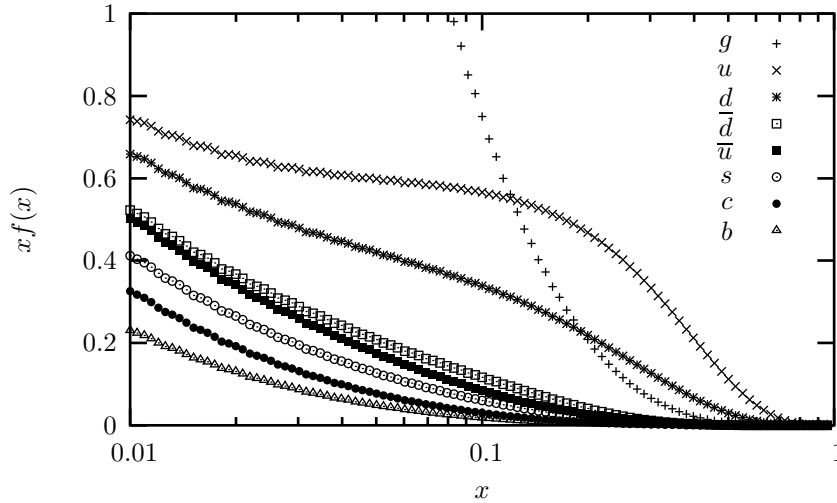


Figure 5.5: The parton distribution functions at scale  $\mu = 175$  GeV.

## The classes LorentzVector and Histogram

Finally, there are two more classes in the program that are quite small but nonetheless important. The LorentzVector class makes calculations for the phase space much easier by offering a large number of operator functions to do simple arithmetics as well as dot products and boosting. Quite useful are also the functions for calculating the rapidity and the pseudo-rapidity of the Lorentz-vector.

The Histogram class is vital for collecting the data needed to draw the histograms of the transverse momentum and the (pseudo)rapidity. When the simulation is finished, the Histograms save their data to a text file with the extension \*.his. The actual drawing is done by a separate program like GnuPlot [26] or ROOT [27], that reads the his-files and plots the histograms. A simple check that the Histogram class is working properly is done by determining the area of the histogram. This should be equal to the total cross section of the process, which is the case for all histograms shown in this thesis.

# Chapter 6

## Topflavor models

After the development of the Standard Model (SM), theoretical physicists have developed a large number of new theories extending the SM. An obvious way to create such an extension is by starting with a Lagrangian with a certain symmetry and then break it to  $SU(3)_c \times SU(2)_w \times U(1)_Y$ , the symmetry structure of the SM. Of course there are many different ways to do this. A lot of these new models were falsified by accurate electroweak measurements, but a number of them survived and a few theories became very popular.

One interesting theory, is the theory of Topflavor<sup>1</sup>. It was introduced in 1996 by David J. Muller and Satyanarayan Nandi [29] as an explanation for the exceptionally heavy mass of the top quark. Topflavor is the Standard Model extended with an extra  $SU(2)$  gauge group, similar to the  $SU(2)$  flavor symmetry of the up and down quark. Only the top-bottom doublet transforms under this new  $SU(2)$ , hence the name Topflavor. The way to implement this, is by simply assigning the proper quantum numbers to the fermions.

In the first section, after determining the symmetric structure of this theory, we determine the Topflavor Lagrangian. This section is followed by two sections that describe what happens during the two steps of symmetry breaking. In these sections the mass eigenstates of the gauge bosons are determined. Subsequently, in Section 6.4 we present the couplings between the fermions and the gauge bosons. These are then used in Section 6.5 for calculating the cross sections of single-top processes. In the final section we present and discuss the results that were found with the Monte Carlo simulations.

### 6.1 The Topflavor Lagrangian

Topflavor is the Standard Model extended with an extra  $SU(2)$  group, i.e. the Topflavor Lagrangian has the gauge symmetry  $SU(3)_c \times SU(2)_l \times SU(2)_h \times U(1)_Y$ . The label  $l$  stands for light and the label  $h$  for heavy. The first and second generation of the (left-handed) fermions transforms as doublets under  $SU(2)_l$  and as singlets under  $SU(2)_h$ . For the heavy fermions in the third generation the story is exactly the opposite: they transform as doublets under  $SU(2)_h$  and as singlets under  $SU(2)_l$ .

For energies lower than the electroweak breaking scale,  $\mathcal{O}(v \approx 175 \text{ GeV})$ , the model must reduce to the Standard Model. In the Topflavor model discussed in this chapter we shall use a complex Higgs scalar  $\Sigma$  that spontaneously breaks the original Topflavor symmetry by acquiring a vacuum expectation value (VEV) of  $u$ :

$$SU(2)_l \times SU(2)_h \times U(1)_Y \rightarrow SU(2)_w \times U(1)_Y. \quad (6.1)$$

For simplicity we ignore the color group, because it plays no active role in the symmetry breaking process. At even lower energies the theory breaks down as usual,

$$SU(2)_w \times U(1)_Y \rightarrow U(1)_{em}, \quad (6.2)$$

which happens when a second complex Higgs scalar doublet  $H$  acquires its VEV at scale  $v$ , with  $v \ll u$ . The second breaking is called electroweak symmetry breaking (EWSB).

---

<sup>1</sup>This model can be considered as being part of a much larger class of models called *Technicolor*. An excellent review about this topic is given in [28]. A similar theory to Topflavor is *Topcolor* which uses a  $SU(3)$  gauge group, similar to the color group of QCD.

Now that we have determined the symmetric structure of our theory, it is not hard to write down the Lagrangian. The Topflavor Lagrangian consists of the same parts as in the Standard Model:

$$\mathcal{L}_{\text{TF}} = \mathcal{L}_{\text{kF}} + \mathcal{L}_{\text{kGB}} + \mathcal{L}_{\text{kH}} + \mathcal{L}_{\text{pH}} + \mathcal{L}_Y. \quad (6.3)$$

However, the covariant derivative here is extended with an extra set of gauge bosons<sup>2</sup>,

$$D_\mu = \partial_\mu - ig' B_\mu Y - ig_l W_{l\mu}^a \frac{\tau^a}{2} - ig_h W_{h\mu}^a \frac{\tau^a}{2}. \quad (6.4)$$

Apart from the  $D_\mu$ , the kinetic fermion term remains the same:

$$\mathcal{L}_{\text{kF}} = i\bar{L}_\ell \not{D} L_\ell + i\bar{R}_\ell \not{D} R_\ell + i\bar{L}_{u^i} \not{D} L_{u^i} + i\bar{R}_{u^i} \not{D} R_{u^i} + i\bar{R}_{d^i} \not{D} R_{d^i}, \quad (6.5)$$

with summation over leptons  $\ell = e, \mu, \tau$  and quarks  $u^i = u, c, t$  and  $d^i = d, s, b$  implied. The kinetic term for the gauge bosons obtains one extra term for the extra three gauge bosons,

$$\mathcal{L}_{\text{kGB}} = -\frac{1}{4} B^{\mu\nu} B_{\mu\nu} - \frac{1}{4} W_l^{a\mu\nu} W_{l\mu\nu}^a - \frac{1}{4} W_h^{a\mu\nu} W_{h\mu\nu}^a, \quad (6.6)$$

with the field strengths given by

$$B_{\mu\nu} = \partial_\mu B_\nu - \partial_\nu B_\mu, \quad (6.7a)$$

$$W_{l\mu\nu}^a = \partial_\mu W_{l\nu}^a - \partial_\nu W_{l\mu}^a + g_l \epsilon^{abc} W_{l\mu}^b W_{l\nu}^c, \quad (6.7b)$$

$$W_{h\mu\nu}^a = \partial_\mu W_{h\nu}^a - \partial_\nu W_{h\mu}^a + g_h \epsilon^{abc} W_{h\mu}^b W_{h\nu}^c. \quad (6.7c)$$

All fermions in Topflavor theory transform as

$$\psi(x) \rightarrow \psi'(x) = \exp(ig'Y) \exp\left(ig_l T_l^a \frac{\tau^a}{2}\right) \exp\left(ig_h T_h^a \frac{\tau^a}{2}\right) \psi(x), \quad (6.8)$$

Here the  $Y$  is the hypercharge of fermion, and  $T_l, T_h$  are new quantum numbers similar to the weak-isospin  $T$  of the SM. The quantum numbers for each field in the theory are listed in Table 6.1.

## The Higgs sector

The Higgs sector of the Topflavor Lagrangian is much different then in the Standard Model. This time we have two Higgs fields that we need construct in such a way that they produce the correct symmetry breaking. The simplest of the two is the  $H$  doublet. This doublet must play the same role as the Higgs in the SM and must therefore have the same quantum numbers and representations. Under  $\text{SU}(2)_l \times \text{SU}(2)_h \times \text{U}(1)_Y$  it transforms as<sup>3</sup>

$$H : (\mathbf{2}, \mathbf{1})_{1/2}. \quad (6.9)$$

With this choice for the  $H$  we can use it to generate masses for the light fermions. In order to obtain mass terms for the heavy fermions we can add another  $H$  to the theory that transform as  $(\mathbf{1}, \mathbf{2})_{1/2}$ . However, in the next subsection we introduce an alternative method.

It is clear that we can give  $H$  the same shape as in the Standard Model,

$$H(x) = \begin{pmatrix} \phi_1(x) + \phi_2(x) \\ v + h(x) + i\phi_4(x) \end{pmatrix}. \quad (6.10)$$

The  $\phi_1, \phi_2$ , and  $\phi_4$  are the Goldstone bosons that will be eaten by the three gauge bosons  $W_\mu^\pm$  and  $Z_\mu$  after the electroweak symmetry breaking (EWSB). The  $h(x)$  then becomes a massive Higgs particle.

The Higgs field  $\Sigma(x)$  cannot be written as a complex doublet, because if we want to use  $\Sigma$  to break  $\text{SU}(2)_l \times \text{SU}(2)_h \rightarrow \text{SU}(2)_w$ , it has to transform under both  $\text{SU}(2)$  groups. In other words,  $\Sigma$  transforms as

$$\Sigma : (\mathbf{2}, \mathbf{2})_0. \quad (6.11)$$

<sup>2</sup>As stated before, we leave out the QCD part of this theory.

<sup>3</sup>Often the  $H$  field is given  $Y = 1$  with  $D_\mu = \partial_\mu - ig' B_\mu \frac{Y}{2}$ . However, we shall follow here the same approach as in Chapter 3 and take  $Y = 1/2$  with  $D_\mu = \partial_\mu - ig' B_\mu Y$ .



Explicitly, the  $\Sigma$  must transform as

$$\Sigma^{cd} \rightarrow \Sigma'^{cd} = R_l^{ca} R_h^{db} \Sigma^{ab}, \quad (6.12)$$

where  $R_l$  and  $R_h$  are transformation matrices belonging to the groups  $SU(2)_l$  and  $SU(2)_h$ . Note that these must have different indices, otherwise they are not independent. We see from the indices that  $\Sigma(x)$  can be written as a  $2 \times 2$  matrix,

$$\Sigma(x) = u + \sigma(x) + i\tau^a \chi^a(x) = \begin{pmatrix} u + \sigma + i\chi_3 & i\chi_1 + \chi_2 \\ i\chi_1 - \chi_2 & u + \sigma - i\chi_3 \end{pmatrix}. \quad (6.13)$$

As usual the  $\tau^a$  here are the Pauli matrices. We shall later see that the  $\chi_1$ ,  $\chi_2$ , and  $\chi_3$  are Goldstone bosons that will be eaten by the three heavy gauge bosons  $W'_\mu{}^\pm$  and  $Z'_\mu$  after the first symmetry breaking. The  $u$  is the VEV of the field and  $\sigma(x)$  becomes a massive Higgs particle just like  $h(x)$ .

Without using the tensor notation, we see that  $\Sigma$  transform as

$$\Sigma' = (\Sigma')^{cd} = (R_l)^{ca} (\Sigma)^{ab} (R_h)^{db} = (R_l)^{ca} (\Sigma)^{ab} (R_h^\dagger)^{bd} = R_l \Sigma R_h^\dagger. \quad (6.14)$$

To reverse the indices in  $R_h$  we could also use the transpose. However,  $R_h^T$  does not belong to  $SU(2)_h$ , which is easy to see by looking at the second Pauli matrix:

$$\tau_2^T = -\tau_2. \quad (6.15)$$

Taking the Hermitian conjugate leaves all Pauli matrices invariant and hence  $R_h^\dagger$  does belong to  $SU(2)_h$ .

By using the quantum numbers in (6.9) we see that the covariant derivative for  $H$  is

$$D_\mu H = \partial_\mu H - \frac{ig'}{2} B_\mu H - \frac{ig_l}{2} W_\mu^a \tau^a H. \quad (6.16)$$

For  $\Sigma$  we need to keep in mind how the field transforms. We find

$$\begin{aligned} D_\mu \Sigma &= \partial_\mu \Sigma + \left( -ig_l W_\mu^a \frac{\tau^a}{2} \right) \Sigma + \Sigma \left( -ig_h W_{h\mu}^a \frac{\tau^a}{2} \right)^\dagger \\ &= \partial_\mu \Sigma - ig_l W_\mu^a \frac{\tau^a}{2} \Sigma + ig_h \Sigma W_{h\mu}^a \frac{\tau^a}{2}. \end{aligned} \quad (6.17)$$

Finally, in order to have spontaneous symmetry breaking via the Higgs mechanism, we must of course include a Higgs potential. For the  $H$  we choose the usual potential,

$$V_H = -\mu_H^2 (H^\dagger H) + \lambda_H (H^\dagger H)^2, \quad (6.18)$$

with

$$H^\dagger H = (v + h)^2 + \phi_1^2 + \phi_2^2 + \phi_4^2. \quad (6.19)$$

We need a similar potential for  $\Sigma(x)$ . However,  $\Sigma^\dagger \Sigma$  is a  $2 \times 2$  matrix, not a scalar:

$$\begin{aligned} \Sigma^\dagger \Sigma &= (u + \sigma - i\chi_a^T \tau_a) (u + \sigma + i\tau_b \chi_b) \\ &= (u + \sigma)^2 + \chi_a^T \tau_a \tau_b \chi_b \\ &= (u + \sigma)^2 + \chi_a^T (\delta_{ab} + i\epsilon_{abc} \tau_c) \chi_b \\ &= (u + \sigma)^2 + \chi_a^T \chi_a + i\chi_a^T \epsilon_{abc} \tau_c \chi_b \end{aligned} \quad (6.20)$$

To obtain a real scalar value similar to the term  $H^\dagger H$ , we must remove the last term by taking the trace:

$$\begin{aligned} \frac{1}{2} \text{Tr}(\Sigma^\dagger \Sigma) &= \frac{1}{2} \text{Tr} \left( (u + \sigma)^2 + \chi_a^T \chi_a + i\chi_a^T \epsilon_{abc} \tau_c \chi_b \right) \\ &= (u + \sigma)^2 + \chi_1^2 + \chi_2^2 + \chi_3^2. \end{aligned} \quad (6.21)$$

The Higgs sector of the Topflavor Lagrangian can be written as

$$\mathcal{L}_H = \mathcal{L}_{kH} + \mathcal{L}_{pH}, \quad (6.22)$$

with the kinetic terms

$$\mathcal{L}_{\text{KH}} = (D_\mu H)^\dagger (D^\mu H) + \frac{1}{2} \text{Tr} \left( (D_\mu \Sigma)^\dagger (D^\mu \Sigma) \right), \quad (6.23)$$

and potentials

$$\begin{aligned} \mathcal{L}_{\text{pH}} &= -V_H (H^\dagger H) - V_\Sigma (\text{Tr} (\Sigma^\dagger \Sigma)) \\ &= -\mu_H^2 H^\dagger H + \lambda_H (H^\dagger H)^2 - \frac{\mu_\Sigma^2}{2} \text{Tr} (\Sigma^\dagger \Sigma) + \frac{\lambda_\Sigma}{4} (\text{Tr} (\Sigma^\dagger \Sigma))^2. \end{aligned} \quad (6.24)$$

## Topflavor with seesaw mechanism

We also need Yukawa terms to generate masses for the fermions using the Higgs bosons. Instead of using the original model of [29], we shall use an extension called Topflavor with Seesaw Mechanism [30]. The main difference is that in the original theory the whole third generation transforms under  $\text{SU}(2)_h$ , while in this new model only the top-bottom family transform under  $\text{SU}(2)_h$ , with the tau lepton transforming in the same way as the lighter families. This can explain why the top is so much heavier than the tau lepton.

We can explain the principle of the seesaw mechanism [31] with a  $2 \times 2$  matrix like

$$\mathbf{M}^2 = \begin{pmatrix} 0 & m \\ m & b \end{pmatrix}. \quad (6.25)$$

The value of  $b$  has to be large, and  $m$  is of an intermediate size. In order to find the mass eigenstates of the particles, we need to diagonalize this matrix. Their masses follow from the eigenvalues:

$$\lambda_\pm = \frac{b \pm \sqrt{b^2 + 4m^2}}{2}. \quad (6.26)$$

Since  $b \gg m$ , one particle receives a really large mass,

$$\lambda_+ \approx b. \quad (6.27)$$

The determinant of the matrix is equal to

$$|\mathbf{M}^2| = \lambda_- \lambda_+ = -m^2. \quad (6.28)$$

This means that if one mass goes up, the other goes down – just like a seesaw. Indeed, the other particle has a really small mass,

$$\lambda_- = \frac{b - \sqrt{b^2 + 4m^2}}{2} = -\frac{m^2}{b} + \mathcal{O}(m^4). \quad (6.29)$$

The seesaw mechanism can be used to explain e.g. the small neutrino masses. In our Topflavor model the mechanism is used to generate a top mass, which is small compared to the masses of two new quarks,  $\mathcal{T}$  and  $\mathcal{B}$ . These left-handed quarks are doublet under  $\text{SU}(2)_l$ ,

$$S_L = \begin{pmatrix} \mathcal{T}_L \\ \mathcal{B}_L \end{pmatrix}, \quad (6.30)$$

while the right-handed quarks form a doublet under  $\text{SU}(2)_h$ ,

$$S_R = \begin{pmatrix} \mathcal{T}_R \\ \mathcal{B}_R \end{pmatrix}. \quad (6.31)$$

The Yukawa terms for the third quark family are

$$\mathcal{L}_{\text{Y,3rd}} = -\frac{y_s}{\sqrt{2}} \bar{S}_L \Sigma S_R - y_{st} \bar{S}_L H^c t_R - y_{sb} \bar{S}_L H b_R - \kappa \bar{L}_t S_R + \text{h.c.}, \quad (6.32)$$

where  $H^c$  is the anti-Higgs doublet,

$$H^c = -i\tau_2 H^*. \quad (6.33)$$

particle	SU(3) <sub>c</sub>	SU(2) <sub>l</sub>	SU(2) <sub>h</sub>	U(1) <sub>Y</sub>
$(t_L, b_L)^T$	<b>3</b>	<b>1</b>	<b>2</b>	+1/6
$t_R$	<b>3</b>	<b>1</b>	<b>1</b>	+2/3
$b_R$	<b>3</b>	<b>1</b>	<b>1</b>	-1/3
$(\mathcal{T}_L, \mathcal{B}_L)^T$	<b>3</b>	<b>2</b>	<b>1</b>	+1/6
$(\mathcal{T}_R, \mathcal{B}_R)^T$	<b>3</b>	<b>1</b>	<b>2</b>	+1/6
$(\nu_{\tau L}, \tau_L)^T$	<b>1</b>	<b>2</b>	<b>1</b>	-1/2
$\tau_R$	<b>1</b>	<b>1</b>	<b>1</b>	-1
$\Sigma$	<b>1</b>	<b>2</b>	<b>2</b>	0
$H$	<b>1</b>	<b>2</b>	<b>1</b>	+1/2

Table 6.1: Representations of all fields in the Topflavor model (taken from [30]). The representations for the first and second family of leptons and quarks do not change in Topflavor, they are all singlets under the SU(2)<sub>h</sub>.

When  $H$  and  $\Sigma$  obtain there VEV's,

$$\langle H \rangle = \frac{1}{\sqrt{2}} \begin{pmatrix} 0 \\ v \end{pmatrix}, \quad \langle \Sigma \rangle = \frac{1}{\sqrt{2}} \begin{pmatrix} u & 0 \\ 0 & u \end{pmatrix}, \quad (6.34)$$

the Yukawa terms turn into

$$\begin{aligned} \mathcal{L}_{Y,3rd} = & - (\bar{t}_L \quad \bar{\mathcal{T}}_L) \begin{pmatrix} 0 & \kappa \\ m_{st} & M_S \end{pmatrix} \begin{pmatrix} t_R \\ \mathcal{T}_R \end{pmatrix} \\ & - (\bar{b}_L \quad \bar{\mathcal{B}}_L) \begin{pmatrix} 0 & \kappa \\ m_{sb} & M_S \end{pmatrix} \begin{pmatrix} b_R \\ \mathcal{B}_R \end{pmatrix} + \text{h.c.} \end{aligned} \quad (6.35)$$

where  $M_S \equiv y_s u / \sqrt{2}$ ,  $m_{st} \equiv y_{st} v / \sqrt{2}$ , and  $m_{sb} \equiv y_{sb} v / \sqrt{2}$ . The values of  $y_s$ ,  $y_{st}$  and  $y_{sb}$  are all of order 1. Because  $u \gg v$ , we see that these matrices cause a seesaw mechanism. The masses of the quarks are

$$\begin{aligned} m_t &= \frac{m_{st}\kappa}{M_S\sqrt{1+r}} \left[ 1 - \frac{(m_{st}/M_S)^2}{2(1+r)^2} + \mathcal{O}\left(\frac{m_t^4}{M_S^4}\right) \right], \\ m_b &= \frac{m_{sb}\kappa}{M_S\sqrt{1+r}} \left[ 1 - \frac{(m_{sb}/M_S)^2}{2(1+r)^2} + \mathcal{O}\left(\frac{m_b^4}{M_S^4}\right) \right], \\ M_{\mathcal{T}} &= M_S\sqrt{1+r} \left[ 1 + \frac{z_t^2}{2(1+r)} + \frac{4r+3}{8(1+r)^2} z_t^4 + \mathcal{O}(z_t^6) \right], \\ M_{\mathcal{B}} &= M_S\sqrt{1+r} \left[ 1 + \frac{z_b^2}{2(1+r)} + \frac{4r+3}{8(1+r)^2} z_b^4 + \mathcal{O}(z_b^6) \right], \end{aligned} \quad (6.36)$$

where  $r \equiv (\kappa/M_S)^2 \sim \mathcal{O}(1)$  and  $z_{t,b} \equiv m_{t,b}/\kappa$  with  $z_b \ll z_t \ll 1$ .

In the remainder of this chapter we shall not go further into the properties of the  $\mathcal{T}$  and  $\mathcal{B}$  quarks, we shall focus on the gauge bosons. For us, the only difference between the original Topflavor model and the one with the seesaw mechanism, is the fact that tau lepton will not couple strongly to the heavy gauge bosons.

Finally, we must mention that the Yukawa terms for the light families are simply the same as in the Standard Model:

$$\mathcal{L}_Y = -\lambda_\ell \bar{L}_\ell H R_\ell - \lambda_{d^i} \bar{L}_{u^i} H R_{d^i} - \lambda_{u^i} \bar{L}_{u^i} H^c R_{u^i} + \text{h.c.}, \quad (6.37)$$

summation over leptons  $\ell = e, \mu, \tau$  and the light quarks  $u^i = u, c$  and  $d^i = d, s$  implied. There are no Yukawa terms with light fermions and the  $\Sigma$  field. This is because there are no light right-handed doublets.

## 6.2 Breaking of $SU(2)_l \times SU(2)_h \rightarrow SU(2)_w$

In this section we determine which gauge bosons obtain a mass when  $\Sigma$  acquires its VEV,

$$\langle \Sigma \rangle = \frac{1}{\sqrt{2}} \begin{pmatrix} u & 0 \\ 0 & u \end{pmatrix}. \quad (6.38)$$

As stated in Table 3.2 in Chapter 3, we can find the masses and mass eigenstates of the gauge bosons by substituting  $\Sigma = \langle \Sigma \rangle$  into the kinetic Higgs term  $\mathcal{L}_{\text{kH}}$  of (6.23). Because the  $H$  field has no influence on the breaking of  $SU(2)_l \times SU(2)_h \rightarrow SU(2)_w$ , we only need to examine the kinetic term of  $\Sigma$ :

$$\mathcal{L}_{\text{kH},\Sigma} = \frac{1}{2} \text{Tr} \left( (D_\mu \Sigma)^\dagger (D^\mu \Sigma) \right). \quad (6.39)$$

We find

$$\begin{aligned} D_\mu \langle \Sigma \rangle &= \partial_\mu \langle \Sigma \rangle - ig_l W_{l\mu}^a \frac{\tau^a}{2} \langle \Sigma \rangle + ig_h \langle \Sigma \rangle W_{h\mu}^a \frac{\tau^a}{2} \\ &= -\frac{i u}{2\sqrt{2}} (g_l W_{l\mu}^a - g_h W_{h\mu}^a) \tau^a, \end{aligned} \quad (6.40)$$

and

$$D_\mu \langle \Sigma \rangle^\dagger = \frac{i u}{2\sqrt{2}} (g_l W_{l\mu}^a - g_h W_{h\mu}^a) \tau^a. \quad (6.41)$$

Their product is

$$(D_\mu \langle \Sigma \rangle)^\dagger (D^\mu \langle \Sigma \rangle) = \frac{u^2}{8} (g_l W_{l\mu}^a - g_h W_{h\mu}^a) (g_l W_l^{b\mu} - g_h W_h^{b\mu}) \tau^a \tau^b, \quad (6.42)$$

and the kinetic Higgs term is therefore

$$\begin{aligned} \mathcal{L}_{\text{kH},\langle \Sigma \rangle} &= \frac{u^2}{16} (g_l W_{l\mu}^a - g_h W_{h\mu}^a) (g_l W_l^{b\mu} - g_h W_h^{b\mu}) \text{Tr} (\tau^a \tau^b) \\ &= \frac{u^2}{16} (g_l W_{l\mu}^a - g_h W_{h\mu}^a) (g_l W_l^{b\mu} - g_h W_h^{b\mu}) (2\delta^{ab}) \\ &= \frac{u^2}{8} \left[ g_l^2 (W_{l\mu}^a)^2 - 2g_l g_h W_{l\mu}^a W_h^{a\mu} + g_h^2 (W_{h\mu}^a)^2 \right] \\ &= \frac{1}{2} \begin{pmatrix} W_{l\mu}^a & W_{h\mu}^a \end{pmatrix} \mathbf{M}^2 \begin{pmatrix} W_l^{a\mu} \\ W_h^{a\mu} \end{pmatrix}. \end{aligned} \quad (6.43)$$

The mass matrix  $\mathbf{M}^2$  is given by

$$\mathbf{M}^2 = \frac{u^2}{4} \begin{pmatrix} g_l^2 & -g_l g_h \\ -g_l g_h & g_h^2 \end{pmatrix}. \quad (6.44)$$

This is exactly the same matrix as in (3.71) The eigenvalues of this matrix are

$$M_1^2 = 0, \quad (6.45a)$$

$$M_2^2 = \frac{u^2}{4} (g_l^2 + g_h^2), \quad (6.45b)$$

with the normalized eigenstates

$$W_1^{a\mu} = (g_h W_l^{a\mu} + g_l W_h^{a\mu}) / \sqrt{g_l^2 + g_h^2}, \quad (6.46a)$$

$$W_2^{a\mu} = (-g_l W_l^{a\mu} + g_h W_h^{a\mu}) / \sqrt{g_l^2 + g_h^2}. \quad (6.46b)$$

In the Standard Model we simplified these expressions by introducing the mixing angle  $\theta_w$ . We can do this again with a different mixing angle  $\phi$  defined by

$$\cos \phi = \frac{g_h}{\sqrt{g_l^2 + g_h^2}}, \quad \sin \phi = \frac{g_l}{\sqrt{g_l^2 + g_h^2}}, \quad (6.47)$$

such that

$$W_1^{a\mu} = \cos \phi W_l^{a\mu} + \sin \phi W_h^{a\mu}, \quad (6.48a)$$

$$W_2^{a\mu} = -\sin \phi W_l^{a\mu} + \cos \phi W_h^{a\mu}. \quad (6.48b)$$

We have found that the breaking  $SU(2)_l \times SU(2)_h \times U(1)_Y \rightarrow SU(2)_w \times U(1)_Y$  using  $\langle \Sigma \rangle$  causes three gauge bosons to obtain a mass:  $W_2^{a\mu}$ . The remaining gauge bosons  $W_1^{a\mu}$  and  $B^\mu$  (the gauge boson of  $U(1)_Y$ ) are left massless. It is clear that the massless  $W_1^{a\mu}$  and  $B^\mu$  can be identified with the Standard Model gauge bosons before electroweak symmetry breaking.

### 6.3 Electroweak symmetry breaking

In order to compare the Topflavor model with the Standard Model, we must determine the masses and mass eigenstates of the gauge bosons after EWSB. The VEV of the  $H$  field is

$$\langle H \rangle = \frac{1}{\sqrt{2}} \begin{pmatrix} 0 \\ v \end{pmatrix}. \quad (6.49)$$

This has no influence on the  $\Sigma$  part of  $\mathcal{L}_{\text{kH}}$ ,

$$\mathcal{L}_{\text{kH},(\Sigma)} = \frac{1}{2} M_1^2 (W_1^{a\mu})^2 + \frac{1}{2} M_2^2 (W_2^{a\mu})^2 \quad (6.50)$$

$$= \frac{1}{2} \frac{u^2}{4} (g_l^2 + g_h^2) (W_2^{a\mu})^2, \quad (6.51)$$

but only changes

$$\mathcal{L}_{\text{kH},H} = (D_\mu H)^\dagger (D^\mu H). \quad (6.52)$$

First we calculate

$$\begin{aligned} D_\mu \langle H \rangle &= \partial_\mu \langle H \rangle - \frac{ig'}{2} B_\mu \langle H \rangle - \frac{ig_l}{2} W_{l\mu}^a \tau^a \langle H \rangle \\ &= -\frac{ig'}{2\sqrt{2}} B_\mu \begin{pmatrix} 0 \\ v \end{pmatrix} - \frac{ig_l}{2\sqrt{2}} \begin{pmatrix} W_{l\mu}^3 & W_{l\mu}^1 - iW_{l\mu}^2 \\ W_{l\mu}^1 + iW_{l\mu}^2 & -W_{l\mu}^3 \end{pmatrix} \begin{pmatrix} 0 \\ v \end{pmatrix} \\ &= -\frac{ig'v}{2\sqrt{2}} \begin{pmatrix} 0 \\ B_\mu \end{pmatrix} - \frac{ig_lv}{2\sqrt{2}} \begin{pmatrix} W_{l\mu}^1 - iW_{l\mu}^2 \\ -W_{l\mu}^3 \end{pmatrix} \\ &= -\frac{iv}{2\sqrt{2}} \begin{pmatrix} g_l (W_{l\mu}^1 - iW_{l\mu}^2) \\ g' B_\mu - g_l W_{l\mu}^3 \end{pmatrix}, \end{aligned} \quad (6.53)$$

and

$$D_\mu \langle H \rangle^\dagger = \frac{iv}{2\sqrt{2}} \begin{pmatrix} g_l (W_{l\mu}^1 + iW_{l\mu}^2) & g' B_\mu - g_l W_{l\mu}^3 \end{pmatrix}. \quad (6.54)$$

The result is

$$\mathcal{L}_{\text{kH},\langle H \rangle} = \frac{1}{2} \frac{v^2 g_l^2}{4} |W_{l\mu}^1 - iW_{l\mu}^2|^2 + \frac{1}{2} \frac{v^2}{4} (g' B_\mu - g_l W_{l\mu}^3)^2 \quad (6.55)$$

$$= \frac{1}{2} \frac{v^2 g_l^2}{4} [(W_{l\mu}^1)^2 + (W_{l\mu}^2)^2] + \frac{1}{2} \frac{v^2}{4} (g' B_\mu - g_l W_{l\mu}^3)^2. \quad (6.56)$$

The most straightforward way of determining the mass eigenstates of all 7 gauge bosons, is by determining the  $7 \times 7$  mass matrix:

$$\mathcal{L}_{\text{kH}} = \mathcal{L}_{\text{kH},\langle H \rangle} + \mathcal{L}_{\text{kH},(\Sigma)} = \frac{1}{2} G^\dagger \mathbf{M}^2 G, \quad (6.57)$$

with the vector  $G$  defined by

$$G^\dagger = ( W_{l\mu}^1 \quad W_{h\mu}^1 \quad W_{l\mu}^2 \quad W_{h\mu}^2 \quad W_{l\mu}^3 \quad W_{h\mu}^3 \quad B_\mu ). \quad (6.58)$$

With this choice for  $G$  the mass matrix obtains a nice diagonal form:

$$\mathbf{M}^2 = \begin{pmatrix} \mathbf{A}^2 & 0 & 0 \\ 0 & \mathbf{A}^2 & 0 \\ 0 & 0 & \mathbf{B}^2 \end{pmatrix}, \quad (6.59)$$

with

$$\mathbf{A}^2 = \frac{u^2}{4} \begin{pmatrix} (v^2/u^2 + 1) g_l^2 & -g_l g_h \\ -g_l g_h & g_h^2 \end{pmatrix} = \frac{v^2 x}{4} \begin{pmatrix} (1/x + 1) g_l^2 & -g_l g_h \\ -g_l g_h & g_h^2 \end{pmatrix}, \quad (6.60)$$

and

$$\mathbf{B}^2 = \frac{v^2 x}{4} \begin{pmatrix} (1/x + 1) g_l^2 & -g_l g_h & -g' g_l/x \\ -g_l g_h & g_h^2 & 0 \\ -g' g_l/x & 0 & g'^2/x \end{pmatrix}. \quad (6.61)$$

Here we have defined  $x$  as

$$x \equiv \frac{u^2}{v^2}. \quad (6.62)$$

Note that because  $u \gg v$  we have  $x \gg 1$ .

## Mass eigenstate of the photon

We expect after diagonalization to find only one massless gauge boson, the photon. In the SM the photon mass eigenstate was a linear combination of fields including the  $B_\mu$  field. Indeed, when we diagonalize the  $\mathbf{B}^2$  matrix, we find again that it has one eigenvalue equal to zero. The normalized eigenstate associated with this eigenvalue is

$$A_\mu = \frac{g' g_h W_{l\mu}^3 + g' g_l W_{h\mu}^3 + g_l g_h B_\mu}{\sqrt{g'^2 g_l^2 + g'^2 g_h^2 + g_l^2 g_h^2}} = \frac{1}{\sqrt{1/g_e^2}} \left( \frac{1}{g_l} W_{l\mu}^3 + \frac{1}{g_h} W_{h\mu}^3 + \frac{1}{g'} B_\mu \right), \quad (6.63)$$

where we have defined  $g_e$  with

$$\frac{1}{g_e^2} = \frac{1}{g_l^2} + \frac{1}{g_h^2} + \frac{1}{g'^2}. \quad (6.64)$$

We could imagine  $A_\mu$  as a unit vector in the 3-dimensional space of  $(W_{l\mu}^3, W_{h\mu}^3, B_\mu)$ . The coupling constants then determine the direction of this vector:

$$A_\mu = \left( \frac{g_e}{g_l}, \frac{g_e}{g_h}, \frac{g_e}{g'} \right). \quad (6.65)$$

Because we have here a normal 3-dimensional space, we could introduce spherical coordinates. A common choice is

$$\frac{g_e}{g_l} = \sin \theta \cos \phi, \quad \frac{g_e}{g_h} = \sin \theta \sin \phi, \quad \frac{g_e}{g'} = \cos \theta. \quad (6.66)$$

Note that the  $\phi$  here is the same as in (6.47). In terms of these mixing angles, we have

$$A_\mu = \sin \theta \left( \cos \phi W_{l\mu}^3 + \sin \phi W_{h\mu}^3 \right) + \cos \theta B_\mu. \quad (6.67)$$

## Mass eigenstates of the $Z$ and $Z'$

The other two eigenvalues of the  $\mathbf{B}^2$  matrix are

$$M_\pm^2 = \frac{M_0^2 (x + \sin^4 \phi)}{2 \sin^2 \phi \cos^2 \theta} + \frac{M_0^2}{2 \cos^2 \theta} \pm \frac{M_0^2 \sqrt{(\sin^2 \phi \cos^2 \phi - (x + \sin^4 \phi) \cos^2 \theta)^2 + 4 \sin^6 \phi \cos^2 \phi \cos^2 \theta}}{2 \cos^2 \theta \sin^2 \phi \cos^2 \phi}, \quad (6.68)$$

with

$$M_0^2 \equiv \frac{g_e^2 v^2}{4 \sin^2 \theta}. \quad (6.69)$$

For very large values of  $x = u^2/v^2 \gg 1$  we see that these masses become

$$\lim_{x \rightarrow \infty} M_\pm^2 = \frac{M_0^2}{2 \sin^2 \phi \cos^2 \theta} x \pm \frac{M_0^2}{2 \sin^2 \phi \cos^2 \phi} x. \quad (6.70)$$

Evidently  $M_-$  vanishes when  $u \rightarrow \infty$ . This means that  $M_-$  must be the mass of the light  $Z$  boson and  $M_+$  the mass of much heavier  $Z'$ -boson. If we expand the expressions around  $1/x = 0$  we find

$$M_Z^2 = M_-^2 = \frac{M_0^2}{\cos^2 \theta} \left[ 1 - \frac{\sin^4 \phi}{x} + \mathcal{O}\left(\frac{1}{x^2}\right) \right] \quad (6.71)$$

and for  $Z'$ ,

$$M_{Z'}^2 = M_+^2 = M_0^2 \left[ \frac{x}{\sin^2 \phi \cos^2 \phi} + \frac{\sin^2 \phi}{\cos^2 \phi} + \frac{\sin^4 \phi}{x \cos^2 \theta} + \mathcal{O}\left(\frac{1}{x^2}\right) \right]. \quad (6.72)$$

In the limit  $x \rightarrow \infty$  one finds that the eigenstates are

$$\lim_{x \rightarrow \infty} Z_\mu \equiv Z_{1\mu} = \cos \theta (\cos \phi W_{l\mu}^3 + \sin \phi W_{h\mu}^3) - \sin \theta B_\mu, \quad (6.73a)$$

$$\lim_{x \rightarrow \infty} Z'_\mu \equiv Z_{2\mu} = -\sin \phi W_{l\mu}^3 + \cos \phi W_{h\mu}^3. \quad (6.73b)$$

The eigenstates of  $Z_\mu$  and  $Z'_\mu$  for finite values of  $x$  can be nicely written as a perturbation of the states  $Z_{1\mu}$  and  $Z_{2\mu}$ . To order  $\mathcal{O}(x^{-2})$  we find

$$Z_\mu = Z_{1\mu} + \frac{\sin^3 \phi \cos \phi}{x \cos \theta} Z_{2\mu}, \quad (6.74a)$$

$$Z'_\mu = -\frac{\sin^3 \phi \cos \phi}{x \cos \theta} Z_{1\mu} + Z_{2\mu}. \quad (6.74b)$$

## Mass eigenstates of the $W$ and $W'$

The masses and mass eigenstates of the  $W$  and  $W'$  follow from the matrix  $\mathbf{A}^2$ , in a similar manner. The mass of the  $W$  is

$$M_W^2 = M_0^2 \left[ 1 - \frac{\sin^4 \phi}{x} - \frac{(2 \cos^2 \phi - 1) \sin^6 \phi}{x^2} + \mathcal{O}\left(\frac{1}{x^3}\right) \right], \quad (6.75)$$

and for the  $W'$ ,

$$M_{W'}^2 = M_0^2 \left[ \frac{x}{\sin^2 \phi \cos^2 \phi} + \frac{\sin^2 \phi}{\cos^2 \phi} + \frac{\sin^4 \phi}{x} + \mathcal{O}\left(\frac{1}{x^2}\right) \right]. \quad (6.76)$$

Their ratio is

$$\frac{M_W^2}{M_{W'}^2} = \frac{\sin^2 \phi \cos^2 \phi}{x} + \mathcal{O}\left(\frac{1}{x^2}\right). \quad (6.77)$$

For the eigenstates we have to use

$$W_{l\mu}^\pm = (W_{l\mu}^1 \mp iW_{l\mu}^2) / \sqrt{2}, \quad (6.78a)$$

$$W_{h\mu}^\pm = (W_{h\mu}^1 \mp iW_{h\mu}^2) / \sqrt{2}, \quad (6.78b)$$

in order to have mass eigenstates that correspond to the same particles as in the SM. The eigenstates of the  $W_\mu^\pm$  and  $W_{\mu'}^\pm$  are then [32]

$$W_\mu^\pm = W_{1\mu}^\pm + \frac{\sin^3 \phi \cos \phi}{x} W_{2\mu}^\pm, \quad (6.79a)$$

$$W_{\mu'}^\pm = -\frac{\sin^3 \phi \cos \phi}{x} W_{1\mu}^\pm + W_{2\mu}^\pm, \quad (6.79b)$$

where the  $W_{1\mu}^\pm$  and  $W_{2\mu}^\pm$  correspond to the eigenstates in the limit  $x \rightarrow \infty$ ,

$$W_{1\mu}^\pm = \cos \phi W_{l\mu}^\pm + \sin \phi W_{h\mu}^\pm, \quad (6.80a)$$

$$W_{2\mu}^\pm = -\sin \phi W_{l\mu}^\pm + \cos \phi W_{h\mu}^\pm. \quad (6.80b)$$

We can make some interesting remarks. For example, in contrary to the gauge bosons of the SM, the heavy gauge bosons  $W'^\pm$  and  $Z'$  all have the same mass,

$$M_{W'}^2 = M_{Z'}^2 = M_0^2 \left[ \frac{x}{\sin^2 \phi \cos^2 \phi} + \frac{\sin^2 \phi}{\cos^2 \phi} \right], \quad (6.81)$$

up to the order  $\mathcal{O}(x^0) = \mathcal{O}(1)$ . A more important remark can be made about the ratio  $M_W/M_Z$  for which

$$\frac{M_W}{M_Z} = \cos \theta, \quad (6.82)$$

up to order  $\mathcal{O}(x^{-1})$ . Not surprisingly, the angle  $\theta$  is the same as the weak mixing angle  $\theta_w$  of the SM. This is actually a very important property of the Topflavor theory, because this ratio has been measured to high accuracy. If this theory would predict a ratio that is too far off, it would indicate that theory is flawed.

## 6.4 Fermion - gauge boson couplings

Before we can calculate any cross sections with the Topflavor model, we need to determine the vertices. i.e. the couplings. The way to do this, is by evaluating the kinetic term for the fermions in our Lagrangian,

$$\mathcal{L}_{\text{kF}} = i\bar{L}_f\gamma^\mu D_\mu L_f + i\bar{R}_f\gamma^\mu D_\mu R_f. \quad (6.83)$$

The covariant derivative is

$$D_\mu = \partial_\mu - ig'B_\mu Y - ig_l W_{l\mu}^a T_l^a - ig_h W_{h\mu}^b T_h^b, \quad (6.84)$$

with  $T_l^a = \tau^a/2$  the generators of the  $SU(2)_l$ , and  $T_h^b = \tau^b/2$  the generators of  $SU(2)_h$ . As we have seen in Chapter 3 with the Standard Model, it is better to use here

$$T^\pm = \frac{1}{2}\tau^\pm = \frac{1}{2\sqrt{2}}(\tau^1 \pm i\tau^2) = \frac{1}{\sqrt{2}}(T^1 \pm iT^2), \quad (6.85a)$$

such that

$$\begin{aligned} W_{l\mu}^1 T_l^1 + W_{l\mu}^2 T_l^2 &= W_{l\mu}^1 (T^+ + T^-) - iW_{l\mu}^2 (T^+ - T^-) \\ &= \frac{1}{2}(W_{l\mu}^+ + W_{l\mu}^-)(T^+ + T^-) + \frac{1}{2}(W_{l\mu}^+ - W_{l\mu}^-)(T^+ - T^-) \\ &= W_{l\mu}^- T^- + W_{l\mu}^+ T^+. \end{aligned} \quad (6.86)$$

The covariant derivative is then

$$\begin{aligned} D_\mu &= \partial_\mu - ig'B_\mu Y - ig_l (W_{l\mu}^- T_l^- + W_{l\mu}^+ T_l^+ + W_{l\mu}^3 T_l^3) \\ &\quad - ig_h (W_{h\mu}^- T_h^- + W_{h\mu}^+ T_h^+ + W_{h\mu}^3 T_h^3). \end{aligned} \quad (6.87)$$

The next step is to write  $D_\mu$  in terms of the mass eigenstates. To keep things simple, we examine here only the eigenstate  $A_\mu$ . Solving for  $W_{l\mu}^3$ ,  $W_{h\mu}^3$ , and  $B_\mu$  we obtain

$$W_{l\mu}^3 = [\sin\theta \cos\phi] A_\mu + \dots, \quad (6.88a)$$

$$W_{h\mu}^3 = [\sin\theta \sin\phi] A_\mu + \dots, \quad (6.88b)$$

$$B_\mu = [\cos\theta] A_\mu + \dots, \quad (6.88c)$$

where the dots stand for expressions with  $Z_\mu$  and  $Z'_\mu$ . Substituting this into  $D_\mu$  brings us

$$\begin{aligned} D_\mu &= \partial_\mu - ig'Y [\cos\theta] A_\mu - ig_l T_l^3 [\sin\theta \cos\phi] A_\mu - ig_h T_h^3 [\sin\theta \sin\phi] A_\mu + \dots \\ &= \partial_\mu - i \left( \frac{g_e}{\cos\theta} Y \cos\theta + \frac{g_e}{\sin\theta \cos\phi} T_l^3 \sin\theta \cos\phi + \frac{g_e}{\sin\theta \sin\phi} T_h^3 \sin\theta \sin\phi \right) A_\mu + \dots \\ &= \partial_\mu - ig_e (Y + T_l^3 + T_h^3) A_\mu + \dots \\ &= \partial_\mu - ig_e Q A_\mu + \dots \end{aligned} \quad (6.89)$$

From this it is clear that the charge operator  $Q$  is

$$Q = Y + T_l^3 + T_h^3, \quad (6.90)$$

and that  $g_e = e$  is the QED coupling constant.

We can do all of this also for the other gauge bosons. To order  $\mathcal{O}(x^{-1})$  the complete expression is

$$\begin{aligned} D_\mu &= \partial_\mu - ig_e Q A_\mu - ig_w \left[ T_l^\pm + T_h^\pm + \frac{\sin^2\phi}{x} (T_h^\pm \cos^2\phi - T_l^\pm \sin^2\phi) \right] W_\mu^\pm \\ &\quad - i \frac{g_w}{\cos\theta} \left[ T_l^3 + T_h^3 - Q \sin^2\theta + \frac{\sin^2\phi}{x} (T_h^3 \cos^2\phi - T_l^3 \sin^2\phi) \right] Z_\mu \\ &\quad - ig_w \left[ \frac{\cos\phi}{\sin\phi} T_h^\pm - \frac{\sin\phi}{\cos\phi} T_l^\pm - \frac{\sin^3\phi \cos\phi}{x} (T_h^\pm + T_l^\pm) \right] W_\mu^{\pm} \\ &\quad - ig_w \left[ \frac{\cos\phi}{\sin\phi} T_h^3 - \frac{\sin\phi}{\cos\phi} T_l^3 - \frac{\sin^3\phi \cos\phi}{x \cos^2\theta} (T_h^3 + T_l^3 - Q \sin^2\theta) \right] Z'_\mu. \end{aligned} \quad (6.91)$$



The weak coupling constant is again  $g_w = g_e / \sin \theta$ .

To find the coupling between a fermion and a gauge boson, you simply substitute this  $D_\mu$  into the Lagrangian  $\mathcal{L}_{\text{kF}}$  with the quantum numbers corresponding to the fermion. As an example, the interaction between a fermion and the  $W'^-$  boson is

$$\begin{aligned}\mathcal{L}_{\text{kF},W'} &= i\bar{L}_f\gamma^\mu D_\mu L_f + i\bar{R}_f\gamma^\mu D_\mu R_f \\ &= g_w\bar{L}_f\gamma^\mu \left[ \frac{\cos\phi}{\sin\phi}T_h^- - \frac{\sin\phi}{\cos\phi}T_l^- - \frac{\sin^3\phi\cos\phi}{x}(T_h^- + T_l^-) \right] L_f W_\mu'^-, \quad (6.92)\end{aligned}$$

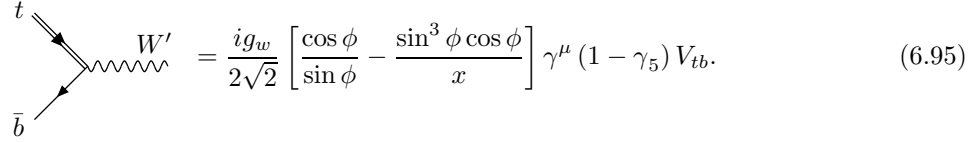
where we have used the fact that for right-handed particles  $T_l = T_h = 0$ . If the fermion is top quark then  $T_l = 0$  also for the left-handed part, and therefore

$$\begin{aligned}\mathcal{L}_{\text{kF},W't} &= g_w\bar{L}_t\gamma^\mu \left[ \frac{\cos\phi}{\sin\phi} - \frac{\sin^3\phi\cos\phi}{x} \right] \frac{\tau^-}{2} L_t W_\mu'^- \\ &= \frac{g_w}{\sqrt{2}} \begin{pmatrix} \bar{t}_L & \bar{b}'_L \end{pmatrix} \gamma^\mu \left[ \frac{\cos\phi}{\sin\phi} - \frac{\sin^3\phi\cos\phi}{x} \right] \begin{pmatrix} 0 \\ t_L \end{pmatrix} W_\mu'^- \\ &= \frac{g_w}{\sqrt{2}} \left[ \frac{\cos\phi}{\sin\phi} - \frac{\sin^3\phi\cos\phi}{x} \right] \bar{b}'_L \gamma^\mu t_L W_\mu'^-. \quad (6.93)\end{aligned}$$

Using the helicity operators  $P_L$  and  $P_R$ ,

$$\begin{aligned}\mathcal{L}_{\text{kF},W't} &= \frac{g_w}{2\sqrt{2}} \left[ \frac{\cos\phi}{\sin\phi} - \frac{\sin^3\phi\cos\phi}{x} \right] \bar{b}' \gamma^\mu (1 - \gamma_5) t W_\mu'^- \\ &= \frac{g_w}{2\sqrt{2}} \left[ \frac{\cos\phi}{\sin\phi} - \frac{\sin^3\phi\cos\phi}{x} \right] (V_{td}\bar{d} + V_{ts}\bar{s} + V_{tb}\bar{b}) \gamma^\mu (1 - \gamma_5) t W_\mu'^-, \quad (6.94)\end{aligned}$$

with  $V_{ij}$  the CKM matrix. This translates into the vertices like



$$t \text{ and } \bar{b} \text{ vertex } = \frac{ig_w}{2\sqrt{2}} \left[ \frac{\cos\phi}{\sin\phi} - \frac{\sin^3\phi\cos\phi}{x} \right] \gamma^\mu (1 - \gamma_5) V_{tb}. \quad (6.95)$$

In a similar way we find the interactions between the  $W^-$  boson and the top:

$$\begin{aligned}\mathcal{L}_{\text{kF},Wt} &= g_w\bar{L}_f\gamma^\mu \left[ T_l^- + T_h^- + \frac{\sin^2\phi}{x}(T_h^- \cos^2\phi - T_l^- \sin^2\phi) \right] L_f W_\mu^- \\ &= \frac{g_w}{2\sqrt{2}} \left[ 1 + \frac{\sin^2\phi\cos^2\phi}{x} \right] (V_{td}\bar{d} + V_{ts}\bar{s} + V_{tb}\bar{b}) \gamma^\mu (1 - \gamma_5) t W_\mu^-. \quad (6.96)\end{aligned}$$

For the  $W^-$  boson with other quarks ( $q = u, c$  such that  $T_h = 0$ ):

$$\mathcal{L}_{\text{kF},Wq} = \frac{g_w}{2\sqrt{2}} \left[ 1 - \frac{\sin^4\phi}{x} \right] (V_{qd}\bar{d} + V_{qs}\bar{s} + V_{qb}\bar{b}) \gamma^\mu (1 - \gamma_5) q W_\mu^-, \quad (6.97)$$

and for the  $W'^-$  boson with  $q = u, c$ :

$$\mathcal{L}_{\text{kF},W'q} = \frac{g_w}{2\sqrt{2}} \left[ -\frac{\sin\phi}{\cos\phi} - \frac{\sin^3\phi\cos\phi}{x} \right] (V_{qd}\bar{d} + V_{qs}\bar{s} + V_{qb}\bar{b}) \gamma^\mu (1 - \gamma_5) q W_\mu'^-. \quad (6.98)$$

From the equations (6.94), (6.96), (6.97), and (6.98) we find the following changes in the couplings. When we compare SM  $\rightarrow$  Topflavor we find for the  $W$  bosons

$$g_w V_{tb} \rightarrow g_w U_{tb} = g_w \left[ 1 + \frac{\sin^2\phi\cos^2\phi}{x} \right] V_{tb} \quad (\text{same for } V_{td}, V_{ts}), \quad (6.99a)$$

$$g_w V_{ud} \rightarrow g_w U_{ud} = g_w \left[ 1 - \frac{\sin^4\phi}{x} \right] V_{ud} \quad (\text{same for } V_{us}, V_{ub}, V_{cd}, V_{cs}, V_{cb}). \quad (6.99b)$$

Apparently the couplings in Topflavor model are a bit different from the SM. The couplings of the  $W'$  are

$$g_w U'_{tb} = g_w \left[ \frac{\cos \phi}{\sin \phi} - \frac{\sin^3 \phi \cos \phi}{x} \right] V_{tb} \quad (\text{same for } V_{td}, V_{ts}), \quad (6.100a)$$

$$g_w U'_{ud} = g_w \left[ -\frac{\sin \phi}{\cos \phi} - \frac{\sin^3 \phi \cos \phi}{x} \right] V_{ud} \quad (\text{same for } V_{us}, V_{ub}, V_{cd}, V_{cs}, V_{cb}). \quad (6.100b)$$

## 6.5 Single-top in the Topflavor model

The  $s$ -channel single-top process is influenced a lot by the introduction of new gauge bosons. Instead of having only the  $W$  as the propagator, it is now also possible to have the heavy  $W'$  boson as propagator<sup>4</sup>. The new Feynman diagram is:



Calculating the invariant amplitude for this process is not that hard. In Chapter 4 we have already determined the  $\mathcal{M}$  for  $s$ -channel single-top without the heavy  $W'$ :

$$\begin{aligned} |\overline{\mathcal{M}}|^2 &= \frac{1}{4} \sum_{\text{all spin}} \frac{g_w^4}{64} \left| [\bar{v}_d \gamma^\mu (1 - \gamma_5) u_u] \left[ \frac{V_{ud} V_{tb} g_{\mu\nu}}{k^2 - m_W^2} \right] [\bar{u}_t \gamma^\nu (1 - \gamma_5) v_{\bar{b}}] \right|^2 \\ &= \frac{1}{256} g_w^4 X^{\mu\kappa} Y_{\mu\kappa\nu\lambda} Z^{\nu\lambda}. \end{aligned} \quad (6.102)$$

with  $k = p_u + p_{\bar{d}}$  the momentum of the  $W$ . The tensors  $X^{\mu\kappa}$ ,  $Y_{\mu\kappa\nu\lambda}$  and  $Z^{\nu\lambda}$  are

$$X^{\mu\kappa} = \text{Tr} \left[ \not{p}_{\bar{d}} \gamma^\mu (1 - \gamma_5) \not{p}_u \gamma^\kappa (1 - \gamma_5) \right], \quad (6.103a)$$

$$Y_{\mu\kappa\nu\lambda} = |V_{ud}|^2 |V_{tb}|^2 \left[ \frac{g_{\mu\nu}}{k^2 - m_W^2} \right] \left[ \frac{g_{\kappa\lambda}}{k^2 - m_W^2} \right]^*, \quad (6.103b)$$

$$Z^{\nu\lambda} = \text{Tr} \left[ (\not{p}_t + m_t) \gamma^\nu (1 - \gamma_5) \not{p}_{\bar{b}} \gamma^\lambda (1 - \gamma_5) \right]. \quad (6.103c)$$

The only thing that changes in the Topflavor model is the tensor  $Y_{\mu\kappa\nu\lambda}$ ,

$$Y_{\mu\kappa\nu\lambda} = \left| \frac{U_{tb} U_{ud}}{k^2 - M_W^2} + \frac{U'_{tb} U'_{ud}}{k^2 - M_{W'}^2 + i M_{W'} \Gamma_{W'}} \right|^2 g_{\mu\nu} g_{\kappa\lambda}. \quad (6.104)$$

The decay width  $\Gamma_{W'}$  of the heavy  $W'$  is needed to prevent the occurrence of a singularity at  $k^2 = M_{W'}^2$ . The width of the light  $W$  is not needed because the energy of the partons  $\hat{s} = k^2$  will be in general much larger than  $M_W^2$ . According to [33] the width of the  $W'$  gauge boson is given by

$$\Gamma_{W'} = \frac{g_w^2}{12\pi^2} \left( \frac{2}{\tan^2 \phi} + \tan^2 \phi \right) M_{W'}. \quad (6.105)$$

The products  $U_{tb} U_{ud}$  and  $U'_{tb} U'_{ud}$  are

$$\begin{aligned} U_{tb} U_{ud} &= \left( 1 + \frac{\sin^2 \phi \cos^2 \phi}{x} \right) \left( 1 - \frac{\sin^4 \phi}{x} \right) V_{tb} V_{ud} \\ &= \left( 1 - \frac{\sin^4 \phi}{x} + \frac{\sin^2 \phi \cos^2 \phi}{x} + \mathcal{O}(x^{-2}) \right) V_{tb} V_{ud}, \end{aligned} \quad (6.106)$$

<sup>4</sup>At CM-energies of several TeV's the partons can acquire energies a much higher than the VEV of the electroweak scale,  $v \approx 175$  GeV. One could argue that at this level the Higgs doublet now also contains a positively charged Higgs boson,  $H^+$ , which can also act as the propagator! Even though this is essentially true, we do not have to include this particle. The fact is that the  $H^+$  is actually a Goldstone boson which is 'hidden' inside the  $W$  boson as its longitudinal polarization state.

and

$$\begin{aligned}
U'_{tb}U'_{ud} &= \left( \frac{\cos \phi}{\sin \phi} - \frac{\sin^3 \phi \cos \phi}{x} \right) \left( -\frac{\sin \phi}{\cos \phi} - \frac{\sin^3 \phi \cos \phi}{x} \right) V_{tb}V_{ud} \\
&= \left( -1 + \frac{\sin^4 \phi}{x} - \frac{\sin^2 \phi \cos^2 \phi}{x} + \mathcal{O}(x^{-2}) \right) V_{tb}V_{ud} \\
&= -U_{tb}U_{ud}.
\end{aligned} \tag{6.107}$$

The squared value of  $U_{tb}U_{ud}$  is

$$|U_{tb}|^2 |U_{ud}|^2 = \left( 1 - 2\frac{\sin^4 \phi}{x} + 2\frac{\sin^2 \phi \cos^2 \phi}{x} + \mathcal{O}(x^{-2}) \right) |V_{tb}|^2 |V_{ud}|^2 \tag{6.108}$$

We prefer to write this in terms of  $M_{W'}$  instead of  $x$ . Using (6.77),

$$\frac{\sin^2 \phi \cos^2 \phi}{x} = \frac{M_W^2}{M_{W'}^2}, \tag{6.109}$$

we find

$$\begin{aligned}
|U_{tb}|^2 |U_{ud}|^2 &= \left( 1 - 2\frac{\sin^4 \phi}{x} + 2\frac{\sin^2 \phi \cos^2 \phi}{x} \right) |V_{tb}|^2 |V_{ud}|^2 \\
&= \left( 1 + 2(-\tan^2 \phi + 1) \frac{M_W^2}{M_{W'}^2} \right) |V_{tb}|^2 |V_{ud}|^2.
\end{aligned} \tag{6.110}$$

The tensor  $Y_{\mu\kappa\nu\lambda}$  can now be written as

$$Y_{\mu\kappa\nu\lambda} = |U_{tb}|^2 |U_{ud}|^2 \left| \frac{1}{k^2 - M_W^2} + \frac{-1}{k^2 - M_{W'}^2 + iM_{W'}\Gamma_{W'}} \right|^2 g_{\mu\nu}g_{\kappa\lambda}. \tag{6.111}$$

The invariant amplitude for the  $s$ -channel is then

$$\begin{aligned}
|\overline{\mathcal{M}}|^2 &= \frac{1}{4}g_w^4 |V_{ud}|^2 |V_{tb}|^2 [(\hat{u} - m_t^2) \hat{u}] \left[ 1 + 2(1 - \tan^2 \phi) \frac{M_W^2}{M_{W'}^2} \right] \\
&\times \left[ \frac{1}{(\hat{s} - M_W^2)^2} - \frac{2(\hat{s} - M_{W'}^2)}{\hat{s}((\hat{s} - M_{W'}^2)^2 + M_{W'}^2\Gamma_{W'}^2)} + \frac{1}{(\hat{s} - M_{W'}^2)^2 + M_{W'}^2\Gamma_{W'}^2} \right],
\end{aligned} \tag{6.112}$$

with  $\hat{s} = k^2 = (p_u + p_{\bar{d}})^2$  and  $\hat{u} = (p_{\bar{d}} - p_t)^2$ . This equation is equal to the one stated in [33].

We do not expect a big change in the cross section for the  $t$ -channel process. The contribution of the  $W'$  goes like  $1/(\hat{t} - M_{W'}^2)^2$ , where  $\hat{t}$  is the difference between the momenta of the initial partons squared. This difference can be neglected if we compare it to the mass of the heavy gauge bosons,  $\hat{t} \ll M_{W'}^2$ , and therefore the contribution of the  $W'$  can be ignored. I.e. the results for the Topflavor  $t$ -channel are the same as those for the  $t$ -channel in the Standard Model.

Also for the  $Wt$ -associated process we do not expect much change, the presence of a heavy  $W'$  has little influence on the  $Wtb$ -coupling. We do expect however to see a similar process,

$$b + g \rightarrow t \rightarrow t + W'. \tag{6.113}$$

The cross section for this process will have the shape of a Breit-Wigner resonance with its maximum at  $s = M_{W'}^2$ .

## 6.6 Monte Carlo results

Precise electroweak measurements give bounds to the values of the free parameters of the Topflavor model. As can be seen from the equations for the  $W$  and  $Z$  masses in (6.75) and (6.71), the parameters  $\sin^2 \phi$  and  $1/x$  must be small enough to ensure that the Topflavor predictions agree with experimental results. The masses of the  $W'$  and  $Z'$  are directly related to  $\sin^2 \phi$  and  $1/x$ , via Equation (6.77).

Therefore one can also use  $M_{Z'}^2 = M_{W'}^2$ , as a free Topflavor parameter, instead of the ratio  $x = u^2/v^2$ . According to [34] valid ranges are

$$800 \text{ GeV} \leq M_{W'} \leq 2000 \text{ GeV}, \quad (6.114a)$$

$$0.05 \leq \sin^2 \phi \leq 0.25. \quad (6.114b)$$

In Figures 6.1 and 6.2 the cross sections for the  $s$ -channel single-top process are shown, for different values of  $\sin^2 \phi$  and  $M_{W'}$ . For comparison we have included in Figure 6.3 the same graphs, but for next-to-leading order [34]. One can see that for the Tevatron the NLO values are about 1.4 times larger than the LO values. We can find approximately the same factor in Table 4.2: the ratio  $\sigma_{\text{NLO}}/\sigma_{\text{LO}}$  for the  $s$ -channel at the Tevatron with  $\sqrt{s} = 2 \text{ TeV}$ , is 1.47. Of course this is no solid proof that Figure 6.2 absolutely agrees with Figure 6.3; the values of Table 4.2 are for the Standard Model, while the plots presented here are for Topflavor. But we do recognize that the curves of Figures 6.1 and 6.2 nicely follow the curves of Figure 6.3, e.g. none of the LO curves crosses its NLO curve. Also for the LHC we find that ratio  $\sigma_{\text{NLO}}/\sigma_{\text{LO}}$  in the Topflavor plots roughly agrees with the values in Table 4.2, in all cases around 1.4. If we compare the  $s$ -channel cross sections of the Standard Model to those of the Topflavor, we see that the Topflavor  $s$ -channel cross sections can be up to four times larger for the LHC. Even if  $M_{W'}$  has a large mass of around 2 TeV the cross section is increased by about 25%. At the Tevatron there are no big differences between the Standard Model cross section and those in Topflavor. Therefore it is unlikely that the Tevatron will discover the  $W'$  via the  $s$ -channel.

The  $p_T$  of the top quark for different values of  $M_{W'}$  is presented in Figure 6.4-6.7, and for different values of  $\sin^2 \phi$  in Figure 6.8 and 6.9. It is clear that the heavy  $W'$  has a strong influence on the  $s$ -channel single-top process. If the mass is relatively low (below 1 TeV) then the  $p_T$  shows a clear peak near  $p_T = M_{W'}/2$ . This can be easily explained with kinematics. The left peak is the same maximum as the one in the  $p_T$  plots of the Standard Model (Figure 4.7 and 4.8). By introducing a second, heavier  $W$  boson, we introduce a second peak. The  $p_T$  of the top quark has its second maximum around half the mass of the  $W'$ , because there the  $W$  is close to becoming a real particle. If there is enough energy then it is easier to create a real particle than a virtual one<sup>5</sup>, hence the increase in cross section. The mass of the top quark is small compared to the  $W'$  mass. This means that when the heavy boson decays ( $W'^+ \rightarrow t\bar{b}$ ), each quark will receive about half the energy of the  $W'$ , i.e. the momentum of the top will be  $p_t \approx M_{W'}/2$ .

As one can see in Figure 6.8 and 6.9, a small mixing angle leads to a small second peak. How can we explain this? The answer is inside Equation (6.105): the decay width of the  $W'$ . The decay width is included in the invariant amplitude to avoid a singularity when  $W'$  becomes real;  $k^2 \approx M_{W'}^2$ . Evidently, when  $\Gamma_{W'}$  becomes smaller, the resonance quickly increase in size. The width is proportional to

$$\Gamma_{W'} \propto \frac{2}{\tan^2 \phi} + \tan^2 \phi = \frac{2 \cos^2 \phi}{\sin^2 \phi} + \frac{\sin^2 \phi}{\cos^2 \phi} = \frac{2(1 - \sin^2 \phi)}{\sin^2 \phi} + \frac{\sin^2 \phi}{(1 - \sin^2 \phi)}. \quad (6.115)$$

If  $\sin^2 \phi$  becomes really small, then

$$\Gamma_{W'} \propto \frac{2(1 - \sin^2 \phi)^2 + \sin^4 \phi}{\sin^2 \phi (1 - \sin^2 \phi)} \approx \frac{2}{\sin^2 \phi}, \quad (6.116)$$

and this becomes very large for small values of  $\sin^2 \phi$ . Therefore a small  $\sin^2 \phi$  results into a smaller resonance, hence a small second peak.

Figures 6.10-6.17 show the pseudo(rapidity) of the top. These are quite similar to the ones in the Standard Model, except for having a larger area (which is because the cross section is higher than in the SM). The only noticeable thing is that in the pseudorapidity for the LHC (Figure 6.13) the small dip disappears when  $M_{W'}$  is large and  $\sin^2 \phi$  is low.

The results for the  $\bar{t}$  at the Tevatron are the same as the results for the  $t$ . For the LHC the  $\bar{t}$  cross sections are all roughly 50% lower than the  $t$  values. That is because the LHC collides two protons, each built from two  $u$ -quarks and one  $d$ -quark. To produce an  $s$ -channel top quark, we need a  $u$ -quark (and a  $\bar{d}$ -quark). To produce an  $s$ -channel top antiquark, we need a  $d$ -quark (and a  $\bar{u}$ -quark). Hence, the cross section for the top is twice as large.

<sup>5</sup>In mathematical terms: if the particle is (almost) real, then  $k^2 \approx m^2$  and the denominator in the propagator of the  $s$ -channel becomes very small. This results into a large increase of the invariant implitude, i.e. a large cross section near  $k^2 = m^2$ .

Figure 6.1: Cross section of the  $s$ -channel single-top in the Topflavor model, as a function of  $M_{W'} = M_{Z'}$ . The  $\sigma$  here is the cross section for the Tevatron ( $p\bar{p}$ ,  $\sqrt{s} = 2$  TeV). At the Tevatron the results for  $t$  are equal to those for the  $\bar{t}$ .

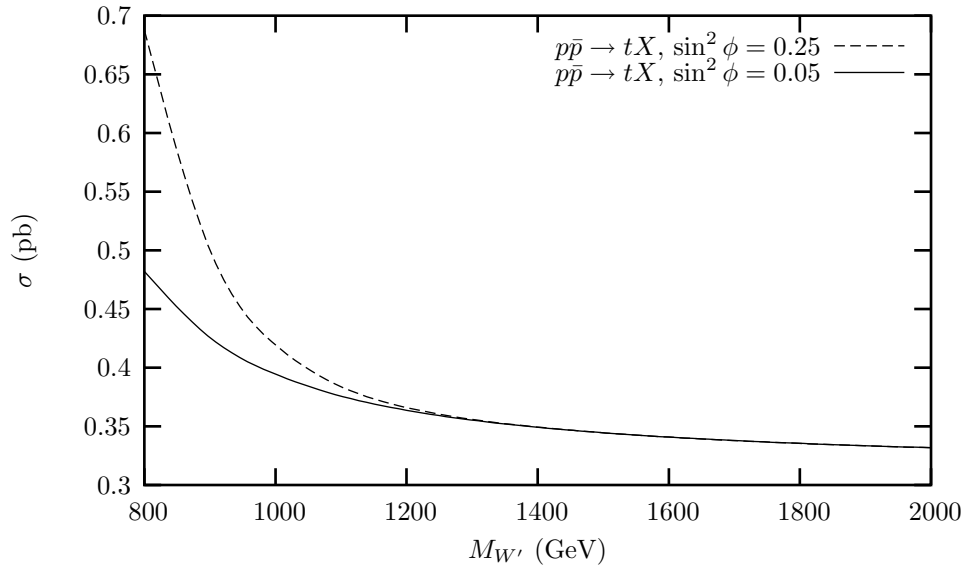
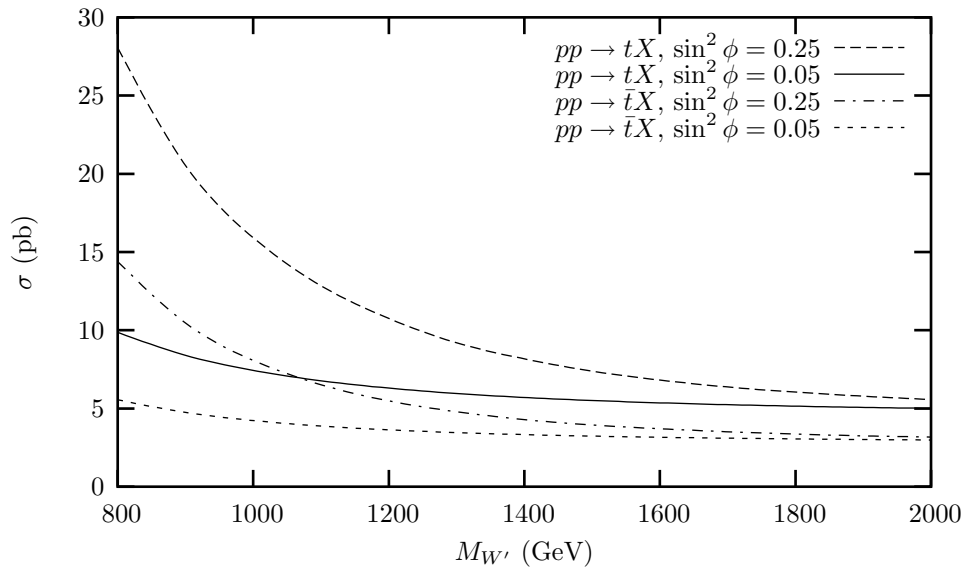


Figure 6.2: Cross section of the  $s$ -channel single-top in the Topflavor model, as a function of  $M_{W'} = M_{Z'}$ . The  $\sigma$  here is the cross section for the LHC ( $pp$ ,  $\sqrt{s} = 14$  TeV).



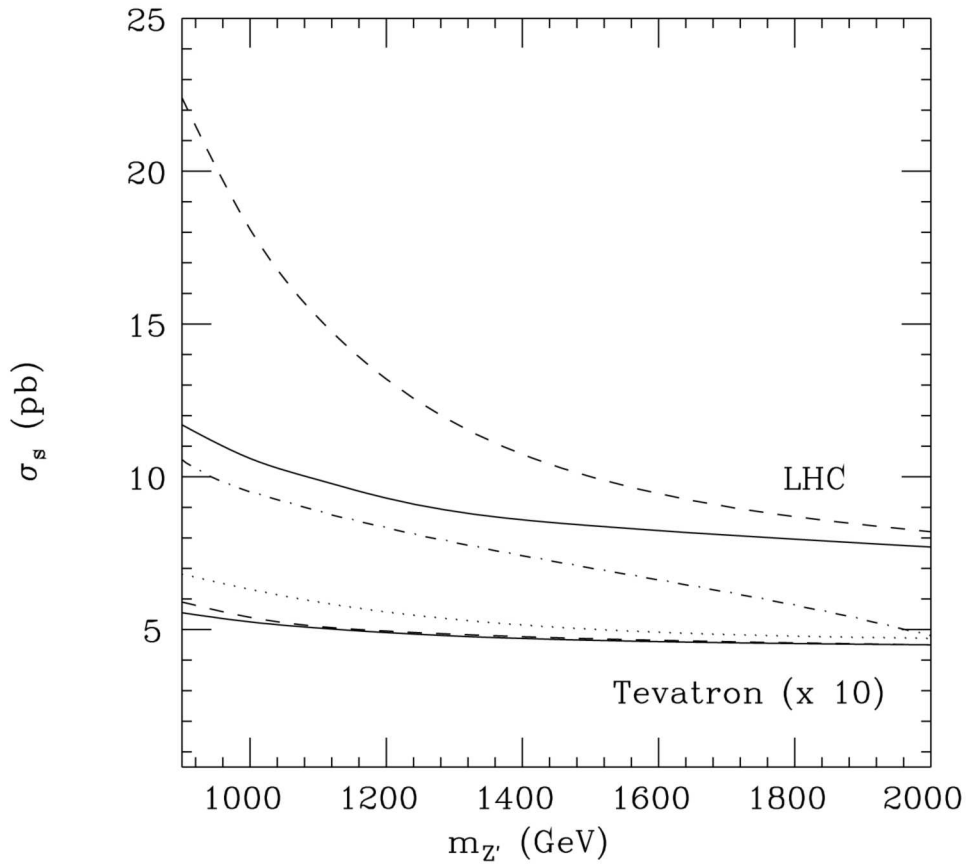


Figure 6.3: The NLO rate of the  $s$ -channel process  $q\bar{q}' \rightarrow W, W' \rightarrow t\bar{t}$  in pb at the Tevatron (lower curves) and LHC (upper curves), for the Topflavor model with  $\sin^2 \phi = 0.05$  (solid curves) and  $\sin^2 \phi = 0.25$  (dashed curves), as a function of  $M_{Z'} = M_{W'}$ . The Tevatron cross sections are multiplied by a factor of 10. At the Tevatron, the  $\bar{t}$  production rate is equal to the  $t$  rate. At the LHC the  $\bar{t}$  rates are shown for  $\sin^2 \phi = 0.05$  (dotted curve) and  $\sin^2 \phi = 0.25$  (dot-dashed curve). Taken from [34].

Figure 6.4: Transverse momentum for  $s$ -channel single-top in the Topflavor model, at the Tevatron ( $p\bar{p}$ ,  $\sqrt{s} = 2$  TeV). We have plotted here the  $p_T$  of the  $t$ -quark for different values of  $M_{W'}$ , always with  $\sin^2 \phi = 0.25$ . At the Tevatron the results for  $t$  are equal to those for the  $\bar{t}$ .

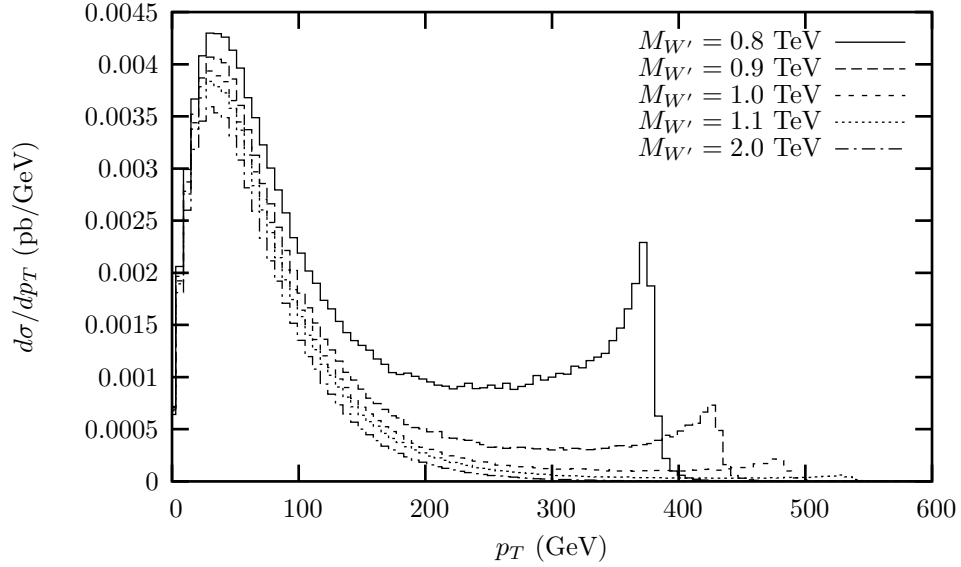


Figure 6.5: Transverse momentum for  $s$ -channel single-top in the Topflavor model, at the Tevatron ( $p\bar{p}$ ,  $\sqrt{s} = 2$  TeV). We have plotted here the  $p_T$  of the  $t$ -quark for different values of  $M_{W'}$ , always with  $\sin^2 \phi = 0.05$ . At the Tevatron the results for  $t$  are equal to those for the  $\bar{t}$ .

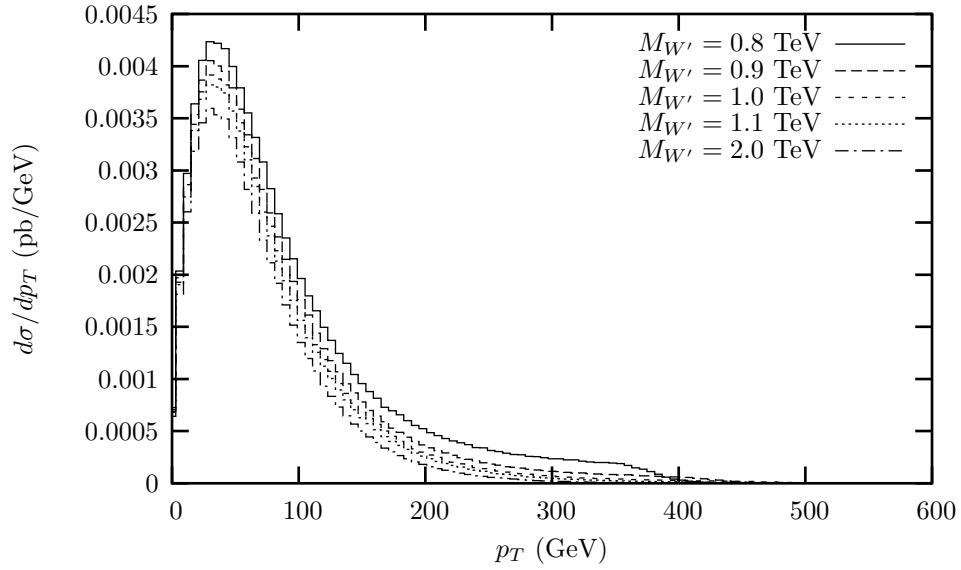


Figure 6.6: Transverse momentum for  $s$ -channel single-top in the Topflavor model, at the LHC ( $pp$ ,  $\sqrt{s} = 14$  TeV). We have plotted here the  $p_T$  of the  $t$ -quark for different values of  $M_{W'}$ , always with  $\sin^2 \phi = 0.25$ . The  $p_T$  of the  $\bar{t}$ -quark has the same shape as the  $t$ -quark, but is roughly 50% lower.

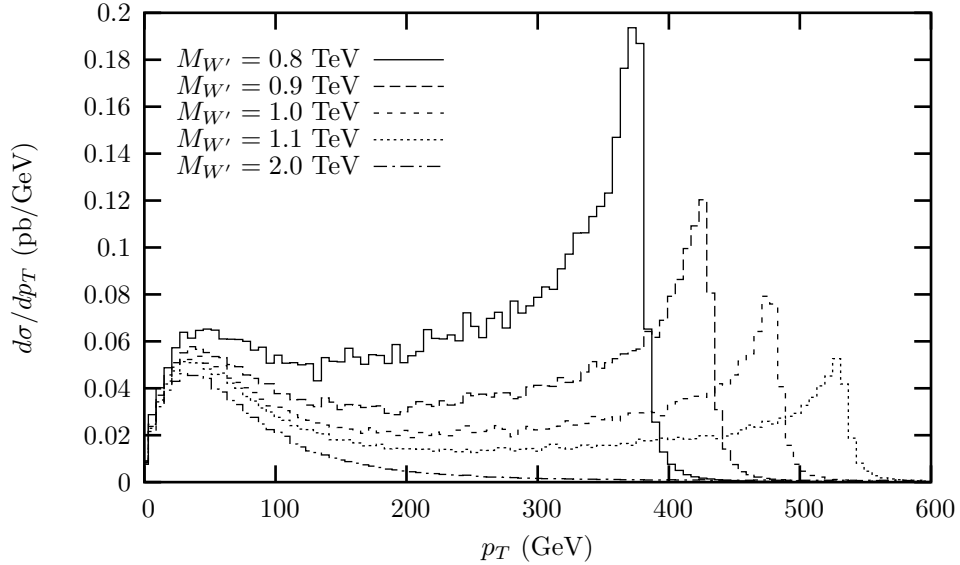


Figure 6.7: Transverse momentum for  $s$ -channel single-top in the Topflavor model, at the LHC ( $pp$ ,  $\sqrt{s} = 14$  TeV). We have plotted here the  $p_T$  of the  $t$ -quark for different values of  $M_{W'}$ , always with  $\sin^2 \phi = 0.05$ . The  $p_T$  of the  $\bar{t}$ -quark has the same shape as the  $t$ -quark, but is roughly 50% lower.

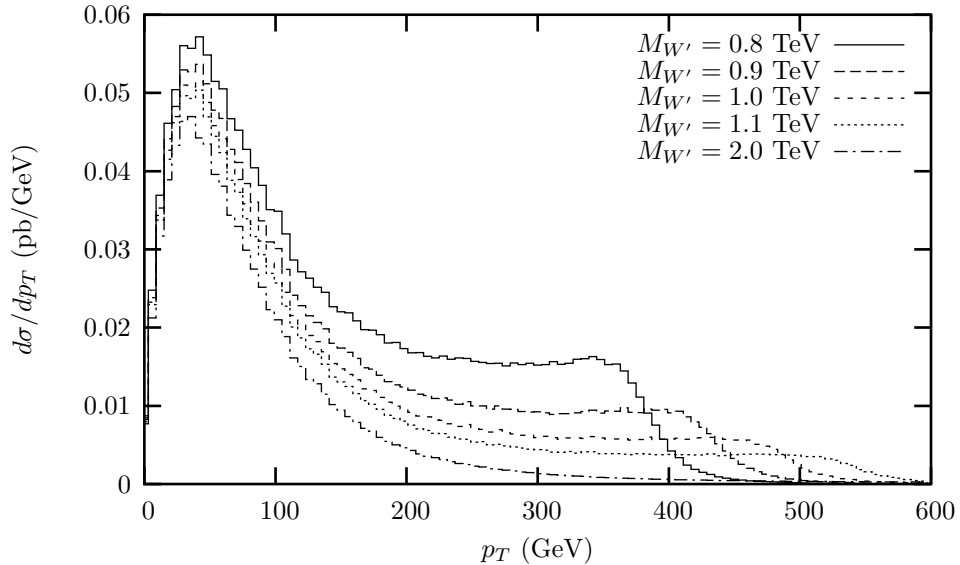




Figure 6.8: Transverse momentum for  $s$ -channel single-top in the Topflavor model, at the Tevatron ( $p\bar{p}$ ,  $\sqrt{s} = 2$  TeV). We have plotted here the  $p_T$  of the  $t$ -quark for different values of  $\sin^2 \phi$ . The mass of the heavy  $W$  boson is here  $M_{W'} = 800$  GeV. At the Tevatron the results for  $t$  are equal to those for the  $\bar{t}$ .

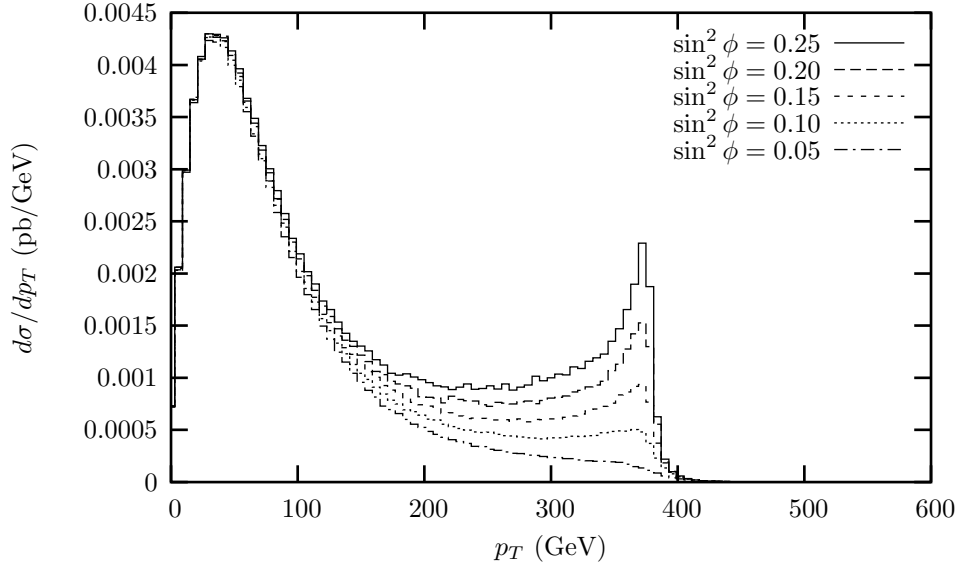


Figure 6.9: Transverse momentum for  $s$ -channel single-top in the Topflavor model, at the LHC ( $pp$ ,  $\sqrt{s} = 14$  TeV). We have plotted here the  $p_T$  of the  $t$ -quark for different values of  $\sin^2 \phi$ . The mass of the heavy  $W$  boson is here  $M_{W'} = 800$  GeV. The  $p_T$  of the  $\bar{t}$ -quark has the same shape as the  $t$ -quark, but is roughly 50% lower.

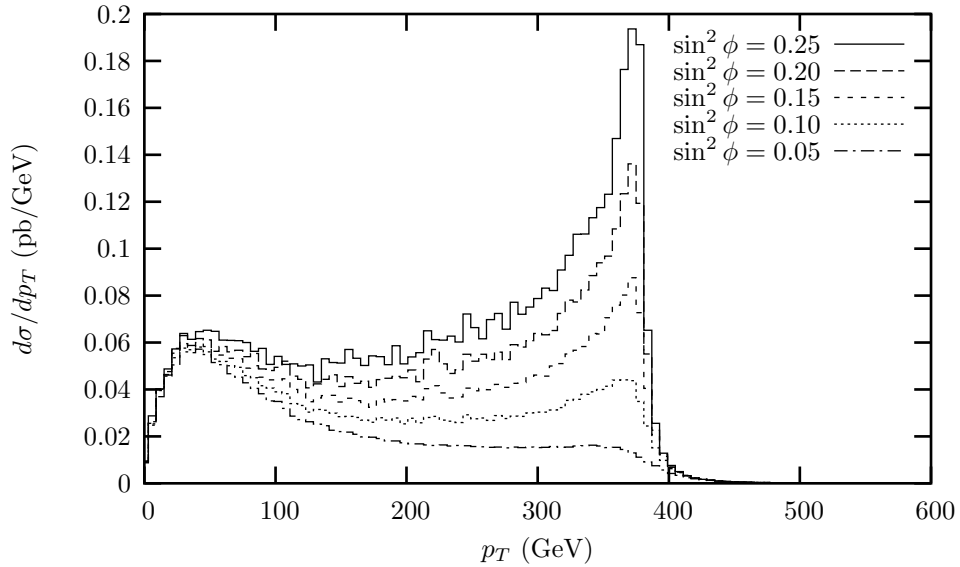


Figure 6.10: Pseudorapidity for  $s$ -channel single-top in the Topflavor model, at the Tevatron ( $p\bar{p}$ ,  $\sqrt{s} = 2$  TeV). We have plotted here the  $\eta$  of the  $t$ -quark for different values of  $M_{W'}$ , always with  $\sin^2 \phi = 0.25$ . At the Tevatron the results for  $t$  are equal to those for the  $\bar{t}$ .

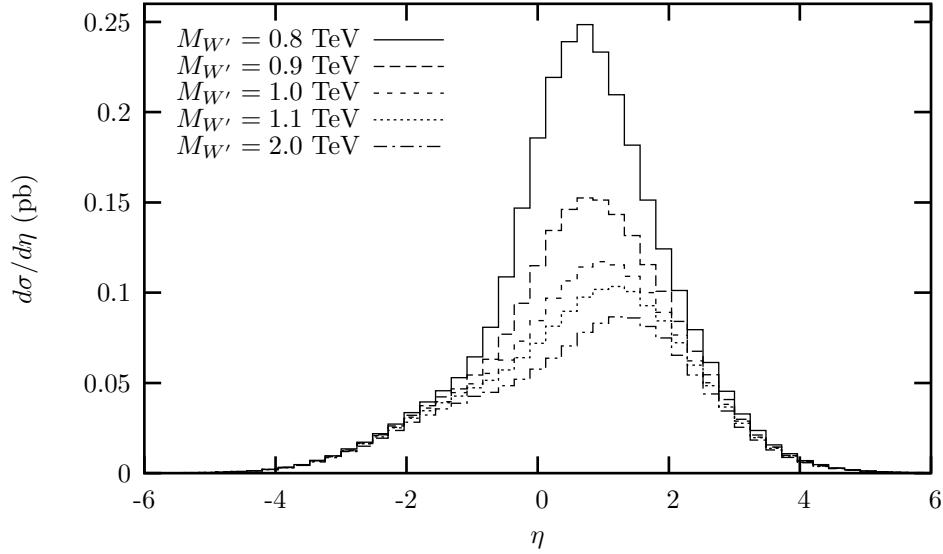


Figure 6.11: Pseudorapidity for  $s$ -channel single-top in the Topflavor model, at the Tevatron ( $p\bar{p}$ ,  $\sqrt{s} = 2$  TeV). We have plotted here the  $\eta$  of the  $t$ -quark for different values of  $M_{W'}$ , always with  $\sin^2 \phi = 0.05$ . At the Tevatron the results for  $t$  are equal to those for the  $\bar{t}$ .

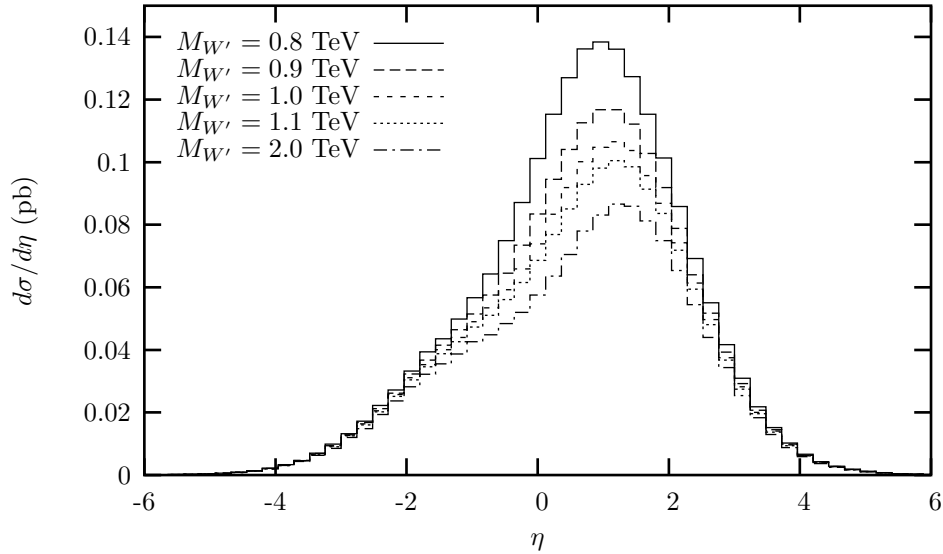


Figure 6.12: Pseudorapidity for  $s$ -channel single-top in the Topflavor model, at the LHC ( $pp$ ,  $\sqrt{s} = 14$  TeV). We have plotted here the  $\eta$  of the  $t$ -quark for different values of  $M_{W'}$ , always with  $\sin^2 \phi = 0.25$ . The  $p_T$  of the  $\bar{t}$ -quark has the same shape as the  $t$ -quark, but is roughly 50% lower.

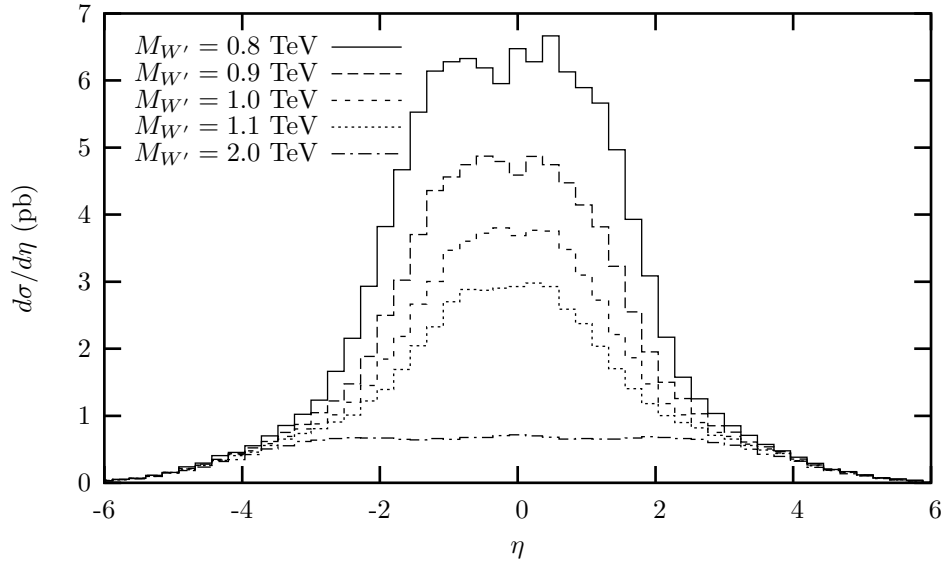


Figure 6.13: Pseudorapidity for  $s$ -channel single-top in the Topflavor model, at the LHC ( $pp$ ,  $\sqrt{s} = 14$  TeV). We have plotted here the  $\eta$  of the  $t$ -quark for different values of  $M_{W'}$ , always with  $\sin^2 \phi = 0.05$ . The  $p_T$  of the  $\bar{t}$ -quark has the same shape as the  $t$ -quark, but is roughly 50% lower.

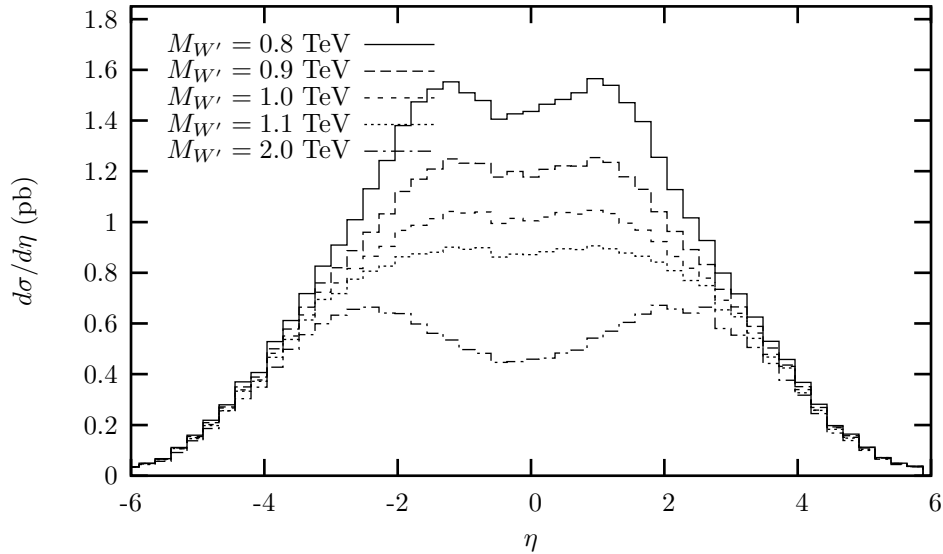


Figure 6.14: Rapidity for  $s$ -channel single-top in the Topflavor model, at the Tevatron ( $p\bar{p}$ ,  $\sqrt{s} = 2$  TeV). We have plotted here the  $y$  of the  $t$ -quark for different values of  $M_{W'}$ , always with  $\sin^2 \phi = 0.25$ . At the Tevatron the results for  $t$  are equal to those for the  $\bar{t}$ .

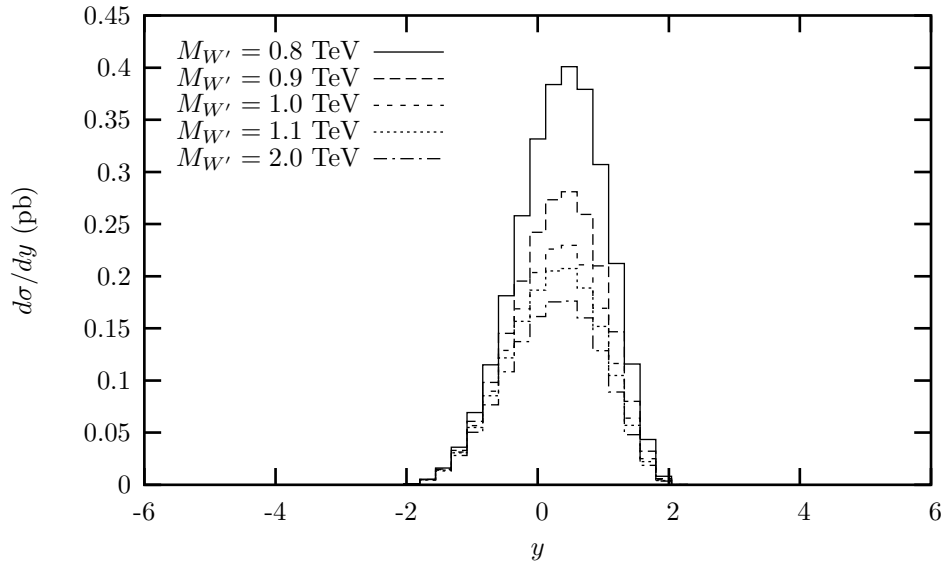


Figure 6.15: Rapidity for  $s$ -channel single-top in the Topflavor model, at the Tevatron ( $p\bar{p}$ ,  $\sqrt{s} = 2$  TeV). We have plotted here the  $y$  of the  $t$ -quark for different values of  $M_{W'}$ , always with  $\sin^2 \phi = 0.05$ . At the Tevatron the results for  $t$  are equal to those for the  $\bar{t}$ .

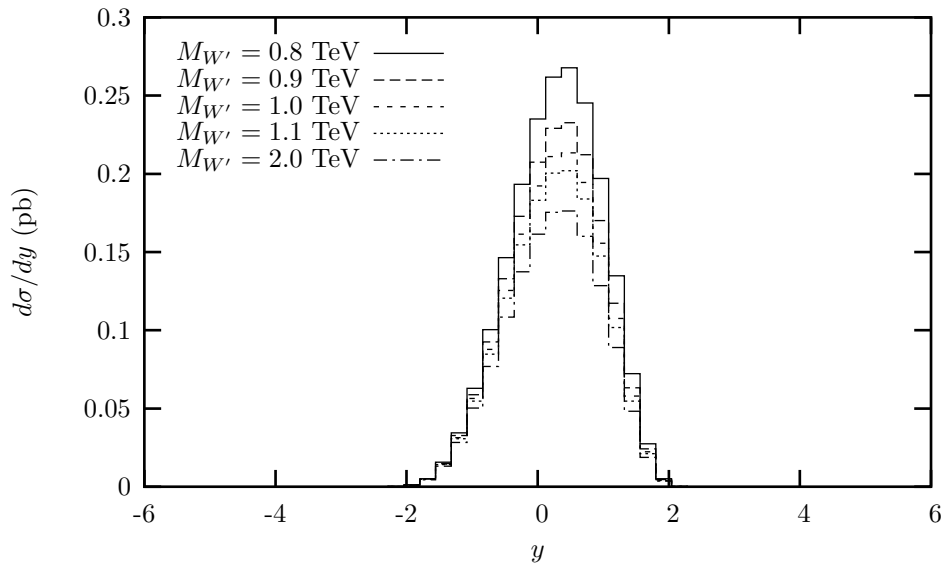


Figure 6.16: Rapidity for  $s$ -channel single-top in the Topflavor model, at the LHC ( $pp$ ,  $\sqrt{s} = 14$  TeV). We have plotted here the  $y$  of the  $t$ -quark for different values of  $M_{W'}$ , always with  $\sin^2 \phi = 0.25$ . The  $p_T$  of the  $\bar{t}$ -quark has the same shape as the  $t$ -quark, but is roughly 50% lower.

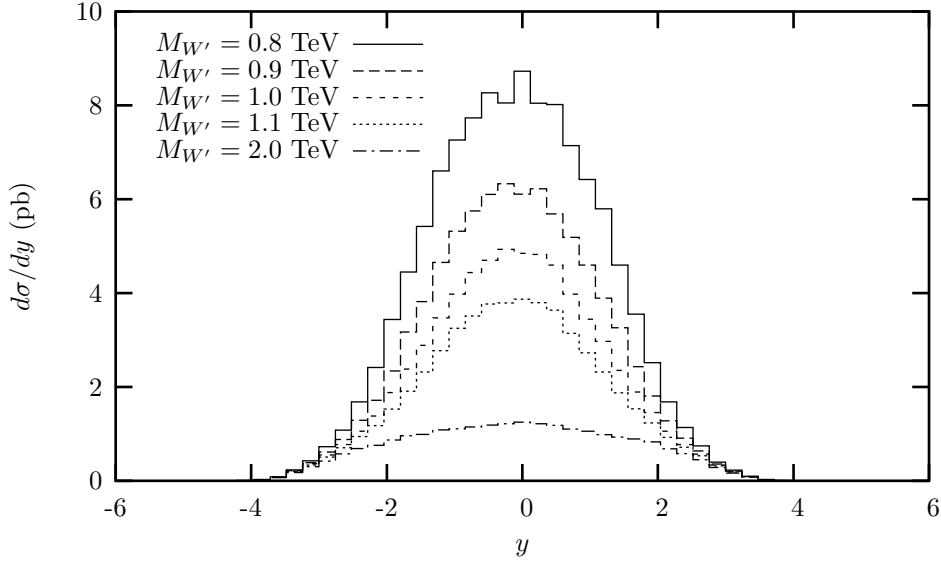
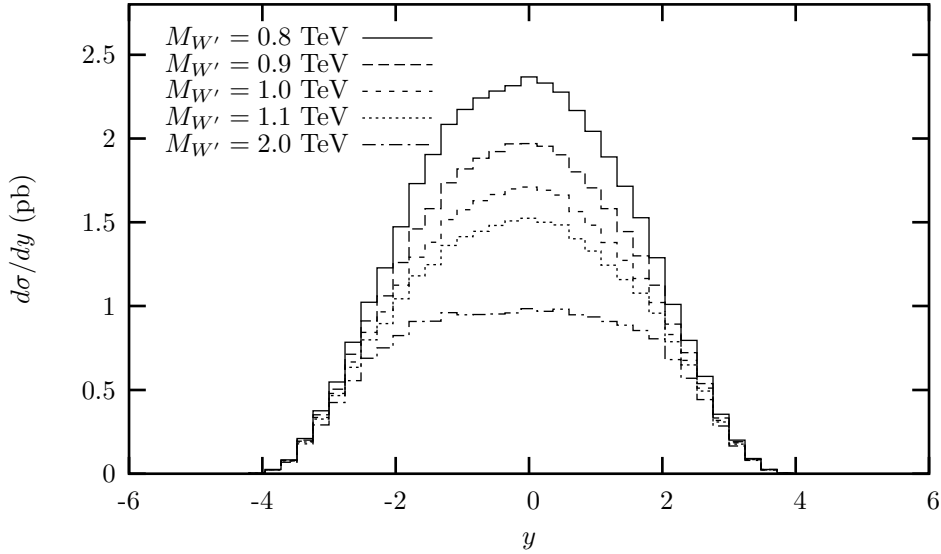


Figure 6.17: Rapidity for  $s$ -channel single-top in the Topflavor model, at the LHC ( $pp$ ,  $\sqrt{s} = 14$  TeV). We have plotted here the  $y$  of the  $t$ -quark for different values of  $M_{W'}$ , always with  $\sin^2 \phi = 0.05$ . The  $p_T$  of the  $\bar{t}$ -quark has the same shape as the  $t$ -quark, but is roughly 50% lower.



# Chapter 7

## Little Higgs models

Recently, a new class of extensions to the Standard Model has been developed. These *Little Higgs models* provide a natural way of giving the Higgs boson its mass. In the Standard Model the Higgs mass suffers from the so-called hierarchy problem, something that is solved in Little Higgs theory. We shall explain more about the hierarchy problem in the first section of this chapter. After that we focus more on one particular model: *the Littlest Higgs*. This model has become quite popular in a short period of time. In Section 7.2 we present the symmetric structure of this model, followed by the calculation of the mass eigenstates of the gauge bosons in Section 7.3. In Section 7.4. the invariant amplitudes for single-top are determined, with the results presented and discussed in Section 7.5.

### 7.1 The hierarchy problem

At tree level the Standard Model is a stable, well-behaving quantum field theory, but problems arise when we include diagrams with loops. To calculate loop diagrams we need integrate over the momenta of the fermions inside the loops. These integrals are often quadratically divergent and need to cancel with the integrals of other loop diagrams. In the Standard Model the calculation of the Higgs mass is a problem. There are three diagrams that give a large contribution to the Higgs mass, see Figure 7.1. Assuming that the Standard Model remains valid up to a cut-off scale of  $\Lambda \sim 10$  TeV, the three diagrams give [35]

$$\text{top loop} \quad -\frac{3}{8\pi^2}\lambda_t^2\Lambda^2 \sim -(2 \text{ TeV})^2, \quad (7.1a)$$

$$\text{gauge boson loop} \quad \frac{1}{16\pi^2}g^2\Lambda^2 \sim (700 \text{ GeV})^2, \quad (7.1b)$$

$$\text{Higgs loop} \quad \frac{1}{16\pi^2}\lambda^2\Lambda^2 \sim (500 \text{ GeV})^2. \quad (7.1c)$$

The Higgs mass is then

$$m_h^2 = m_{\text{tree}}^2 - (2 \text{ TeV})^2 + (700 \text{ GeV})^2 + (500 \text{ GeV})^2. \quad (7.2)$$

The parameters  $\lambda_t$ ,  $g$ , and  $\lambda$  need some careful fine-tuning to make sure that all divergences are exactly cancelled (Figure 7.2). This is possible, but is however a very unnatural situation. We would prefer to have a theory where all quadratic divergences are canceled because of symmetries or some other property of the theory. The need for fine-tuning is called the *hierarchy problem*.

There are several extensions of the Standard Model that solve the hierarchy problem. In supersymmetric theories each particle has a superpartner that gives the same loop diagrams, but with the

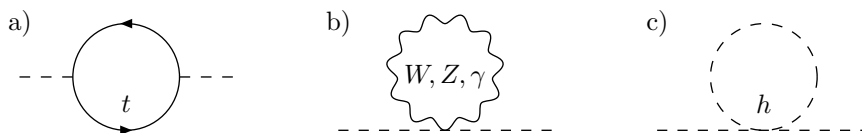


Figure 7.1: The three most significant loop contributions to the Higgs mass. In (a) the top loop diagram, in (b) the Higgs loop diagram, and in (c) the gauge boson loop diagram.

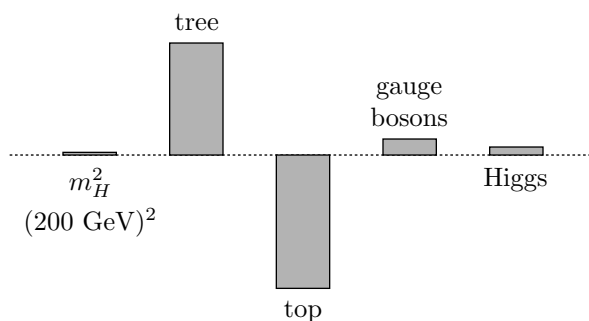


Figure 7.2: The fine-tuning required to obtain an acceptable Higgs mass in the Standard Model with cut-off scale  $\Lambda \sim 10$  TeV (taken from [36]).

opposite sign. Therefore the supersymmetry causes a perfect cancellation of quadratic divergences. There are still logarithmic divergences, but these do not invoke any fine-tuning. In this chapter we examine a different class of theories: Little Higgs models. In these models the Higgs boson has a stable mass because it is a pseudo-Goldstone boson<sup>1</sup>. Such a boson results from a spontaneously broken approximate global symmetry. A small mass term or Yukawa term breaks the global symmetry explicitly, providing a small mass for the otherwise massless Goldstone boson. This term must be small to prevent the theory from losing the symmetry completely.

Early attempts to create such a theory were unsuccessful: the quadratic divergences to the Higgs mass remained. The first successful Little Higgs model which canceled all relevant quadratic divergences was constructed by Arkani-Hamed, Cohen, and Georgi in 2001 [37]. Subsequently, a lot of new Little Higgs models were constructed, e.g. [38], [39], [40]. In this chapter we treat one of the most popular models, the so-called Littlest Higgs [41].

## 7.2 The Littlest Higgs

Little Higgs models can be categorized by the symmetry breaking they are based upon. In the case of the Littlest Higgs we have the breaking of  $\underline{\text{SU}(5)} \rightarrow \underline{\text{SO}(5)}$ , which occurs at a scale  $f$  of the order of 1 TeV. We introduce here an old notation: when the symmetry is global, the group is underlined. Within the global  $\underline{\text{SU}(5)}$  symmetry we imbed an  $\text{SU}(2)_1 \times \text{U}(1)_1 \times \text{SU}(2)_2 \times \text{U}(1)_2$  gauge symmetry. After the breaking  $\underline{\text{SU}(5)} \rightarrow \underline{\text{SO}(5)}$  the gauge symmetry will break down to the Standard Model symmetry:  $[\text{SU}(2)_j \times \text{U}(1)_j]^2 \rightarrow \text{SU}(2)_w \times \text{U}(1)_Y$ . Of course, at scale  $v$  we have again the electroweak symmetry breaking.

Even though the symmetry breaking to  $\text{U}(1)_{em}$  goes into two steps (just like Topflavor), this theory only needs one Higgs field: a  $5 \times 5$  matrix field called  $\Sigma$ . When  $\Sigma$  acquires a vacuum expectation value, Goldstone bosons appear to the theory. These are then identified with the SM Higgs fields.

For the correct breaking to happen, we need the VEV of the  $\Sigma$  to be

$$\langle \Sigma \rangle = \Sigma_0 = \begin{pmatrix} & & & & \mathbf{1}_{2 \times 2} \\ & & & & \\ & & 1 & & \\ & & & & \\ \mathbf{1}_{2 \times 2} & & & & \end{pmatrix}. \quad (7.3)$$

What causes  $\Sigma$  to acquire exactly this VEV is not explained in the theory. But that this VEV leads to the correct symmetry breaking can be shown by writing

$$\Sigma_0 = A^2 = A^T A, \quad (7.4)$$

where the matrix  $A$  is given by

$$A = \frac{1}{2} \begin{pmatrix} 1+i & & 1-i \\ & 2 & \\ 1-i & & 1-i \end{pmatrix}. \quad (7.5)$$

With  $A$  we can define a new set of  $\text{SU}(5)$  generators  $X_a \equiv A \lambda_a A^{-1}$ , where  $\lambda_a$  are the usual  $\text{SU}(5)$  generators as stated in Appendix B. It is easy to see that just like the  $\lambda_a$ , the  $X_a$  also satisfy the Lie

<sup>1</sup>This is a natural idea; the same principle occurs also for pions, which can be regarded as pseudo-Goldstone bosons generated by the chiral symmetry breaking  $\text{U}(3)_L \times \text{U}(3)_R \rightarrow \text{U}(3)_{L+R}$  in QCD.

algebra of  $SU(5)$ . If

$$[\lambda_a, \lambda_b] = if_{abc}\lambda_c, \quad (7.6)$$

then

$$\begin{aligned} [X_a, X_b] &= [A\lambda_a A^{-1}, A\lambda_b A^{-1}] = A\lambda_a A^{-1} A\lambda_b A^{-1} - A\lambda_b A^{-1} A\lambda_a A^{-1} \\ &= A\lambda_a \lambda_b A^{-1} - A\lambda_b \lambda_a A^{-1} = A[\lambda_a, \lambda_b] A^{-1} = A(if_{abc}\lambda_c) A^{-1} \\ &= if_{abc} A\lambda_c A^{-1} = if_{abc} X_c. \end{aligned} \quad (7.7)$$

The  $X_a$  are defined in such a way that

$$X_a \Sigma_0 = (A\lambda_a A^{-1}) A^2 = A\lambda_a A = \pm (A\lambda_a A)^T = \pm (X_a \Sigma_0)^T = \pm \Sigma_0 X_a^T, \quad (7.8)$$

with the plus sign for the 14 symmetric  $\lambda_a$  and the minus sign for the 10 antisymmetric  $\lambda_a$ .

The matrix field  $\Sigma$  transforms as

$$\Sigma \rightarrow \Sigma' = U\Sigma U^T = \exp(i\alpha_a X_a) \Sigma \exp(i\alpha_a X_a^T), \quad (7.9)$$

where  $U$  is a  $SU(5)$  operator. The generators of the unbroken symmetry  $\underline{SO(5)}$  are the ones that leave the vacuum invariant:

$$\exp(i\alpha_a X_a) \Sigma_0 \exp(i\alpha_a X_a^T) = \Sigma_0 \quad (7.10)$$

Up to order  $\mathcal{O}(\alpha_a^2)$  we find

$$(1 + i\alpha_a X_a) \Sigma_0 (1 + i\alpha_a X_a^T) = \Sigma_0 + i\alpha_a (X_a \Sigma_0 + \Sigma_0 X_a^T) + \mathcal{O}(\alpha_a^2), \quad (7.11)$$

and therefore the  $\underline{SO(5)}$  generators are given by:

$$X_a \Sigma_0 + \Sigma_0 X_a^T = 0. \quad (7.12)$$

We see that these generators are the 10 matrices  $T_a \equiv A\lambda_a A^{-1}$  for which  $\lambda_a$  is antisymmetric. The other 14 generators  $S_a \equiv A\lambda_a A^{-1}$  with symmetric  $\lambda_a$ , are broken.

## Introducing the gauge symmetries

Sofar we have only demonstrated the breaking of the global symmetries. We shall now gauge a part of the  $\underline{SU(5)}$  symmetry to introduce gauge bosons to the theory. We cannot turn the whole  $\underline{SU(5)}$  into a local symmetry, because then all Goldstone bosons would be eaten by the gauge bosons and we would not have any Goldstone bosons left that can be identified as the Standard Model Higgs. Therefore we only gauge a small part of the  $\underline{SU(5)}$ .

The kinetic term of  $\Sigma$  is given by

$$\mathcal{L}_{\text{kH}} = \frac{f^2}{4} \text{Tr} \left[ (D_\mu \Sigma)^\dagger (D^\mu \Sigma) \right] = \frac{f^2}{4} \text{Tr} |D_\mu \Sigma|^2, \quad (7.13)$$

with the covariant derivative  $D_\mu$  chosen in such a way that we have a  $[SU(2)_j \times U(1)_j]^2$  gauge symmetry:

$$D_\mu \Sigma = \partial_\mu \Sigma - i \sum_{j=1}^2 [g_j W_{\mu j}^a (Q_j^a \Sigma + \Sigma Q_j^{aT}) + g'_j B_{\mu j} (Y_j \Sigma + \Sigma Y_j^T)]. \quad (7.14)$$

The generators  $Q_j^a$  correspond to the  $SU(2)_j$  gauge symmetry and the generators  $Y_j$  to the  $U(1)_j$ . A good way to embed these subgroups into the  $\underline{SU(5)}$  is:

$$Q_1^a = \frac{1}{2} \begin{pmatrix} \tau^a & & \\ & \mathbf{0}_{3 \times 3} & \\ & & \end{pmatrix}, \quad Y_1 = \frac{1}{10} \text{diag}(-3, -3, 2, 2, 2), \quad (7.15a)$$

$$Q_2^a = \frac{1}{2} \begin{pmatrix} & & \\ \mathbf{0}_{3 \times 3} & & \\ & & -\tau^a \end{pmatrix}, \quad Y_2 = \frac{1}{10} \text{diag}(-2, -2, -2, 3, 3). \quad (7.15b)$$

With this choice one can easily check that their linear combinations,

$$Q^a = \frac{1}{\sqrt{2}} (Q_1^a + Q_2^a), \quad Y = Y_1 + Y_2, \quad (7.16)$$



remain unbroken after the symmetry breaking:

$$Q_a \Sigma_0 + \Sigma_0 Q_a^T = 0 \quad (7.17a)$$

$$Y \Sigma_0 + \Sigma_0 Y^T = 0 \quad (7.17b)$$

Therefore the generators  $Q_a$  and  $Y$  are identified as the generators of the SM electroweak group  $SU(2)_w \times U(1)_Y$ .

The  $Q_1^a$  and  $Y_1$  still allow for a global  $SU(3)$  symmetry in the lower  $3 \times 3$  block. Also the  $Q_2^a$  and  $Y_2$  allow for a global  $SU(3)$  symmetry, but there the symmetry is in the upper  $3 \times 3$  block. These are two different symmetries, the first will be notated with  $\underline{SU(3)}_1$  and the latter with  $\underline{SU(3)}_2$ .

## Goldstone bosons

Goldstone's theorem tells us that the symmetry breaking  $SU(5) \rightarrow SO(5)$  leaves us with 14 massless Goldstone bosons, because there are 14 broken generators. At the same time the Higgs mechanism tells us that breaking the gauge symmetry  $[SU(2)_j \times U(1)_j]^2 \rightarrow SU(2)_w \times U(1)_Y$  causes four gauge bosons to become massive. This means that we are left with only 10 physical Goldstone fields.

To handle these fields, it is convenient to expand  $\Sigma$  about the expectation value:

$$\begin{aligned} \Sigma &= \exp(i\alpha_a S_a) \Sigma_0 \exp(i\alpha_a S_a^T) = (1 + i\alpha_a S_a) \Sigma_0 (1 + i\alpha_a S_a^T) + \mathcal{O}(\alpha_a^2) \\ &= \Sigma_0 + i\alpha_a (S_a \Sigma_0 + \Sigma_0 S_a^T) + \mathcal{O}(\alpha_a^2) \\ &= \Sigma_0 + 2i\alpha_a S_a \Sigma_0 + \mathcal{O}(\alpha_a^2) \\ &= \Sigma_0 \exp(2i\alpha_a S_a) \\ &\equiv \Sigma_0 \exp(2i\Pi/f), \end{aligned} \quad (7.18)$$

where we have used  $S_a \Sigma_0 = \Sigma_0 S_a^T$  and defined the matrix

$$\Pi \equiv \pi_a S_a \equiv f \alpha_a S_a. \quad (7.19)$$

Using  $S_a$  as defined before, we can write  $\Pi$  explicitly as [42]

$$\Pi = \begin{pmatrix} \chi + \eta/(2\sqrt{5}) & h^*/\sqrt{2} & \phi^\dagger \\ h^T/\sqrt{2} & -2\eta/\sqrt{5} & h^\dagger/\sqrt{2} \\ \phi & h/\sqrt{2} & \chi^T + \eta/(2\sqrt{5}) \end{pmatrix}, \quad (7.20)$$

with  $\eta$  a real singlet,  $\chi = \chi^a \tau^a / 2$  a Hermitian, traceless  $2 \times 2$  matrix,  $h$  a complex doublet and  $\phi$  a  $2 \times 2$  symmetric matrix. These fields represent the 14 Goldstone bosons. Under  $SU(2)_w \times U(1)_Y$  they transform as

$$\mathbf{1}_0 \oplus \mathbf{3}_0 \oplus \mathbf{2}_{\pm\frac{1}{2}} \oplus \mathbf{3}_{\pm 1}. \quad (7.21)$$

The breaking of the gauge group  $[SU(2)_j \times U(1)_j]^2$  causes the  $\eta$  and  $\chi$  to be eaten. What remains left are the  $h$  and  $\phi$  which are identified as two Higgs fields:

$$h = \begin{pmatrix} h^+ \\ h^0 \end{pmatrix}, \quad \phi = \begin{pmatrix} \phi^{++} & \frac{\phi^+}{\sqrt{2}} \\ \frac{\phi^+}{\sqrt{2}} & \phi^0 \end{pmatrix}. \quad (7.22)$$

When these reach their VEV the electroweak symmetry breaking occurs.

Because the VEV  $f$  has such a large value, it is useful to expand  $\Sigma$  in powers of  $1/f$ ,

$$\begin{aligned} \Sigma &= \Sigma_0 \exp(2i\Pi/f) = \Sigma_0 + \frac{2i}{f} \Sigma_0 \Pi + \mathcal{O}\left(\frac{1}{f^2}\right) \\ &= \Sigma_0 + \frac{2i}{f} \begin{pmatrix} \mathbf{0}_{2 \times 2} & h^*/\sqrt{2} & \phi^\dagger \\ h^T/\sqrt{2} & 0 & h^\dagger/\sqrt{2} \\ \phi & h/\sqrt{2} & \mathbf{0}_{2 \times 2} \end{pmatrix} + \mathcal{O}\left(\frac{1}{f^2}\right). \end{aligned} \quad (7.23)$$

## Gauge bosons and their interaction with Higgs bosons

Now that we have determined the structure of the Littlest Higgs theory, it is time to determine the mass eigenstates of the gauge bosons after the  $\Sigma$  has acquired its VEV. Substituting  $\Sigma_0$  into the Lagrangian gives

$$\begin{aligned}
\mathcal{L}_{\text{kH},\Sigma_0} &= \frac{1}{2} \frac{f^2}{4} \text{Tr} |D_\mu \Sigma_0|^2 \\
&= \frac{1}{2} \frac{f^2}{4} (g_1 W_{1\mu}^a - g_2 W_{2\mu}^a)^2 + \frac{1}{2} \frac{f^2}{4} \frac{1}{5} (g'_1 B_{1\mu} - g'_2 B_{2\mu})^2 \\
&= \frac{1}{2} \frac{f^2}{4} (g_1^2 W_{1\mu}^a W_1^{a\mu} + g_2^2 W_{2\mu}^a W_2^{a\mu} - 2g_1 g_2 W_{1\mu}^a W_2^{a\mu}) \\
&\quad + \frac{1}{2} \frac{f^2}{4} \frac{1}{5} (g_1'^2 B_{1\mu} B_1^\mu + g_2'^2 B_{2\mu} B_2^\mu - 2g'_1 g'_2 B_{1\mu} B_2^\mu) \\
&= \frac{1}{2} M_W^2 (W_\mu^a)^2 + \frac{1}{2} M_B^2 (B_\mu)^2 + \frac{1}{2} M_{W'}^2 (W_\mu'^a)^2 + \frac{1}{2} M_{B'}^2 (B_\mu')^2. \tag{7.24}
\end{aligned}$$

To find the mass eigenstates of the  $W$  and  $B$  fields we first read off the mass matrices,

$$\mathbf{M}_W^2 = \frac{f^2}{4} \begin{pmatrix} g_1^2 & -g_1 g_2 \\ -g_1 g_2 & g_2^2 \end{pmatrix}, \tag{7.25a}$$

$$\mathbf{M}_B^2 = \frac{f^2}{4} \frac{1}{5} \begin{pmatrix} g_1'^2 & -g'_1 g'_2 \\ -g'_1 g'_2 & g_2'^2 \end{pmatrix}, \tag{7.25b}$$

and diagonalize them. Note that these are again the same matrices as with the Standard Model, so the eigenstates are the orthogonal transformations

$$W_\mu^a = s W_{1\mu}^a + c W_{2\mu}^a, \quad W_\mu'^a = -c W_{1\mu}^a + s W_{2\mu}^a, \tag{7.26a}$$

$$B_\mu = s' B_{1\mu} + c' B_{2\mu}, \quad B_\mu' = -c' B_{1\mu} + s' B_{2\mu}, \tag{7.26b}$$

where the mixing angles are given by

$$s = \frac{g_2}{\sqrt{g_1^2 + g_2^2}}, \quad c = \frac{g_1}{\sqrt{g_1^2 + g_2^2}}, \tag{7.27a}$$

$$s' = \frac{g_2'}{\sqrt{g_1'^2 + g_2'^2}}, \quad c' = \frac{g_1'}{\sqrt{g_1'^2 + g_2'^2}}. \tag{7.27b}$$

The masses are then

$$m_W^2 = 0, \quad M_{W'}^2 = \frac{f^2}{4} (g_1^2 + g_2^2), \tag{7.28a}$$

$$m_B^2 = 0, \quad M_{B'}^2 = \frac{f^2}{4} \frac{1}{5} (g_1'^2 + g_2'^2). \tag{7.28b}$$

The  $W'$  and the  $B'$  are new heavy gauge bosons and the  $W$  and the  $B$  are the gauge bosons from the Standard Model.

For this model it is interesting to also take a look at the interactions between the gauge bosons and the Higgs bosons  $h$  and  $\phi$ . To find these interactions we simply substitute the expansion (7.23) of  $\Sigma(x)$  into the Lagrangian, and substitute the  $W_{1,2}^{\mu a}$ ,  $B_{1,2}^\mu$  fields for their mass eigenstates. The relevant terms are

$$\begin{aligned}
\mathcal{L}_{\text{kH},W} &= \frac{g^2}{4} \left[ W_\mu^a W^{b\mu} - \frac{(c^2 - s^2)}{sc} W_\mu^a W'^{b\mu} \right] \text{Tr} \left[ h^\dagger h \delta^{ab} + 2\phi^\dagger \phi \delta^{ab} + 2\sigma^a \phi^\dagger \sigma^{bT} \phi \right] \\
&\quad - \frac{g^2}{4} \left[ W_\mu'^a W'^{a\mu} \text{Tr} \left[ h^\dagger h + 2\phi^\dagger \phi \right] - \frac{(c'^4 - s'^4)}{2s'^2 c'^2} W_\mu'^a W'^{b\mu} \text{Tr} \left[ 2\sigma^a \phi^\dagger \sigma^{bT} \phi \right] \right], \tag{7.29}
\end{aligned}$$

and

$$\begin{aligned}
\mathcal{L}_{\text{kH},B} &= g'^2 \left[ B_\mu B^\mu - \frac{(c'^2 - s'^2)}{s'c'} B_\mu B'^\mu \right] \text{Tr} \left[ \frac{1}{4} h^\dagger h + \phi^\dagger \phi \right] \\
&\quad - g'^2 \left[ B_\mu' B'^\mu \text{Tr} \left[ \frac{1}{4} h^\dagger h \right] - \frac{(c'^2 - s'^2)^2}{4s'^2 c'^2} B_\mu' B'^\mu \text{Tr} \left[ \phi^\dagger \phi \right] \right]. \tag{7.30}
\end{aligned}$$

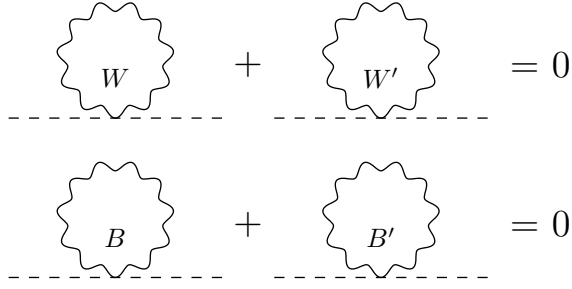


Figure 7.3: Cancellation of the quadratic divergences due to the gauge bosons [43].

The  $g$  and  $g'$  are the same couplings as in the Standard Model,

$$g = g_1 s = g_2 c, \quad (7.31a)$$

$$g' = g'_1 s' = g'_2 c', \quad (7.31b)$$

and the weak mixing angle is defined as usual:

$$s_w = \frac{g'}{\sqrt{g^2 + g'^2}}, \quad c_w = \frac{g}{\sqrt{g^2 + g'^2}}. \quad (7.32)$$

In the Standard Model these interaction terms between the gauge bosons and the Higgs lead to quadratically divergent contributions to the Higgs boson mass (Figure 7.1b). However, in this model the Higgs does not only have interactions with the  $W$  and the  $B$ , but also with the heavy  $W'$  and  $B'$ . As can be seen in the equations (7.29) and (7.30) the couplings are equally strong, but have opposite sign. Therefore the contributions cancel each other exactly, see Figure 7.3.

## The Higgs potential

To make the electroweak symmetry breaking possible, the Higgs bosons need a quartic potential. In the Littlest Higgs model this potential is not explicitly added to the Lagrangian, but comes from radiative corrections at one- and higher-loop level. This potential was invented by Coleman and Weinberg in 1973 and is therefore most often referred to as the Coleman-Weinberg potential [44]. For the Higgs fields  $h$  and  $\phi$  it can be written as

$$V(h, \phi) = \lambda_{\phi^2} f^2 \text{Tr}(\phi^\dagger \phi) + i\lambda_{h\phi h} f (h^\text{T} \phi^\dagger h - h^\dagger \phi h^*) - \mu^2 h^\dagger h + \lambda_{h^4} (h^\dagger h)^2, \quad (7.33)$$

where we have left out small terms that involve  $\phi^4$  and  $h^2 \phi^2$ . This potential allows for the proper electroweak breaking, with

$$\langle h \rangle = \frac{1}{\sqrt{2}} \begin{pmatrix} 0 \\ v \end{pmatrix}, \quad \langle \phi \rangle = -i \begin{pmatrix} 0 & 0 \\ 0 & v' \end{pmatrix}. \quad (7.34)$$

The coefficients  $\lambda_{\phi^2}$ ,  $\lambda_{h\phi h}$  and  $\lambda_{h^4}$  depend on the VEV's  $f, v', v$  and on  $\mu$ . Their relationship is [45]

$$\lambda_{h^4} = \frac{1}{4} \lambda_{\phi^2}, \quad v^2 = \frac{\mu^2}{\lambda_{h^4} - \lambda_{h\phi h}^2 / \lambda_{\phi^2}}, \quad v' = \frac{\lambda_{h\phi h} v^2}{2\lambda_{\phi^2} f}. \quad (7.35)$$

From this we find

$$\lambda_{h\phi h} = 2\lambda_{\phi^2} \frac{fv'}{v^2}, \quad (7.36a)$$

$$\lambda_{\phi^2} = \frac{4\mu^2}{v^2} \frac{1}{[1 - (4v'f/v^2)^2]}. \quad (7.36b)$$

By diagonalizing the Higgs mass matrix, we find the mass eigenstates  $\Phi$  and  $H$  with masses

$$M_\Phi^2 \simeq 2m_H^2 \frac{f^2}{v^2} \frac{1}{[1 - (4v'f/v^2)^2]}, \quad (7.37a)$$

$$m_H^2 \simeq 2\mu^2. \quad (7.37b)$$

Because we want  $M_{\Phi}^2 > 0$ , we also find that

$$\frac{v'^2}{v^2} < \frac{v^2}{16f^2}. \quad (7.38)$$

The self-interactions of the Higgs fields  $\Phi$  and  $H$  lead again to divergent loop diagrams, but at one-loop order these are logarithmically divergent and not quadratically divergent like in the Standard Model. This is much better, because a logarithmically divergent integral diverges much slower than a quadratically divergent one. In other words, the needed cancellations are much smaller in this case. The two-loop diagrams still lead to quadratically divergent integrals, but because they are two-loop also their contribution is small.

## Fermion masses

By introducing a new set of gauge bosons we were able to cancel the loop diagram of Figure 7.1b. In a similar way we can cancel the loop diagram of Figure 7.1a by introducing a new set of quarks,  $\tilde{t}$  and  $\tilde{t}'^c$ . They transform under the two global  $\underline{\text{SU}}(3)$ s as  $(\mathbf{3}, \mathbf{1})$  and  $(\bar{\mathbf{3}}, \mathbf{1})$ . These only need to interact with the third family of quarks, because we only need to cancel the diagrams with the top-loops.

The Yukawa term can be written as

$$\mathcal{L}_Y = \frac{1}{2} \lambda_1 f \epsilon_{ijk} \epsilon_{xy} \chi_i \Sigma_{jx} \Sigma_{ky} u_3^c + \lambda_2 f \tilde{t} \tilde{t}'^c + \text{h.c.}, \quad (7.39)$$

where  $\chi$  is the row vector  $\chi_i = (b_3, t_3, \tilde{t})$  and  $u_3^c$  is the right-handed top quark of the SM. The indices  $i, j, k$  are summed over 1, 2, 3 and the indices  $x, y$  are summed over 4, 5. Note that the Yukawa term is invariant under the  $\underline{\text{SU}}(3)_2$  if  $\lambda_1 = 0$ , and that it is invariant under the  $\underline{\text{SU}}(3)_1$  if  $\lambda_2 = 0$ .

If we expand  $\mathcal{L}_Y$  with the  $\Sigma$  as given in (7.23), we find

$$\mathcal{L}_Y = -\frac{\lambda_1}{f} \tilde{t} h^\dagger h u_3^c + \lambda_1 f \tilde{t} u_3^c - i \lambda_1 \sqrt{2} q_3 h^\dagger u_3^c + \lambda_2 f \tilde{t} \tilde{t}'^c + \text{h.c.} + \dots \quad (7.40)$$

In this expansion we have left out the contribution of the heavier  $\phi$  boson. The  $q_3$  is a row vector defined by  $q_3 = (b_3, t_3)$ . The terms  $\lambda_1 f \tilde{t} u_3^c$  and  $\lambda_2 f \tilde{t} \tilde{t}'^c$  should be combined to yield the mass eigenstate  $\tilde{t}^c$ :

$$\tilde{t}^c = \frac{1}{\sqrt{\lambda_1^2 + \lambda_2^2}} (\lambda_1 u_3^c + \lambda_2 \tilde{t}'^c), \quad (7.41)$$

By substituting this mass eigenstate into (7.40) we find the mass term for the  $\tilde{t}$ :

$$-m_{\tilde{t}} \tilde{t} \tilde{t}'^c = f \sqrt{\lambda_1^2 + \lambda_2^2} \tilde{t} \tilde{t}'^c, \quad (7.42)$$

and the Standard Model Yukawa coupling for the top quark:

$$\lambda_t q_3 h u_3^c = \frac{\lambda_1 \lambda_2}{\sqrt{\lambda_1^2 + \lambda_2^2}}. \quad (7.43)$$

The mixing between the right-handed top quark  $u_3^c$  and the new quark  $\tilde{t}$  can be parameterized with

$$x_L = \frac{\lambda_1^2}{\lambda_1^2 + \lambda_2^2}. \quad (7.44)$$

Note that  $0 < x_L < 1$ , and that there is no mixing when  $x_L = \lambda_1 = 0$ . If  $x_L = 1$  (i.e.  $\lambda_2 = 0$ ) then the mass eigenstate  $\tilde{t}^c$  is equal to the right-handed top quark.

In the Yukawa term (7.40) the top loop of Figure 7.1a is cancelled. One can show this with the use of the mass eigenstates  $t$  and  $\tilde{t}$ , but it can also be explained in terms of  $q_3$ ,  $u_3^c$ , and  $\tilde{t}'$ . How this cancellation happens is shown in Figure 7.4.

$$2\lambda_1^2 \quad + \quad -\lambda_1^2 \quad + \quad -\lambda_1^2 \quad = \quad 0$$

Figure 7.4: Cancellation of the quadratic divergences due to the top quark, from (7.40). Taken from [43].

### 7.3 Electroweak symmetry breaking

We have seen how the Littlest Higgs theory solves the hierarchy problem, now we must determine the mass eigenstates of the gauge bosons after the EWSB. We substitute the VEV's (7.34) into the  $\Sigma(x)$  of (7.23) to get

$$\Sigma = \begin{pmatrix} 0 & 0 & 0 & 1 & 0 \\ 0 & 0 & iv/f & 0 & 1 - 2v'/f \\ 0 & iv/f & 1 & 0 & iv/f \\ 1 & 0 & 0 & 0 & 0 \\ 0 & 1 + 2v'/f & iv/f & 0 & 0 \end{pmatrix} + \mathcal{O}\left(\frac{1}{f^2}\right). \quad (7.45)$$

This expression we insert into

$$\mathcal{L}_{\text{kH}} = \frac{1}{2} \frac{f^2}{4} \text{Tr} |D_\mu \Sigma|^2, \quad (7.46)$$

and then we diagonalize the resulting mass matrix. These calculations with  $5 \times 5$  matrices can best be done with the aid of a program like Maple or Mathematica. After some patience one finds the following mass eigenstates. There are four neutral gauge bosons,<sup>2</sup>

$$A_L = s_w W^3 + c_w B, \quad (7.47a)$$

$$Z_L = c_w W^3 - s_w B + x_Z^{W'} \frac{v^2}{f^2} W'^3 + x_Z^{B'} \frac{v^2}{f^2} B', \quad (7.47b)$$

$$A_H = B' + x_H \frac{v^2}{f^2} W'^3 - x_Z^{B'} \frac{v^2}{f^2} (c_w W^3 - s_w B), \quad (7.47c)$$

$$Z_H = W'^3 - x_H \frac{v^2}{f^2} B' - x_Z^{W'} \frac{v^2}{f^2} (c_w W^3 - s_w B), \quad (7.47d)$$

where

$$x_H = \frac{5}{2} g g' \frac{s c s' c'}{(5g^2 s'^2 c'^2 - g'^2 s^2 c^2)}, \quad (7.48a)$$

$$x_Z^{W'} = -\frac{1}{2c_w} s c (c^2 - s^2), \quad (7.48b)$$

$$x_Z^{B'} = -\frac{5}{2s_w} s' c' (c'^2 - s'^2). \quad (7.48c)$$

Their masses are given by

$$M_{A_L}^2 = 0, \quad (7.49a)$$

$$M_{Z_L}^2 = m_z^2 \left[ 1 - \frac{v^2}{f^2} \left( \frac{1}{6} + \frac{1}{4} (c^2 - s^2)^2 + \frac{5}{4} (c'^2 - s'^2)^2 \right) + 8 \frac{v'^2}{v^2} \right], \quad (7.49b)$$

$$M_{A_H}^2 = m_z^2 s_w^2 \left( \frac{f^2}{5s'^2 c'^2 v^2} - 1 + \frac{x_H c_w^2}{4s^2 c^2 s_w^2} \right), \quad (7.49c)$$

$$M_{Z_H}^2 = m_w^2 \left( \frac{f^2}{s^2 c^2 v^2} - 1 - \frac{x_H s_w^2}{s'^2 c'^2 c_w^2} \right), \quad (7.49d)$$

<sup>2</sup>In order to write  $A_L$  and  $Z_L$  in the standard form, we have absorbed a minus sign into the definition of  $B$ .

where  $m_w$  and  $m_z$  are the masses of the Standard Model  $W$  and  $Z$ , given by

$$m_w = \frac{gv}{2}, \quad (7.50a)$$

$$m_z = \frac{gv}{2c_w}. \quad (7.50b)$$

The  $A_L$  is the photon, and the  $Z_L$  is the  $Z$  boson of the Standard Model. The gauge bosons  $A_H$  and  $Z_H$  are new heavy particles.

Besides the neutral bosons, the Littlest Higgs model also predicts two charged gauge bosons,

$$W_L^\pm = W^\pm + \frac{v^2}{2f^2} sc (c^2 - s^2) W'^\pm, \quad (7.51a)$$

$$W_H^\pm = W'^\pm - \frac{v^2}{2f^2} sc (c^2 - s^2) W^\pm. \quad (7.51b)$$

The masses are

$$M_{W_L^\pm}^2 = m_w^2 \left[ 1 - \frac{v^2}{f^2} \left( \frac{1}{6} + \frac{1}{4} (c^2 - s^2)^2 \right) + 4 \frac{v'^2}{v^2} \right], \quad (7.52a)$$

$$M_{W_H^\pm}^2 = m_w^2 \left( \frac{f^2}{s^2 c^2 v^2} - 1 \right). \quad (7.52b)$$

The  $W_L$  is the Standard Model  $W$  boson, the  $W_H$  is a new heavy charged gauge boson.

## Couplings

To find the couplings between the fermions and the gauge bosons, we follow the usual recipe. First we rewrite the covariant derivative  $D_\mu$  in terms of the mass eigenstates, and then we substitute that expression into the kinetic Lagrangian term of the fermions. The resulting interactions for the charged gauge bosons with quarks are (up to order  $v^2/f^2$ )

$$\begin{array}{c} u \\ \searrow \\ \text{---} W \\ \nearrow \\ \bar{d} \end{array} = \frac{ig_w}{2\sqrt{2}} \left[ 1 - \frac{1}{2} \frac{v^2}{f^2} c^2 (c^2 - s^2) \right] \gamma^\mu (1 - \gamma_5) V_{ud}, \quad (7.53a)$$

$$\begin{array}{c} t \\ \searrow \\ \text{---} W \\ \nearrow \\ \bar{b} \end{array} = \frac{ig_w}{2\sqrt{2}} \left[ 1 - \frac{v^2}{f^2} \left( \frac{1}{2} x_L^2 + \frac{1}{2} c^2 (c^2 - s^2) \right) \right] \gamma^\mu (1 - \gamma_5) V_{tb}, \quad (7.53b)$$

for the light Standard Model  $W$  boson, and

$$\begin{array}{c} u \\ \searrow \\ \text{---} W_H \\ \nearrow \\ \bar{d} \end{array} = -\frac{ig_w}{2\sqrt{2}} \frac{c}{s} \gamma^\mu (1 - \gamma_5) V_{ud}, \quad (7.54a)$$

$$\begin{array}{c} t \\ \searrow \\ \text{---} W_H \\ \nearrow \\ \bar{b} \end{array} = -\frac{ig_w}{2\sqrt{2}} \frac{c}{s} \gamma^\mu (1 - \gamma_5) V_{tb}, \quad (7.54b)$$

for the heavy  $W_H$  boson. See Equation (7.44) for the definition of  $x_L$ . Note that the coupling with the  $W_H$  is the same for each combination of quarks (apart from the value of  $V_{ij}$  of course). For the couplings with the  $W$ , the  $(u, d)$  can be replaced by  $(u, s)$ ,  $(u, b)$ ,  $(c, d)$ ,  $(c, s)$ , or  $(c, b)$ , and the  $(t, b)$  can be replaced by  $(t, d)$  or  $(t, s)$ .

All of the results presented in this subsection have been checked with [46].

## 7.4 Single-top in the Littlest Higgs model

The Littlest Higgs has almost the same gauge symmetry as Topflavor. Therefore we can copy a lot of the formulas that we have used in Chapter 6. For the  $s$ -channel single-top process  $u\bar{d} \rightarrow W, W_H \rightarrow t\bar{b}$  the invariant amplitude is again

$$|\overline{\mathcal{M}}|^2 = \frac{1}{256} g_w^4 X^{\mu\kappa} Y_{\mu\kappa\nu\lambda} Z^{\nu\lambda}, \quad (7.55)$$

with

$$X^{\mu\kappa} = \text{Tr} \left[ \not{p}_{\bar{d}} \gamma^\mu (1 - \gamma_5) \not{p}_u \gamma^\kappa (1 - \gamma_5) \right], \quad (7.56)$$

$$Z^{\nu\lambda} = \text{Tr} \left[ (\not{p}_t + m_t) \gamma^\nu (1 - \gamma_5) \not{p}_{\bar{b}} \gamma^\lambda (1 - \gamma_5) \right], \quad (7.57)$$

and

$$Y_{\mu\kappa\nu\lambda} = \left| \frac{U_{tb}U_{ud}}{k^2 - M_{W_L}^2} + \frac{U'_{tb}U'_{ud}}{k^2 - M_{W_H}^2 + iM_{W_H}\Gamma_{W_H}} \right|^2 g_{\mu\nu}g_{\kappa\lambda}. \quad (7.58)$$

Just like with Topflavor, we need to use the decay width  $\Gamma_{W_H}$  of the heavy  $W_H$  to prevent the occurrence of a singularity at  $k = p_u + p_{\bar{d}} = M_{W_H}$ . However, because the couplings in the Littlest Higgs are much different from those in Topflavor, we have here a different expression for the width [46]:

$$\Gamma_{W_H} = \frac{g_w^2 c^2}{16\pi s^2} M_{W_H}. \quad (7.59)$$

For the Littlest Higgs the expressions for  $U_{ij}$  and  $U'_{ij}$  follow from

$$g_w U_{tb} = g_w \left[ 1 - \frac{v^2}{f^2} \left( \frac{1}{2} x_L^2 + \frac{1}{2} c^2 (c^2 - s^2) \right) \right] V_{tb}, \quad (7.60a)$$

$$g_w U_{ud} = g_w \left[ 1 - \frac{1}{2} \frac{v^2}{f^2} c^2 (c^2 - s^2) \right] V_{ud}, \quad (7.60b)$$

and

$$g_w U'_{ij} = -g_w \frac{c}{s} V_{ij}. \quad (7.61)$$

To make a comparison with the Topflavor easier, we shall use (7.52b),

$$\frac{v^2}{f^2} = \frac{1}{s^2 c^2} \frac{m_w^2}{M_{W_H^\pm}^2 + m_w^2} \approx \frac{1}{s^2 c^2} \frac{m_w^2}{M_{W_H^\pm}^2}, \quad (7.62)$$

to write all expressions in terms of the heavy mass,  $M_{W_H}$ . The product  $U_{tb}U_{ud}$  becomes

$$\begin{aligned} U_{tb}U_{ud} &= \left( 1 - \frac{v^2}{f^2} \left( \frac{1}{2} x_L^2 + \frac{1}{2} c^2 (c^2 - s^2) \right) \right) \left( 1 - \frac{1}{2} \frac{v^2}{f^2} c^2 (c^2 - s^2) \right) V_{tb}V_{ud} \\ &= \left[ 1 - \frac{v^2}{f^2} \left( c^4 + c^2 s^2 - \frac{1}{2} x_L^2 \right) + \mathcal{O}(v^4/f^4) \right] V_{tb}V_{ud} \end{aligned} \quad (7.63)$$

$$= \left[ 1 - \frac{2c^2 - x_L^2}{2s^2 c^2} \frac{m_w^2}{M_{W_H^\pm}^2} \right] V_{tb}V_{ud}, \quad (7.64)$$

and the  $U'_{tb}U'_{ud}$  is simply

$$|U'_{tb}|^2 |U'_{ud}|^2 = \frac{c^4}{s^4} |V_{tb}|^2 |V_{ud}|^2.$$

Putting everything together, we see that the invariant amplitude for the  $s$ -channel is

$$\begin{aligned} |\overline{\mathcal{M}}|^2 &= \frac{1}{4} g_w^4 |V_{ud}|^2 |V_{tb}|^2 [(\hat{u} - m_t^2) \hat{u}] \\ &\times \left[ \frac{\alpha^2}{\hat{s}^2} + \frac{2\alpha\beta (\hat{s} - M_{W_H}^2)}{\hat{s} \left( (\hat{s} - M_{W_H}^2)^2 + M_{W_H}^2 \Gamma_{W_H}^2 \right)} + \frac{\beta^2}{(\hat{s} - M_{W_H}^2)^2 + M_{W_H}^2 \Gamma_{W_H}^2} \right], \end{aligned} \quad (7.65)$$

(taking  $\hat{s} \gg M_{W_L}^2$ ) with

$$\alpha = 1 - \frac{2c^2 - x_L^2}{2s^2c^2} \frac{m_w^2}{M_{W_H^\pm}^2}, \quad (7.66a)$$

$$\beta = \frac{c^2}{s^2}. \quad (7.66b)$$

The Mandelstam variables are as usual:  $\hat{s} = k^2 = (p_u + p_{\bar{d}})^2$  and  $\hat{u} = (p_{\bar{d}} - p_t)^2$ .

At tree-level the  $t$ -channel in the Littlest Higgs will not differ much from the Standard Model  $t$ -channel. The argument is the same as with Topflavor: the contribution  $1/(\hat{t} - M_{W_H}^2)^2$  is just too small to have an influence. Also for the  $Wt$ -associated process we have the same thing as with Topflavor. The  $Wtb$  coupling in (7.60a) does not differ enough from the SM coupling to cause a noticeable effect in experiment.

We must make one additional note here. The Littlest Higgs model has a much larger Higgs sector than the Standard Model (from the 14 pseudo-Goldstone bosons we had, only 7 were eaten). Therefore one could expect to have an extra  $s$ -channel process like  $u\bar{d} \rightarrow h^+ \rightarrow t\bar{b}$ . In fact, there exists an interaction vertex between  $u$ ,  $\bar{d}$ , and  $\Phi^+$  where [46]

$$\Phi^+ = \frac{v}{\sqrt{v^2 + 4v'^2}} \phi^+ - \frac{2v'}{\sqrt{v^2 + 4v'^2}} h^+, \quad (7.67)$$

but there is no interaction between  $t$ ,  $\bar{b}$ , and  $\Phi^+$ . The reason for this is that the  $(u, d)$  has a different Yukawa term than the  $(t, b)$ . However, there are extra  $s$ -channel processes possible that have the  $t$  and a  $\bar{T}$  in its final state (the  $T$  is a mass eigenstate of the  $\hat{t}$ -quark).

## 7.5 Monte Carlo results

The valid ranges for the free parameters in the Littlest Higgs model are [47]:

$$f \geq 1 \text{ TeV}, \quad (7.68a)$$

$$0.4 \leq x_L \leq 0.6, \quad (7.68b)$$

$$0 \leq c \leq 0.5. \quad (7.68c)$$

The lower bound for the mass  $M_{W_H}$  is about the same as for the  $M_{W'}$  in Topflavor ( $\sim 800$  GeV), therefore we have used in our Littlest Higgs (LH) simulations the same range as with Topflavor.

Note that the mixing angle  $c^2$  in the LH has the same meaning as the  $\sin^2 \phi$  in Topflavor. The notation  $c$  is used to indicate that it is the cosine of some mixing angle. It is a bit unfortunate that the cosine is used in the Little Higgs, while the sine is used in Topflavor.

An interesting difference between the Littlest Higgs and Topflavor, is that we have here an extra parameter that the Topflavor does not have:  $x_L$ . Unfortunately the range of  $x_L$  is rather narrow and small changes do not influence the single-top equations much. We only encounter  $x_L$  in the equation for  $|\mathcal{M}|^2$ , where it changes the value of  $\alpha$  a bit, see Equation (7.66a). The result of this, is that any changes of  $x_L$  have not led to a significant change of the cross section in any way.

We present the cross sections for the Tevatron and the LHC in Figures 7.5 - 7.10. In Figure 7.5 the cross section is presented as a function of  $M_{W_H}$ , in a similar way as Figure 6.1 and 6.2 in the Topflavor chapter. The LH cross sections are of about the same size, up to 30 pb for  $t$ -production at the LHC. This has been checked with [48], we come again to the conclusion that the  $W_H$  should be easy to find, if it has a relatively small mass.

The results are somewhat disappointing because a lot is the same as in the Topflavor model. Changing the value of  $c^2$  has exactly the same effect as changing  $\sin^2 \phi$  in the previous chapter (compare Figure 7.7 and 7.8 with Figure 6.8 and 6.9). The only interesting difference is that the parameter  $c^2$  is allowed to be larger than the  $\sin^2 \phi$  is allowed to. This larger parameter space results the possibility of higher peaks in the  $p_T$ , as can be seen in Figure 7.7 and 7.8.

Also the pseudo(rapidity) plots show a large similarity with those of Topflavor. As an example we have included Figure 7.10 which shows the mass dependence of the top quark pseudorapidity at the Tevatron.



Figure 7.5: Cross section of the  $s$ -channel single-top in the Littlest Higgs model, as a function of  $M_{W_H}$ . Here we have used  $c^2 = 0.3$  and  $x_L = 0.5$ . For the Tevatron the results for  $t$  are equal to those for the  $\bar{t}$ . Note that the cross sections of the Tevatron has been multiplied by a factor of 10.

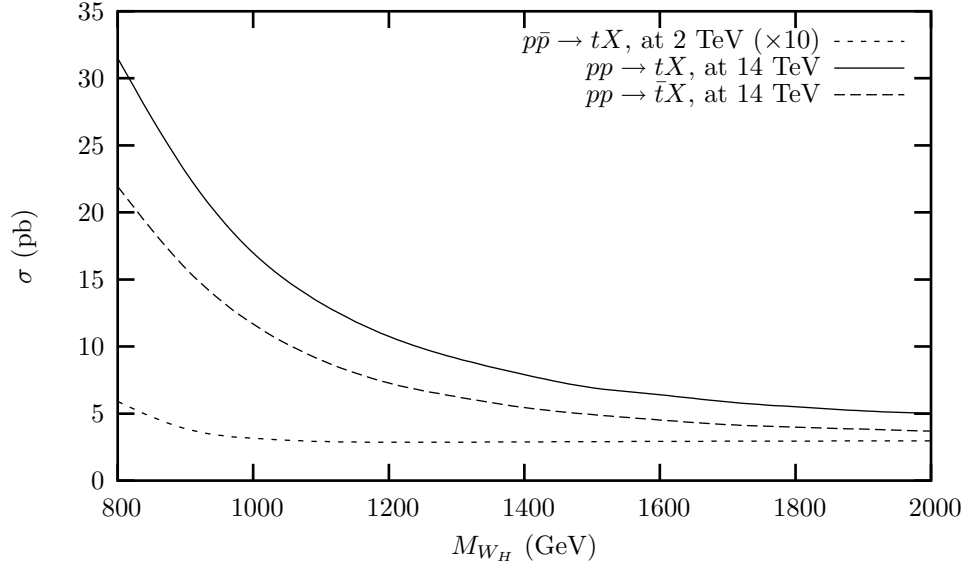


Figure 7.6: Cross section of the  $s$ -channel single-top in the Littlest Higgs model, as a function of  $c^2$ . Here we have used  $M_{W_H} = 1000$  GeV and  $x_L = 0.5$ . For the Tevatron the results for  $t$  are equal to those for the  $\bar{t}$ . Note that the cross sections of the Tevatron has been multiplied by a factor of 10.

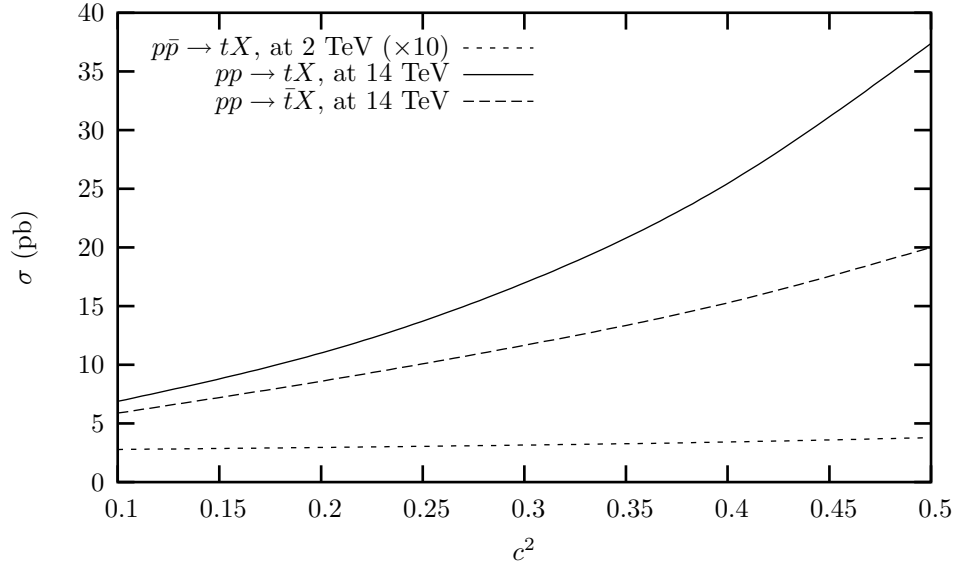


Figure 7.7: Transverse momentum for  $s$ -channel single-top in the Littlest Higgs model, at the Tevatron ( $p\bar{p}$ ,  $\sqrt{s} = 2$  TeV), for different values of  $M_{W_H}$ . In all cases  $c^2 = 0.3$  and  $x_L = 0.5$ . The results for  $\bar{t}$  are equal to those shown here.

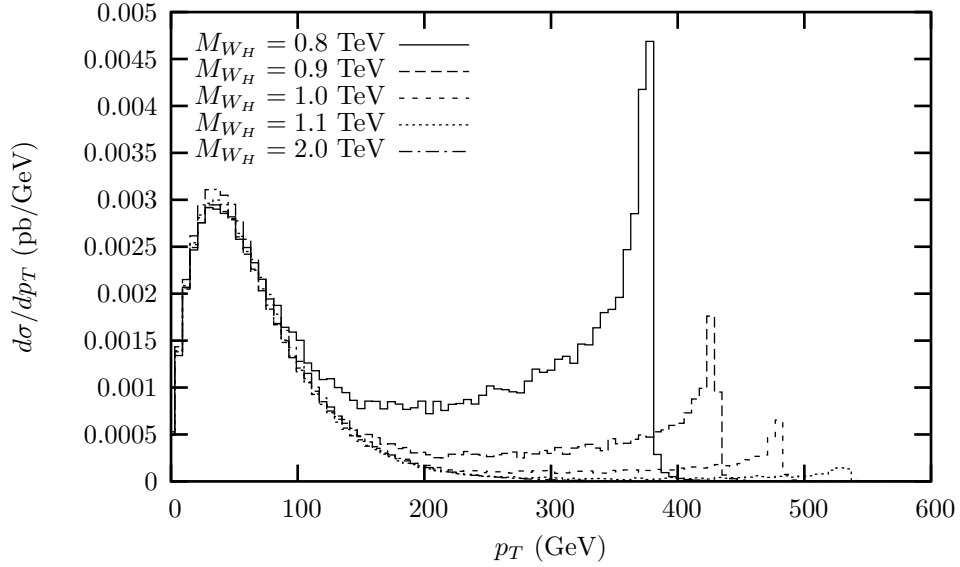


Figure 7.8: Transverse momentum for  $s$ -channel single-top in the Littlest Higgs model, at the LHC ( $pp$ ,  $\sqrt{s} = 14$  TeV), for different values of  $M_{W_H}$ . In all cases  $c^2 = 0.3$  and  $x_L = 0.5$ . The results for  $\bar{t}$  have the same shape, but are roughly 50% lower.

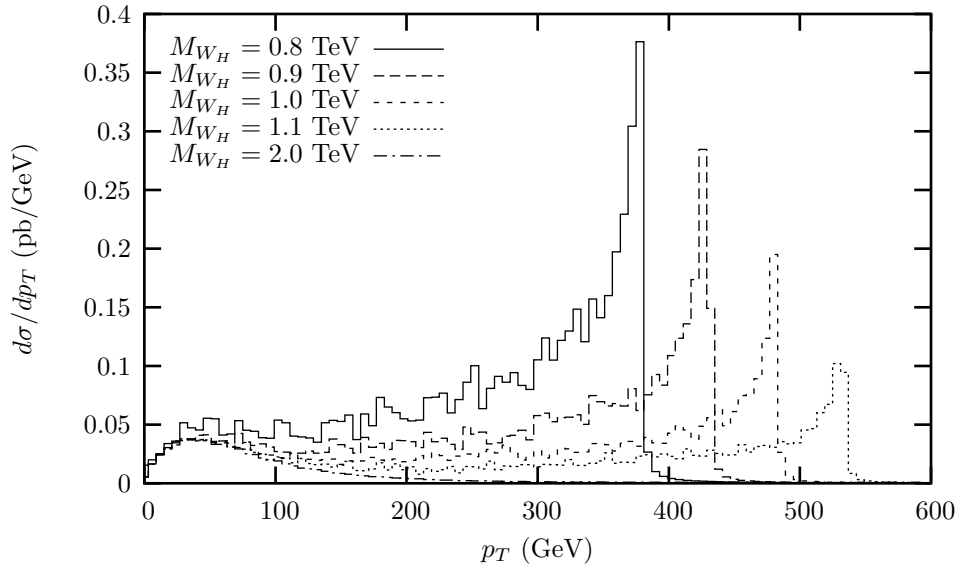


Figure 7.9: Transverse momentum for  $s$ -channel single-top in the Littlest Higgs model, at the Tevatron ( $p\bar{p}$ ,  $\sqrt{s} = 2$  TeV), for different values of  $c^2$ . In all cases  $M_{W_H} = 1000$  GeV and  $x_L = 0.5$ . The results for  $\bar{t}$  are equal to those shown here.

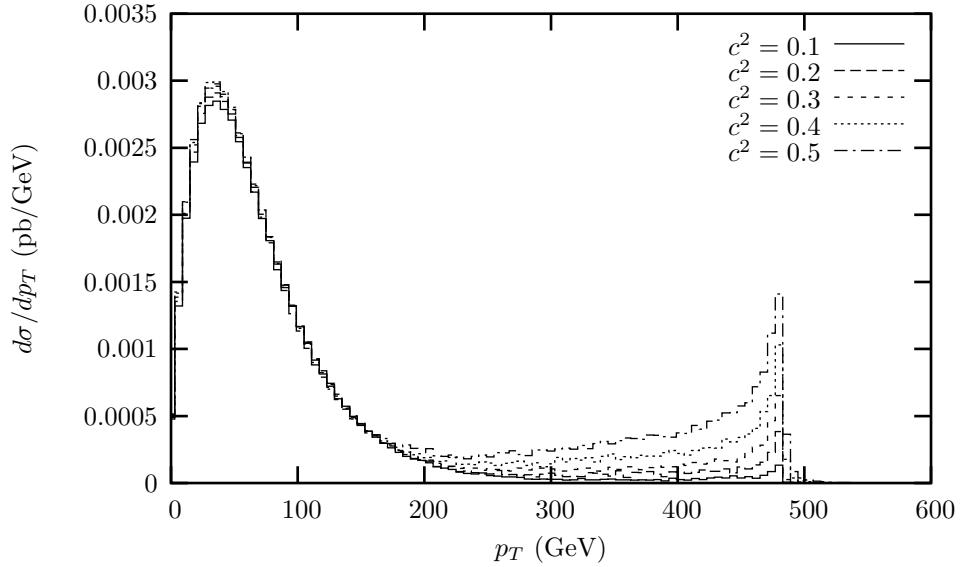
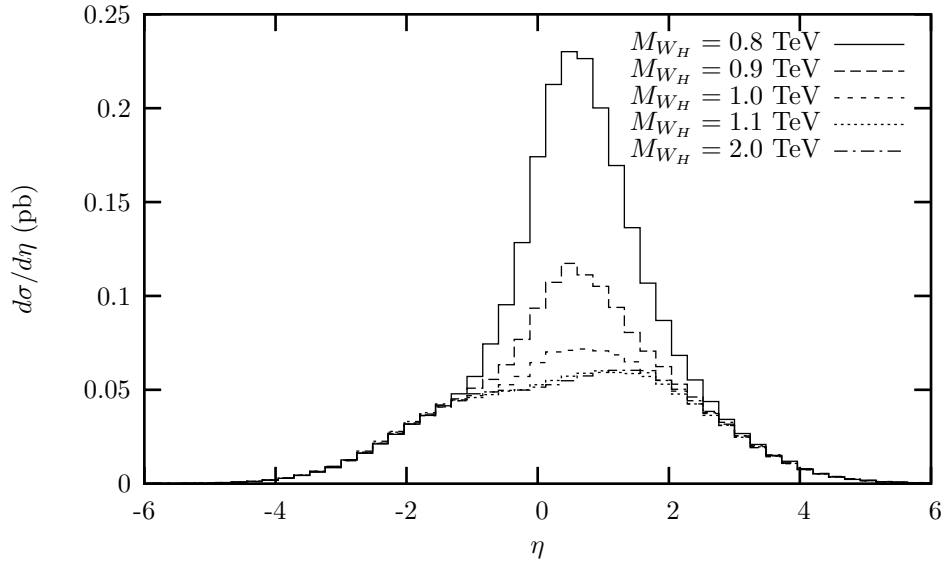


Figure 7.10: Pseudorapidity for  $s$ -channel single-top in the Littlest Higgs model, at the Tevatron ( $p\bar{p}$ ,  $\sqrt{s} = 2$  TeV). We have plotted here the  $\eta$  of the  $t$ -quark for different values of  $M_{W_H}$ , always with  $c^2 = 0.3$  and  $x_L = 0.5$ . At the Tevatron the results for  $t$  are equal to those for the  $\bar{t}$ .



# Chapter 8

## Conclusions

If we assume that there is physics beyond the Standard Model, then one could ask ‘If so, what could we discover?’ Now that we have reached the end of this thesis, we can answer this question simply with ‘More particles and higher cross sections!’. The time to finish a thesis project is limited and it was therefore impossible to examine more models and more processes. We have however learned a great deal and found that the existence of an extra set of gauge bosons is a realistic option, as well as extra quarks. One of the most important discoveries shall be the verification of the existence of Higgs bosons. These particles are crucial for gauge theories with spontaneous symmetry breaking<sup>1</sup>.

The results of this thesis can be best described with Table 8.1, which summarizes our findings of the chapters 4, 6, and 7. We see that the event rates for single-top at the Tevatron are rather low. More importantly we see that it is virtually impossible to distinguish between the different models at the Tevatron using only the  $s$ -channel single-top cross sections. Only if the heavy  $W$  is light enough, the Tevatron will have a chance to find any signature of new physics this way. Especially the large spike in the  $p_T$  graphs could then be used as a potential smoking-gun signature.

The chance of discovering a sign of the Littlest Higgs or Topflavor is fortunately much higher at the LHC. Even if the heavy  $W$  boson has a mass of around 2 TeV, it would be possible to see a clear difference between the Standard Model  $s$ -channel and that of the other models. It is even possible to see the difference between the Littlest Higgs and Topflavor, if we compare the  $t$  cross sections and the  $\bar{t}$  cross sections.

The Monte Carlo program seems to be working fine, but it is a bit worrying that our cross sections of Table 4.3 do not perfectly agree with those of Table 4.4. It might be necessary to perform more elaborate tests, but we do not expect large changes in the results presented in this thesis. Extensive testing is mandatory however, if the Monte Carlo program would ever be extended. Many extensions of the program are possible. The program could be extended with the  $Wt$ -associated production, or it could even be upgraded to do next-to-leading order (NLO) calculations.

As stated in Section 4.4 about top decay, the  $s$ -channel and the  $t$ -channel both give exactly the same signal in an experiment. One can only make a distinction using the  $b$ -tagging technique, but this

<sup>1</sup>It must be mentioned that the electroweak symmetry breaking is also possible with the usual Higgs boson [49].

	LHC ( $pp \rightarrow tX$ )		LHC ( $pp \rightarrow \bar{t}X$ )		Tevatron	
	$\sigma$ in pb	ev/day	$\sigma$ in pb	ev/day	$\sigma$ in pb	ev/day
Standard Model ( $t$ -channel)	144.8	125,000	83.4	72,000	0.948	8
Standard Model ( $s$ -channel)	4.53	3,900	2.74	2,400	0.315	3
Topflavor ( $M_{W'} = 1$ TeV)	16	13,800	8.1	7,000	0.42	4
Topflavor ( $M_{W'} = 2$ TeV)	5.6	4,800	3.2	2,800	0.33	3
Littlest Higgs ( $M_{W_H} = 1$ TeV)	17	14,700	11.7	10,100	0.32	3
Littlest Higgs ( $M_{W_H} = 2$ TeV)	5.0	4,300	3.7	3,200	0.30	3

Table 8.1: Cross sections and event rates for single-top processes in the Standard Model, the Topflavor model (with  $\sin^2 \phi = 0.25$ ), and the Littlest Higgs model (with  $c^2 = 0.3$  and  $x_L = 0.5$ ). The  $t$ -channel cross section is the same for all three models. We have used here  $\sqrt{s} = 2$  TeV for the Tevatron, and high-luminosity for the LHC ( $L = 10^{34} \text{ cm}^{-2}\text{s}^{-1}$ ). The Standard Model cross sections are copied from Table 4.4 and the data of Table 1.1 has been used to calculate the event rates.

is not always possible for each event. To account for this, one should simulate the detector by including hadronization and apply the proper cutoffs. Even though these options are already available in the current program, they have not been used. This could be an interesting subject for further research, as well as a more elaborate analysis of the background signals for single-top production. Finally, there are still a lot of more theoretical explorations possible. One could investigate the possibility of flavor changing neutral currents (FCNC) and custodial  $SU(2)$  symmetry in the Littlest Higgs model. Another interesting topic is to do more research about Topflavor and its big brother, Technicolor.

The gauge symmetry of the Littlest Higgs model is, apart from an extra  $U(1)$ , the same as in Topflavor. We have seen the result of this: both models predict an extra set of  $W, Z$  bosons. Even though Topflavor and the Little Higgs have a lot in common, there are some distinct differences. One clear example is the width of the  $W'$  (or  $W_H$ ), which is different for both models. Probably the best way to check which model describes nature correctly, is by measuring the  $W'$ -couplings with the quarks. Chapters 6 and 7 predict some clear relations between  $U'_{tb}$  and  $U'_{ud}$  the Standard Model CKM matrix. Also relations like

$$|U'_{tb}|^2 |U'_{ud}|^2 = |U_{tb}|^2 |U_{ud}|^2 \quad (8.1)$$

as in Topflavor, are strong predictions that provide for an easy way to check the model. But the main difference between the models does not lie in the experimental results, but in their theoretical structure. The Littlest Higgs model treats the Higgs as a pseudo-Goldstone boson, while in Topflavor it is the usual scalar boson. With Topflavor the third generation of quarks transforms differently than the other generations, while in the Littlest Higgs there is no such distinction. It is interesting to see that we can find two theories that are so different theoretically, are so similar in experiment.

# Appendix A

## Differential cross sections

Because the top has such a high mass, we can ignore the mass of the other quarks. We therefore take a look at the differential cross section for the process  $A + B \rightarrow C + D$  where  $m_A = m_B = 0$ . We define

$$\begin{aligned} s &= (p_A + p_B)^2 = m_A^2 + m_B^2 + 2p_A \cdot p_B \\ &= (p_C + p_D)^2 = m_C^2 + m_D^2 + 2p_C \cdot p_D, \end{aligned} \quad (\text{A.1a})$$

$$\begin{aligned} t &= (p_A - p_C)^2 = m_A^2 + m_C^2 - 2p_A \cdot p_C \\ &= (p_B - p_D)^2 = m_B^2 + m_D^2 - 2p_B \cdot p_D, \end{aligned} \quad (\text{A.1b})$$

$$\begin{aligned} u &= (p_B - p_C)^2 = m_B^2 + m_C^2 - 2p_B \cdot p_C \\ &= (p_A - p_D)^2 = m_A^2 + m_D^2 - 2p_A \cdot p_D. \end{aligned} \quad (\text{A.1c})$$

The differential cross section can be written as

$$d\sigma = \frac{|\overline{\mathcal{M}}|^2}{F} dQ, \quad (\text{A.2})$$

with  $F$  the flux

$$F = 4\sqrt{(p_A \cdot p_B)^2 - m_A^2 m_B^2} = 4\sqrt{\left(\frac{1}{2}s\right)^2} = 2s. \quad (\text{A.3})$$

and  $dQ$  the Lorentz-invariant phase space,

$$\begin{aligned} dQ &= (2\pi)^4 \delta^{(4)}(p_C + p_D - p_A - p_B) \frac{d^3\mathbf{p}_C}{(2\pi)^3 2E_C} \frac{d^3\mathbf{p}_D}{(2\pi)^3 2E_D} \\ &= \frac{1}{(2\pi)^2} \delta^{(4)}(p_C + p_D - p_A - p_B) d^4p_C \delta_+(p_C^2 - m_C^2) d^4p_D \delta_+(p_D^2 - m_D^2), \end{aligned} \quad (\text{A.4})$$

where  $\delta_+(p^2 - m^2) \equiv \theta(p^0) \delta(p^2 - m^2)$ . We now define two new invariants,

$$t_1 = t - m_C^2, \quad (\text{A.5a})$$

$$u_1 = u - m_D^2, \quad (\text{A.5b})$$

such that  $s + t_1 + u_1 = 0$ . With the use of  $E_C + E_D = \sqrt{s}$  we then find

$$\begin{aligned} dQ &= \frac{1}{(2\pi)^2} \delta^{(4)}(p_C + p_D - p_A - p_B) \delta_+(p_C^2 - m_C^2) \theta(E_D) \delta(p_D^2 - m_D^2) d^4p_D d^4p_C \\ &= \frac{1}{(2\pi)^2} \delta_+(p_C^2 - m_C^2) \theta(\sqrt{s} - E_C) \delta\left((p_A + p_B - p_C)^2 - m_D^2\right) d^4p_C \\ &= \frac{1}{(2\pi)^2} \delta_+(p_C^2 - m_C^2) \theta(\sqrt{s} - E_C) \delta\left((p_A + p_B)^2 + p_C^2 - 2p_C \cdot (p_A + p_B) - m_D^2\right) d^4p_C \\ &= \frac{1}{(2\pi)^2} \delta_+(p_C^2 - m_C^2) \theta(\sqrt{s} - E_C) \delta\left(s + m_C^2 - 2(p_C \cdot p_A) - 2(p_C \cdot p_B) - m_D^2\right) d^4p_C \\ &= \frac{1}{(2\pi)^2} \delta_+(p_C^2 - m_C^2) \theta(\sqrt{s} - E_C) \delta\left(s + m_C^2 + t - m_C^2 + u - m_C^2 - m_D^2\right) d^4p_C \\ &= \frac{1}{4\pi^2} \delta_+(p_C^2 - m_C^2) \theta(\sqrt{s} - E_C) \delta(s + t_1 + u_1) d^4p_C \end{aligned} \quad (\text{A.6})$$

It is useful to switch to the lightcone coordinates,

$$p^+ = \frac{p_C^0 + p_C^3}{\sqrt{2}}, \quad p^- = \frac{p_C^0 - p_C^3}{\sqrt{2}}, \quad \mathbf{p}_T = (p_C^1, p_C^2), \quad (\text{A.7})$$

such that

$$p_C^0 = \frac{p^+ + p^-}{\sqrt{2}}, \quad p_C^3 = \frac{p^+ - p^-}{\sqrt{2}}. \quad (\text{A.8})$$

In the CM frame we then have

$$p_A = (E_A, 0, 0, E_A) = \frac{1}{2}\sqrt{s}(1, 0, 0, 1), \quad (\text{A.9a})$$

$$p_B = (E_B, 0, 0, -E_B) = \frac{1}{2}\sqrt{s}(1, 0, 0, -1), \quad (\text{A.9b})$$

and therefore

$$\begin{aligned} 2p_A \cdot p_C &= \sqrt{s}(1, 0, 0, 1) \cdot (p_C^0, p_C^1, p_C^2, p_C^3) \\ &= \sqrt{s}(p_C^0 - p_C^3) = \sqrt{2s}p^- = -t_1, \end{aligned} \quad (\text{A.10})$$

and

$$\begin{aligned} 2p_B \cdot p_C &= \sqrt{s}(1, 0, 0, -1) \cdot (p_C^0, p_C^1, p_C^2, p_C^3) \\ &= \sqrt{s}(p_C^0 + p_C^3) = \sqrt{2s}p^+ = -u_1. \end{aligned} \quad (\text{A.11})$$

It is then easy to see that

$$\begin{aligned} d^4 p_C &= dp_C^0 dp_C^1 dp_C^2 dp_C^3 = \left| \left( \begin{array}{cc} \frac{\partial p_C^0}{\partial p^+} & \frac{\partial p_C^0}{\partial p^-} \\ \frac{\partial p_C^3}{\partial p^+} & \frac{\partial p_C^3}{\partial p^-} \end{array} \right) \right| dp^+ dp^- d^2 \mathbf{p}_T \\ &= \left| \left( \begin{array}{cc} \frac{1}{\sqrt{2}} & \frac{1}{\sqrt{2}} \\ \frac{1}{\sqrt{2}} & -\frac{1}{\sqrt{2}} \end{array} \right) \right| dp^+ dp^- d^2 \mathbf{p}_T = dp^+ dp^- d^2 \mathbf{p}_T \\ &= \left| \left( \begin{array}{cc} \frac{\partial p^+}{\partial t_1} & \frac{\partial p^+}{\partial u_1} \\ \frac{\partial p^-}{\partial t_1} & \frac{\partial p^-}{\partial u_1} \end{array} \right) \right| dt_1 du_1 d^2 \mathbf{p}_T = \left| \left( \begin{array}{cc} 0 & -\frac{1}{\sqrt{2s}} \\ -\frac{1}{\sqrt{2s}} & 0 \end{array} \right) \right| dt_1 du_1 d^2 \mathbf{p}_T \\ &= \frac{1}{2s} dt_1 du_1 d^2 \mathbf{p}_T, \end{aligned} \quad (\text{A.12})$$

and

$$\begin{aligned} p_C^2 &= (p_C^0)^2 - (p_C^1)^2 - (p_C^2)^2 - (p_C^3)^2 \\ &= \frac{1}{2}(p^+ + p^-)^2 - (\mathbf{p}_T)^2 - \frac{1}{2}(p^+ - p^-)^2 \\ &= 2p^+ p^- - \mathbf{p}_T^2 \\ &= \frac{u_1 t_1}{s} - \mathbf{p}_T^2. \end{aligned} \quad (\text{A.13})$$

Hence,  $dQ$  becomes

$$\begin{aligned} dQ &= \frac{1}{4\pi^2} \theta\left(\frac{p^+ + p^-}{\sqrt{2}}\right) \delta\left(\frac{u_1 t_1}{s} - \mathbf{p}_T^2 - m_C^2\right) \theta\left(\sqrt{s} - \frac{p^+ + p^-}{\sqrt{2}}\right) \frac{1}{2s} dt_1 du_1 d^2 \mathbf{p}_T \\ &= \frac{1}{8\pi^2 s} \theta\left(\frac{-u_1 - t_1}{\sqrt{2}\sqrt{2s}}\right) \delta\left(\frac{u_1 t_1}{s} - m_C^2 - \mathbf{p}_T^2\right) \theta\left(\sqrt{s} - \frac{-u_1 - t_1}{\sqrt{2}\sqrt{2s}}\right) dt_1 du_1 d^2 \mathbf{p}_T \\ &= \frac{1}{8\pi^2 s} \theta(-[u_1 + t_1]) \delta\left(\frac{u_1 t_1}{s} - m_C^2 - \mathbf{p}_T^2\right) \theta(2s + u_1 + t_1) dt_1 du_1 d^2 \mathbf{p}_T, \end{aligned} \quad (\text{A.14})$$

where we have left off the delta function  $\delta(s + t_1 + u_1)$ , implying the constraint  $s + t_1 + u_1 = 0$ . We can use this constraint to get rid of the theta functions:

$$\begin{aligned} dQ &= \frac{1}{8\pi^2 s} \theta(s) \delta\left(\frac{u_1 t_1}{s} - m_C^2 - \mathbf{p}_T^2\right) \theta(s) dt_1 du_1 d^2 \mathbf{p}_T \\ &= \frac{1}{8\pi^2 s} \delta\left(\frac{u_1 t_1}{s} - m_C^2 - \mathbf{p}_T^2\right) dt_1 du_1 d^2 \mathbf{p}_T. \end{aligned} \quad (\text{A.15})$$

Here we have used  $\theta(s) = 1$  because  $s = E_A + E_B \geq 0$ . This delta function can be rewritten as

$$\begin{aligned} \delta\left(\frac{u_1 t_1}{s} - m_C^2 - \mathbf{p}_T^2\right) &= \frac{1}{2\sqrt{\frac{u_1 t_1}{s} - m_C^2}} \delta\left(|\mathbf{p}_T| - \sqrt{\frac{u_1 t_1}{s} - m_C^2}\right) \\ &+ \frac{1}{2\sqrt{\frac{u_1 t_1}{s} - m_C^2}} \delta\left(|\mathbf{p}_T| + \sqrt{\frac{u_1 t_1}{s} - m_C^2}\right). \end{aligned} \quad (\text{A.16})$$

The latter term is zero because  $|\mathbf{p}_T| > 0$ . The 2-dimensional vector  $\mathbf{p}_T = (p_C^1, p_C^2)$  can be rewritten in the polar coordinates  $(|\mathbf{p}_T|, \phi)$ . The infinitesimal area is then

$$d^2 \mathbf{p}_T = |\mathbf{p}_T| d|\mathbf{p}_T| d\phi. \quad (\text{A.17})$$

Integrating  $dQ$  over  $|\mathbf{p}_T|$  and  $\phi$  results in

$$\begin{aligned} dQ &= \frac{1}{8\pi^2 s} \frac{1}{2\sqrt{\frac{u_1 t_1}{s} - m_C^2}} \left[ \delta\left(|\mathbf{p}_T| - \sqrt{\frac{u_1 t_1}{s} - m_C^2}\right) |\mathbf{p}_T| d|\mathbf{p}_T| d\phi \right] dt_1 du_1 \\ &= \frac{1}{8\pi^2 s} \frac{1}{2\sqrt{\frac{u_1 t_1}{s} - m_C^2}} \left[ \sqrt{\frac{u_1 t_1}{s} - m_C^2} d\phi \right] \delta(s + t_1 + u_1) dt_1 du_1 \\ &= \frac{2\pi}{8\pi^2 s} \frac{1}{2} \delta(s + t_1 + u_1) dt_1 du_1 \\ &= \frac{1}{8\pi s} \delta(s + t_1 + u_1) dt_1 du_1. \end{aligned} \quad (\text{A.18})$$

This we substitute in the expression for the differential cross section,

$$\frac{d^2 \sigma}{dt_1 du_1} = \frac{1}{16\pi s^2} |\overline{\mathcal{M}}|^2 \delta(s + t_1 + u_1). \quad (\text{A.19})$$

The  $\delta$ -function is often left off:

$$\frac{d^2 \sigma}{dt_1 du_1} = \frac{1}{16\pi s^2} |\overline{\mathcal{M}}|^2 \quad (\text{with } s + t_1 + u_1 = 0). \quad (\text{A.20})$$



# Appendix B

## Special unitary groups

The special unitary group  $SU(N)$  is the set of  $N \times N$  unitary matrices with determinant  $+1$ . One encounters these groups quite often in quantum mechanics, because quantum mechanical operators are unitary. An arbitrary unitary matrix can always be written as

$$U = \exp(iH), \quad (\text{B.1})$$

where  $H$  is an Hermitian, traceless matrix,

$$H^\dagger = H, \quad \text{Tr } H = 0. \quad (\text{B.2})$$

That  $H$  must be traceless follows from  $\det U = 1$ . Each traceless Hermitian  $N \times N$  matrix can be written as a linear combination of  $N^2 - 1$  Hermitian matrices:

$$H = \alpha^a T^a, \quad (\text{B.3})$$

where summation over  $a = 1, 2, \dots, N^2 - 1$  is implied. The constant matrices  $T^a$  are called the *generators* of the  $SU(N)$  group, because with these matrices it is possible to generate every possible unitary transformation  $U$ . For an infinitesimal small rotation we find

$$U = \exp(i\alpha^a T^a) = 1 + i\alpha^a T^a + \mathcal{O}(\alpha^2). \quad (\text{B.4})$$

A special property of the  $SU(N)$  group is that an arbitrary unitary transformation can be obtained by performing multiple rotations subsequently:

$$U = \lim_{n \rightarrow \infty} (1 + i\alpha^a T^a)^n = \exp(i\alpha^a T^a). \quad (\text{B.5})$$

A continuous group with this structure is called a *Lie group*. Such a group is characterized by its *Lie algebra*, i.e. the commutator of two generators can be written as a linear combination of the other generators:

$$[T^a, T^b] = i f^{abc} T^c, \quad (\text{B.6})$$

where  $f^{abc}$  are the *structure constants* of the group. If we choose the set of generators in such a way that

$$\text{Tr}(T^a T^b) = C_R \delta^{ab}, \quad (\text{B.7})$$

with  $C_R$  a constant (a so-called Casimir number), then we can write the  $f^{abc}$  as

$$f^{abc} = -\frac{i}{C_R} \text{Tr}([T^a, T^b] \cdot T^c). \quad (\text{B.8})$$

With this, one can show that the structure constants are completely antisymmetry, i.e.  $f^{abc} = -f^{bac} = f^{bca}$ . From the identity

$$[T^a, [T^b, T^c]] + [T^b, [T^c, T^a]] + [T^c, [T^a, T^b]] = 0 \quad (\text{B.9})$$

follows that the structure constants must also obey

$$f^{ade} f^{bcd} + f^{bde} f^{cad} + f^{cde} f^{abd} = 0. \quad (\text{B.10})$$

This relation is called the *Jacobi identity*.

Let us define a set of matrices  $\mathcal{T}^a$ , whose element  $(b, c)$  is given by

$$(\mathcal{T}^a)_{bc} = -if^{abc}. \quad (\text{B.11})$$

The commutator is

$$\begin{aligned} [\mathcal{T}^a, \mathcal{T}^b] &= (\mathcal{T}^a)_{cd}(\mathcal{T}^b)_{de} - (\mathcal{T}^b)_{cd}(\mathcal{T}^a)_{de} \\ &= -f^{acd}f^{bde} + f^{bcd}f^{ade} = f^{cad}f^{bde} + f^{bcd}f^{ade} \\ &= -f^{cde}f^{abd} = if^{abd}(if^{dce}) = if^{abd}(\mathcal{T}^d)_{ce} \\ &= if^{abc}\mathcal{T}^c. \end{aligned} \quad (\text{B.12})$$

We see that the matrices  $\mathcal{T}^a$  have the same Lie algebra and therefore belong to the group  $\text{SU}(N)$ , just like the  $T^a$  do. The  $T^a$  are called the *fundamental representation*, because they are  $N \times N$  matrices. The  $\mathcal{T}^a$  are  $(N^2 - 1) \times (N^2 - 1)$  matrices and are called the *adjoint representation*. There are many other representations possible, each with matrices of a certain dimension. The trivial, or *singlet representation*, is the set of  $1 \times 1$  matrices. To obey the Lie algebra (B.6), it is clear that each generator in the trivial representation must be equal to zero.

Probably the most famous unitary group is  $\text{SU}(2)$ . The generators of  $\text{SU}(2)$  are

$$T_{\text{SU}(2)}^a = \frac{1}{2}\tau^a, \quad (\text{B.13})$$

where  $\tau^a$  are the Pauli matrices:

$$\tau^1 = \begin{pmatrix} 0 & 1 \\ 1 & 0 \end{pmatrix}, \quad \tau^2 = \begin{pmatrix} 0 & -i \\ i & 0 \end{pmatrix}, \quad \tau^3 = \begin{pmatrix} 1 & 0 \\ 0 & -1 \end{pmatrix}. \quad (\text{B.14})$$

The generators are chosen such that

$$\text{Tr}(T^a T^b) = C_R \delta^{ab} = \frac{1}{2} \delta^{ab}. \quad (\text{B.15})$$

It is often useful to work with the  $\tau^\pm$  defined by

$$\tau^\pm \equiv \frac{1}{\sqrt{2}}(\tau^1 \pm i\tau^2), \quad (\text{B.16})$$

or written explicitly,

$$\tau^+ = \sqrt{2} \begin{pmatrix} 0 & 1 \\ 0 & 0 \end{pmatrix}, \quad \tau^- = \sqrt{2} \begin{pmatrix} 0 & 0 \\ 1 & 0 \end{pmatrix}. \quad (\text{B.17})$$

The structure constants of  $\text{SU}(2)$  are given by

$$f^{abc} = \epsilon^{abc} = \begin{cases} +1 & \text{if } abc \text{ is an even permutation of } 123, \\ -1 & \text{if } abc \text{ is an odd permutation of } 123, \\ 0 & \text{otherwise} \end{cases}, \quad (\text{B.18})$$

which is known as the Levi-Civita tensor.

The  $\text{SU}(3)$  generators are usually defined as

$$T_{\text{SU}(3)}^a = \frac{1}{2}\lambda^a, \quad (\text{B.19})$$

with  $a = 1, 2, \dots, 8$  and  $\lambda$  the Gell-Mann matrices given by

$$\begin{aligned} \lambda_1 &= \begin{pmatrix} 0 & 1 & 0 \\ 1 & 0 & 0 \\ 0 & 0 & 0 \end{pmatrix}, & \lambda_2 &= \begin{pmatrix} 0 & -i & 0 \\ i & 0 & 0 \\ 0 & 0 & 0 \end{pmatrix}, & \lambda_3 &= \begin{pmatrix} 1 & & \\ & -1 & \\ & & 0 \end{pmatrix}, \\ \lambda_4 &= \begin{pmatrix} 0 & 0 & 1 \\ 0 & 0 & 0 \\ 1 & 0 & 0 \end{pmatrix}, & \lambda_5 &= \begin{pmatrix} 0 & 0 & -i \\ 0 & 0 & 0 \\ i & 0 & 0 \end{pmatrix}, & \lambda_6 &= \begin{pmatrix} 0 & 0 & 0 \\ 0 & 0 & 1 \\ 0 & 1 & 0 \end{pmatrix}, \\ \lambda_7 &= \begin{pmatrix} 0 & 0 & 0 \\ 0 & 0 & -i \\ 0 & i & 0 \end{pmatrix}, & \lambda_8 &= \frac{1}{\sqrt{3}} \begin{pmatrix} 1 & & \\ & 1 & \\ & & -2 \end{pmatrix}. \end{aligned} \quad (\text{B.20})$$

The generators are again chosen in such a way that

$$\text{Tr}(T^a T^b) = \frac{1}{2} \delta^{ab}. \quad (\text{B.21})$$

There are  $8^3 = 512$  structure constants for  $\text{SU}(3)$ , but most of them are zero. One can obtain all of them with

$$\begin{aligned} f^{123} &= 1, & f^{458} &= f^{678} = \sqrt{3}/2, \\ f^{147} &= f^{246} = f^{257} = f^{345} = f^{516} = f^{637} = \frac{1}{2}, \end{aligned} \quad (\text{B.22})$$

and by making use of the fact that  $f^{abc}$  is completely antisymmetric.

Finally we shall present here all the generators of  $\text{SU}(5)$ . These are

$$T_{\text{SU}(5)}^a = \frac{1}{2} \tilde{\lambda}^a, \quad (\text{B.23})$$

with

$$\begin{aligned} \tilde{\lambda}_1 &= \begin{pmatrix} 0 & 1 & 0 \\ 1 & 0 & 0 \\ 0 & 0 & 0 \end{pmatrix}, & \tilde{\lambda}_2 &= \begin{pmatrix} 0 & -i & 0 \\ i & 0 & 0 \\ 0 & 0 & 0 \end{pmatrix}, & \tilde{\lambda}_3 &= \begin{pmatrix} 1 & & & & \\ & -1 & & & \\ & & 0 & & \\ & & & 0 & \\ & & & & 0 \end{pmatrix}, \\ \tilde{\lambda}_4 &= \begin{pmatrix} 0 & 0 & 1 \\ 0 & 0 & 0 \\ 1 & 0 & 0 \end{pmatrix}, & \tilde{\lambda}_5 &= \begin{pmatrix} 0 & 0 & -i \\ 0 & 0 & 0 \\ i & 0 & 0 \end{pmatrix}, & \tilde{\lambda}_6 &= \begin{pmatrix} 0 & 0 & 0 \\ 0 & 0 & 1 \\ 0 & 1 & 0 \end{pmatrix}, \\ \tilde{\lambda}_7 &= \begin{pmatrix} 0 & 0 & 0 \\ 0 & 0 & -i \\ 0 & i & 0 \end{pmatrix}, & \tilde{\lambda}_8 &= \frac{1}{\sqrt{3}} \begin{pmatrix} 1 & & & & \\ & 1 & & & \\ & & -2 & & \\ & & & 0 & \\ & & & & 0 \end{pmatrix}, \\ \tilde{\lambda}_9 &= \begin{pmatrix} & & 1 & 0 \\ & & 0 & 0 \\ & & 0 & 0 \\ 1 & 0 & 0 & 0 \\ 0 & 0 & 0 & 0 \end{pmatrix}, & \tilde{\lambda}_{10} &= \begin{pmatrix} & & -i & 0 \\ & & 0 & 0 \\ & & 0 & 0 \\ i & 0 & 0 & 0 \\ 0 & 0 & 0 & 0 \end{pmatrix}, & \tilde{\lambda}_{11} &= \begin{pmatrix} & & 0 & 0 \\ & & 1 & 0 \\ & & 0 & 0 \\ 0 & 1 & 0 & 0 \\ 0 & 0 & 0 & 0 \end{pmatrix}, \\ \tilde{\lambda}_{12} &= \begin{pmatrix} & & 0 & 0 \\ & & -i & 0 \\ & & 0 & 0 \\ 0 & i & 0 & 0 \\ 0 & 0 & 0 & 0 \end{pmatrix}, & \tilde{\lambda}_{13} &= \begin{pmatrix} & & 0 & 0 \\ & & 0 & 0 \\ & & 1 & 0 \\ 0 & 0 & 1 & 0 \\ 0 & 0 & 0 & 0 \end{pmatrix}, & \tilde{\lambda}_{14} &= \begin{pmatrix} & & 0 & 0 \\ & & 0 & 0 \\ & & -i & 0 \\ 0 & 0 & i & 0 \\ 0 & 0 & 0 & 0 \end{pmatrix}, \\ \tilde{\lambda}_{15} &= \begin{pmatrix} & & 0 & 1 \\ & & 0 & 0 \\ & & 0 & 0 \\ 0 & 0 & 0 & 0 \\ 1 & 0 & 0 & 0 \end{pmatrix}, & \tilde{\lambda}_{16} &= \begin{pmatrix} & & 0 & -i \\ & & 0 & 0 \\ & & 0 & 0 \\ 0 & 0 & 0 & 0 \\ i & 0 & 0 & 0 \end{pmatrix}, & \tilde{\lambda}_{17} &= \begin{pmatrix} & & 0 & 0 \\ & & 0 & 1 \\ & & 0 & 0 \\ 0 & 0 & 0 & 0 \\ 0 & 1 & 0 & 0 \end{pmatrix}, \\ \tilde{\lambda}_{18} &= \begin{pmatrix} & & 0 & 0 \\ & & 0 & -i \\ & & 0 & 0 \\ 0 & 0 & 0 & 0 \\ 0 & i & 0 & 0 \end{pmatrix}, & \tilde{\lambda}_{19} &= \begin{pmatrix} & & 0 & 0 \\ & & 0 & 0 \\ & & 0 & 1 \\ 0 & 0 & 0 & 0 \\ 0 & 0 & 1 & 0 \end{pmatrix}, & \tilde{\lambda}_{20} &= \begin{pmatrix} & & 0 & 0 \\ & & 0 & 0 \\ & & 0 & -i \\ 0 & 0 & 0 & 0 \\ 0 & 0 & i & 0 \end{pmatrix}, \\ \tilde{\lambda}_{21} &= \begin{pmatrix} & & & & \\ & & & & \\ & & & & \\ & & 0 & 1 & \\ & & 1 & 0 & \end{pmatrix}, & \tilde{\lambda}_{22} &= \begin{pmatrix} & & & & \\ & & & & \\ & & & & \\ & & 0 & -i & \\ & & i & 0 & \end{pmatrix}, & \tilde{\lambda}_{23} &= \begin{pmatrix} 0 & & & & \\ & 0 & & & \\ & & 0 & & \\ & & & 1 & \\ & & & & -1 \end{pmatrix}, \end{aligned}$$

and

$$\tilde{\lambda}_{24} = \frac{1}{\sqrt{15}} \begin{pmatrix} -2 & & & & \\ & -2 & & & \\ & & -2 & & \\ & & & 3 & \\ & & & & 3 \end{pmatrix}. \quad (\text{B.24})$$

# Bibliography

- [1] J.B. Marion and S.T. Thornton, *Classical Dynamics of Particles and Systems* (1995) Harcourt Inc. (p. 234)
- [2] M.E. Peskin and D.V. Schroeder, *An Introduction to Quantum Field Theory* (1995) Westview Press (p. 488)
- [3] D.J. Griffiths, *Introduction to Elementary Particles* (1987) John Wiley & Sons, Inc. (pp. 119-120)
- [4] M.E. Peskin and D.V. Schroeder, *An Introduction to Quantum Field Theory* (1995) Westview Press
- [5] L.H. Ryder, *Quantum field theory* 2nd ed. (1999) Cambridge University Press
- [6] L.H. Ryder, *Quantum field theory* 2nd ed. (1999) Cambridge University Press (p. 154)
- [7] F. Halzen and A.D. Martin, *Quarks & Leptons* (1984) John Wiley & Sons, Inc. (p. 139)
- [8] M.E. Peskin and D.V. Schroeder, *An Introduction to Quantum Field Theory* (1995) Westview Press (p. 735)
- [9] M.E. Peskin and D.V. Schroeder, *An Introduction to Quantum Field Theory* (1995) Westview Press (pp. 801-802)
- [10] M.E. Peskin and D.V. Schroeder, *An Introduction to Quantum Field Theory* (1995) Westview Press (p. 691)
- [11] J.A.M. Vermaseren, *New features of FORM* (2000), [math-ph/0010025]  
<http://www.nikhef.nl/~form/>
- [12] V.D. Barger and R.J.N. Phillips, *Collider Physics* (1987) Addison-Wesley Publishing Company (p. 374)
- [13] F. Halzen and A.D. Martin, *Quarks & Leptons* (1984) John Wiley & Sons, Inc. (p. 193)
- [14] S. Willenbrock, *The Standard Model and the Top Quark*, 16 Dec 2002, [hep-ph/0211067] (Fig. 8)
- [15] B.W. Harris, E. Laenen, L. Phaf, Z. Sullivan, S. Weinzierl, *The fully differential single-top-quark cross section in next-to-leading order QCD*, Phys. Rev. D **66** (2002), 054024 [hep-ph/0207055]
- [16] S. Willenbrock, *The Standard Model and the Top Quark*, 16 Dec 2002, [hep-ph/0211067] (Table 5)
- [17] S. Willenbrock, *The Standard Model and the Top Quark*, 16 Dec 2002, [hep-ph/0211067]
- [18] S. Willenbrock, *The Standard Model and the Top Quark*, 16 Dec 2002, [hep-ph/0211067] (Table 3)
- [19] Particle Physics Booklet, July 2004. Extracted from S. Eidelman *et al.*, *Review of Particle Physics*, Phys. Lett. B **592**, 1 (2004)
- [20] S. Weinzierl, *Introduction to Monte Carlo methods* (2000), [hep-ph/0006269]
- [21] E.W. Weinstein, *Gaussian Quadrature*. From *Mathworld*—A Wolfram Web Resource.  
<http://mathworld.wolfram.com/GaussianQuadrature.html>
- [22] G.P. Lepage, *A New Algorithm for Adaptive Multidimensional Integration*, Journal of Computational Physics **27**, 192-203, (1978)

- [23] G. Marsaglia, A. Zaman, and W.-W. Tsang, *Stat. prob. Lett.* **9**, (1990), 35
- [24] I.M. Sobol', *USSR Comp. Math. Math. Phys.* **7**, (1967), 86
- [25] F. Halzen and A.D. Martin, *Quarks & Leptons* (1984) John Wiley & Sons, Inc. (p. 91)
- [26] Gnuplot  
<http://www.gnuplot.info>
- [27] ROOT, *An Object-Oriented Data Analysis Framework*  
<http://root.cern.ch>
- [28] C.T. Hill and E.H. Simmons, *Strong Dynamics and Electroweak Symmetry Breaking*, *Phys. Rept.* **381** (2003) 235-402, [hep-ph/0203079]
- [29] D. Muller and S. Nandi, *Topflavor: Separate SU(2) for the Third Family*, *Phys. Lett. B* **383** (1996) 345-350, [hep-ph/9602390]
- [30] H.-J. He, T.M.P. Tait, and C.-P. Yuan, *New Topflavor Models with Seesaw Mechanism*, *Phys. Rev. D* **62** (2000) 011702, [hep-ph/9911266]
- [31] Wikipedia, Seesaw mechanism,  
[http://en.wikipedia.org/wiki/Seesaw\\_mechanism](http://en.wikipedia.org/wiki/Seesaw_mechanism) (as of May 20th 2006, 20:30 GMT)
- [32] E. Malkawi, T. Tait, and C.-P. Yuan, *A Model of Strong Flavor Dynamics for the Top Quark*, *Phys. Lett. B* **385** (1996) 304-310, [hep-ph/9603349]
- [33] E.H. Simmons *New Gauge Interactions and Single Top Quark Production*, *Phys. Rev. D* **55** (1997) 5494-5500, [hep-ph/9612402]
- [34] T.M.P. Tait and C.-P. Yuan, *Single Top Production as a Window to Physics Beyond the Standard Model.*, *Phys. Rev. D* **63** (2001) 014018, [hep-ph/0007298]
- [35] M. Schmaltz, D. Tucker-Smith, *Little Higgs Review*, *Ann. Rev. Nucl. Part. Sci.* **55** (2005) 229-270, [hep-ph/0502182]
- [36] M. Schmaltz, *Introducing the Little Higgs*, *Nucl. Phys. Proc. Suppl.* **117** (2003) 40-49, [hep-ph/0210415]
- [37] N. Arkani-Hamed, A.G. Cohen, and H. Georgi, *Electroweak symmetry breaking from dimensional deconstruction*, *Phys. Lett. B* **513** (2001) 232-240, [hep-ph/0105239]
- [38] I. Low, W. Skiba, and D. Smith, *Little Higgses from an Antisymmetric Condensate*, *Phys. Rev. D* **66** (2002) 072001, [hep-ph/0207243]
- [39] N. Arkani-Hamed, A.G. Cohen, T. Gregoire, E. Katz, A.E. Nelson, and J.G. Wacker, *The Minimal Moose for a Little Higgs*, *JHEP* **0208** (2002) 021, [hep-ph/0206020]
- [40] T. Gregoire and J.G. Wacker, *Moose, Topology and Higgs*, *JHEP* **0208** (2002) 019, [hep-ph/0206023]
- [41] N. Arkani-Hamed, A.G. Cohen, E. Katz, A.E. Nelson, *The Littlest Higgs* *JHEP* **0207** (2002) 034, [hep-ph/0206021]
- [42] M. Schmaltz, D. Tucker-Smith, *Little Higgs Review*, *Ann. Rev. Nucl. Part. Sci.* **55** (2005) 229-270, [hep-ph/0502182] (p. 29)
- [43] M.C. Brak, *The Hierarchy Problem in the Standard Model and Little Higgs Theories*, Master's thesis (2004)  
<http://www.nikhef.nl/pub/theory/masters-theses/maarten.brak.pdf>
- [44] S.R. Coleman and E. Weinberg, *Phys. Rev. D* **7**, 1888 (1973)
- [45] T. Han, H.E. Logan, B. McElrath, and L.-T. Wang, *Phenomenology of the little Higgs model*, *Phys. Rev. D* **67** (2003) 095004, [hep-ph/0301040] (Eq. A24 and A25)

- [46] T. Han, H.E. Logan, B. McElrath, and L.-T. Wang, *Phenomenology of the little Higgs model*, Phys. Rev. D **67** (2003) 095004, [hep-ph/0301040]
- [47] C.-X. Yue, L. Zhou, and S. Yang, *Little Higgs models and single top production at the LHC*, [hep-ph/0604001]
- [48] Z. Sullivan, How to rule out Little Higgs (and constrain many other models) at the LHC, talk given at the XXXVIIIth Rencontres de Moriond: QCD and Hadronic interactions (2003), [hep-ph/0306266]
- [49] C. Csaki, C. Grojean, L. Pilo, and J. Terning, *Towards a Realistic Model of Higgsless Electroweak Symmetry Breaking*, Phys. Rev. Lett. **92** (2004) 101802, [hep-ph/0308038]
- [50] J.A.M. Vermaseren, *Axodraw*, Comp. Phys. Comm. 83:45-58 (1994)  
<http://www.nikhef.nl/~t68/axodraw/>